Large scale structure in the Durham/UKST galaxy Redshift survey

Ratcliffe, Andrew

Large Scale Structure in the Durham/UKST Galaxy Redshift Survey

Andrew Ratcliffe

A thesis submitted to the University of Durham
in accordance with the regulations for
admittance to the Degree of Doctor of Philosophy.

Department of Physics
University of Durham
March 1996

Abstract

The initial results from the Durham/UKST Galaxy Redshift Survey are presented here. Using this redshift survey the luminosity, clustering and dynamical properties of galaxies in the Universe are investigated.

The 3-D distribution of galaxies in the Durham/UKST survey appears "cellular" on 50-100h^{-1}Mpc scales (where h is Hubble's constant in units of 100 kms^{-1} Mpc^{-1}) and is clearly more complex than a simple 1-D periodic pattern.

The optical galaxy luminosity function of the Durham/UKST survey is estimated and can be fit by a Schechter function. Comparison with other determinations of the luminosity function shows good agreement, favouring a flat faint end slope to $M_{b_J} \sim -14$.

The *redshift* space 2-point correlation function clustering statistic is estimated from the Durham/UKST survey. Comparison with previous estimates from other redshift surveys again shows good agreement and the Durham/UKST survey gives a detection of large scale power above and beyond that of the standard cold dark matter cosmological model on 10-40h^{-1}Mpc scales. The projected correlation function is also estimated from the Durham/UKST survey and is compared with models for the *real* space 2-point correlation function. To estimate this *real* space correlation function directly, a new application of the Richardson-Lucy inversion technique is developed, tested and then applied to the Durham/UKST survey.

The effects of redshift space distortions on the 2-point correlation function are investigated and modelled in the non-linear and linear regimes. The 1-D pairwise velocity dispersion of galaxies is measured to be 416 ± 36 kms^{-1} which, while being consistent with the canonical value of ~ 350 kms^{-1}, is slightly smaller than recently measured values. However, this value is inconsistent with the ~ 1000 kms^{-1} value as measured in the standard cold dark matter cosmological model at a high level of significance. The ratio of the mean mass density of the Universe, Ω, and the linear bias factor, b (relating the galaxy and light distributions), is then calculated to be $\Omega^{0.6}/b = 0.45 \pm 0.38$. This favours either an open ($\Omega < 1$) and unbiased ($b = 1$) Universe or a flat ($\Omega = 1$) and biased ($b \sim 2$) Universe.

Preface

The work described in this thesis was undertaken between 1992 and 1995 whilst the author was a research student under the supervision of Dr. T. Shanks in the Department of Physics at the University of Durham. This work has not been submitted for any other degree at the University of Durham or at any other University.

All of the observations presented in chapter 2 and appendix A were undertaken in collaboration with Dr. A. Broadbent, Dr. T.Shanks, (Durham University), Dr. Q.A. Parker (AAO) and Dr. C.A. Collins (Liverpool-John-Moores University). Other collaborators in this project were Dr. R. Fong (Durham University), Dr. F.G. Watson (AAO) and Dr. A.P. Oates (RGO). However, the vast majority of the analysis presented in chapters 3, 4, 5 and 6 was the author's own work.

A number of the results presented here have appeared in the following papers :

Ratcliffe, A., Shanks, T., Broadbent, A., Parker, Q.A., Watson, F.G., Oates, A.P. & Collins, C.A., (1996), submitted to *Mon. Not. R. astr. Soc.*

This thesis is dedicated to the memory of my Mother.

It's always tougher to win when everyone expects you to.

Dave Johnson

You can remember me any way you want to. I don't really care, to be honest.

Jimmy Connors

Contents

Chapter 1

Introduction

1.1 The Standard Cosmology

The standard cosmological model ("The Hot Big Bang") assumes that the observable Universe and its properties are spatially homogeneous and isotropic on sufficiently large scales. Such a spatially homogeneous and isotropic Universe is described by the Friedmann-Robertson-Walker metric. The Universe itself is seen to be expanding (Hubble, 1929) and according to General Relativity this is interpreted as a property of the metric which describes the space-time around us. Also, the Universe is observed in all directions to be full of a very uniform background radiation which has a spectral distribution consistent with that of a nearly perfect black body at a temperature of a few K (Penzias & Wilson, 1965). The uniformity of this so-called Cosmic Microwave Background Radiation (of order 1 part in 10^5, see Smoot *et al.* 1992) implies that the early Universe, at the time of baryonic matter-radiation decoupling, was also homogeneous and isotropic. Running the clock backwards from the boundary conditions observed today (namely that of expansion and temperature of a few K) implies that the Universe was hotter and denser in the past, eventually becoming an infinitely small, infinitely dense point (a mathematical singularity) at an infinite temperature, this is what is meant by the "Hot Big Bang" ! However, the laws of physics probably break down as the Universe reaches these extreme conditions.

1.2 Motivation

While the Cosmic Microwave Background Radiation (and hence the early Universe) is very uniform, the Universe today is not and, among other things, consists of stars, galaxies and galaxy clusters. One of the questions which should be asked is, "How did the Universe become so clumpy from such a uniform beginning ?" In the past two decades cosmologists believe they have begun to answer this question. Basically, it is thought that small primordial imhomogeneities in the density field have grown via gravitational instability, ie. some initial form of perturbations in the Friedmann-Robertson-Walker metric have been amplified by gravity. The "Inflationary paradigm" of Guth (1981) gives a possible explanation of the origin of these initial perturbations and, during the inflationary phase, quantum fluctuations in the energy-density field are responsible for producing a specific spectrum of primordial perturbations (Hawking, 1982). Microphysical processes then alter this initial form depending on the amount and character of the mass density. Perhaps the most successful cosmological model of structure formation is the cold dark matter (CDM) model (eg. Blumenthal *et al.* 1984, Davis *et al.* 1985) where the mass of the Universe is dominated by slowly moving non-baryonic dark matter. Therefore, the major problem in cosmology today is to observe the form of the density fluctuations and compare with various theoretical predictions. In doing this one can hopefully determine both the initial perturbation spectrum and the contents of the mass density, hence specifying a complete cosmological model. Of course, one must remember that the perturbations observed at the present day are not exactly the same as those after the microphysical processes have occured because they have been evolving and growing with time. In order for a correct comparison to be made the fluctuations predicted by these theoretical models must also be similarly evolved with time. This can be done by the use of numerical N-body simulations.

In the statistical analysis of the density field the fundamental object of interest is the power spectrum of the density fluctuations, $P(k)$. (Assuming that the density field is a Gaussian Random Field.) Essentially this gives the relative amount of structure, or "power", at a given length scale and is defined as follows. Consider the density contrast

$$\delta(\mathbf{x}) = \frac{\rho(\mathbf{x}) - \bar{\rho}}{\bar{\rho}}, \tag{1.1}$$

where $\rho(\mathbf{x})$ is the density field as a function of position, $\mathbf{x}$, and $\bar{\rho}$ is the mean density. One can Fourier expand this field

$$\delta(\mathbf{x}) = \frac{1}{(2\pi)^3} \int \delta_k \exp[-i\mathbf{k}.\mathbf{x}] d^3k, \tag{1.2}$$

such that its Fourier transform is

$$\delta_k = \int \delta(\mathbf{x}) \exp[i\mathbf{k}.\mathbf{x}] d^3x. \tag{1.3}$$

The power spectrum of the density fluctuations is simply the mean square modulus of these Fourier coefficients

$$P(k) = \left\langle |\delta_k|^2 \right\rangle, \tag{1.4}$$

where the angular brackets denote averaging over different regions of space which by the Spatial Ergodic Hypothesis is equivalent to ensemble averaging over different Universes.

It can be shown (eg. Kolb & Turner, 1990, or Strauss & Willick, 1995) that the power spectrum of the density fluctuations can be related to other cosmologically interesting quantities. These include the variance of the density fluctuations, $(\delta\rho/\rho)^2$, the mean square peculiar velocity field (the "bulk" peculiar velocity flow), the large angle gravitationally induced temperature fluctuations in the Cosmic Microwave Background Radiation (the Sachs-Wolfe effect) and the 2-point correlation function (the Fourier transform of the power spectrum). Therefore, one can extract information about the fluctuation spectrum by measuring one or more of these quantities. At this point in time, the research in the fields involving these quantities is probably more limited by the observations and the biases inherent in them and not the physics behind them. Hence, the observational datasets only give information, of varying reliability, on different scales. For example, when this Ph.D. was started in 1992, the local peculiar velocity field had just been measured out to $\sim 50h^{-1}$Mpc (Bertschinger *et al.* 1990), the largest redshift survey in existence consisted of a few thousand galaxies mapping out to $\sim 100h^{-1}$Mpc (Saunders *et al.* 1991) and fluctuations in the cosmic microwave background radiation had just been detected (Smoot *et al.* 1992). Reliable information about the fluctuations on small scales ($<$ 10-20h^{-1}Mpc) mainly came from the redshift and velocity surveys while the cosmic microwave background radiation gave information on much larger scales ($\sim 1000h^{-1}$Mpc). On the scales in between these there was little concrete observational information about the form of the fluctuations.

In the 1980's a great deal of time and effort went into probing the fluctuations by constructing galaxy redshift surveys with well defined selection criterion (for a recent review see Strauss & Willick, 1995). The overall picture that developed from these redshift surveys was one of spectacular structures in the galaxy distribution. Indeed, the Universe appeared not to be a bland homogeneous and isotropic place but was full of "filaments" and "sheets" of galaxies on $\sim 50h^{-1}$Mpc scales which surrounded large empty regions almost devoid of galaxies. This was most prominently seen in the CfA1 survey (Geller *et al.* 1987) where the Coma cluster and "Great Wall" dominated the observed distribution. Unfortunately, the surveys were limited by the total number of galaxies that could be observed on a realistic timescale. However, rapid improvements in instrumentation were also made during this time, most noticeably the advent of wide-field multi-object spectroscopy which enabled simultaneous measurement of many galaxy redshifts. This allowed the limiting number of redshifts to increase dramatically from a couple of hundred to a couple of thousand. There existed a number of observational strategies designed to maximise the information one could get out of a survey ; one could go for quite large angles with a full sampling rate but not very deep (eg. the CfA1 survey of Geller *et al.* 1987), or very deep and fully sampled but only cover a very small angle (eg. the pencil-beam survey of Broadhurst *et al.* 1990), or moderately deep, covering a very large angle but only with a sparse sampling (eg. the APM-Stromlo survey of Loveday *et al.* 1992b, or the IRAS surveys of Saunders *et al.* 1991 and Fisher *et al.* 1994). Indeed, even the largest survey in existence at the time of writing is limited by having a very narrow "slice" geometry of angular width 1.5° (Shectman *et al.* 1995). Therefore, when the Durham/UKST project was started in earnest in 1991 the aim was to maximise the information obtained from these different approaches, namely to observe a moderately deep sample, covering a reasonably large area on the sky with a quite high sampling rate.

1.3 Scientific Aims

With the above observing strategy the aims (and hopes !) of the Durham/UKST Galaxy Redshift Survey were to enable a good measurement of clustering statistics on large scales up to $\sim 100h^{-1}$Mpc (ie. the survey would be big enough such that individual structures would not dominate the survey) and also to measure a strong signal on small scales less than $\sim 10h^{-1}$Mpc (ie. that the sampling rate would be high enough such that the signal would not be totally washed out). Since redshifts are measured and not direct distances, the intrinsic galaxy clustering pattern also has the imprint of the galaxy peculiar velocity field on top of it. Therefore, by measuring clusting statistics on the aforementioned scales, important dynamical information in both the non-linear and linear regimes can also be obtained.

The redshift survey itself was constructed by spectroscopically observing over 4000 galaxies sampled at a rate of 1 in 3 from the Edinburgh/Durham Southern Galaxy Catalogue of Collins *et al.* (1988) to $b_J \leq 17.5^m$. The resulting survey, complete to $b_J \simeq 17^m$, has ~ 2500 measured redshifts, covers a $\sim 20° \times 75°$ contiguous area of the sky at the South Galactic Pole and probes to a depth of $> 300h^{-1}$Mpc with a median depth of $\sim 150h^{-1}$Mpc. The total volume of space surveyed is $\sim 4 \times 10^6 h^{-3}$Mpc^3.

The Durham/UKST survey itself is described in more detail in chapter 2. As will be seen in chapters 5 and 6 this combination of depth, high sampling rate and large area on the sky does allow the accurate determination of clustering statistics which in turn give information on the structure and dynamics of the Universe on the above scales.

Chapter 2

The Durham/UKST Galaxy Redshift Survey – Construction of the Data Set

2.1 Introduction

In this chapter the construction of the Durham/UKST Galaxy Redshift Survey is described. The format of the chapter is as follows. The parent 2-D catalogue is briefly described followed by a zero-point correction to the photometry used in the Durham/UKST survey. The observational and data reduction procedures are then outlined. The Durham/UKST redshift catalogue is described, the accuracy of the redshifts checked and then the completeness of the Durham/UKST survey is given for a few different magnitude limited samples. (The full redshift catalogue is presented in appendix A.) Redshift-cone plots are then shown and described, along with the number-distance histogram for this survey. The chapter ends with the main conclusions on the construction of this redshift catalogue.

2.2 The Parent 2-D Galaxy Sample

The Durham/UKST galaxy redshift survey uses the right ascension and declination positions (α, δ) and b_J photometry (with a small correction, see section 2.3) of galaxies selected from the Edinburgh/Durham Southern Galaxy Catalogue (EDSGC) of Collins *et al.* (1988), also see Collins *et al.* (1992). The EDSGC consists of a mosaic of 60 UKST b_J survey plates around the South Galactic Pole to a limiting apparent magnitude depth of $b_J \simeq 20$, containing $\sim 10^6$ galaxies. Each plate was scanned by the Edinburgh COSMOS measuring machine and covers a $5.3° \times 5.3°$ region on the sky with an overlap of $0.3°$ at the edges, therefore each UKST field measures $5.0° \times 5.0°$. Galaxies from each of the 60 fields were selected to $b_J = 17.5$ using the

EDSGC 1 in 1 lists. This magnitude limit was almost 0.5^m fainter than the nominal limit of the survey, this was necessary to ensure that all of the fibres were used in the actual observations given the fluctuations seen in the number density on the sky. The objects in the 1 in 1 lists were then eyeballed by A. Broadbent using copies of the original UKST plates. Objects which were misidentified by the COSMOS machine as galaxies were then removed from the lists, these spurious objects were generally double stars or star/galaxy mergers and amounted to < 10% of the total number. The remaining objects were ordered into increasing apparent magnitude and objects selected at a rate of 1 in 3. These final lists form the observational target samples of the Durham/UKST galaxy redshift survey.

2.3 The Zero-Point Photometry Correction

Metcalfe *et al.* (1995a) have carried out a photometry comparison between the APM and COSMOS catalogues using CCD photometry in a few overlapping fields. Although dealing with small numbers of galaxies the indications were that the APM photometry was more accurate with respect to the CCD photometric zero-points. Therefore, in an effort to correct the photometry used in this thesis a small zero-point correction is applied to each field. Table 2.1 shows the UKST field number, the right ascension and declination (α,δ) coordinates of the field center (1950), the field widths and the photometry zero-point correction used in each of the 60 UKST fields. The photometry correction is simply an offset in each field and is derived from a comparison between the APM catalogue of Maddox *et al.* (1990a) and the EDSGC of Collins *et al.* (1988). Dalton (1995) has kindly supplied the number of matched APM and COSMOS galaxies and the mean magnitude difference between these magnitudes (as measured by the respective machines) in each field as a function of b_J, see Dalton *et al.* (1995). The average cumulative magnitude offset to $b_J = 19.5$ was calculated (in the sense APM − COSMOS) and is used to correct the COSMOS magnitudes to have the same zero-point as the APM magnitudes. These corrections are plotted in figure 2.1 as a function of the field center (α,δ) coordinates. These offsets do not appear to be random and there seems to be a difference of ~ 0.3 mags as a function of α across the sky. This will not be investigated any further here.

Table 2.1: Table showing the (α,δ) coordinates (1950), field widths and the photometry correction for each field.

Field #	α (h m s)	δ ($^\circ$ $'$ $''$)	α width (m)	δ width ($^\circ$)	Δb_J
531	21 38 00	−25 00 00	22.0	5.00	+0.1633
532	22 00 00	−25 00 00	22.0	5.00	+0.1325
533	22 22 00	−25 00 00	22.0	5.00	+0.1888
534	22 44 00	−25 00 00	22.0	5.00	+0.0066
535	23 06 00	−25 00 00	22.0	5.00	−0.0088
536	23 28 00	−25 00 00	22.0	5.00	−0.0488
537	23 50 00	−25 00 00	22.0	5.00	−0.1810
472	00 06 00	−25 00 00	10.0	5.00	−0.0672
473	00 22 00	−25 00 00	22.0	5.00	−0.0676
474	00 44 00	−25 00 00	22.0	5.00	−0.0047
475	01 06 00	−25 00 00	22.0	5.00	−0.1542
476	01 28 00	−25 00 00	22.0	5.00	−0.1758
477	01 50 00	−25 00 00	22.0	5.00	−0.0983
478	02 12 00	−25 00 00	22.0	5.00	−0.0634
479	02 34 00	−25 00 00	22.0	5.00	−0.0593
480	02 56 00	−25 00 00	22.0	5.00	−0.1006
481	03 18 00	−25 00 00	22.0	5.00	−0.2179
466	21 51 00	−30 00 00	23.0	5.00	+0.1536
467	22 14 00	−30 00 00	23.0	5.00	−0.0039
468	22 37 00	−30 00 00	23.0	5.00	+0.0822
469	23 00 00	−30 00 00	23.0	5.00	+0.0953
470	23 23 00	−30 00 00	23.0	5.00	+0.0126
471	23 46 00	−30 00 00	23.0	5.00	−0.1004
409	00 04 30	−30 00 00	14.0	5.00	−0.1031
410	00 23 00	−30 00 00	23.0	5.00	−0.1708
411	00 46 00	−30 00 00	23.0	5.00	+0.0990
412	01 09 00	−30 00 00	23.0	5.00	−0.2165
413	01 32 00	−30 00 00	23.0	5.00	−0.1412
414	01 55 00	−30 00 00	23.0	5.00	−0.1705
415	02 18 00	−30 00 00	23.0	5.00	−0.0821
416	02 41 00	−30 00 00	23.0	5.00	−0.1348
417	03 04 00	−30 00 00	23.0	5.00	−0.0922

Table 2.1: Table showing the (α,δ) coordinates (1950), field widths and the photometry correction for each field.

Field #	α (h m s)	δ (° ′ ″)	α width (m)	δ width (°)	Δb_J
404	22 00 00	−35 00 00	24.0	5.00	+0.0929
405	22 24 00	−35 00 00	24.0	5.00	−0.0286
406	22 48 00	−35 00 00	24.0	5.00	+0.0049
407	23 12 00	−35 00 00	24.0	5.00	−0.0234
408	23 36 00	−35 00 00	24.0	5.00	−0.0260
349	00 00 00	−35 00 00	24.0	5.00	−0.0990
350	00 24 00	−35 00 00	24.0	5.00	−0.1955
351	00 48 00	−35 00 00	24.0	5.00	−0.0471
352	01 12 00	−35 00 00	24.0	5.00	−0.2069
353	01 36 00	−35 00 00	24.0	5.00	−0.1934
354	02 00 00	−35 00 00	24.0	5.00	−0.1905
355	02 24 00	−35 00 00	24.0	5.00	−0.1724
356	02 48 00	−35 00 00	24.0	5.00	+0.1510
357	03 12 00	−35 00 00	24.0	5.00	−0.0957
344	22 06 00	−40 00 00	26.0	5.00	+0.2166
345	22 32 00	−40 00 00	26.0	5.00	+0.1016
346	22 58 00	−40 00 00	26.0	5.00	+0.1164
347	23 24 00	−40 00 00	26.0	5.00	+0.0449
348	23 50 00	−40 00 00	26.0	5.00	−0.0944
293	00 08 00	−40 00 00	10.0	5.00	−0.1940
294	00 26 00	−40 00 00	26.0	5.00	−0.0406
295	00 52 00	−40 00 00	26.0	5.00	−0.0271
296	01 18 00	−40 00 00	26.0	5.00	−0.0311
297	01 44 00	−40 00 00	26.0	5.00	−0.0805
298	02 10 00	−40 00 00	26.0	5.00	−0.1575
299	02 36 00	−40 00 00	26.0	5.00	−0.1145
300	03 02 00	−40 00 00	26.0	5.00	+0.0328
301	03 28 00	−40 00 00	26.0	5.00	−0.1834

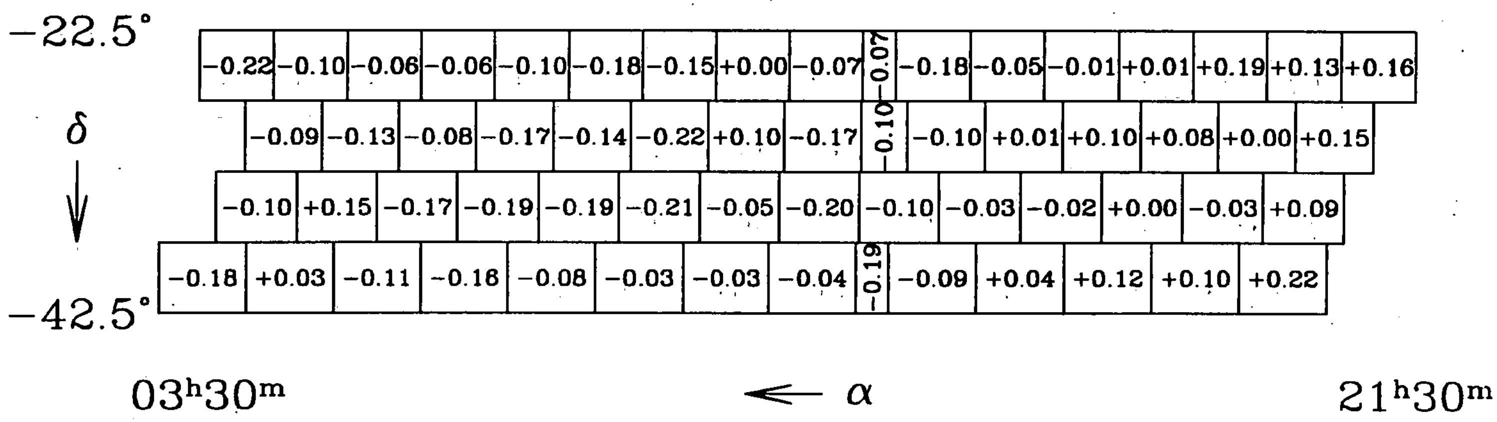

Figure 2.1: The photometry corrections of each UKST field as a function of (α,δ) on the sky.

2.4 The Observational Procedures

The observations for the Durham/UKST survey were carried out in the 4 year period from early 1991 to late 1994 using the FLAIR multi-object spectroscopy system on the UK Schmidt Telescope (UKST) at Siding Spring, Australia. The FLAIR system and its improvements were recently described by Parker & Watson (1995), an earlier description can be found in Watson *et al.* (1991) where the pilot redshift survey from FLAIR is presented (also see Hale-Sutton, 1990). This initial survey determined the feasibility of the larger Durham/UKST project. During this period generous allocations of telescope time (> 60 nights in total) were given to this project. Also, the FLAIR instrument changed from a single plateholder system with 35 fibres and a $\sim 300 \times 400$ pixel CCD (FLAIR-I) to a two plateholder system with 92 & 73 fibres and a $\sim 600 \times 400$ pixel CCD (FLAIR-II). These (and other more subtle) changes in the hardware allowed the project to proceed ~ 8 times as fast in the last 2 years with respect to the first 2 years. The observational goal was simply to measure as many redshifts as possible with well defined selection criteria. Therefore as many fibres as possible were filled with galaxies as far down on each field's target list. To accomplish this only 5-10 fibres in each field were allocated to observe the night sky, the so-called "sky" fibres. The observations themselves were carried out by A. Broadbent, Q. Parker, T. Shanks and myself. Each field was observed only once and for the FLAIR-II system an integration time of ~ 15000s was required to produce > 75% completeness. Unfortunately, the readout noise of the CCD was large (~ 12 e/ADU), therefore the exposures had to be multiple and shorter in length (5×3000s) and then combined during the data reduction procedure. For a typical night when two plateholders were available the observing strategy was as follows. At the start of the night 5-10 bias frames were taken, then 3 frames each of the Hg-Cd arc lamp, the Ne arc lamp, the dome flat fields and the twilight flat fields. Of course, more of these calibration frames were taken if time allowed but experience showed that 3 of each type was the minimum necessary for multiple combining to get rid of cosmic rays, CCD readout glitches etc. The object field was then acquired and the 5 (or more) exposure frames were taken. A final Mercury-Cadmium arc lamp frame was taken to ensure that the fibre aperatures on the CCD had not moved during the observing. The plateholders were then changed and frames were taken in reverse order to the above, ie. starting with the Mercury-Cadmium arc lamp frame and finishing with the bias frames. This minimised the amount of time that was lost due to changing fields while ensuring that all the calibrations were in order. On a typical night the total time lost due to swapping plateholders and acquiring the new field was ~ 45 minutes.

2.5 The Redshift Data Reduction Techniques

The majority of the data reduction was done by myself using the IRAF data analysis package. However, Q. Parker reduced 8 fields in the center of the $\delta = -35°$ strip with the same IRAF packages as part of a 1 in 1 survey to a similar magnitude limit

(Parker, 1995). Also, A. Broadbent reduced the first 12 fields observed (with the FLAIR-I system) in the $\delta = -30°$ strip using the FIGARO data analysis package. The methods of reduction and measurement of redshifts are very similar for all cases and are outlined below using the IRAF package. The reduction procedures for the FLAIR system follow those described by Holman & Drinkwater (1994) :

(i) The bias frames were first eyeballed using the **display** task and then had their mean and standard deviation measured with the **imstat** task. Any frames which appeared out of the ordinary were rejected and the remaining ones were combined using the **zerocombine** task in the **imred.ccdred** package with a min/max rejection algorithm.

(ii) The flat field frames were eyeballed and their mean and standard deviation measured. Any strange frames were rejected and the rest combined using the **flatcombine** task in the **imred.ccdred** package with an average sigma clipping rejection algorithm. This algorithm essentally estimates a standard deviation at each pixel using the input frames and rejects according to if each individual pixel is above or below the mean with a certain threshold, $\pm 4\sigma$ was used. Dome flats and twilight-sky flats were kept separate.

(iii) The combined flat frames, the arc frames and the object frames were all "processed", namely de-biased, overscan corrected and trimmed using the **ccdproc** task in the **imred.ccdred** package. Flat fielding was done at a later stage.

(iv) The arc frames were eyeballed and blinked with one another to check that there was no shift in the arc lines before and after the object field was observed. In the vast majority of cases no shift was seen (at the < 1 pixel level). However, if one was detected then the frames which gave the night sky lines at the correct wavelengths were used (see (vi) for wavelength calibrations). The Hg-Cd and Ne frames were separately combined using the **combine** task in the **imred.ccdred** package with an average sigma clipping ($\pm 4\sigma$) rejection algorithm. The resulting two frames were then added with the **imarith** task to produce a final arc frame containing ~ 20 emission lines of various strengths.

(v) The object frames were eyeballed and their mean and standard deviation measured. Any strange frames were rejected and the rest were combined using the **combine** task in the **imred.ccdred** package with a CCD clipping rejection algorithm. This algorithm uses the gain and readout noise of the CCD to reject pixels above or below the mean with a certain threshold, $\pm 5\sigma$ was used. Obviously the object frames are very important and as few as possible are rejected. While cosmic rays are effectively removed by this process, glitches and other defects are not. The easiest way of removing these defects was to set the pixels in the region equal to a negative value (-1000 was used) and then combine as above. The CCD clipping rejection algorithm then rejects these negative pixels and scales up the remaining pixels to the correct mean.

(vi) Spectra were extracted from the combined object frame using the **dohydra** task in the **imred.hydra** package. This is a multi-task procedure which automatically finds the fibre aperatures on the CCD. It then extracts and flat

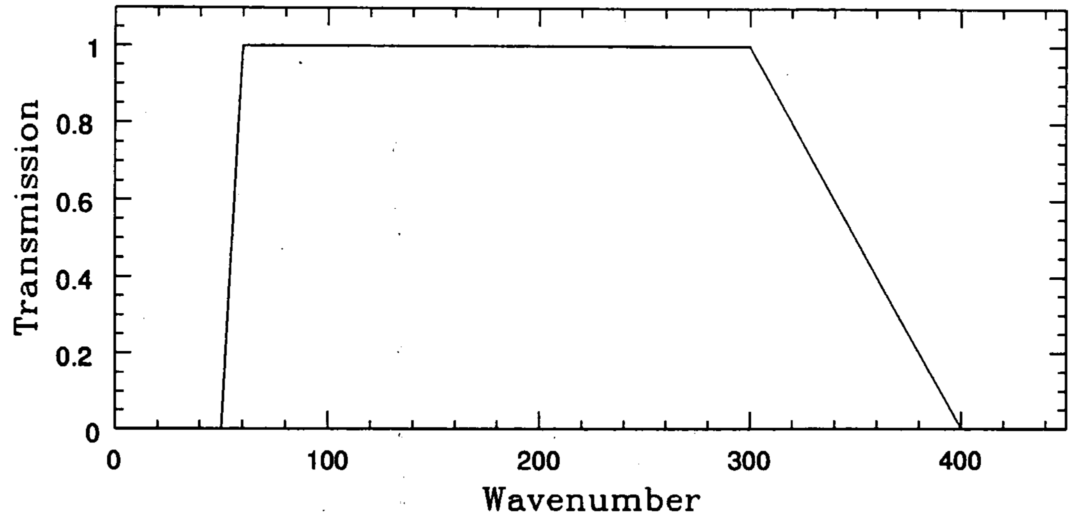

Figure 2.2: Schematic view of the ramp filter used in the cross-correlation of the power spectrum of the continuum subtracted spectra.

fields the spectra using these aperatures and the appropriate flat field frame. The arc frames were calibrated in a semi-automated way using input line lists of the wavelengths of the Hg, Cd and Ne emission lines with the user finding the first few points before a low order polynomial fit was done to ~ 15 of the strongest lines in the region 4000-7500Å. The object spectra are then wavelength calibrated using this fit. The sky spectra are then combined and subtracted from the object spectra. All of the above procedures were carefully monitored at every stage by the user and any mistakes made by the automated process were corrected. The results of this task are a set of wavelength calibrated, sky subtracted, object spectra.

(vii) Any remaining sky lines were removed from the spectra by hand and then cross-correlated using the methods of Tonry & Davis (1979) with the template spectra using the **fxcor** task in the **rv** package. The template spectra were of galaxies observed using the FLAIR system and reduced with the above procedures. These templates had their redshift measured by hand from emission & absorption lines and also had known redshifts from the literature (see section 2.6.2 for more details). The templates were good quality specta with high signal to noise and generally had many emission/absorption features (the emission lines were removed by hand before cross-correlation). As the templates came from the FLAIR spectra themselves their number increased as the data reduction proceeded and between 10–40 templates were used for each field. The cross-correlation procedure starts by continuum subtracting the spectra and then Fourier transforming (and squaring) the results. This power spectrum is then filtered by a ramp function, schematically shown in figure 2.2. This process filters away small scale noise and any large scale features left behind by the continuum subtraction process. The resulting filtered power spectrum is then cross-correlated with the templates which have undergone the same procedure and an estimated object redshift (with respect to the template) is produced as well as the Tonry & Davis (1979) r-factor.

(viii) These cross-correlated redshifts are then corrected to produce a radial velocity with respect to the local (observer) frame. Consider a template of known radial velocity with respect to the local frame, $v_{1/0}$, and a galaxy of estimated radial velocity with respect to the template frame, $v_{2/1}$, but unknown radial velocity with respect to the local frame, $v_{2/0}$. Using the definition of redshift (eg. Peebles, 1993) and its relation to the radial recession velocity, $v = cz = (\lambda_o - \lambda_e)/\lambda_e$, where c is the speed of light ($\sim 3 \times 10^5$ kms^{-1}) and λ_o, λ_e are the observed and emitted wavelengths of the line, respectively, gives

$$\frac{v_{1/0}}{c} = \frac{\lambda_1 - \lambda_0}{\lambda_0}, \tag{2.1}$$

$$\frac{v_{2/1}}{c} = \frac{\lambda_2 - \lambda_1}{\lambda_1}, \tag{2.2}$$

$$\frac{v_{2/0}}{c} = \frac{\lambda_2 - \lambda_0}{\lambda_0}. \tag{2.3}$$

λ_1 can be eliminated from equations 2.1 and 2.2 to give the radial velocity of the galaxy with respect to the local frame

$$\frac{v_{2/0}}{c} = \frac{v_{1/0} + v_{2/1} + \frac{v_{1/0} \cdot v_{2/1}}{c}}{c}. \tag{2.4}$$

A heliocentric correction is not carried out, analysis of the measured redshifts shows that this correction is not significant and therefore was not necessary, see section 2.6.2. All of the wavelength calibrated, sky subtracted, object spectra are then eyeballed and any emission lines measured. Also, any absorption features implied from the cross-correlation process were confirmed by eye. It was found that a Tonry & Davis (1979) r-factor > 4 had very believable redshifts, $r \sim$ 3-4 produced reliable redshifts $\sim 50\%$ of the time, while for $r < 3$ the redshifts could not really be trusted. The poor efficiency of the FLAIR-II CCD in the blue region of the spectrum ($<$ 5000Å) means that it is difficult to get reliable redshifts using the Calcium H & K (3968Å & 3934Å) absorption lines, this is unfortunate given that these are probably the most commonly observed lines in galaxies. Therefore the absorption lines that were mainly used were the Mg band (5175Å), Na (5893Å) and occasionally the G band (4304Å). The most common emission lines seen were H_β (4861Å), OIII (4959Å & 5007Å), H_α (6563Å) and occasionally SII (6724Å). The author had the final choice whether to believe the measured redshift or not and was quite stringent in his decisions.

2.6 The Redshift Data

2.6.1 The Durham/UKST Galaxy Redshift Catalogue

The Durham/UKST Galaxy Redshift Catalogue is formally presented in appendix A. In this appendix, table A.1 gives the UKST field number, the (α,δ) coordinates (1950), the EDSGC b_J apparent magnitude (after the zero-point correction of section 2.3) and the measured radial velocity (from the FLAIR observations) of all of the galaxies in the Durham/UKST survey. Published redshifts were found in the literature (mainly from the Southern Sky Redshift Survey of da Costa *et al.* 1991 and the previous Durham surveys of Peterson *et al.* 1986 and Metcalfe *et al.* 1989) for $\sim$ 200 galaxies in the Durham/UKST survey. Of these literature redshifts approximately three-quarters also had reliable redshifts measured from the FLAIR observations and comparisons are shown in section 2.6.2. That leaves a total of $\sim$ 50 which are presented here which were not actually measured by FLAIR. When there were not enough galaxies to fill all the fibres (to $b_J = 17.5$) other objects from the original 1 in 1 list were observed. These extra objects were reduced using the methods of section 2.5 and provided $>$ 100 new galaxy redshifts. These are not presented here because they were randomly observed and hence do not have the same well defined selection criteria as the magnitude limited sample.

2.6.2 Accuracy of the Measured Redshifts

The aims of this survey are to investigate the structure and dynamics of the Universe on a large range of scales from 1 to $100h^{-1}$Mpc. Therefore, to be successful in its goals, it is necessary to have accurate radial velocity estimates of the redshifts in this survey. It was shown by Watson *et al.* (1991), also see Hale-Sutton (1990), that the FLAIR-I system (using the observational procedures, integration times and reduction techniques of sections 2.4 and 2.5) could produce reliable redshifts which were accurate to ± 150 kms^{-1} for $b_J \simeq 17$ galaxies. Using the $\sim$ 150 radial velocities of galaxies which had reliable measurements from FLAIR (mainly the FLAIR-II system) and also published values in the literature, a mean offset of $\langle \Delta v \rangle = -10$ kms^{-1} and a standard deviation of $\sigma = 136$ kms^{-1} was calculated. Figure 2.3 shows a plot of these differences as a function of apparent magnitude, b_J. The solid line is the mean radial velocity offset and the dotted lines denote the 1σ spread about this value. There appears to be no systematic trend of increasing scatter with magnitude and the radial velocity zero-point is negligible compared to the scatter seen, hence no heliocentric correction is made.

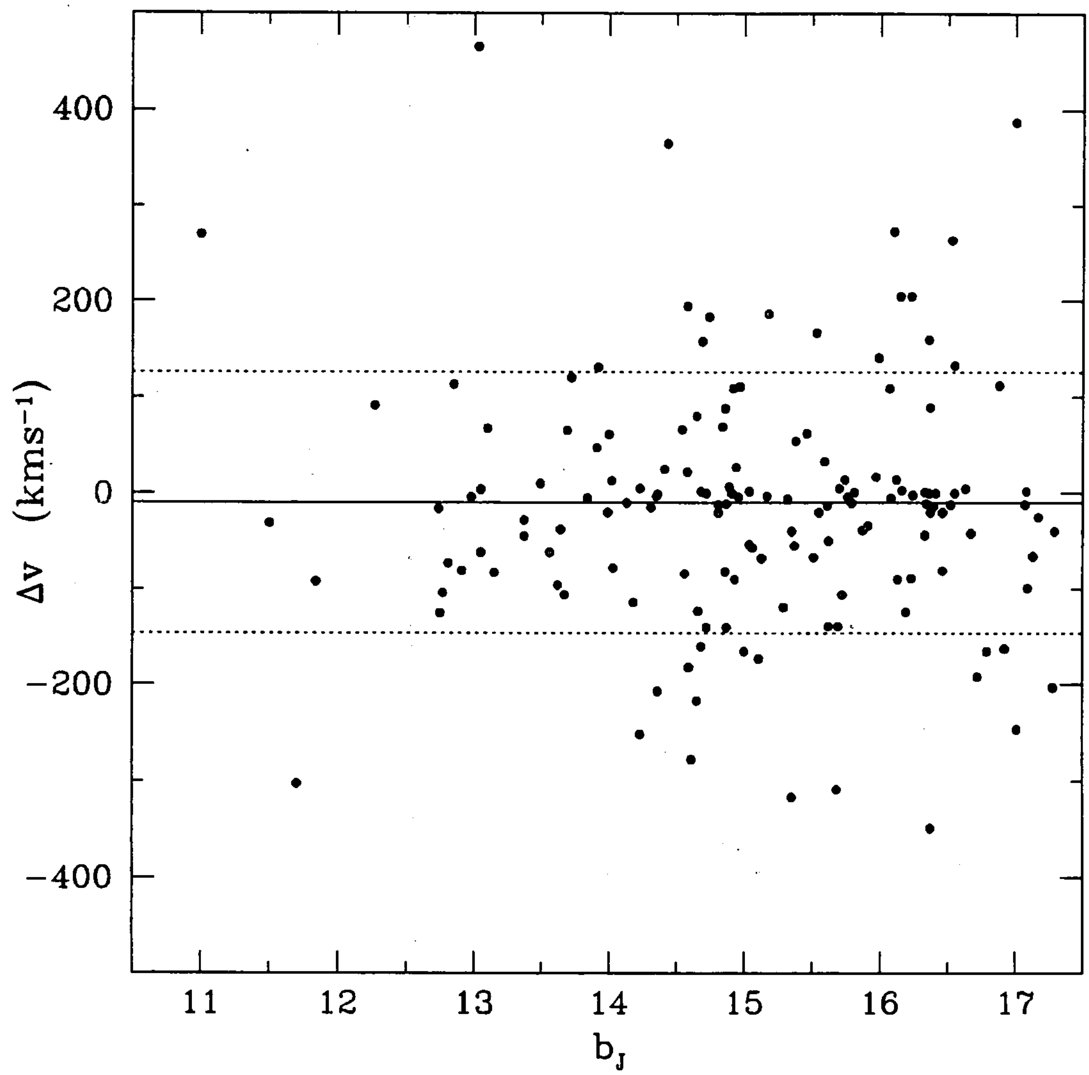

Figure 2.3: A comparison of published galaxy radial velocities with those measured by the FLAIR system for the Durham/UKST survey.

Sample Name	n_z	Mean Completeness (%)	s.d. (%)	Mean m_{lim}	s.d.
16.75	1639	74.5	15.9	16.75	–
best	2055	75.0	11.1	16.86	0.25
all	2501	59.1	17.7	17.23	0.17

Table 2.2: Completeness and magnitude limit statistics for the three samples.

2.7 Field Completeness

The completeness of a given field is defined as follows. Let n_{tot} be the total number of galaxies to a given magnitude limit, m_{lim}, from the original 1 in 3 target list (selected from the EDSGC). Let n_{unobs} be the number of galaxies from this list which were not observed. Let n_{miss} be the number of galaxies which were observed but did not produce a reliable redshift (for whatever reason). Therefore, the number of (reliable) measured redshifts is $n_z = n_{tot} - (n_{unobs} + n_{miss})$. The completeness of the field is simply the number of measured redshifts divided by the maximum number of redshifts it was possible to measure, namely

$$\text{completeness} = \frac{n_{tot} - (n_{unobs} + n_{miss})}{n_{tot}}. \tag{2.5}$$

The completeness of each field is given in appendix B. Three magnitude limits are shown, a uniform limit of $b_J = 16.75$ (table B.1), a "best" limit (table B.2) which was chosen by the author as a compromise between having a faint magnitude limit in each field and keeping the completeness levels quite high ($> 60\%$) and an "all" limit (table B.3) which simply included every measured redshift in the 1 in 3 catalogue. Table 2.2 gives a condensed version of these tables. It is seen that the "best" sample is $\sim 75\%$ complete to $b_J \simeq 16.9$ and contains over 2000 redshifts. This sample will be almost exclusively used in the analysis of the Durham/UKST survey. It is worth noting that the previous Durham surveys mentioned in section 2.6.1 contain ~ 500 redshifts in total, scattered randomly over the sky. Therefore this new survey represents a significant 4-5 increase in the numbers available, with a similar increase seen in the volume sampled.

2.8 Pictures of the Survey

Figures 2.4, 2.5, 2.6 and 2.7 show the redshift-cone plots of all the galaxies in the Durham/UKST survey for four constant declination slices. In these figures each dot is supposed to represent a galaxy. The slices are centered on $\delta = -25°$, $-30°$, $-35°$ and $-40°$, respectively and each slice spans 5° in the δ direction and $\sim 75°$ in the α direction. The depth of this survey is similar to that of the APM-Stromlo survey of Loveday *et al.* (1992b), is twice that of the CFA2 survey of Huchra *et al.* (1995) and half that of the Las Campanas survey of Shectman *et al.* (1995).

These plots of the Durham/UKST survey show the wealth of structure in the galaxy distribution, from clusters to filaments and voids. In fact, this survey gives the striking impression that the galaxy distribution is "cellular" or "bubble-like" on 5000-10000 kms^{-1} scales. The most noticeable structure in the survey is the low density region lying between 0 and 9000 kms^{-1} surrounded by long "walls" of galaxies. This structure is present in the three most southerly slices and has previously been referred to as the Sculptor Void (Fairall & Jones, 1988 and da Costa *et al.* 1991). In the most northerly slice ($\delta = -25°$) there is evidence for the top of this structure and that it is indeed a "cell".

2.9 The Number-Distance Histogram

Figure 2.8 shows the histogram of galaxy number with comoving distance, $n(r)$, in the Durham/UKST survey for the "best" sample of section 2.7. The comoving distances, r, have been calculated from the redshifts, z, assuming a $q_0 = \frac{1}{2}$, $\Lambda = 0$ cosmology and use the relation

$$r(z) = \left(\frac{2c}{H_0}\right)\left[1 - \frac{1}{\sqrt{1+z}}\right], \tag{2.6}$$

where $H_0 = 100h$ kms^{-1}Mpc^{-1} is the Hubble Constant. Equation 2.6 reduces to the familiar Hubble law in the case of small redshift ($z \ll 1$)

$$r \simeq \frac{cz}{H_0}. \tag{2.7}$$

In figure 2.8 the dashed curve shows how a random and homogeneous distribution would appear given the angular/radial selection functions and sampling rate of this "best" sample. The Durham/UKST survey $n(r)$ distribution has several large peaks. In particular there are two strong peaks at ~ 90 and $\sim 170h^{-1}$Mpc signifying "walls" in the galaxy distribution. There is possible evidence for a third such feature at $\sim 270h^{-1}$Mpc. However, at least one of these peaks does not follow the $128h^{-1}$Mpc periodic pattern previously claimed by the Broadhurst *et al.* (1990) pencil-beam survey along the North-South Galactic Pole axis which intersects this survey at $\sim$ 0^h54^m, $-27.5°$, crossing the nearer and further Sculptor superclusters. Also, recent analysis of the Las Campanas redshift survey by Landy *et al.* (1996) with the 2-D power spectrum has shown an excess of power in the $\sim 100h^{-1}$Mpc region, although at a lower level of significance than Broadhurst *et al.* (1990). The arrows indicate where these $128h^{-1}$Mpc periodic "spikes" in the galaxy distribution should appear. In this larger angle survey the galaxy distribution is clearly more complex than any simple periodic pattern. A χ^2 test is applied to the binned $n(r)$ distribution to test the significance of these peaks above the random and homogeneous distribution given by the dashed curve in figure 2.8. A χ^2 of ~ 382 is calculated for 78 degrees of freedom, this has a formal probability of $< 1 \times 10^{-40}$! Therefore, even in such a deep and wide-angled survey as this one, it appears that a fair sample of the Universe has yet to be reached.

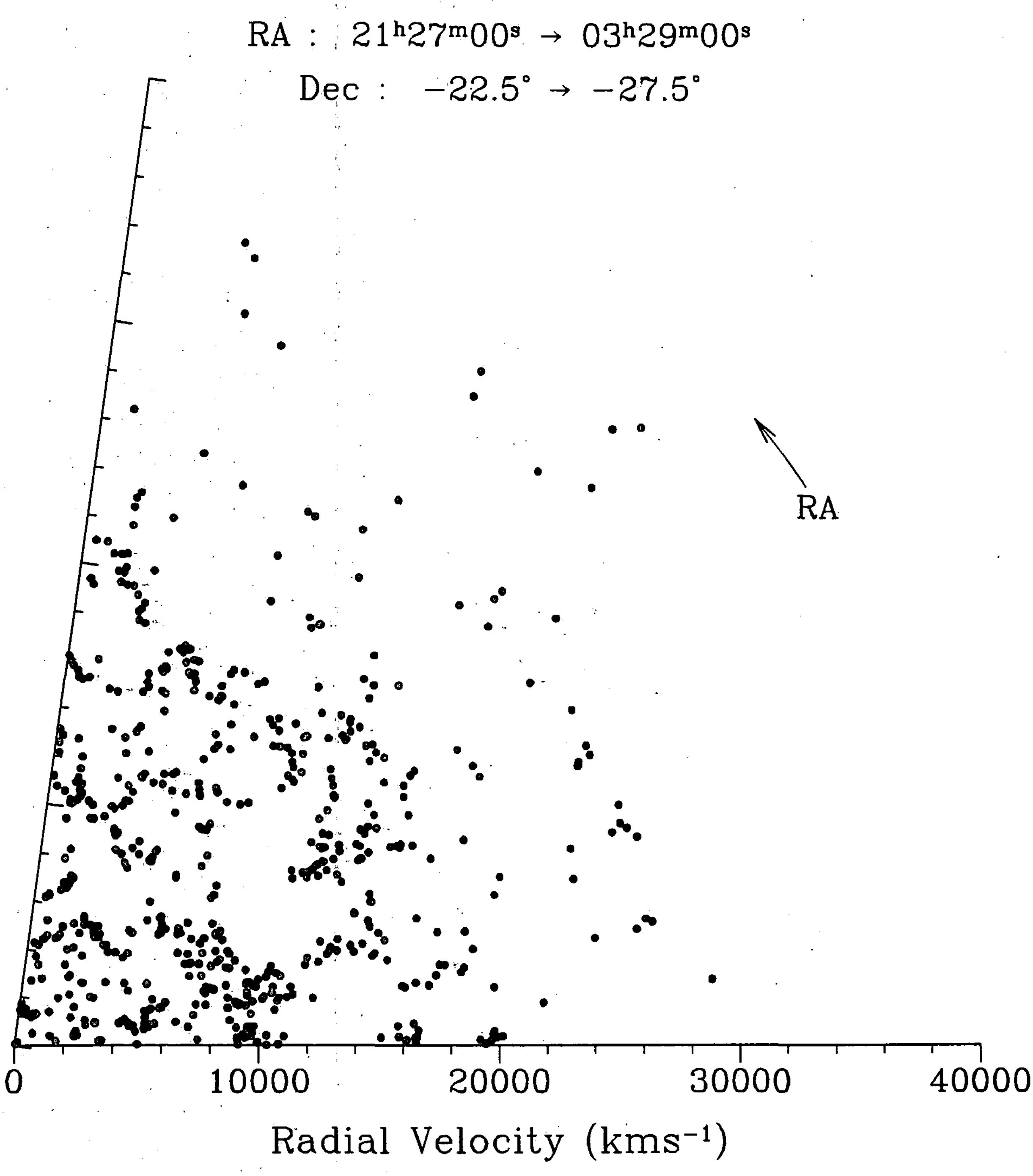

Figure 2.4: Radial velocity (cz) vs. RA (α) for the $\delta = -25°$ slice.

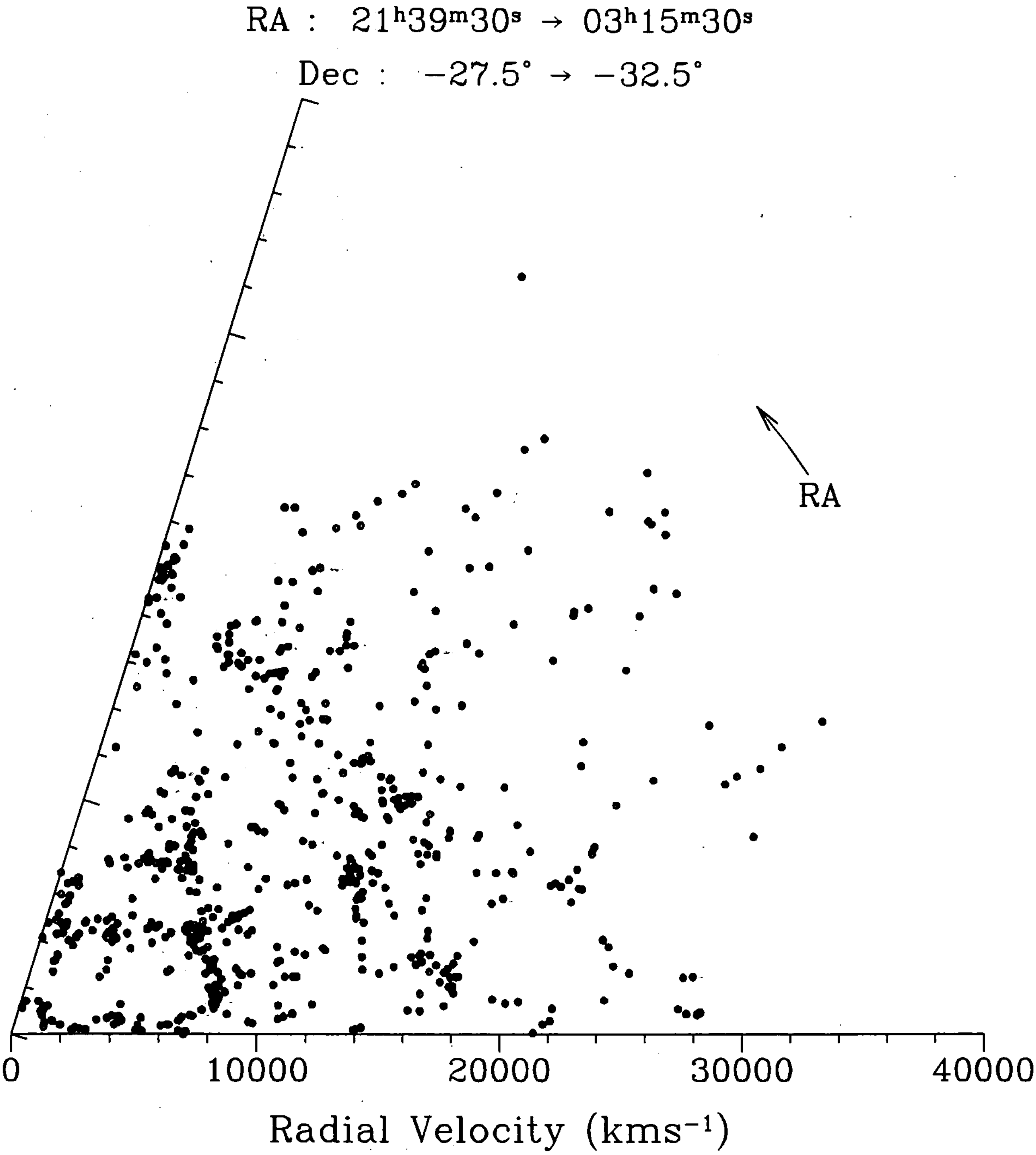

Figure 2.5: Radial velocity (cz) vs. RA (α) for the $\delta = -30°$ slice.

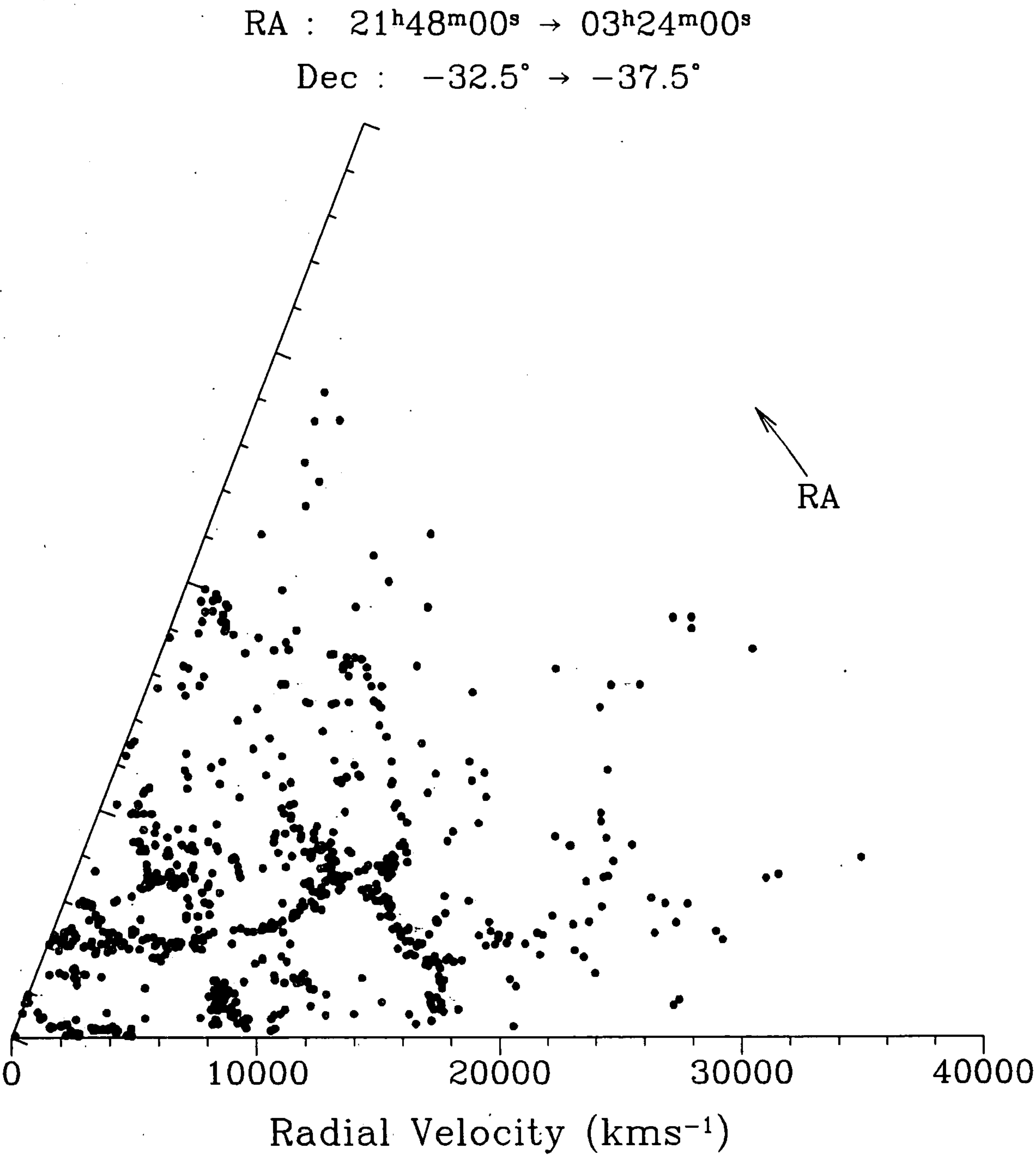

Figure 2.6: Radial velocity (cz) vs. RA (α) for the $\delta = -35°$ slice.

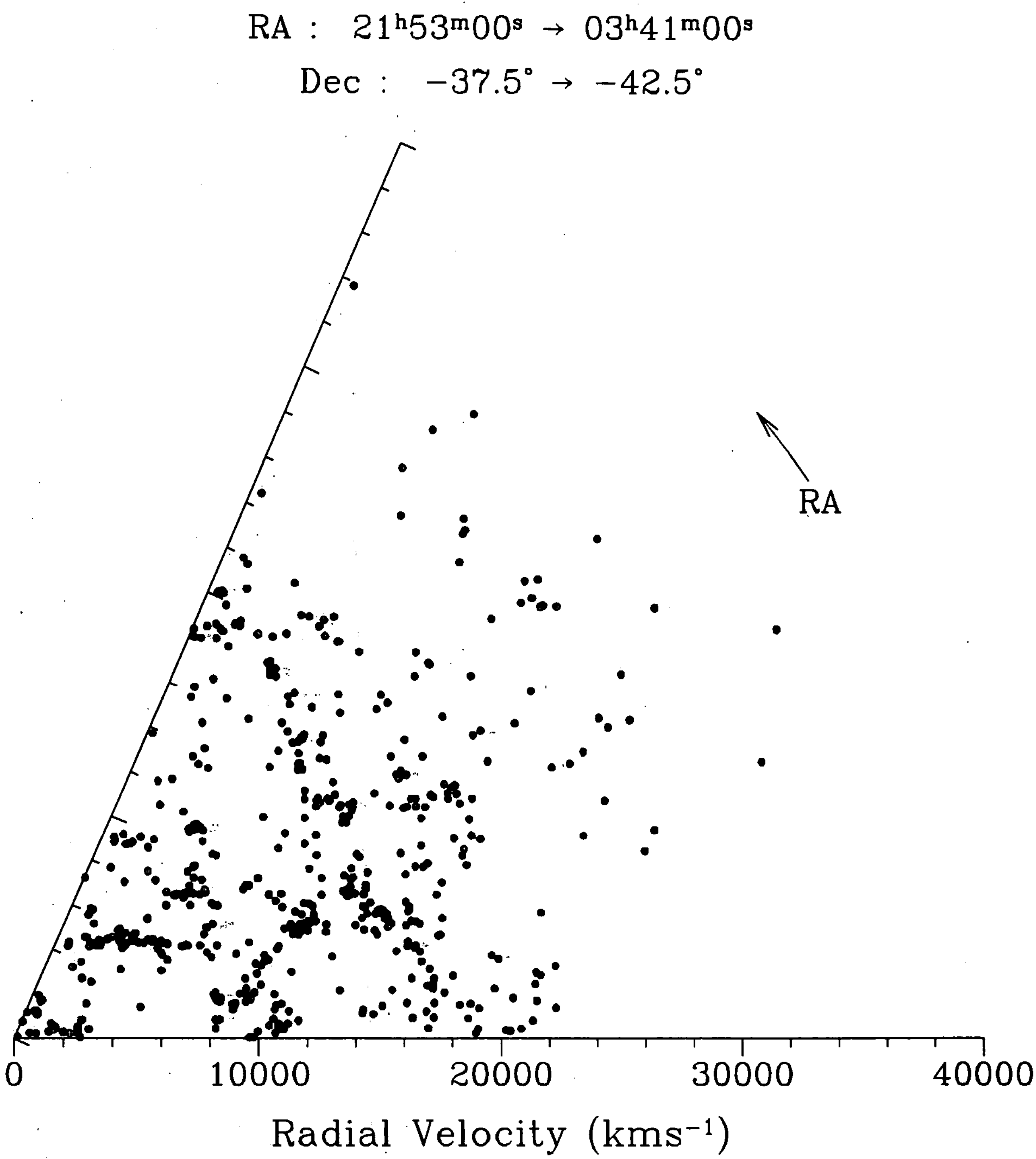

Figure 2.7: Radial velocity (cz) vs. RA (α) for the $\delta = -40°$ slice.

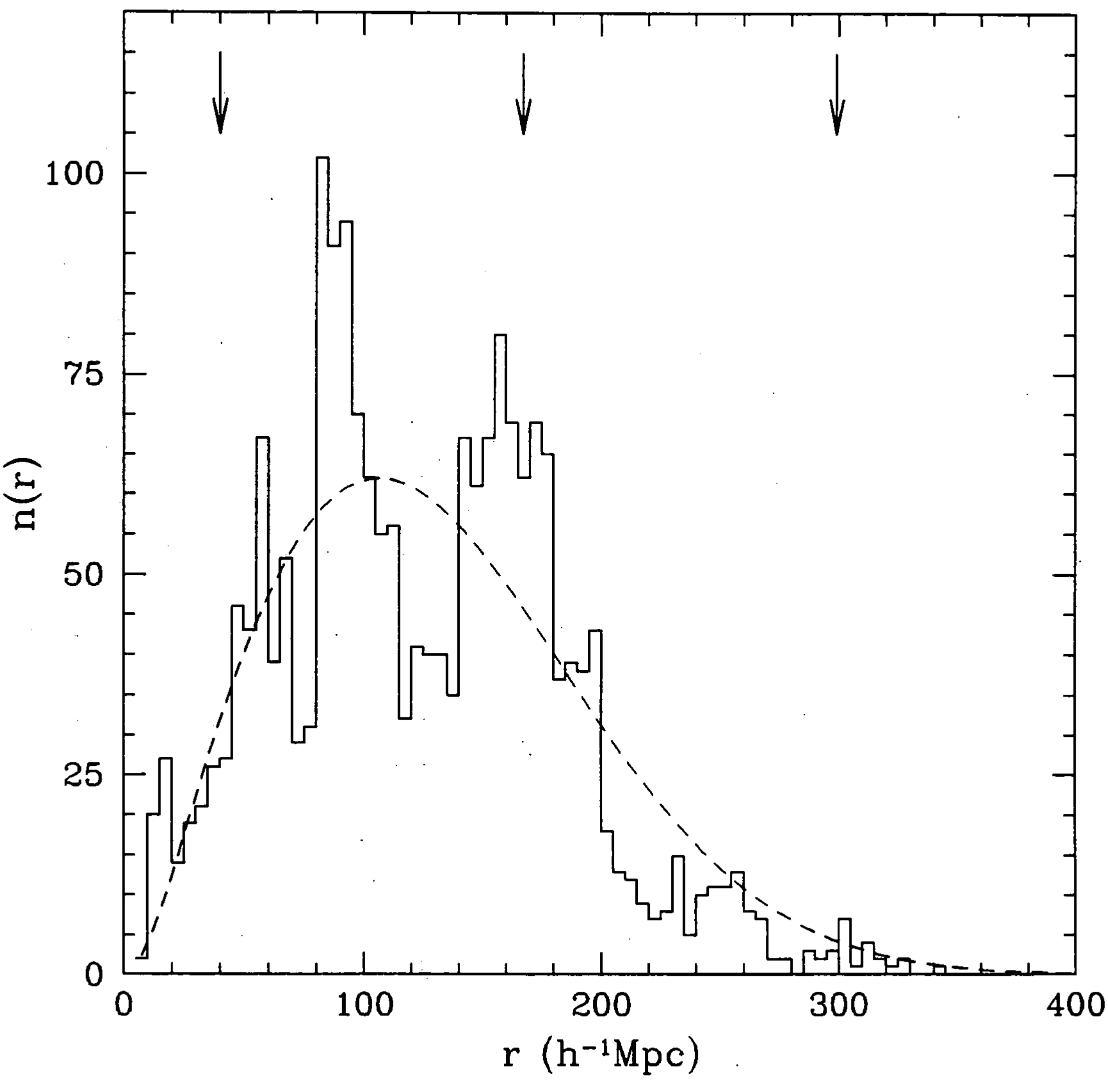

Figure 2.8: The Durham/UKST survey $n(r)$ distribution for the "best" sample.

2.10 Conclusions

The Durham/UKST Galaxy Redshift Survey was constructed from the 2-D parent EDSGC, it was observed using the FLAIR system on the UKST in a 4 year period. A small zero-point photometry correction is applied and the measured redshifts are shown to be accurate to ± 150 kms^{-1}. The "best" magnitude limited sample is $\sim 75\%$ complete to $b_J \simeq 16.9$ and this will be used in the later analysis of the survey. The redshift-cone plots of the Durham/UKST survey itself give a visual impression that the galaxy distribution is "cellular" on scales of 50-100h^{-1}Mpc with the Sculptor cell being particularly prominent in this region of the sky. The galaxy number-distance histogram shows several large peaks some of which agree with the previously seen "spikes" in the galaxy distribution in this region of the sky. A χ^2 test shows that this observed histogram is not consistent with a random and homogeneous distribution. Therefore, the Durham/UKST survey is probably not yet sampling a fair region of the Universe.

Chapter 3

The Optical Galaxy Luminosity Function

3.1 Introduction

In this chapter the optical galaxy luminosity function is estimated from the Durham/UKST galaxy redshift survey. The luminosity function is one of the most basic and fundamentally important quantities in observational cosmology. Indeed, it is essential in the determination of the radial selection function (which is used in galaxy clustering statistics, eg. Efstathiou, 1988) and also for the proper interpretation of the observed galaxy number count data (in the comparison with number count models, eg. Metcalfe *et al* 1995b). In fact there is currently much debate (eg. Ellis *et al.* 1995, Lilly *et al.* 1995) regarding the evolution (or not) of the luminosity function at high redshifts and the resulting effect on the interpretation of the measured galaxy number-magnitude counts. While the Durham/UKST survey is not deep enough to begin to answer the question of evolution it can provide a determination of the local luminosity function and in particular the faint end slope which is needed when attempting to model these number counts to fainter apparent magnitudes.

The format of the chapter is as follows. The standard methods of luminosity function estimation, error analysis and normalisation are briefly reviewed. The parametric and non-parametric forms of the luminosity function (as calculated from the Durham/UKST survey) are then presented followed by their normalisation. Methods of radial density estimation are then briefly reviewed and the results from the Durham/UKST survey presented. This new estimate of the luminosity function is then compared with that from other galaxy redshift surveys. The chapter ends with the main conclusions obtained from this analysis of the Durham/UKST survey.

It is obvious that the luminosity function is a whole research topic in itself and it is important to state that this chapter is not intended to be a complete review or analysis of the luminosity function whatsoever.

3.2 Estimating the Luminosity Function

The galaxy luminosity function, $\phi(L)$, is the number of galaxies per unit volume with a given absolute luminosity L (or magnitude M)

$$dn(L) = \phi(L)dL, \tag{3.1}$$

where $dn(L)$ is the number density of galaxies in the range $[L, L + dL]$. It would be expected that a general luminosity function would be a much more complicated function than this, depending on pass-band of selection, local environment, galaxy morphology etc. However, one might hope that on specification of a given pass-band (in this case the optical) equation 3.1 will become a reasonably good approximation.

3.2.1 Review of the Methods

One of the simplest estimators of $\phi(L)$ is the "$1/V_{max}$" method (Schmidt, 1968)

$$\phi(L)dL = \sum_i \frac{1}{V_{max}(L_i)}, \tag{3.2}$$

where $V_{max}(L_i)$ is the maximum volume (derived from the survey's physical limits) that the galaxy of luminosity L_i could still be seen in (given the apparent magnitude limits of the survey) and the sum extends over all galaxies in the luminosity interval $[L, L+dL]$. This equation will only give an unbiased estimate of $\phi(L)$ if the inhomogeneities of the galaxy distribution in the survey can be neglected. Unfortunately, this is not the case and galaxies are seen to be clustered. It is easy to imagine how a nearby excess of clustering will bias this estimator, in this case shallow samples will be over-represented with respect to distant ones, hence there will be an excess of intrinsically faint galaxies and $\phi(L)$ will be too steep at the faint end. For future reference this estimator will be called the VMAX method.

Other methods of determination have concentrated on maximum likelihood techniques. To overcome the above problems with clustering they have been constructed in a density independent way by decomposing the luminosity function into luminosity dependent and density dependent parts. These methods can in turn be split into two types, parametric and non-parametric.

The parametric estimators assume a given functional form of $\phi(L)$ for insertion into the likelihood formula, one such method is now described :

(i) Historically it has been common to use a "Schechter function" (Schechter, 1976) to describe $\phi(L)$. The Schechter function has three parameters, a normalisation ϕ^*, a faint end slope α, and a characteristic luminosity L^* (or equivalently absolute magnitude M^*)

$$\phi_S(L)dL = \phi^* \left(\frac{L}{L^*}\right)^\alpha \exp\left(-\frac{L}{L^*}\right) d\left(\frac{L}{L^*}\right). \tag{3.3}$$

One then forms a likelihood, $\mathcal{L}$, based on the probability of seeing a galaxy of luminosity L_i at redshift z_i in the survey

$$p_i \propto \phi(L_i) \Big/ \int_{L_{min(z_i)}}^{\infty} \phi(L) dL \,, \tag{3.4}$$

$$\mathcal{L} = \prod_{i=1}^{N} p_i, \tag{3.5}$$

where the product extends over all of the N galaxies in the survey and $L_{min}(z_i)$ is the minimum absolute luminosity that a galaxy at redshift z_i could have and still be included in the survey. The best estimate of $\phi(L)$ is then given when $\mathcal{L}$ (or equivalently $\ln \mathcal{L}$) is maximised with respect to the parameters of this assumed functional form (Sandage *et al.* 1979). One could use standard differentiation techniques to determine this maximum but in practise it is easier to estimate the maximum by probing the (α, L^*) space of likelihoods through direct calculation of

$$\ln \mathcal{L} = \alpha \sum_{i=1}^{N} \ln L_i - (\alpha+1) N \ln L^* - \sum_{i=1}^{N} \frac{L_i}{L^*} - \sum_{i=1}^{N} \ln \Gamma[\alpha+1, L_{min(z_i)}/L^*] + \text{const.}. \tag{3.6}$$

Obviously, one does not have to use a Schechter function and there is freedom to choose other parametric forms which may provide a better fit. Indeed, Efstathiou *et al.* (1988a) choose to do this by considering the effects of random scatter in the measured magnitudes. They approximate these errors by convolving the pure Schechter function, ϕ_S, with a gaussian distribution of zero mean and σ_m rms

$$\phi_C(M) = \frac{1}{\sqrt{2\pi}\sigma_m} \int_{-\infty}^{\infty} \phi_S(M') \exp\left[-\frac{1}{2\sigma_m^2}(M'-M)^2\right] dM'. \tag{3.7}$$

To evaluate the convolution one needs a value of σ_m and Metcalfe *et al.* (1995a) have made a best estimate of $\sigma_m = 0.22$ for COSMOS vs CCD magnitudes.

For future reference this estimator will be called the STY method.

The non-parametric estimators assume that $\phi(L)$ can be written as a series of constant steps across given luminosity intervals, two such methods are now described :

(i) Bean (1983, based on a private communication with Peebles) and Choloniewski (1986) have independently proposed the following method. Consider the 2-D array of absolute magnitude, M, and distance modulus, μ. The expected number of galaxies in an absolute magnitude interval $[M_i - \frac{\Delta}{2}, M_i + \frac{\Delta}{2}]$ and a distance modulus interval $[\mu_j - \frac{\Delta}{2}, \mu_j + \frac{\Delta}{2}]$, where Δ is a constant bin size for both absolute magnitude and distance modulus, is given by

$$\langle n_{ij} \rangle = \phi_i \rho_j, \tag{3.8}$$

where ϕ_i is the luminosity function and ρ_j the number density multiplied by the volume element across the j^{th} bin and both ϕ_i and ρ_j are assumed to be constant in that bin. By binning the galaxies from the survey into this array the observed number, n_{ij}, is deduced. Assuming that Poisson statistics apply the probability that the observed number is seen is given by

$$p = \frac{\langle n_{ij}\rangle^{n_{ij}}}{n_{ij}!} \exp(-\langle n_{ij}\rangle), \tag{3.9}$$

and the likelihood product is formed

$$\mathcal{L} = \prod_i \prod_j^{i+j\leq S} \frac{(\phi_i \rho_j)^{n_{ij}}}{n_{ij}!} \exp(-\phi_i\rho_j), \tag{3.10}$$

where $S = (m_{lim} - M_0 - \mu_0)/\Delta$ (M_0 is the maximum absolute magnitude used and μ_0 is the minumum distance modulus used) and its appearance in the product is due to the fact that galaxies do not populate the whole of the (M, μ) plane because of the apparent magnitude limit. The maximisation conditions ($\frac{\partial \ln \mathcal{L}}{\partial \phi_k} = 0 = \frac{\partial \ln \mathcal{L}}{\partial \rho_k}$) produce the following coupled equations

$$\phi_k = \sum_{j=1}^{S-k} n_{kj} \bigg/ \sum_{j=1}^{S-k} \rho_j \, , \tag{3.11}$$

$$\rho_k = \sum_{i=1}^{S-k} n_{ik} \bigg/ \sum_{i=1}^{S-k} \phi_i \, . \tag{3.12}$$

A solution to these equations is found via iteration until the desired convergence is obtained by assuming an initial trial set of the ϕ_i's. For future reference this estimator will be called the PBC method.

(ii) Efstathiou *et al.* (1988a) propose a stepwise maximum likelihood method devised on the principle of the STY method but with the luminosity function as a set of N_p constant steps instead of a Schechter function

$$\phi(L) = \phi_k, \quad L \in \left[L_k - \tfrac{\Delta L}{2}, L_k + \tfrac{\Delta L}{2}\right], \quad k = 1, \ldots, N_p. \tag{3.13}$$

Using this expression in equations 3.4 and 3.5 the likelihood becomes

$$\ln \mathcal{L} = \sum_{i=1}^{N} W(L_i - L_k) \ln \phi_k - \sum_{i=1}^{N} \ln \left[\sum_{j=1}^{N_p} \phi_j \Delta L H(L_j - L_{min(z_i)})\right] + \text{const.}, \tag{3.14}$$

where the number of galaxies in the survey is again N and

$$W(x) = \begin{cases} 1 & -\frac{\Delta L}{2} \leq x \leq \frac{\Delta L}{2} \\ 0 & \text{otherwise} \end{cases}, \tag{3.15}$$

and

$$H(x) = \begin{cases} 0 & x \leq -\frac{\Delta L}{2} \\ \frac{1}{2} + \frac{x}{\Delta L} & -\frac{\Delta L}{2} \leq x \leq \frac{\Delta L}{2} \\ 1 & x \geq \frac{\Delta L}{2} \end{cases}. \tag{3.16}$$

In this case the maximisation condition ($\frac{\partial \ln \mathcal{L}}{\partial \phi_k} = 0$) produces the following equation

$$\phi_k = \frac{\sum_{i=1}^{N} W(L_i - L_k)}{\sum_{i=1}^{N} \left[\frac{\Delta L H(L_k - L_{min(z_i)})}{\sum_{j=1}^{N_p} \phi_j \Delta L H(L_j - L_{min(z_i)})} \right]}, \tag{3.17}$$

which can be solved via iteration by assuming an initial trial set of the ϕ_k's. For future reference this estimator will be called the SWML method.

It should be noted that the PBC and SWML methods are very similar. However, as the PBC method stands it does not use any bins bisected by the selection line $M + \mu = m_{lim}$. Choloniewski (1986) suggests a way around this problem by assuming that the galaxies populate each (M, μ) pixel in a homogeneous manner. In this case the likelihood in equation 3.10 should be multiplied by the following factor

$$\prod_{i}\prod_{j}^{i+j=S+1} \frac{(\phi_i \rho_j / 2)^{n_{ij}}}{n_{ij}!} \exp(-\phi_i \rho_j / 2), \tag{3.18}$$

which alters the coupled equations 3.11 and 3.12 slightly. However, Choloniewski (1986) also notes that on making this assumption the method is no longer fully non-parametric.

It is also important to note that by their very method of construction these maximum likelihood techniques cannot provide the overall normalisation, this is dealt with in section 3.2.3.

3.2.2 Review of the Error Analysis

The four estimators discussed in section 3.2.1 all have well defined error properties which will now be described.

Firstly consider the VMAX method, the error in each luminosity interval $[L, L + dL]$ is simply given by the rms

$$\Delta\phi = \left(\sum_i \frac{1}{V_{max}^2(L_i)} \right)^{\frac{1}{2}}. \tag{3.19}$$

Secondly consider the STY method, for such a maximum likelihood method the deviation of $\mathcal{L}$ from the maximum value can be used to estimate the asymptotic error properties thereby giving an ellipsoid of acceptable parameter values

$$\ln \mathcal{L} = \ln \mathcal{L}_{max} - \frac{1}{2}\chi_\beta^2(n), \tag{3.20}$$

where $\mathcal{L}_{max}$ is the maximum likelihood, n is the number of free parameters (namely two, α and L^*) and β is the required confidence level for that number of free parameters (eg. Eadie *et al.* 1971). For example, the 68% and 96% confidence levels for $n = 2$ are 2.30 and 6.00, respectively, so to determine the joint error ellipsoids one looks for the values of α and L^* which reduce the maximum likelihood solution by 1.15 and 3.00.

Thirdly consider the PBC and SWML methods, one can use the covariance matrix to estimate the asymptotic error properties of the maximum likelihood ϕ_k's (eg. Eadie *et al.* 1971)

$$\mathrm{Cov}(\phi_k) = -\left(\frac{\partial^2 \ln \mathcal{L}}{\partial \phi_l^2}\right)^{-1}_{\phi_l=\phi_k}. \tag{3.21}$$

For the PBC method this implies that the error estimates are

$$\mathrm{Var}(\phi_k) = \frac{\phi_k^2}{\sum_{j=1}^{S-k} n_{kj}}, \tag{3.22}$$

$$\mathrm{Var}(\rho_k) = \frac{\rho_k^2}{\sum_{i=1}^{S-k} n_{ik}}, \tag{3.23}$$

while for the SWML method they are

$$\mathrm{Var}(\phi_k) = \left(\sum_{i=1}^{N}\left[\frac{W(L_i - L_k)}{\phi_k^2}\right] - \sum_{i=1}^{N}\left[\frac{\Delta L H(L_k - L_{min(z_i)})}{\sum_{j=1}^{N_p}\phi_j \Delta L H(L_j - L_{min(z_i)})}\right]^2\right)^{-1}, \tag{3.24}$$

where, following Saunders *et al.* (1990), the assumption that one can neglect the off-diagonal elements (ie. the cross-derivatives) has been used.

Finally, one of the problems with the STY method is that it will always return a best fit solution regardless of the assumed parametric functional form and how good a representation of the actual luminosity function it is. Therefore, for this method it is necessary to test the goodness of fit. This can be done using the likelihood ratio test (eg. Eadie *et al.* 1971) if one assumes that the non-parametric form of the PBC or SWML methods provides a good estimate of the shape of the actual luminosity function. Specifically, let $\mathcal{L}_1$ be the likelihood calculated using the maximum likelihood solution of the given functional form and let $\mathcal{L}_2$ be the likelihood calculated from either equation 3.10 or 3.14 using the maximum likelihood solution of the ϕ_k's. Then $-2\ln\lambda$, where $\lambda = \frac{\mathcal{L}_1}{\mathcal{L}_2}$, behaves asymptotically as a χ^2 statistic with $(N_p - 1)$ degrees of freedom. However, to get an answer independent of bin size, ΔL, and number of bins, N_p, the likelihood $\mathcal{L}_1$ should be calculated from either equation 3.10 or 3.14 using a set of ϕ_k's calculated from equation 3.25 below rather than simply using the likelihood $\mathcal{L}_1$ straight from the STY method

$$\phi_k \simeq \frac{\int \phi(L) dN(L)}{\int dN(L)} \simeq \frac{\int \phi(L) L^{\frac{3}{2}} dL}{\int L^{\frac{3}{2}} dL}, \tag{3.25}$$

where the integrals in equation 3.25 are over the luminosity interval in question, $[L_k - \frac{\Delta L}{2}, L_k + \frac{\Delta L}{2}]$ (Efstathiou *et al.* 1988a).

3.2.3 Review of the Normalisation

The expected distribution of the number of galaxies as a function of redshift z (or equivalently distance r) is given by

$$n(r) = f\bar{n}\ Vol(r)\ S(r), \tag{3.26}$$

where f is the sampling rate of the survey, $\bar{n}$ is the mean spatial density of the survey, $Vol(r)$ is the volume element of the survey at a distance r and $S(r)$ is the selection function of the survey at that distance

$$S(r) = \frac{\int_{max}^{\infty} \phi(L)dL}{\int_{L_{low}}^{\infty} \phi(L)dL} = \frac{\Gamma\left(\alpha + 1, \frac{max}{L^*}\right)}{\Gamma\left(\alpha + 1, \frac{L_{low}}{L^*}\right)}, \tag{3.27}$$

where a Schechter luminosity function has been assumed, $max = \max[L_{low}, L_{min(r)}]$, L_{low} is the minimum possible absolute luminosity of a galaxy in the survey and $\Gamma(\alpha + 1, x)$ is the standard incomplete Gamma function. The mean spatial density of the survey is also related to the luminosity function by

$$\bar{n} = \int_{L_{low}}^{\infty} \phi(L)dL = \phi^* \Gamma\left(\alpha + 1, \frac{L_{low}}{L^*}\right). \tag{3.28}$$

Two methods of estimating $\bar{n}$ and ϕ^* are now described :

(i) $\bar{n}$ can be determined by a simple rearrangement of equation 3.26

$$\bar{n} = \frac{n(r)/f}{Vol(r)S(r)}, \tag{3.29}$$

and ϕ^* comes from elimination of $\bar{n}$ from equations 3.26 and 3.28

$$\phi^* = \frac{n(r)/f}{Vol(r)\Gamma\left(\alpha + 1, \frac{max}{L^*}\right)}. \tag{3.30}$$

So, if the $n(r)$ data is binned, then an estimate of $\bar{n}$ and ϕ^* is available in each bin. While it would be possible to take a mean or median of these estimates to give an overall normalisation, a better way using this method would be to take the survey as a whole giving

$$\bar{n} = \frac{\sum_r n(r)/f}{\sum_r Vol(r)S(r)}, \tag{3.31}$$

and

$$\phi^* = \frac{\sum_r n(r)/f}{\sum_r Vol(r)\Gamma\left(\alpha + 1, \frac{max}{L^*}\right)}. \tag{3.32}$$

(ii) $\bar{n}$ can be determined using an iterative scheme (Loveday *et al.* 1992b) with the estimator and weighting, w, of Davis & Huchra (1982)

$$\bar{n} = \frac{\sum_{i=1}^{N} w(r_i)/f}{\int_{r_{min}}^{r_{max}} S(r)w(r)dV}, \tag{3.33}$$

where

$$w(r) = \frac{1}{1 + 4\pi f \bar{n} J_3(r_c) S(r)} \quad , \quad J_3(r_c) = \int_0^{r_c} x^2 \xi(x) dx, \tag{3.34}$$

r_c is the scale on which J_3 converges to a maximum value and $\xi(x)$ is the 2-point correlation function of the galaxy distribution, for more information about ξ and J_3 see chapters 4, 5 and 6. ϕ^* is then determined from equation 3.28. This scheme should produce the minimum variance estimate of $\bar{n}$ if $J_3(r_c)$ converges on a scale r_c smaller than the survey (Davis & Huchra, 1982).

For both methods the variance of $\bar{n}$ is given by (Davis & Huchra, 1982)

$$\mathrm{Var}(\bar{n}) = \frac{\bar{n} \int w^2 S dV + f \bar{n}^2 \int w_1 w_2 S_1 S_2 \xi(x_{12}) dV_1 dV_2}{f \left(\int w S dV\right)^2}, \tag{3.35}$$

where $w = 1$ for the first simple estimator and $w = 1/(1 + 4\pi f \bar{n} J_3(r_c) S(r))$ for the second iterative estimator.

3.3 Results from the Durham/UKST Galaxy Redshift Survey

The brightest absolute magnitude of any galaxy seen in the survey is $M_{b_J} \sim -23$. The minimum distance an object could have a reliable redshift distance estimate for (relatively unaffected by peculiar velocities) is $5h^{-1}$Mpc, ie. $z_{low} = 1.67 \times 10^{-3}$. Using an average magnitude limit of $m_{lim} \sim 17$ these two facts imply that the faintest possible absolute magnitude that could be seen is $M_{b_J} \sim -12$ while the maximum apparent magnitude is $m \sim 6$. Note that the actual maximum apparent magnitude is probably fainter than this due to the limitations of the measuring machine itself.

3.3.1 The $\left\langle \frac{\mathbf{V}}{\mathbf{V_{max}}} \right\rangle$ Test

The volumes, V, are calculated using comoving distances, $d_{co}(z)$ (ie. $r(z)$ of equation 2.6), and also use

$$V = \frac{d\Omega}{3} d_{co}^3(z), \tag{3.36}$$

Sample	$\langle V/V_{max}\rangle$
best	0.501 ± 0.006
all	0.450 ± 0.006

Table 3.1: The $\left\langle \frac{V}{V_{max}} \right\rangle$ test for the Durham/UKST survey.

$$5 \lg d_L(z) = m - M - 25 - k_{corr}(z), \tag{3.37}$$

$$d_L(z) = (1 + z)\, d_{co}(z), \tag{3.38}$$

where $d\Omega$ is the solid steradian angle of the survey, c the velocity of light in kms^{-1}, $H_0 = 100h$ kms^{-1}Mpc^{-1} the Hubble constant, z the redshift, d_{co} the comoving distance in h^{-1}Mpc, d_L the luminosity distance in h^{-1}Mpc and k_{corr} the k-correction. A simple k-correction is used

$$k_{corr} = k_1 z + k_2 z^2, \tag{3.39}$$

where $k_1 = +3.15$ and $k_2 = -0.29$ (Broadbent, 1994).

The results of Schmidt's (1968) $\langle V/V_{max}\rangle$ test for the completeness of a survey are given in table 3.1 for the "best" and "all" magnitude limited samples described in section 2.7. The error quoted is the expected standard deviation for a random variable in the range $[0, 1]$ with a uniform probability distribution, $1/\sqrt{12N}$. Table 3.1 shows that the "best" sample does not suffer from incompleteness while the "all" sample is incomplete at a high level of significance. The "best" sample will therefore be used exclusively throughout the rest of this chapter.

3.3.2 The Parametric Shape

The STY maximum likelihood solution has been calculated for a pure Schechter function (equation 3.3) and for a convolved Schechter function (equation 3.7 with $\sigma_m = 0.22$). The maximum likelihood results of α and $M^*_{b_J}$ are shown in table 3.2 and assume $h = 1$. Figure 3.1 shows these two solutions scaled to agree at $M_{b_J} = -19.75$ (the bin containing the most galaxies) although the absolute normalisation is arbitrary at this stage. The inset of figure 3.1 shows the joint 68% error ellipsoids for these two solutions as calculated from equation 3.20. The errors quoted in table 3.2 are the 1σ error on an individual parameter and are estimated from the inset of figure 3.1.

There is reasonably good agreement between the two solutions shown in figure 3.1. It appears that the main effect of the magnitude errors on a luminosity function of this shape is to pull $\phi(M)$ down at faint magnitudes while pushing it up slightly at bright magnitudes, essentially flattening it. In order to determine which of these solutions gives the best fit to the actual luminosity function the likelihood ratio test (see section 3.2.2) has been applied. It is assumed that the shape

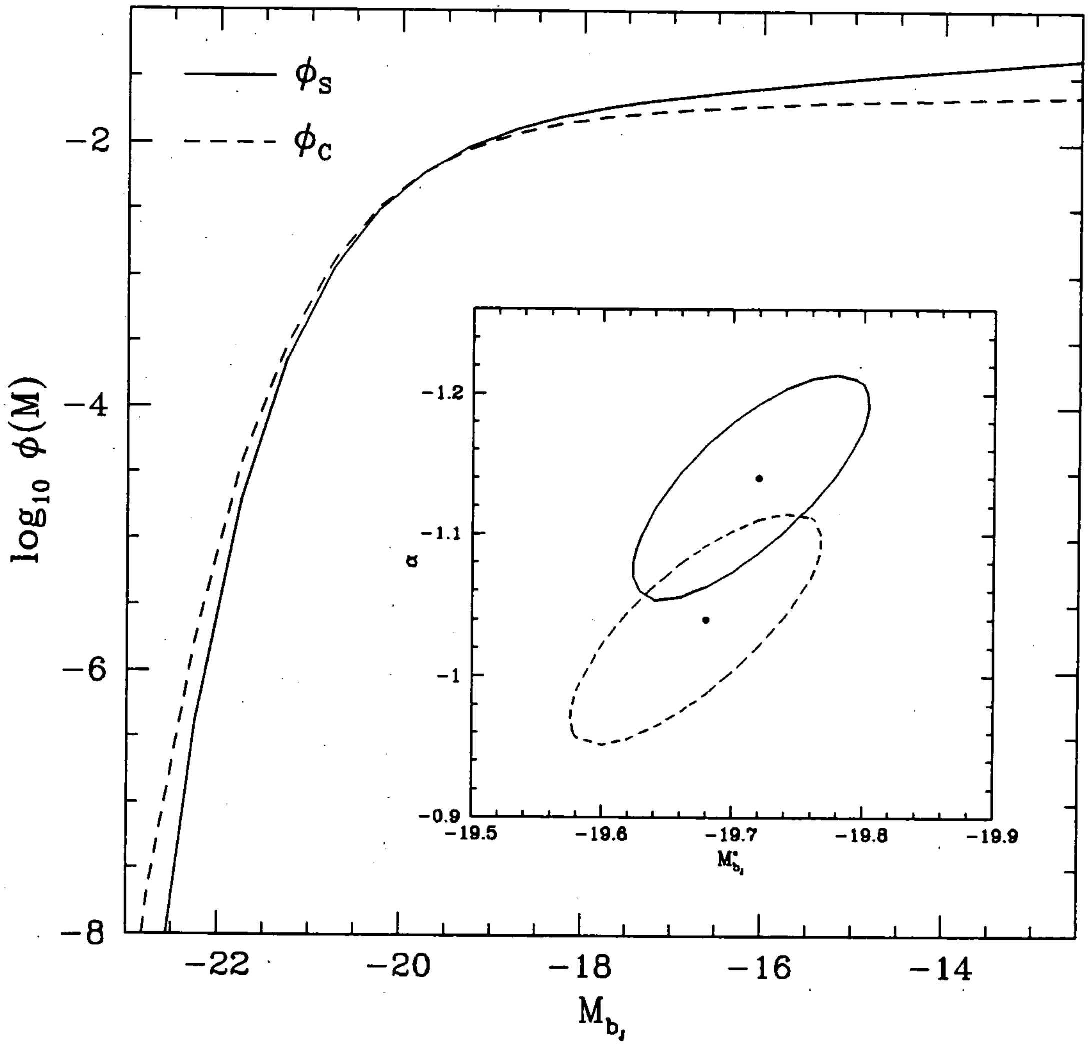

Figure 3.1: The STY maximum likelihood solution for a pure Schechter function (solid curve) and a convolved Schechter function (dashed curve). The two solutions are scaled to agree at $M_{b_J} = -19.75$ but the overall normalisation is arbitrary at this stage. The inset shows these STY likelihood results in the (M_{b_J}, α) plane, complete with the maximum likelihood solution and the joint 68% error ellipsoids on both parameters.

	ϕ_S	ϕ_C
α	-1.14 ± 0.08	-1.04 ± 0.08
$M^*_{b_J}$	-19.72 ± 0.09	-19.68 ± 0.10
χ^2	20.2	18.8
Prob.	0.16	0.22

Table 3.2: STY maximum likelihood results.

of the actual luminosity function can be approximated by the SWML estimate of section 3.3.3. The SWML data is scaled to agree at $M_{b_J} = -19.75$ and any bins in the SWML estimate containing one or fewer galaxies are ignored in the evaluation of the likelihood ratio (ie. the 2 bins at the very bright magnitudes) leaving 16 bins for the likelihood ratio test. The two χ^2's and their associated probabilities are shown in table 3.2. It can be seen that the best fit is achieved using the convolved Schechter function, although this result is marginal. In fact neither of these fits appear to be a very good match to the actual luminosity function. For the sake of simplicity the pure Schechter function is preferred.

3.3.3 The Non-parametric Shape

The VMAX, PBC and SWML estimates of the luminosity function have been calculated and are shown in figure 3.2. No change was seen in the shape of the VMAX estimate when incompleteness was accounted for (only the normalisation was altered). The PBC and SWML methods converged (to 5 *s.f.*) at every point after ~ 20 iterations. The PBC estimator incorporates those galaxies on the $M+\mu = m_{lim}$ selection line using equation 3.18. At this stage the solutions have been scaled to agree at $M_{b_J} = -19.75$ but the overall normalisation is still arbitrary. The error bars have been calculated using equations 3.19, 3.22 and 3.24. It is seen that the PBC and SWML estimates are in excellent agreement at all magnitudes, in fact they are almost identical. The VMAX estimate differs slightly at both the brightest and faintest magnitudes. The SWML and PBC estimates have a flat faint end slope, whereas the VMAX estimate produces a slightly increasing slope. This steeper VMAX faint end slope is probably due to an overdensity in the local galaxy distribution (see section 3.4.2). The best estimate of the non-parametric luminosity function comes from the PBC and SWML methods.

Figure 3.3 shows the two STY maximum likelihood curves from table 3.2 and figure 3.1 plotted against the SWML estimate from figure 3.2. They have been scaled to agree with the SWML estimate at $M_{b_J} = -19.75$ and again the absolute normalisation is arbitrary. The convolved Schechter function appears to give a good fit at the brightest and faintest magnitudes, whereas the pure Schechter function only fits within 1σ in this range. However, in the $-19.5 \leq M_{b_J} \leq -18.0$ region it is the pure Schechter function that gives the better fit although only within 3-4σ. The visual impression is that neither the pure or convolved Schechter functions give a very good fit to the exact details of the non-parametric estimates of the luminos-

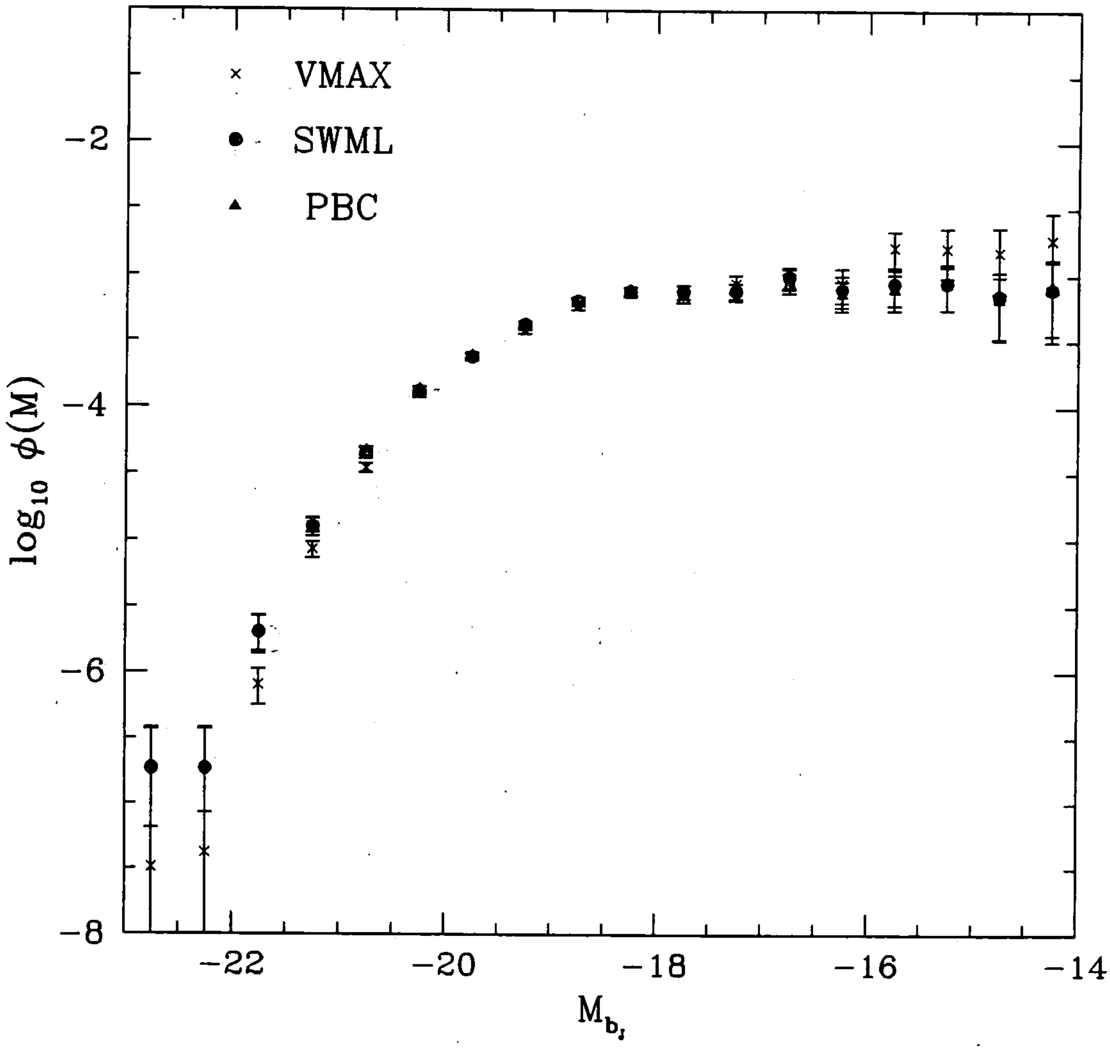

Figure 3.2: The VMAX (crosses), SWML (dots) and PBC (triangles) estimates of the non-parametric form of the galaxy luminosity function. All estimates are scaled to agree at $M_{b_J} = -19.75$ but the absolute normalisation is arbitrary.

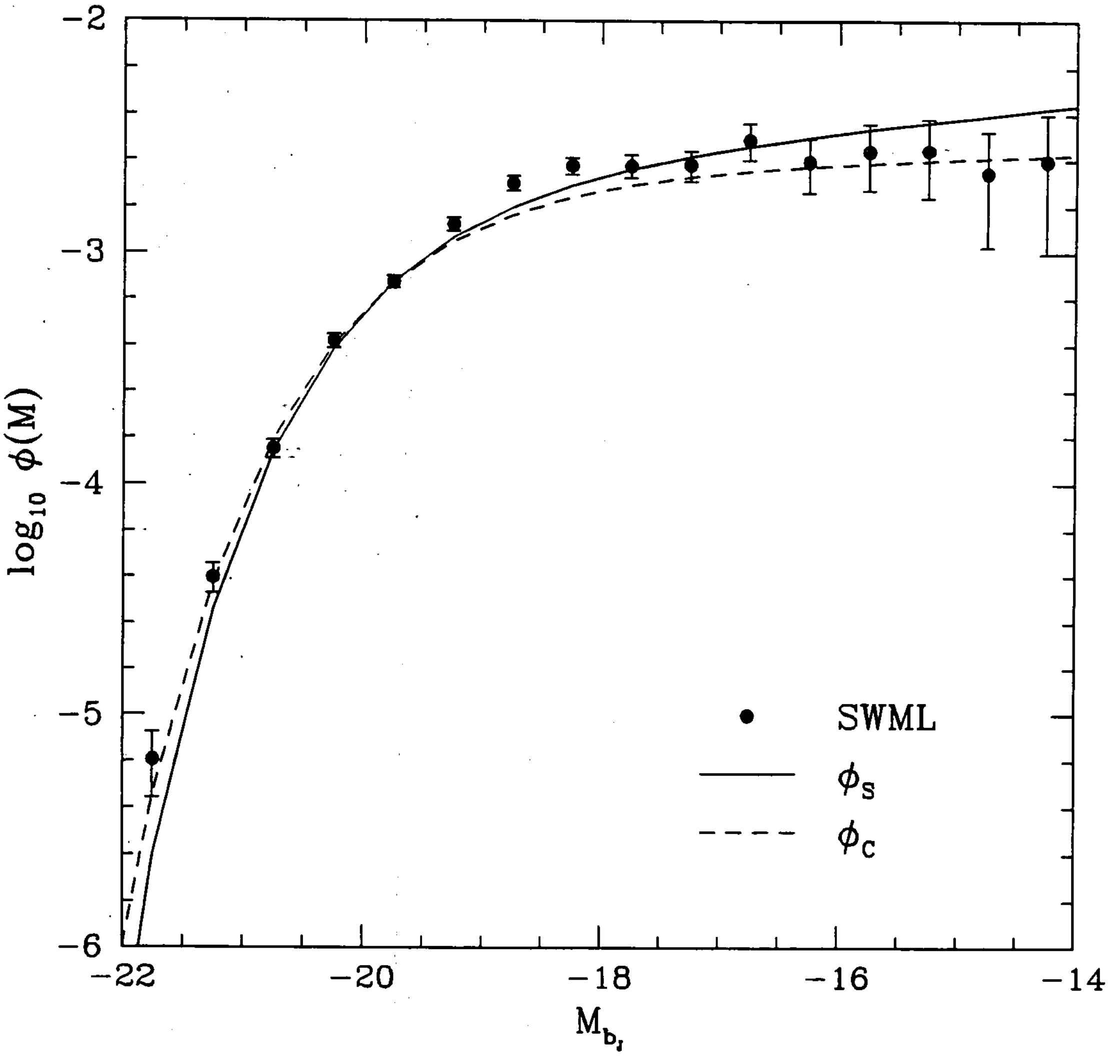

Figure 3.3: The STY maximum likelihood results scaled to agree with the SWML estimator at $M_{b_J} = -19.75$. The absolute normalisation is arbitrary.

$\bar{n}$ (h^3Mpc^{-3})	ϕ_S	ϕ_C
Simple	0.075	0.055
Iterative	0.081	0.053
ϕ^* (h^3Mpc^{-3})	ϕ_S	ϕ_C
Simple	1.12×10^{-2}	1.84×10^{-2}
Iterative	1.21×10^{-2}	1.74×10^{-2}

Table 3.3: Estimates of $\bar{n}$ and ϕ^* for pure and convolved Schechter functions.

ity function. Nevertheless, the general features and shape do agree well although figure 3.3 could be suggesting that something other than a Schechter function is needed to parametrically describe the true form of the galaxy luminosity function. These conclusions about the Schechter function agree with those of section 3.3.2.

3.3.4 The Normalisation

The results of the simple and iterative estimators for $\bar{n}$ and ϕ^* are shown in table 3.3 for the pure and convolved Schechter functions of table 3.2 using the methods described in section 3.2.3. Incompleteness has been corrected for by dividing the sum in the numerators of equations 3.31, 3.32 and 3.33 by the appropriate completeness rate of the field in question. For the iterative estimates a value of $4\pi J_3(r_c) = 5000h^{-3}\mathrm{Mpc}^3$ is used and 5 *s.f.* convergence is achieved after 5 iterations. The method is quite insensitive to the value of J_3 used as doubling or halving it makes only a 4% difference to $\bar{n}$. Using equation 3.35 the variance of $\bar{n}$ in the survey is 10% and 7% with $w = 1$ and $1/(1 + 4\pi f\bar{n}J_3(r_c)S(r))$, respectively. The uncertainty in ϕ^* produced from the errors in the Schechter parameters α and $M^*_{b_J}$ is of the order $\sim$ 15%. Combining this with the variance in $\bar{n}$ gives a total uncertainty in ϕ^* of $\sim$ 18% and 17%, respectively, for the above two weightings.

Table 3.3 shows that for a given parametric function there is little difference between the two methods of estimation. The main source of formal error in both ϕ^* and $\bar{n}$ is the uncertainty in the luminosity function parameters α and $M^*_{b_J}$. However, it is slightly worrying that the choice of parametric form leads to a $\sim$ 40% difference in ϕ^* and $\bar{n}$, especially as both parametric forms gave a similar quality of fit to the actual luminosity function. In conclusion, the best estimates for a pure Schechter function are $\bar{n} = 0.078 \pm 0.014h^3\mathrm{Mpc}^{-3}$ and $\phi^* = 1.17 \pm 0.21 \times 10^{-2}h^3\mathrm{Mpc}^{-3}$, while for a convolved Schechter function $\bar{n} = 0.054 \pm 0.009h^3\mathrm{Mpc}^{-3}$ and $\phi^* = 1.79 \pm 0.30 \times 10^{-2}h^3\mathrm{Mpc}^{-3}$.

3.4 Determining the Radial Density

3.4.1 Review of the Methods and Error Analysis

Non-parametric maximum likelihood methods for the determination of the radial density function are analogous to those proposed for the estimation of the luminosity function. Likelihoods are constructed (see section 3.2.1) which, when maximised, give the density field that best describes the observed radial galaxy distribution. Again, by construction, the normalisation is arbitrary. Two such methods are now briefly reviewed :

(i) The previously described PBC method for determining the luminosity function also gives the radial density function multiplied by the volume element as part of the iteration procedure. To evaluate the actual radial density fluctuations it is a simple matter of dividing the maximum likelihood ρ_j's from equation 3.12 by the appropriate volume, ΔV_j, of the j^{th} distance modulus bin (of constant width Δ). Asymptotic error estimates of the ρ_j's are given in equation 3.23 and it is easy to propagate this error to $\rho_j/\Delta V_j$. This estimator is again referred to as the PBC method.

(ii) Similar to the SWML method, Saunders *et al.* (1990) have proposed maximising the following likelihood to determine the radial density

$$\mathcal{L} = \prod_{i=1}^{N} \frac{\rho(z_i)}{\int_{z_{(min,i)}}^{z_{max(L_i)}} \rho(z_i) \left(\frac{dV}{dz}\right) dz}, \tag{3.40}$$

where $z_{(min,i)} = \max\left[z_{low}, z_{min(L_i)}\right]$ and $z_{max(L_i)}$ are the minimum and maximum redshifts at which a galaxy of luminosity L_i could be seen and still be included in the survey. In this case

$$\ln \mathcal{L} = \sum_{i=1}^{N} W(z_i - z_k) \ln \rho_k - \sum_{i=1}^{N} \ln \left[\sum_{j=1}^{N_p} \rho_j \Delta V_j F(z_{(min,i)}, z_j, z_{max(L_i)})\right], \tag{3.41}$$

where $W(x)$ is defined as in equation 3.15 with Δz replacing ΔL, ΔV_j is the volume of the j^{th} redshift bin (of constant width Δz) and $F(a,x,b)$ is the fraction of the volume bin at redshift x within the integral limits $[a,b]$. When written out explicitly $F(a,x,b)$ is

$$F(a,x,b) = \begin{cases} 0 & x - a \leq -\frac{\Delta z}{2} \\ \frac{\Delta V_{x-a}}{\Delta V_x} & -\frac{\Delta z}{2} \leq x - a \leq \frac{\Delta z}{2} \\ 1 & x - a \geq \frac{\Delta z}{2} \\ 1 & b - x \geq \frac{\Delta z}{2} \\ \frac{\Delta V_b}{\Delta V_x} & -\frac{\Delta z}{2} \leq b - x \leq \frac{\Delta z}{2} \\ 0 & b - x \leq -\frac{\Delta z}{2} \end{cases}. \tag{3.42}$$

The maximisation condition ($\frac{\partial \ln \mathcal{L}}{\partial \rho_k} = 0$) then produces the following equation

$$\rho_k = \frac{\sum_{i=1}^{N} W(z_i - z_k)}{\sum_{i=1}^{N} \left[\frac{\Delta V_k F(z_{(min,i)}, z_k, z_{max(L_i)})}{\sum_{j=1}^{N_p} \rho_j \Delta V_j F(z_{(min,i)}, z_j, z_{max(L_i)})} \right]}, \tag{3.43}$$

which can be solved by iteration as before. The asymptotic error estimates are given by the covariance matrix of equation 3.21 and in this case they are

$$\mathrm{Var}(\rho_k) = \left(\sum_{i=1}^{N} \left[\frac{W(z_i - z_k)}{\rho_k^2} \right] - \sum_{i=1}^{N} \left[\frac{\Delta V_k F(z_{(min,i)}, z_k, z_{max(L_i)})}{\sum_{j=1}^{N_p} \rho_j \Delta V_j F(z_{(min,i)}, z_j, z_{max(L_i)})} \right]^2 \right)^{-1} \tag{3.44}$$

This estimator is again referred to as the SWML method.

The PBC and SWML methods are quite similar. Once again the PBC method does not use any bins bisected by the selection line $M + \mu = m_{lim}$ unless the likelihood is multiplied by the factor in equation 3.18.

3.4.2 Results from the Durham/UKST Galaxy Redshift Survey

The SWML and PBC maximum likelihood estimates of the radial density function are shown in figures 3.4(a) and 3.4(b). Incompleteness is not explicitly corrected for in either method. The SWML and PBC methods converged (to 5 *s.f.*) at every point after $\sim$ 20 iterations. The PBC estimator incorporates those galaxies on the $M + \mu = m_{lim}$ selection line using equation 3.18. The error bars have been calculated using equations 3.23 and 3.44. The solutions are normalised to unity in the region $[25, 350]$ h^{-1}Mpc with an inverse error weighting. Figure 3.5 shows both estimates plotted on the same graph and the agreement between the methods is impressive out to $r \simeq 250h^{-1}$Mpc (although no formal statistical test has been attempted). For larger radial distances it becomes harder to compare the two estimates (because the PBC distance modulus bins increase in size for increasing radial distance).

These figures show that fluctuations in the observed galaxy density (of order $\sim$ 40-70%) occur on $\sim 50h^{-1}$Mpc scales. The radial size of the fluctuations are similar to those seen in the APM-Stromlo survey of Loveday *et al.* (1992b) but at almost twice the amplitude. Also, apart from the large local overdensity at $r < 20h^{-1}$Mpc (which could also be a combination of small volume and poor statistics) the dominant features in the radial distribution are the three peaks at $\sim$ 90, 170 and (possibly) $310h^{-1}$Mpc and the two troughs between them. The radial distances of these peaks and troughs agree well with those in the observed $N(r)$ histogram (section 2.9) and again there is some correspondance with the Broadhurst *et al.* (1990) pencil-beam redshift survey SGP "spikes" (section 2.9).

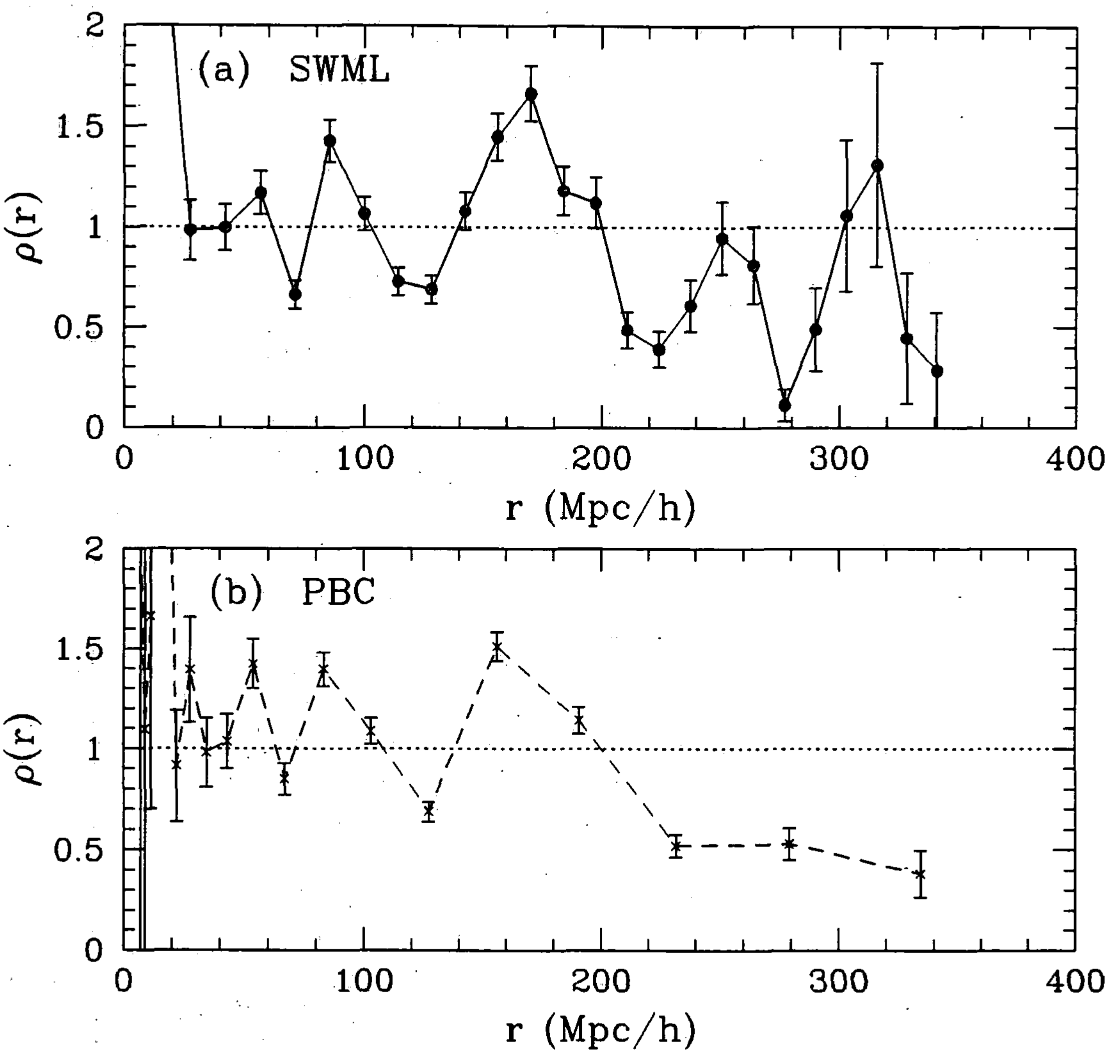

Figure 3.4: The maximum likelihood estimate of the radial density function estimated from the (a) SWML and (b) PBC methods.

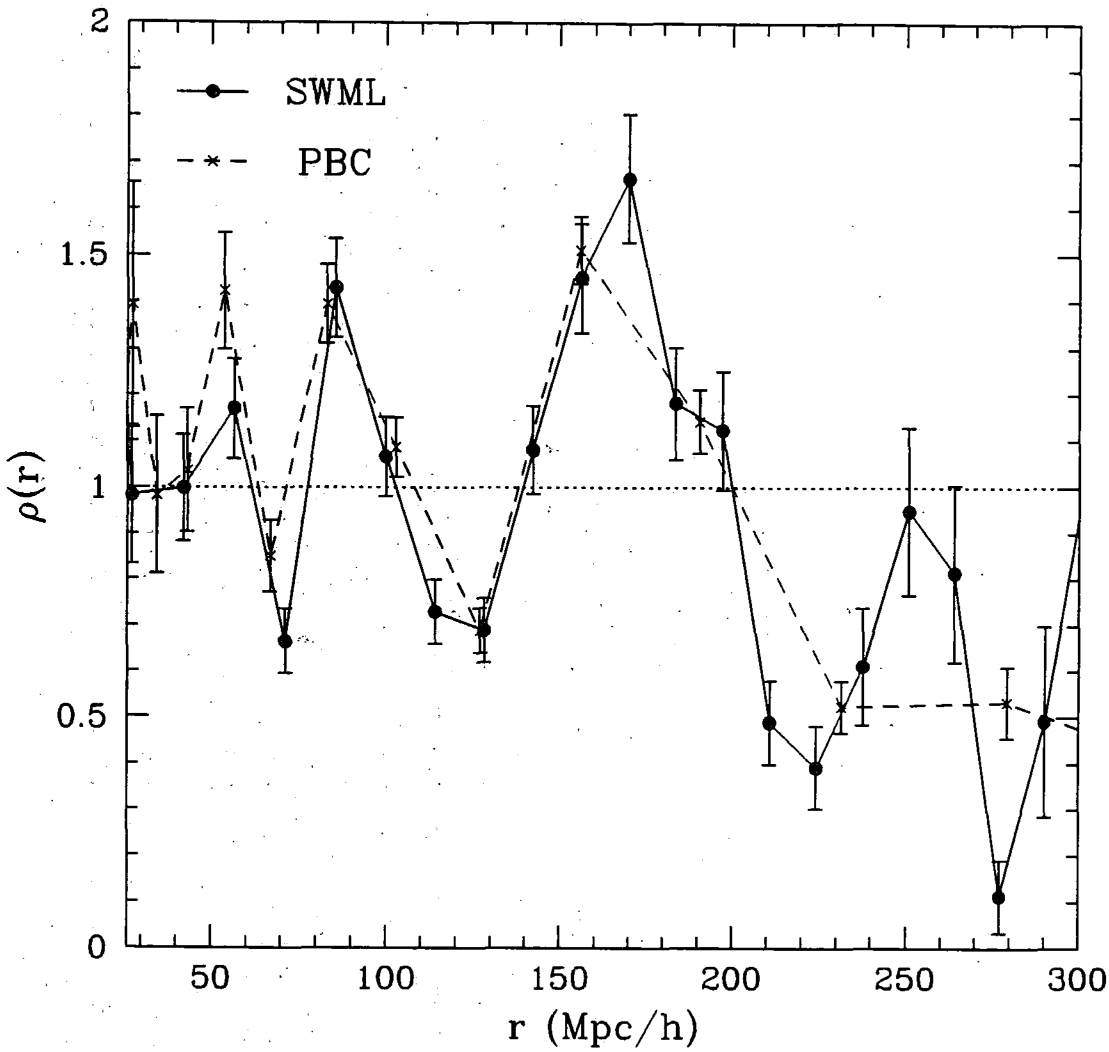

Figure 3.5: The SWML (dots) and PBC (crosses) maximum likelihood estimates of the radial density function (same as figure 3.4).

3.5 Comparison with Other Surveys and Discussion

Table 3.4 shows a comparison between the maximum likelihood convolved Schechter function parameters for the Durham/UKST and other galaxy redshift surveys. The convolved values are used here for consistency (and not the pure Schechter function parameters preferred in section 3.3.2) because, in general, they are the published fits. These luminosity functions are plotted in figure 3.6 assuming the offset between the galaxies as measured in the b_J and Zwicky systems is -0.7 magnitudes and the b_J and Gunn-r is $+1.1$ magnitudes (eg. Lin *et al.* 1995b). The zero-point offset between b_J and Gunn-r comes from the mean rest-frame colour of Las Campanas galaxies, namely $\langle b_J - r \rangle_0 = +1.1$ (Tucker *et al.* 1995), but the zero-point offset between b_J and Zwicky magnitudes remains unexplained (Marzke *et al.* 1994).

Figure 3.6 shows that the convolved Schechter function Durham/UKST estimate agrees very well with that of the APM-Stromlo survey (Loveday *et al.* 1992b). (Note that the pure Schechter function estimate also agrees very well.) This may have been expected given that both surveys come from the same set of UKST plates, albeit scanned by different measuring machines. After the zero-point offset between Zwicky and b_J magnitudes has been applied, the CfA2 luminosity function (Marzke *et al.* 1994) has a similar shape to the Durham/UKST estimate although the CfA2 normalisation appears biased high, probably due to local inhomogeneities in the galaxy distribution (eg. structures such as the "Great Wall"). Similarly, after applying the zero-point offset between Las Campanas Gunn-r galaxies and b_J galaxies, the shape of the Las Campanas luminosity function (Lin *et al.* 1995b) agrees well with the Durham/UKST estimate at bright magnitudes, $M_{b_J} < -17$, although their normalisation is a little low (or alternatively our normalisation is a little high). However, at fainter magnitudes, $M_{b_J} > -16$, their best Schechter function fit does not agree well with the Durham/UKST estimate. This is not thought to be a problem with the Durham/UKST survey as the Las Campanas survey is slightly biased against intrinsically faint galaxies because of their central surface brightness selection cutoff. Overall, the general features of these convolved Schechter luminosity functions are in good agreement with a value of $M^*_{b_J} \sim -19.5$ and a flat faint end slope, $\alpha \sim -1.0$.

The normalisations of these luminosity functions are also given in table 3.4. Note that ϕ^* and $\bar{n}$ are not independent and are related via the integral over the shape of the luminosity function (equation 3.28). All of the values of ϕ^* are roughly consistent within 3σ, with the Las Campanas value providing the estimate with the smallest errors and the CfA2 value appearing to be biased high, albeit with much larger errors. The values of $\bar{n}$ are again pretty much consistent within 3σ, apart from the Las Campanas value which if one believes the quoted errors on these estimates is $\sim 9\sigma$ lower than the APM-Stromlo value. This large discrepency is not apparent in figure 3.6 and can probably be attributed to the falling faint end of the Las Campanas luminosity function with respect to the APM-Stromlo one.

Survey	Durham/UKST	APM-Stromlo	CfA2	Las Campanas
Volume ($h^3\mathrm{Mpc}^{-3}$)	4×10^6	1×10^7	2×10^6	1×10^7
Mag. System	b_J	b_J	Zwicky	Gunn-r
σ_m	0.22	0.30	0.35	0.10
M^*	-19.68 ± 0.08	-19.50 ± 0.13	-18.8 ± 0.3	-20.29 ± 0.02
α	-1.04 ± 0.08	-0.97 ± 0.15	-1.0 ± 0.2	-0.70 ± 0.05
$\phi^* \times 10^2$ ($h^3\mathrm{Mpc}^{-3}$)	1.79 ± 0.30	1.40 ± 0.17	4.0 ± 1.0	1.90 ± 0.10
$\bar{n}$ ($h^3\mathrm{Mpc}^{-3}$)	0.054 ± 0.009	0.047 ± 0.002	0.07 ± 0.02	0.029 ± 0.002

Table 3.4: Comparison of convolved Schechter luminosity function fits of different surveys

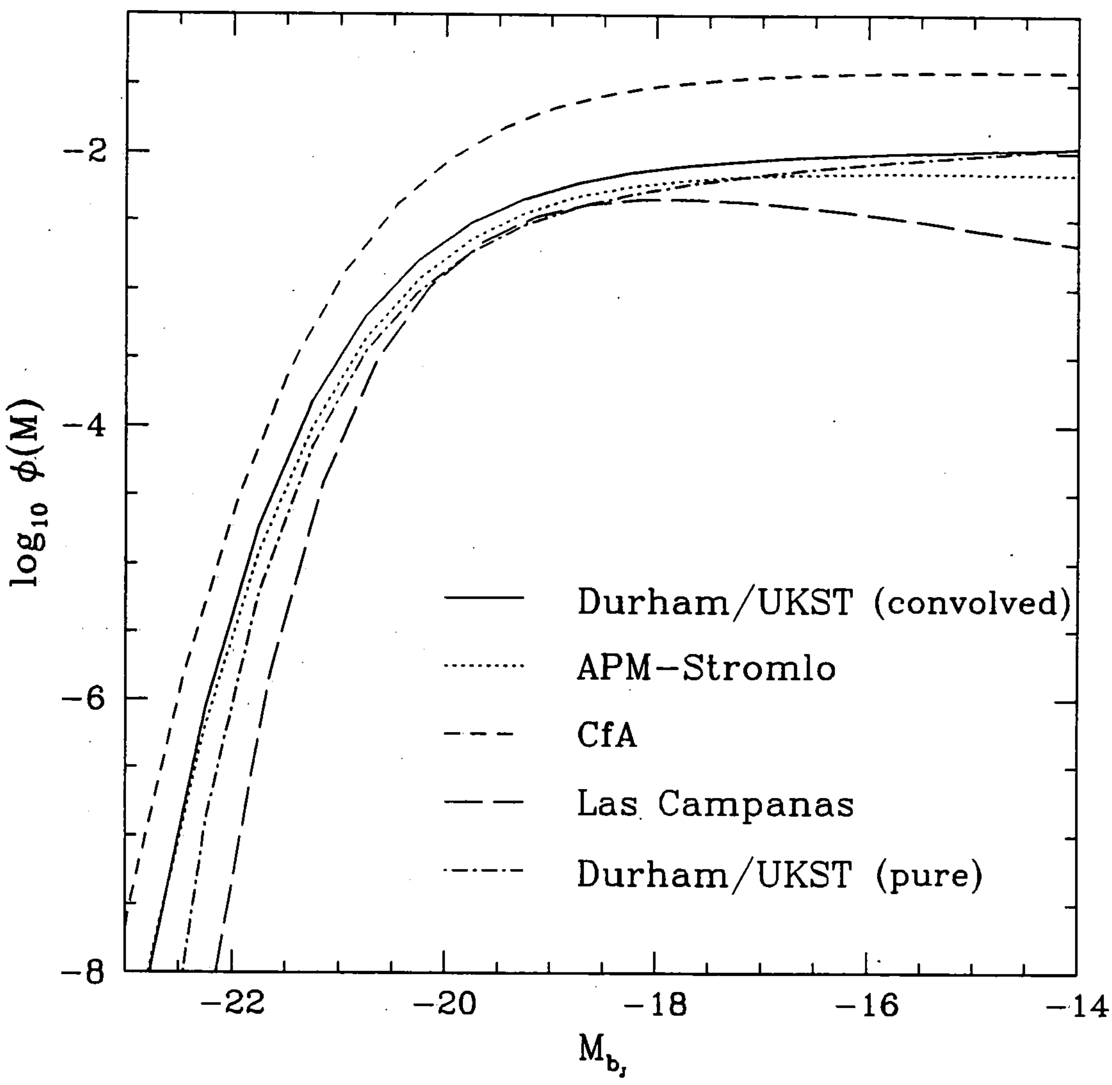

Figure 3.6: Comparison of the Durham/UKST luminosity function with that calculated from other galaxy redshift surveys. The CfA2 Zwicky magnitudes are transformed to the b_J system by the relation $M_{b_J} = M_Z - 0.7$ and the Las Campanas Gunn-r magnitudes by $M_{b_J} = M_r + 1.1$.

Finally, regarding the radial density profile, it is possible that a very large local void, on scales $r \sim 100h^{-1}$Mpc, could explain the low normalisation and steep slope seen in the bright galaxy number-magnitude counts ($b_J \sim 15$-18) without the need for evolution (eg. Shanks, 1990 or Metcalfe *et al.* 1995b). The radial density profiles of other surveys are not shown here but there is no compelling evidence for any such systematic local underdensity in either the Durham/UKST survey or the APM-Stromlo survey (Loveday *et al.* 1992b). However, a $\sim 30\%$ underdensity out to $\sim 150h^{-1}$Mpc is seen in the combined North and South Las Campanas survey regions (Lin *et al.* 1995b), although it should be noted that their selection function is increasing very steeply in this region and hence small changes in it would cause large differences in the estimated radial density. More tentative evidence for a large local void also comes from the Las Campanas survey which has the faintest magnitude limit (ie. probes to the furthest depth) but the highest estimated ϕ^* (ignoring the CfA2 survey). This could indicate that one may have to go to fainter magnitudes to achieve convergence of the normalisation. This interpretation is possibly confirmed by the K-band redshift survey of Glazebrook *et al.* (1995) which measured $\phi^* = 2.6 \pm 0.3 \times 10^{-2} h^3\mathrm{Mpc}^3$ in a sample of 124 galaxies to $K \simeq 17.3$. The issue of a large local void still remains unanswered.

3.6 Conclusions

The "best" magnitude limited sample from the Durham/UKST survey is found **not** to suffer from incompleteness problems. Through the use of maximum likelihood methods the parametric and non-parametric optical galaxy luminosity functions have been estimated from the Durham/UKST survey. Although a Schechter function does not provide a good **formal** fit to the actual (non-parametric) luminosity function the agreement of the **gross** features of this function are good. Attempting to correct for the errors in the measured magnitudes makes little difference to the quality of this parametric fit. Therefore, in the interests of simplicity, a **pure** Schechter function is preferred with best fit parameters $M^*_{b_J} = -19.72 \pm 0.09$, $\alpha = -1.14 \pm 0.08$ and a normalisation of $\phi^* = 1.17 \pm 0.21 \times 10^{-2} h^3\mathrm{Mpc}^{-3}$. This function (and the magnitude error corrected one) is **entirely** consistent with previous determinations of the optical luminosity function and favours a **flat** faint end slope down to $M_{b_J} \sim -14$ in this redshift range ($z < 0.1$). Also, the galaxy radial density profile shows $\sim 50\%$ fluctuations on $50h^{-1}$Mpc scales and good agreement with the peaks in the observed $N(r)$ histogram of section 2.9.

Chapter 4

Optimal Estimation of the 2-Point Correlation Function from a Magnitude Limited Survey

4.1 Introduction

There are many measures of clustering but one of the most fundamental (along with the power spectrum) is the 2-point correlation function, $\xi(x)$, (eg. Peebles, 1980). The 2-point correlation function is a measure of the excess probability (above a random distribution) of finding two objects in volume elements δV_i and δV_j separated by a distance x

$$\delta P_{ij}(x) = \bar{n}^2 \delta V_i \delta V_j [1 + \xi(x)], \tag{4.1}$$

where $\bar{n}$ is the average number density of objects. In our case the objects of interest are galaxies and equation 4.1 is equivalent to saying that

$$\delta P_{ij}(x) = \bar{n} \delta V_{ij} [1 + \xi(x)], \tag{4.2}$$

is the probability of finding another galaxy j at a distance x from a given galaxy i. Therefore, if $\xi > 0$ then the distribution is clustered, if $\xi < 0$ then the distribution is anti-clustered and $\xi = 0$ then the distribution is random.

The aim of this chapter is to determine which weighting/estimator combination most accurately estimates the 2-point correlation function of a magnitude limited catalogue without introducing any systematic biases into the answer. This will be done by analysing specially constructed mock catalogues which have been produced from N-body simulations to mimic the Durham/UKST galaxy redshift survey. Both the bias and minimum variance of the estimates will be considered.

The format of the chapter is as follows. The different methods of estimating the 2-point correlation function are first reviewed. The Cold Dark Matter (CDM) N-body simulations and their parameters are then described. The method of constructing the mock catalogues from these N-body simulations is also described. The 2-point correlation function is then estimated from the N-body simulations and the mock catalogues using different weighting/estimator combinations. A comparison and discussion of these estimates, their errors and the problems in obtaining them is then given. The chapter ends with the main conclusions obtained from this analysis of the simulations.

4.2 Review of the Methods of Estimating the 2-Point Correlation Function

For a volume limited, fair sample galaxy survey of the Universe an unbiased method of calculating the 2-point correlation function is as follows. Imagine a random and homogeneous distribution of galaxies, with mean density $\bar{n}_R$, by definition $\xi = 0$ for this catalogue and the summation over all the individual i, j^{th} volume elements lying within this catalogue at separations x gives the total pair count of this random galaxy distribution, $RR(x)$, at a separation x

$$\begin{aligned} RR(x) &= \sum_i \sum_j \bar{n}_R^2 \delta V_i \delta V_j, & (4.3) \\ &= \bar{n}_R^2 \sum_i \sum_j \delta V_i \delta V_j, & (4.4) \end{aligned}$$

as $\bar{n}_R$ is a constant. Now imagine a similarly constructed catalogue but this time consisting of a non-random galaxy distribution, $\xi \neq 0$, with mean density $\bar{n}_D$. Again summing over all the individual i, j^{th} volume elements lying within this catalogue at separations x gives the total pair count of this non-random galaxy distribution, $DD(x)$, at a separation x

$$\begin{aligned} DD(x) &= \sum_i \sum_j \bar{n}_D^2 \delta V_i \delta V_j [1 + \xi(x)], & (4.5) \\ &= \bar{n}_D^2 [1 + \xi(x)] \sum_i \sum_j \delta V_i \delta V_j, & (4.6) \end{aligned}$$

as $\bar{n}_D$ and $\xi(x)$ are constant at pair separation x. Dividing equation 4.6 by equation 4.4 and rearranging for $\xi(x)$ gives

$$\xi(x) = \frac{DD(x)}{RR(x)} \left(\frac{\bar{n}_R}{\bar{n}_D} \right)^2 - 1. \tag{4.7}$$

However, for an apparent magnitude limited survey which is small enough that the fair sample hypothesis is only an approximation (which may or may not be true) then things are not quite as simple. Not only is the observed galaxy density a function of radial distance (due to the magnitude limit of the survey) but edge effects must be taken into account and the mean galaxy density must be estimated from the sample itself (which could be biased high or low by inhomogeneities in the sample).

In terms of trying to estimate the 2-point correlation function from this sample these two problems manifest themselves as the optimal weighting to use when calculating the relevant pair count and the optimal estimator which is least biased by the mean density and the error in it. If a random and homogeneous catalogue is produced with the same radial and angular selection functions of the magnitude limited survey one can still define the appropriate pair counts. Analogous to equations 4.4 and 4.6 $DD(x)$, $DR(x)$ and $RR(x)$ are the data-data, data-random and random-random pair counts, respectively, namely the cross correlation of the data catalogue with itself, the data catalogue with the random catalogue and the random catalogue with itself. The mean densities estimated from the data and random catalogues again are $\bar{n}_D$ and $\bar{n}_R$, respectively. When calculating the 2-point correlation function two weighting schemes of each data/random point are considered. Firstly, a simple unit weighting that is independent of radial distance (eg. Peebles, 1980)

$$w(r_i) = 1, \tag{4.8}$$

and secondly, the so-called minimum variance weighting (Efstathiou, 1988, also see Peebles, 1973 and Loveday *et al.* 1995b)

$$w(r_i) = \frac{1}{1 + 4\pi n(r_i) J_3(x)}, \tag{4.9}$$

where r_i is the radial distance of the data/random point, $J_3(x) = \int_0^x \xi(y) y^2 dy$ is the volume integral over the 2-point correlation function out to a separation x, $n(r_i) = \bar{n} S(r_i)$ is the density of the data/random catalogue at a radial distance r_i and $S(r_i)$ is the radial selection function, ie. the probability that a data/random point is included in the catalogue at a distance r_i (see section 4.4.1). Also, three methods of estimating the 2-point correlation are considered. Firstly, the standard estimator (eg. Peebles, 1980)

$$\xi_{est}(x) = \frac{DD(x)}{DR(x)} \frac{\bar{n}_R}{\bar{n}_D} - 1, \tag{4.10}$$

secondly, the estimator of Hamilton (1993)

$$\xi_{est}(x) = \frac{DD(x) RR(x)}{DR(x)^2} - 1, \tag{4.11}$$

and thirdly, the estimator of Landy & Szalay (1993)

$$\xi_{est}(x) = \frac{DD(x) - 2DR(x) + RR(x)}{RR(x)}. \tag{4.12}$$

The immediate aim is to determine which of the above combinations of weighting and estimator will produce the most accurate and unbiased estimate of ξ.

4.3 The N-Body Simulations

4.3.1 Technical Details of the Simulations

Cole *et al.* (1994b) have kindly provided me with the results from 10 N-body simulations and Baugh & Gaztañaga (1995) have kindly provided me with the results from 5 N-body simulations. The parameters of these simulations are now described and are also shown in table 4.1.

The 10 simulations of Cole *et al.* (1994b) (also see Eke *et al.* 1995) are cosmological simulations of CDM dominated universes with scale invariant initial conditions and assume the Bardeen *et al.* (1986) CDM transfer function with $\Omega_B = 0$ and $\Gamma = \Omega_{CDM}h = 0.5$. Each simulation consists of $(128)^3$ particles each of mass $2.24 \times 10^{12}h^{-1}M_\odot$ in a cube of comoving side length $256h^{-1}$Mpc. They are evolved to have a bias factor, $b = 1.58$, namely $\sigma_{8\,CDM} = 0.63$, at the present day ($z = 0$). "Galaxies" are then selected from the final particle positions with a probability given by the high peaks bias prescription of Bardeen *et al.* (1986). These parameters describe the "standard" CDM model (SCDM). The first 2 simulations were run using the P^3M code of Efstathiou *et al.* (1985) whereas the final 8 used the AP^3M code of Couchman (1991,1994). It is worth noting that beyond random fluctuations there is no difference in the results found using these different N-body codes. The number of biased galaxies selected from each simulation, ~ 170000, was chosen such that the mean density in the cube would be $\sim 0.01h^3\text{Mpc}^{-3}$. This was deemed a reasonable number given the constraints of disk space and CPU time available to the author.

The 5 simulations of Baugh & Gaztañaga (1995) (also see Gaztañaga & Baugh, 1995) are cosmological simulations of CDM dominated universes with scale invariant initial conditions and assume the Bond & Efstathiou (1984) CDM transfer function with $\Omega_B = 0.03$ and $\Gamma = \Omega_{CDM}h = 0.2$, also included was a non-zero cosmological constant ($\Lambda \neq 0$) to ensure a spatially flat cosmological model. At the end of the simulation $\Omega_{CDM} = 0.2$, hence $\Omega_\Lambda = 0.8$. Each simulation consists of $(126)^3$ particles each of mass $1.52 \times 10^{12}h^{-1}M_\odot$ in a cube of comoving side length $378h^{-1}$Mpc at the final output time, namely when $\Omega_{CDM} = 0.2$. They are evolved to have a bias factor, $b = 1.00$, ie. unbiased, namely $\sigma_{8\,CDM} = 1.0$, at the present day ($z = 0$). "Galaxies" are then selected at random from the final particle positions in an unbiased fashion. These parameters describe a low density/Λ CDM model (LCDM). The 5 simulations were all run using the P^3M code of Efstathiou *et al.* (1985). The number of unbiased galaxies selected from each simulation, ~ 540000, was chosen for the above reasons.

4.3.2 Pictures of the Simulations

An example of the typical visual picture given by the simulations is shown in figures 4.1 and 4.2. They show six $256 \times 256h^{-1}$Mpc slices through the first of the SCDM and LCDM simulations, respectively. Each slice is $42.67h^{-1}$Mpc thick and is

	SCDM	LCDM
l (h^{-1}Mpc)	256	378
No. of Particles	$(128)^3$	$(126)^3$
Mass of Particle	$2.24 \times 10^{12} h^{-1} M_\odot$	$1.52 \times 10^{12} h^{-1} M_\odot$
b	1.58	1.00
$\Omega_{CDM} h$	0.5	0.2
Λ	0.0	0.8
$\sigma_{8\,CDM}$	0.63	1.00
Mean no. of Galaxies	169965	538058

Table 4.1: Parameters of two sets of N-body simulations.

projected along the z axis. Clusters of galaxies are seen in the slices for both CDM models. The LCDM model arguably shows more filaments and voids per slice than the SCDM model on $\sim 50h^{-1}$Mpc scales.

4.4 The Mock Catalogues

4.4.1 Construction of the Mock Catalogues

The simulations of section 4.3 were used to construct mock catalogues which model the angular and radial selection functions of the Durham/UKST galaxy redshift survey. For the SCDM simulations 20 mock catalogues were made (2 per simulation), while for the LCDM simulations 15 mock catalogues were made (3 per simulation). An outline of each step in the construction is given below :

1. The origin of the simulation was transformed to a random point in the cube and all particle positions altered with respect to this new coordinate system. The random point was choosen to be different for each simulation so as to average over any local voids or overdensities.

2. A periodic representation was added to the positive x, y and z directions such that a larger cube was built from 8 ($2 \times 2 \times 2$) of the smaller cubes (see figure 4.3). This was necessary only for the SCDM simulations because they were not quite large enough to include the full spatial dimensions of the Durham/UKST survey.

3. Mock catalogues could be produced in both real and redshift space. For the redshift space catalogues the coordinates of the particles needed to be transformed to redshift space. This was done by adding the x, y and z components of the particle's velocity along the line of sight, in h^{-1}Mpc units, to the x, y and z position of the particle. Specifically,

$$a \rightarrow a + \Delta a_{vel}, \tag{4.13}$$

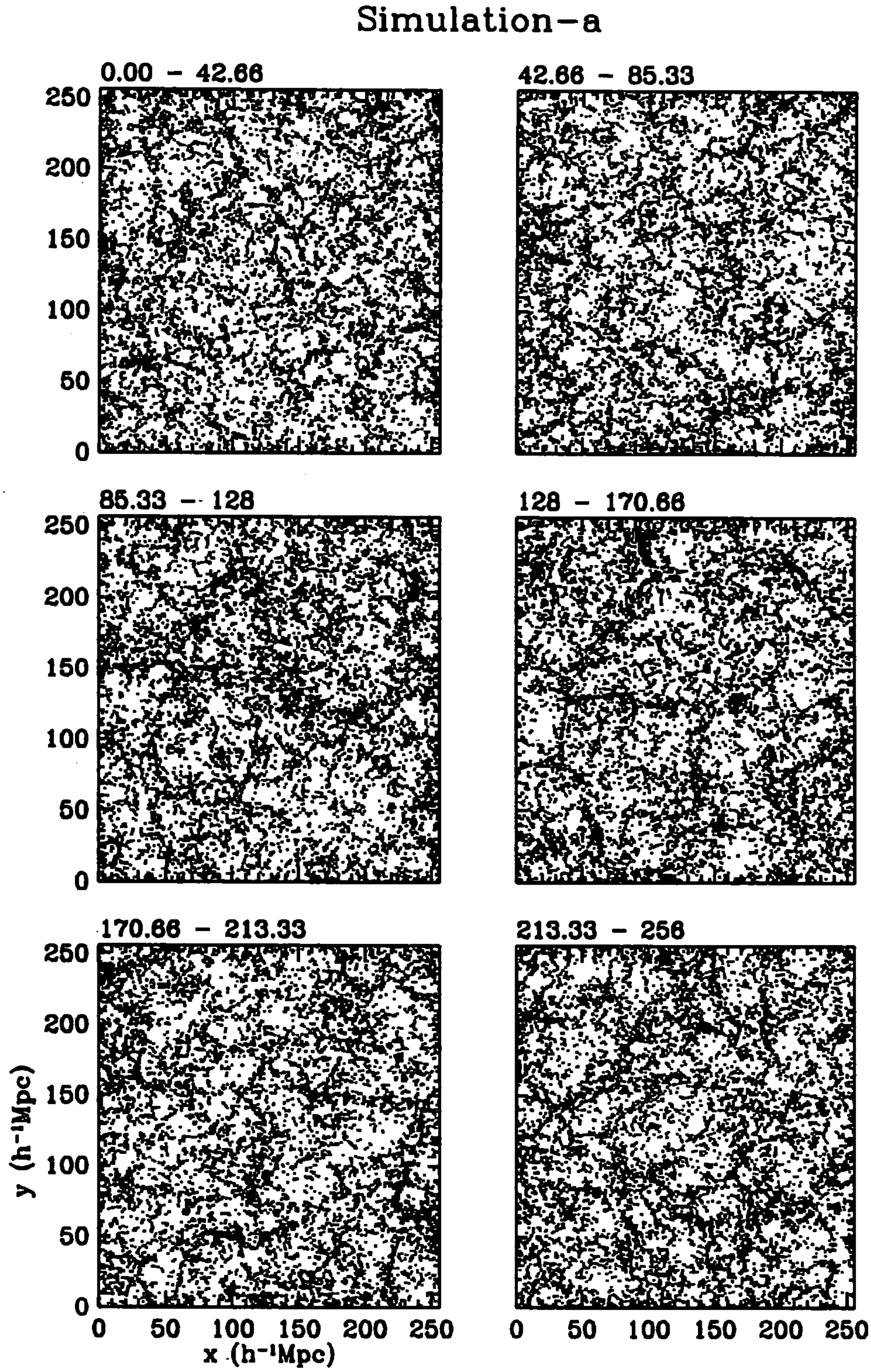

Figure 4.1: Projection along the z-axis of a SCDM simulation.

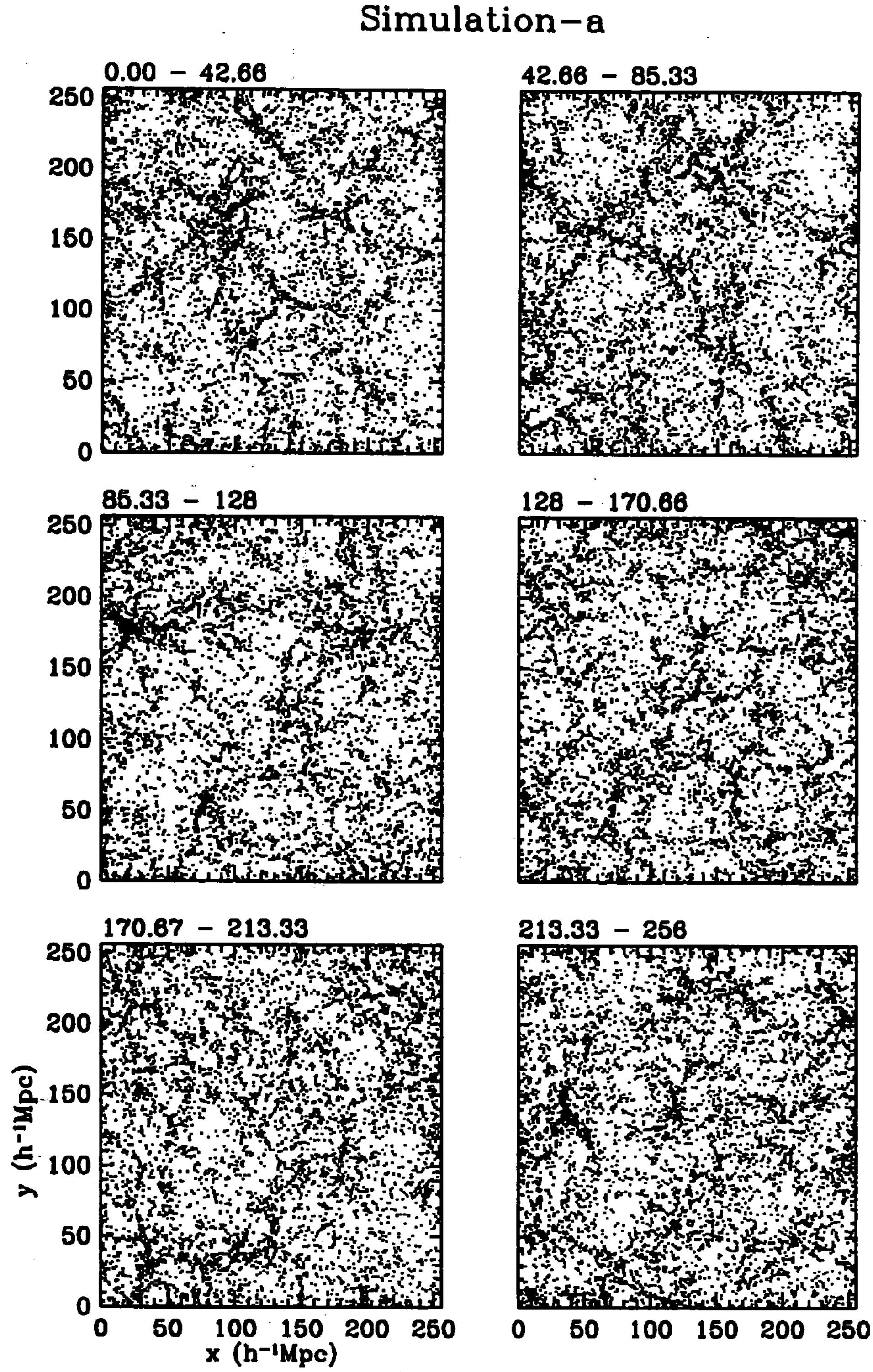

Figure 4.2: Projection along the z-axis of a LCDM simulation.

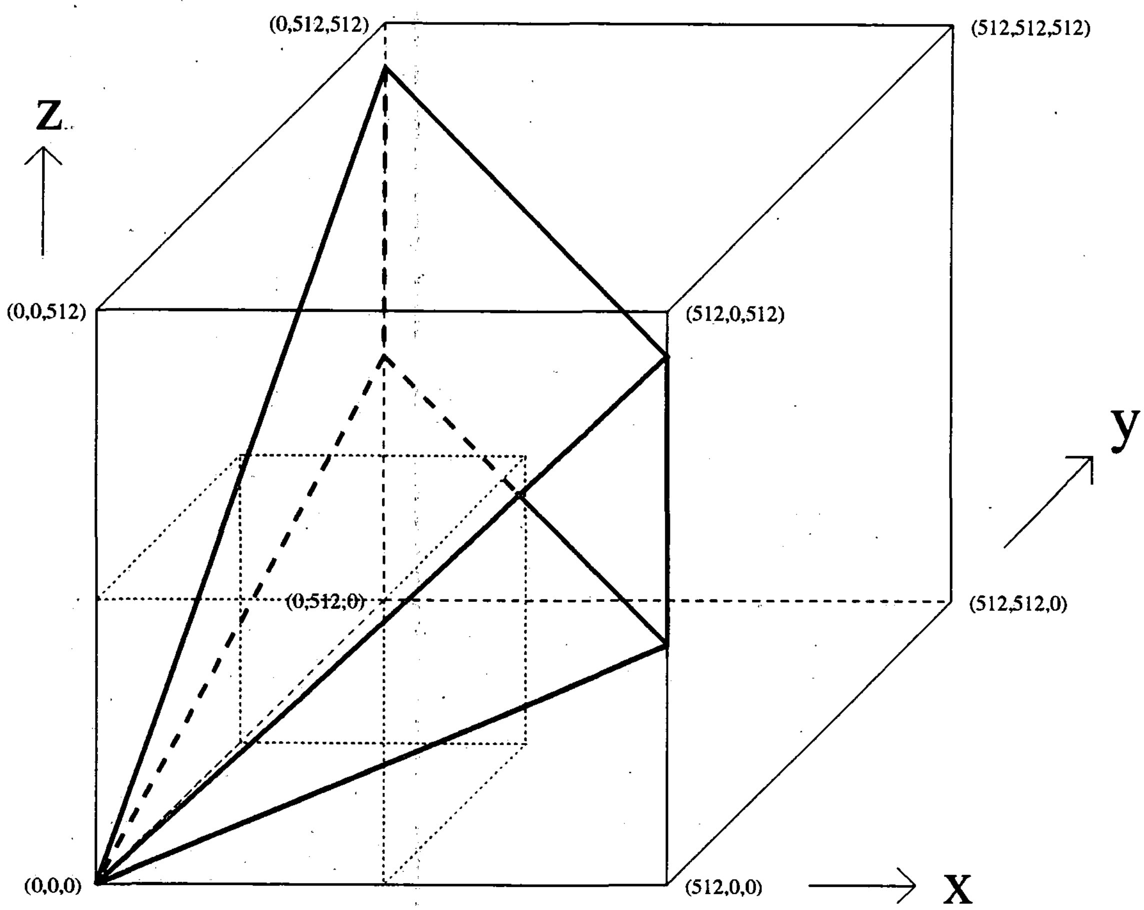

Figure 4.3: Schematic view of the selection/rejection process of the mock catalogues.

$$\Delta a_{vel} = \frac{a}{r^2}(\mathbf{r}.\mathbf{v}), \tag{4.14}$$

where a can be either x, y or z, Δa_{vel} is the velocity component along the a^{th} axis and $\mathbf{r}$, $\mathbf{v}$ are the position, velocity vectors of the particle with respect to the origin.

4. These new (x, y, z) coordinates were transformed to (r, α, δ) using

$$r = \sqrt{x^2 + y^2 + z^2}, \tag{4.15}$$

$$\alpha = \arctan\left(\frac{x}{y}\right), \tag{4.16}$$

$$\delta = -\arcsin\left(\frac{z}{r}\right). \tag{4.17}$$

5. Particles outside the Durham/UKST α and δ ranges are rejected (see figure 4.4). The geometry of the cube implies that α can only span a $[0°, 90°]$ range. However, the actual slices from the Durham/UKST survey at $\delta = -25°$ and $-40°$ extend slightly more than $90°$ in α. Therefore the final $0.5°$ & $3.5°$ of the $\delta = -25°$ & $-40°$ strips, respectively, have been cut off and no particles are selected in these regions. Future analysis of these mock catalogues is not adversely affected by this limitation.

6. Particles with radial distance outside $[5, 400]h^{-1}$Mpc were rejected.

7. The radial selection function, $S(r)$, is the probability that a galaxy at a distance r will be included in the survey and is given by a ratio of integrals over the galaxy luminosity function (see section 3.2.3)

$$S(r) = \frac{\int_{L_{max}}^{\infty} \phi(L)dL}{\int_{L_{low}}^{\infty} \phi(L)dL} = \frac{\Gamma\left(\alpha + 1, \frac{L_{max}}{L^*}\right)}{\Gamma\left(\alpha + 1, \frac{L_{low}}{L^*}\right)}, \tag{4.18}$$

where $L_{max} = \max[L_{low}, L_{min(r)}]$, L_{low} is the minimum possible absolute luminosity of a galaxy in the survey and $L_{min(r)}$ is the minimum absolute luminosity of a galaxy that can be seen at a distance r and still be included in the survey. The RHS of equation 4.18 assumes a Schechter luminosity function (Schechter, 1976) and $\Gamma(\alpha + 1, x)$ is the standard incomplete Gamma function. The parameters of the Schechter function are taken from chapter 3 where it was found that $\alpha = -1.14$ and $M^*_{b_J} = -19.72$ for the Durham/UKST survey.

This radial selection function has to be evaluated for each field because of the variable magnitude limits and is then multiplied by the sampling rate of this field. This produces a 2-D look-up table of probabilities which depends on field number and radial distance only. Particles remaining after steps 5 and 6 are then selected at random to be galaxies in the catalogue according to this 2-D probability table. The normalisation of these probabilities is chosen such that ~ 400 galaxies are selected in every scan of the simulation. Hence, 5 or 6 scans are necessary before stopping at ~ 2000 galaxies and the mean density of each mock catalogue is therefore slightly different.

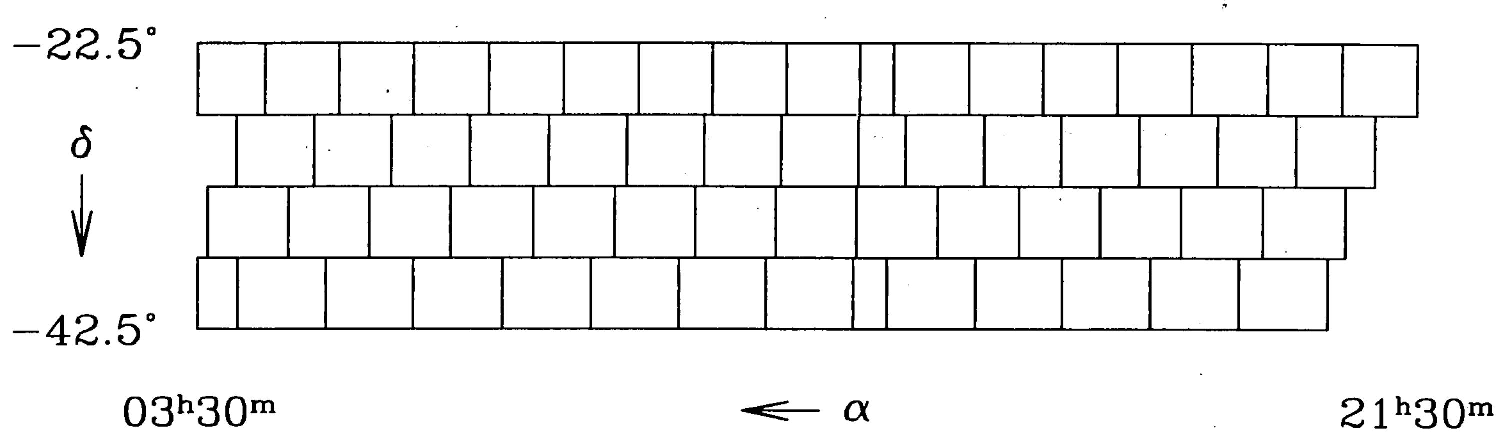

Figure 4.4: A projection of the angular mask used to reject particles.

Name	No. of Galaxies Selected	
	Real Space	Redshift Space
SCDM uniform	2080 ± 139	2077 ± 130
SCDM non-uniform	2092 ± 116	2141 ± 161
LCDM non-uniform	2063 ± 113	2073 ± 147

Table 4.2: The mean number of galaxies selected in each set of mock catalogues.

Two probability tables were considered. Firstly, each field was given both a constant magnitude limit ($b_J = 16.75$) and uniform sampling rate (1.0). Secondly, each field was given the magnitude limits and sampling rates from the "best" Durham/UKST survey sample. More details about these two samples are given in section 2.7. Table 4.2 shows the mean number of galaxies, in real and redshift space, selected using these two different probability tables on the two sets of simulations. The reason for using both a constant and variable magnitude limit/sampling rate in each field is to see if it was possible to correct for the observational constraints. Therefore, there was no need to use the uniform magnitude and sampling rate for the LCDM simulations.

8. The origin is then transformed before repeating steps 2 - 7. The transformation relocates the origin one half (third) of the way up the z-axis and on the other side of the cube for the SCDM (LCDM) simulations. This makes the mock catalogues sample as independent a volume as is possible. Specifically, for the SCDM simulations

$$x \rightarrow 256 - x, \tag{4.19}$$
$$y \rightarrow 256 - y, \tag{4.20}$$
$$z \rightarrow z - 128, \tag{4.21}$$

and for the LCDM simulations

$$x \rightarrow 378 - x, \tag{4.22}$$
$$y \rightarrow 378 - y, \tag{4.23}$$
$$z \rightarrow z - 126. \tag{4.24}$$

4.4.2 Pictures of the Mock Catalogues

The mock catalogues can be split into four declination slices centered on $\delta = -25°$, $-30°$, $-35°$ and $-40°$, spanning 5° in the δ direction. Figures 4.5, 4.6, 4.7 and 4.8 show examples of the SCDM/LCDM real and redshift space catalogues selected from table 4.2 using the non-uniform probabilities which model the Durham/UKST survey. "Fingers of God" are visible in the redshift catalogues of figures 4.7 and 4.8.

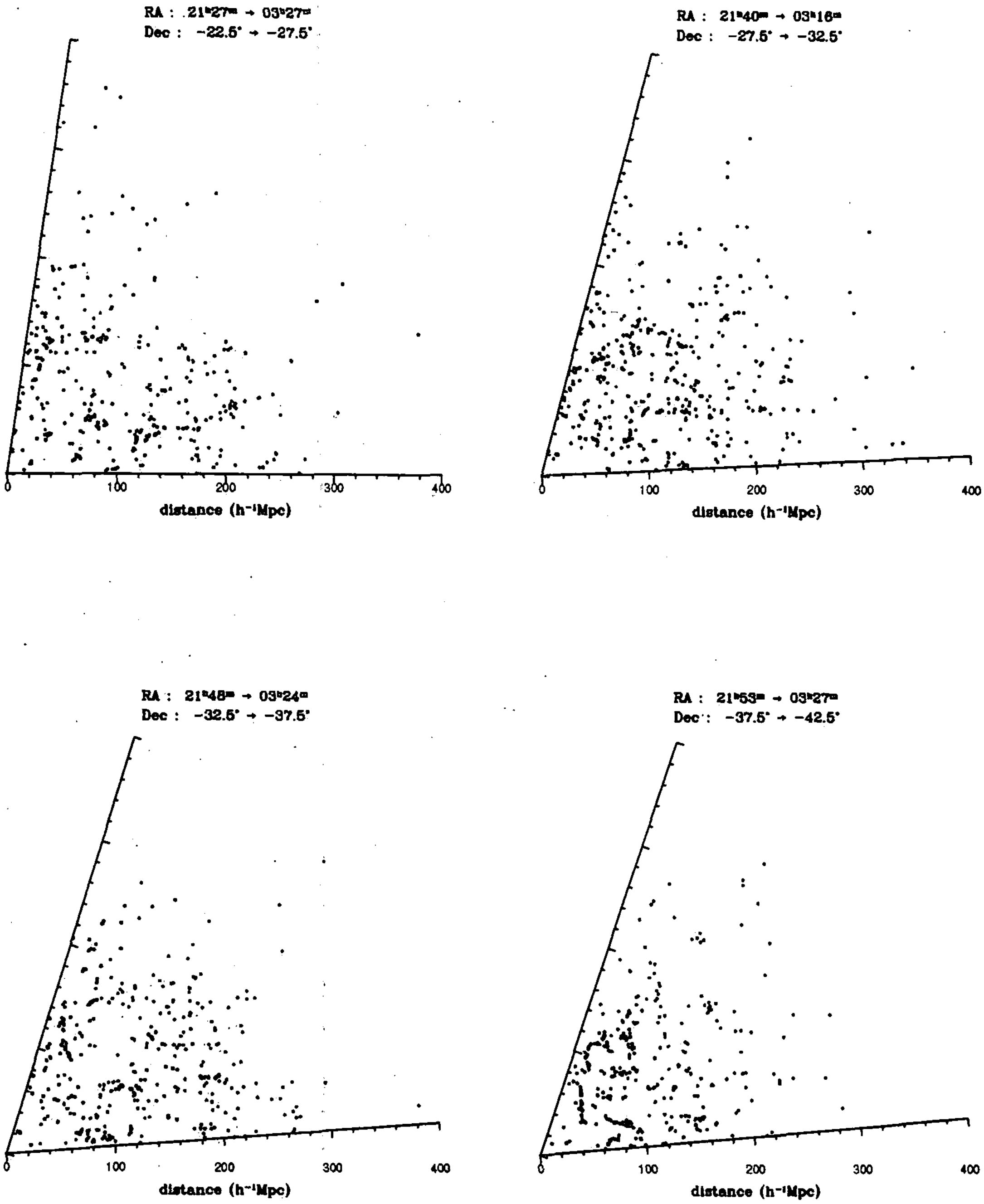

Figure 4.5: The first *real* space mock catalogue selected from the SCDM simulations.

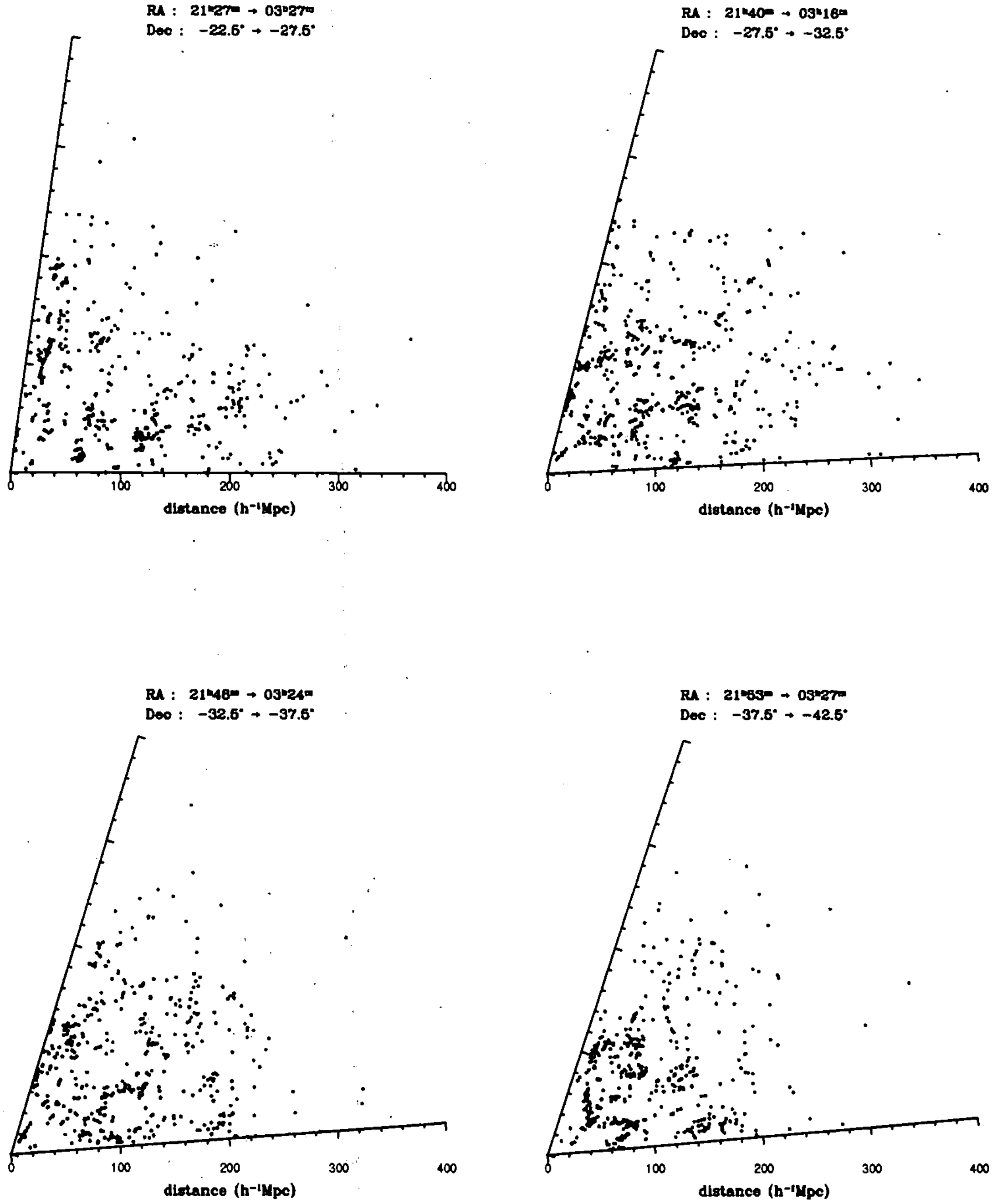

Figure 4.6: The first *redshift* space mock catalogue selected from the SCDM simulations.

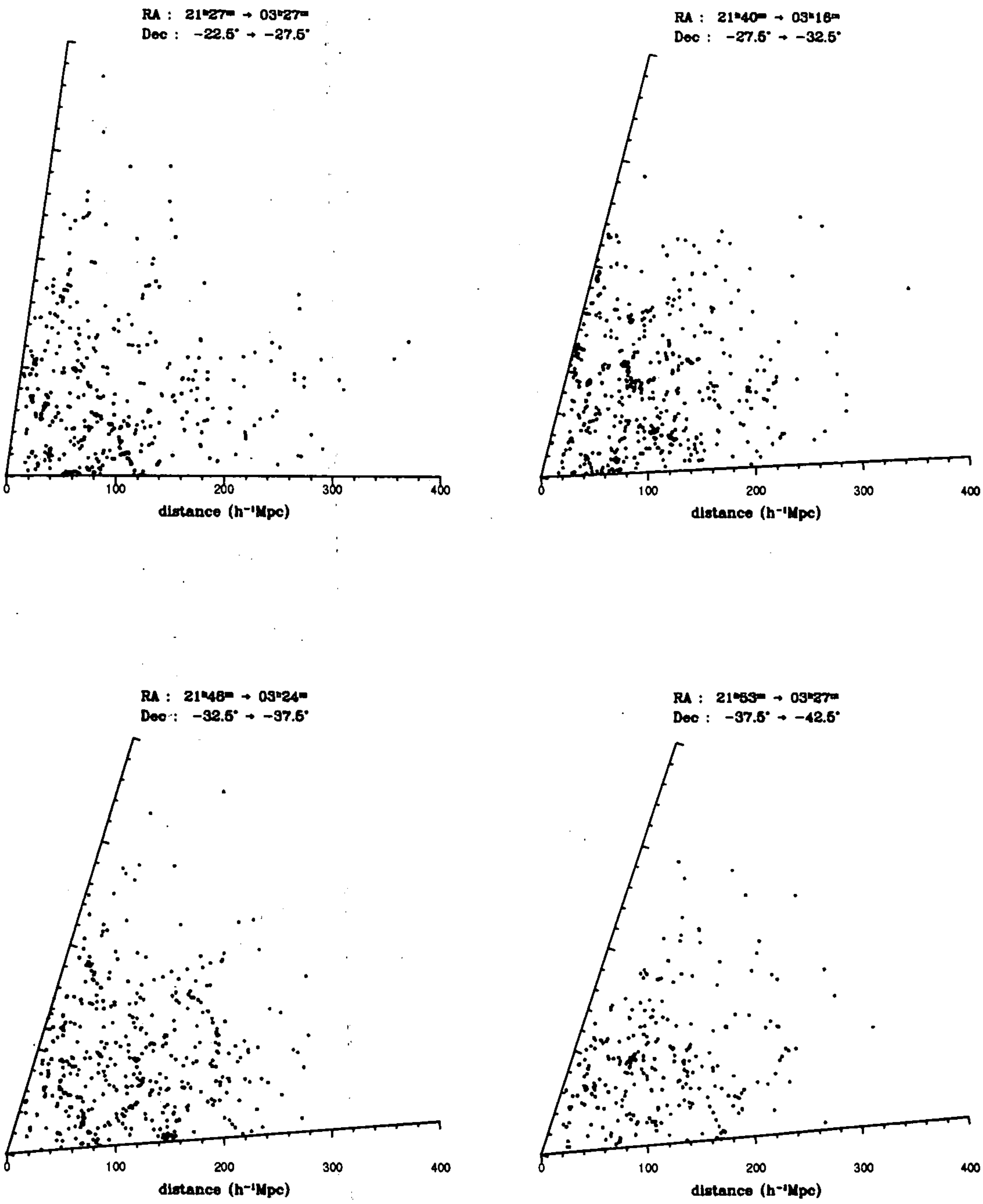

Figure 4.7: The first *real* space mock catalogue selected from the LCDM simulations.

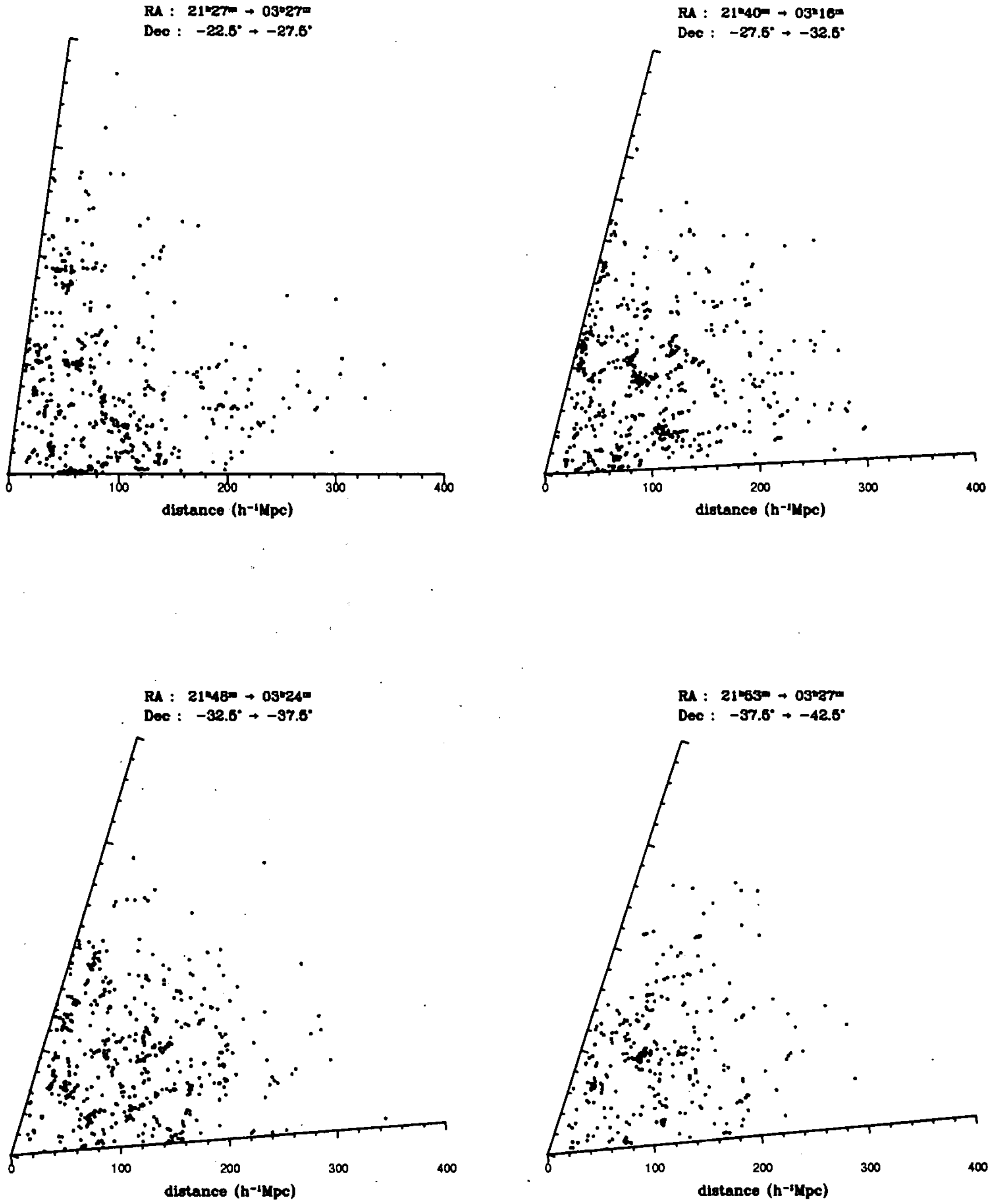

Figure 4.8: The first *redshift* space mock catalogue selected from the LCDM simulations.

4.5 The 2-Point Correlation Function

4.5.1 The N-Body 2-Point Correlation Functions

The 2-point correlation function (in real and redshift space) was evaluated from each SCDM/LCDM simulation cube using the method described below.

(i) Real Space :

To save CPU time a random fraction of $\sim 15\%/5\%$ of the galaxies were chosen from each SCDM/LCDM cube. The cube is then cross correlated with itself summing the DD pair count in 0.1 *dex* bins in pair separation starting at $0.1h^{-1}$Mpc. Since the mean density is known exactly the RR pair count can be calculated using

$$RR = \frac{4\pi}{3}(r_{outer}^3 - r_{inner}^3)\bar{n}N, \tag{4.25}$$

where $[r_{inner}, r_{outer}]$ defines the inner and outer radial distance of each bin and $\bar{n}$ & N are the mean density and total number of galaxies in the cube used in the cross correlation. The periodic boundary conditions of the simulations are implemented when counting the DD pairs. Basically, if any $|x_i - x_j|$, $|y_i - y_j|$ or $|z_i - z_j|$ exceeds half the cube size then because of the periodicity of the boundary conditions the shortest distance between the points is when the point is "wrapped around" to the other side of the cube

$$|a_i - a_j| \rightarrow l - |a_i - a_j|, \tag{4.26}$$

where a can be x, y or z and l is the side length of the cube. The 2-point correlation function is then calculated from equation 4.7 with $\bar{n}_R = \bar{n}_D$.

(ii) Redshift Space :

The pair counts and 2-point correlation function are calculated as above. However, before cross correlation the coordinates are transformed from real to redshift space using the distant observer approximation. Basically, it is assumed that the cube is a large distance away from the observer, such that the line of sight direction can be thought to be the same for all objects in the cube. This direction is arbitrary and, for simplicity, is choosen to be the x direction. To transform from real to redshift space one simply adds the x velocity component (in appropriate h^{-1}Mpc units) to the x component of distance.

The following figures show the mean and 1σ error on ξ under the assumption that each simulation is a statistically independent estimate of ξ. Three phenomenological power law models of ξ are also plotted on each figure, they take the basic form

$$\xi(r) = \left(\frac{r_0}{r}\right)^{\gamma}, \tag{4.27}$$

with different values of the amplitude (or correlation length), r_0, and slope, γ. The canonical value of these parameters in the actual Universe is $r_0 = 4.5h^{-1}$Mpc and $\gamma = 1.8$ (eg. Peebles, 1980). For the SCDM simulations one simulation was found to have an excess DD pair count significantly above that expected in a bin near $2h^{-1}$Mpc. This occured in both the real and redshift space estimates of ξ. The reason for this excess was not discovered but was thought to be due to a corrupted bias file used in producing the "galaxies". This simulation was left out of all subsequent analysis. There were no such problems with any of the LCDM simulations.

SCDM: Figures 4.9 and 4.10 show the real and redshift space ξ's for SCDM on log-log and log-linear plots to emphasise the small ($< 10h^{-1}$Mpc) and large ($> 10h^{-1}$Mpc) scale features of ξ, respectively.

Real space ; On small scales, the slope of ξ is quite steep, $\gamma \simeq 2.2$, with a typical amplitude of $r_0 \simeq 5.0h^{-1}$Mpc. On large scales, there is no evidence of significant large scale power above $20h^{-1}$Mpc.

Redshift space ; On small scales, the slope of ξ is quite flat, $\gamma \simeq 1.3$, with a higher amplitude of $r_0 \simeq 6.0h^{-1}$Mpc. On large scales, there is no evidence of significant large scale power above $20h^{-1}$Mpc.

LCDM: Figures 4.11 and 4.12 show the corresponding plots to figures 4.9 and 4.10 but for LCDM.

Real space ; On small scales, the slope of ξ is again quite steep, $\gamma \simeq 2.2$, but with a higher amplitude of $r_0 \simeq 6.0h^{-1}$Mpc. On large scales, there is evidence for significant large scale power up to $\sim 30h^{-1}$Mpc.

Redshift space ; On small scales, the slope of ξ is again quite flat, $\gamma \simeq 1.3$, but with an even higher amplitude of $r_0 \simeq 7.0h^{-1}$Mpc. On large scales, there is evidence for significant large scale power up to $\sim 30h^{-1}$Mpc.

It is important to note the differences between the shape of the real and redshift space 2-point correlation functions. For both the SCDM and LCDM simulations the effects of peculiar velocities are substantial. In transforming from real to redshift space, ξ appears systematically flattened on small scales, while being extended on large scales. In chapters 5 and 6 these effects will be considered in more detail.

4.5.2 The Mock Catalogue 2-Point Correlation Functions

The 2-point correlation function was evaluated from each of the mock catalogues in table 4.2 using the estimators described in section 4.2. Once again comoving distances and volumes are used. The method of evaluating the DD, DR and RR pair counts is the same in real and redshift space :

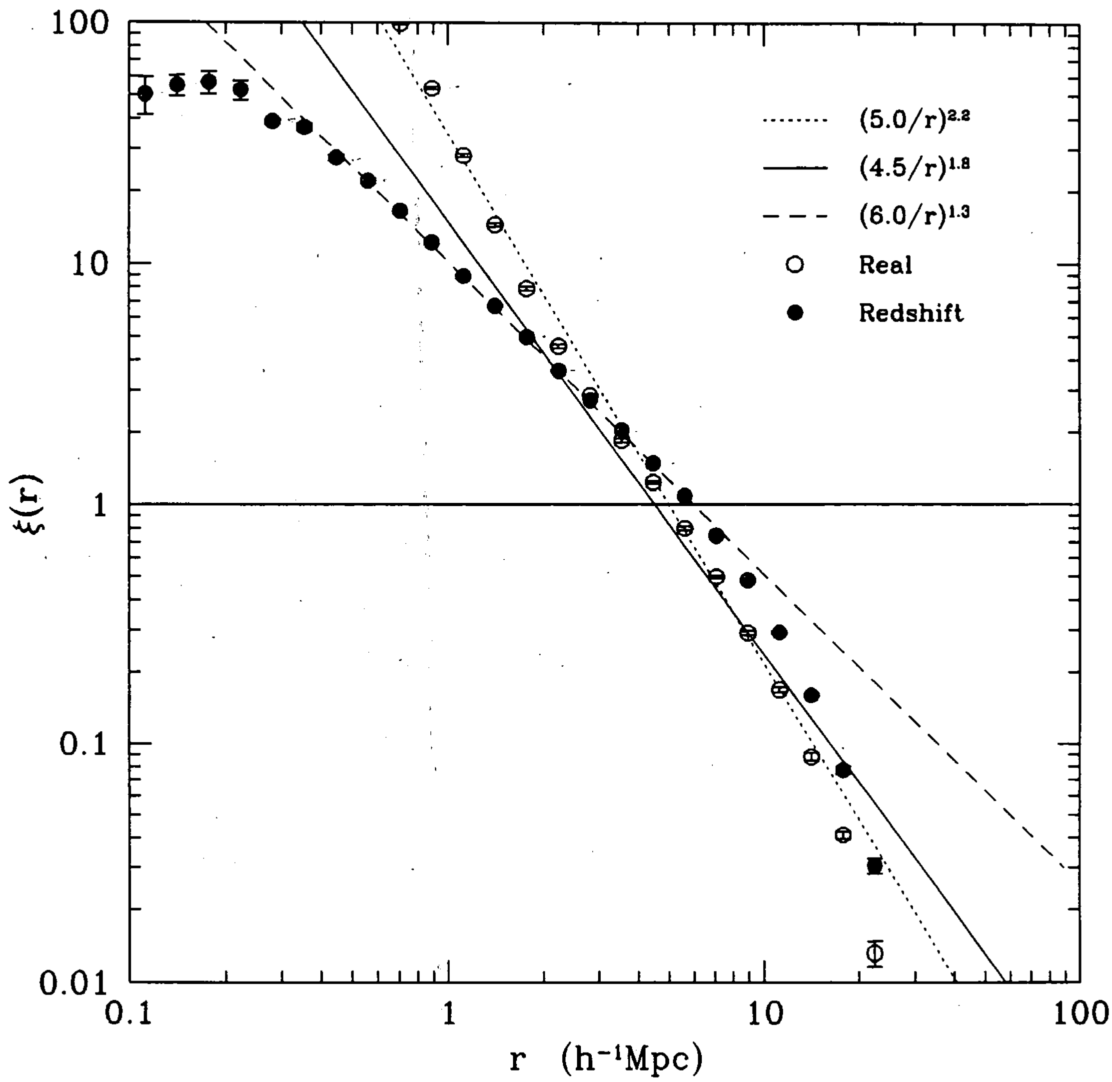

Figure 4.9: The *real* and *redshift* space estimates of ξ for the SCDM N-body simulations on a log-log plot.

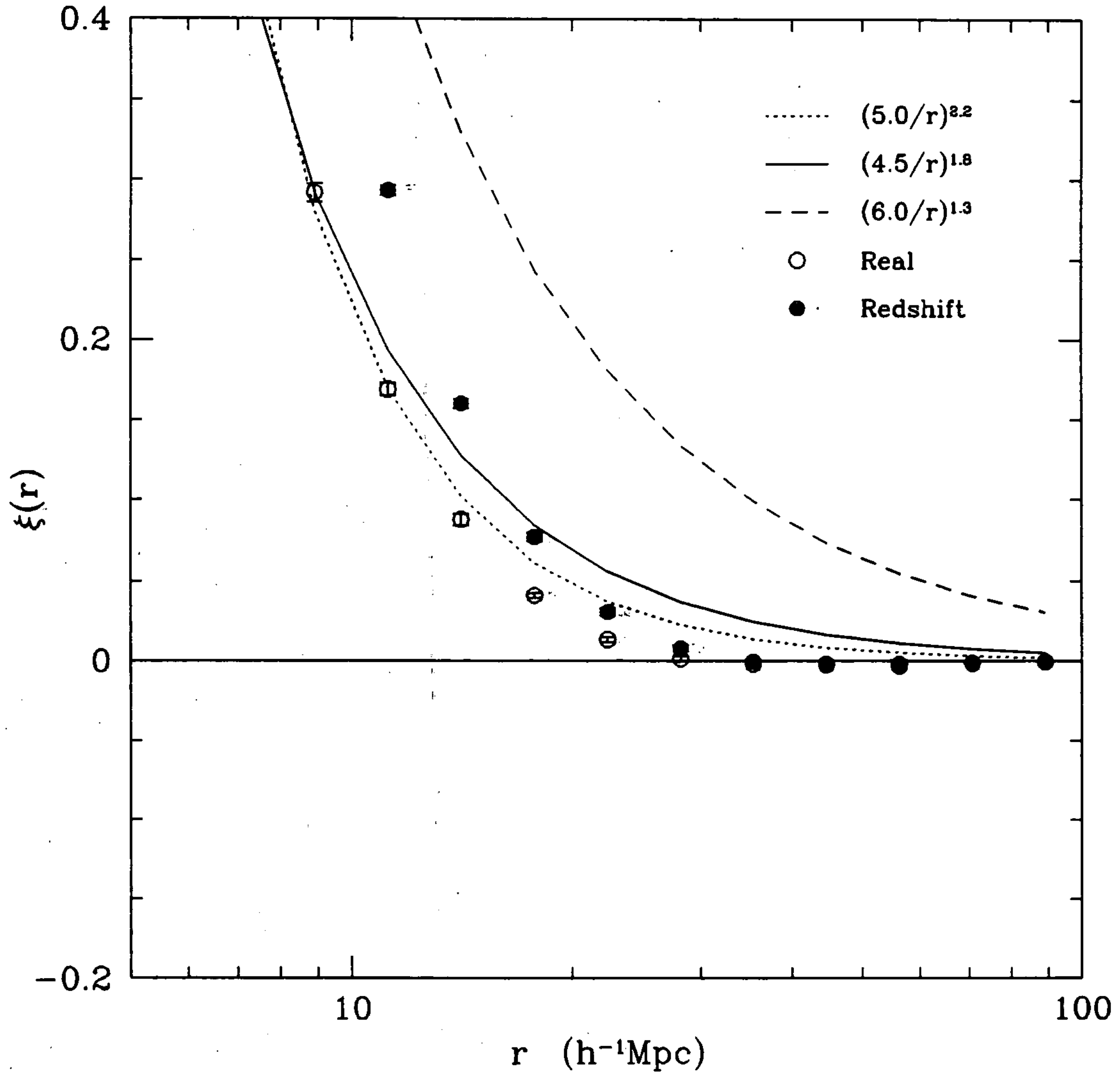

Figure 4.10: The *real* and *redshift* space estimates of ξ for the SCDM N-body simulations on a log-linear plot.

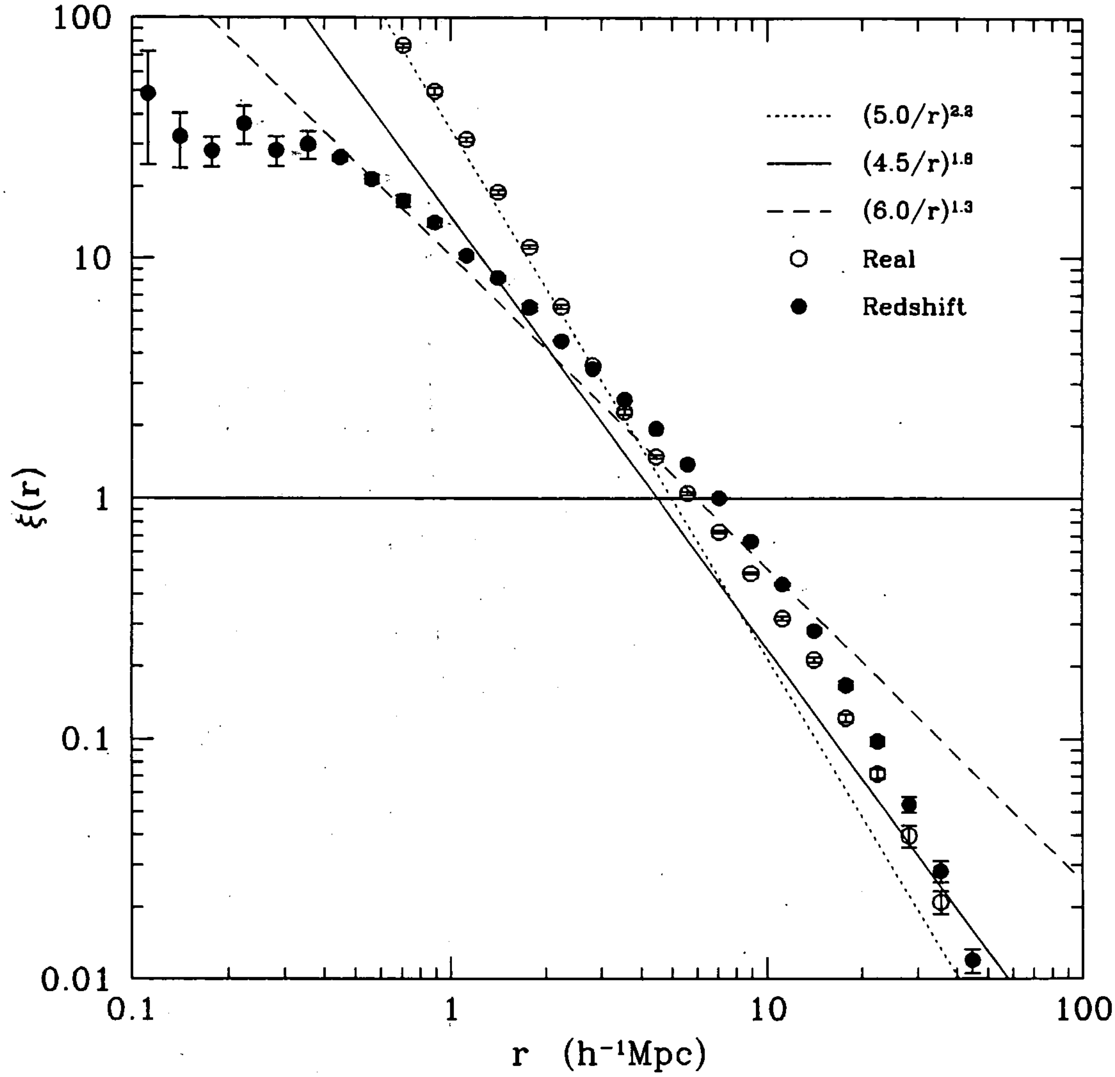

Figure 4.11: The *real* and *redshift* space estimates of ξ for the LCDM N-body simulations on a log-log plot.

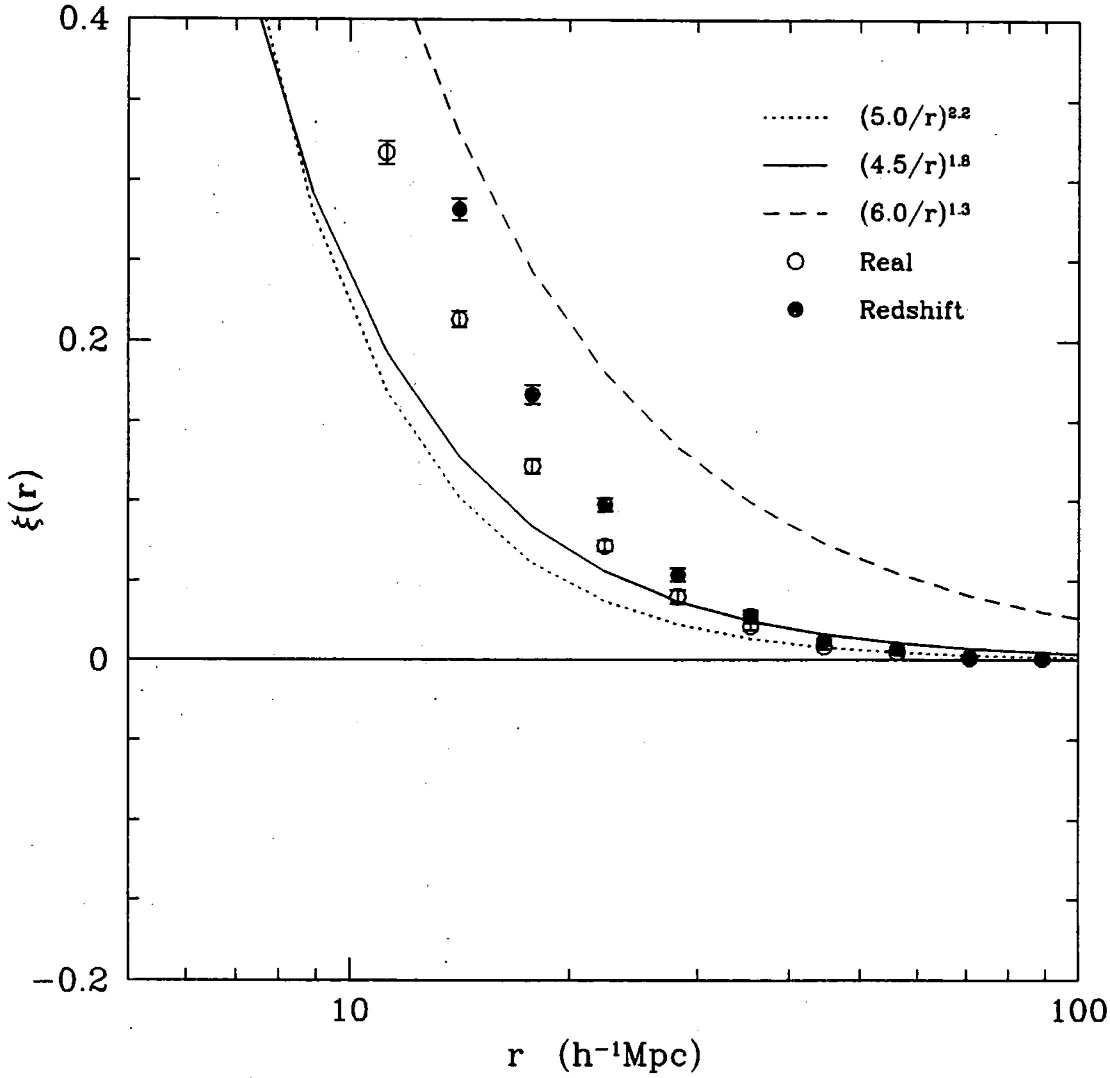

Figure 4.12: The *real* and *redshift* space estimates of ξ for the LCDM N-body simulations on a log-linear plot.

(i) The number of randoms, $N(r_{bin}, n_f)$, at each radial bin, r_{bin}, in each field, n_f, was evaluated using

$$\begin{aligned} N(r_{bin}, n_f) &= f\,\delta V(r_{bin})\,C(n_f)\,n(r_{bin}, n_f), & (4.28)\\ &= f\,\delta V(r_{bin})\,C(n_f)\,\phi^* \int_a^\infty x^\alpha \exp(-x)dx, & (4.29)\end{aligned}$$

where

$$\begin{aligned} \delta V(r_{bin}) &= \frac{\delta\Omega}{3}\left[\left(r_{bin} + \frac{\Delta r_{bin}}{2}\right)^3 - \left(r_{bin} - \frac{\Delta r_{bin}}{2}\right)^3\right],\\ C(n_f) &= \text{Completeness rate of field } n_f,\\ \lg a &= 0.4\left[M^*_{b_J} - (m_{lim}(n_f) - (5\lg d_L(z_{bin}) + 25 + k_{corr}(z_{bin})))\right],\end{aligned}$$

and f is now the ratio of random to data points, r_{bin} & z_{bin} are the centers of the radial bin in units of h^{-1}Mpc & redshift respectively ($\Delta r_{bin} = 5h^{-1}$Mpc), $n(r_{bin}, n_f)$ is the observed mean density at a given radial bin and field, $\delta\Omega$ is the solid angle of the field (in steradians), $C(n_f)$ is the completeness rate of the field (see equation 2.5) and $m_{lim}(n_f)$ is the magnitude limit of the field. The integral on the RHS of equation 4.29 assumes a Schechter luminosity function and ϕ^*, α and $M^*_{b_J}$ are the parameters as described in chapter 3.

(ii) These random galaxies are then distributed uniformly across the field given the above numbers at each radial bin accordingly. In this case $f = 25$ as a compromise between use of CPU time and reducing the noise in the random counts.

(iii) The DD, DR and RR pair counts are then evaluated by the appropriate cross correlation of the data and random catalogues. The pair counts are evaluated using the two weighting schemes of section 4.2 and the counts are stored in 0.1 *dex* bins in distance starting at $0.1h^{-1}$Mpc.

It should be noted that for the minimum variance weighting of Efstathiou (1988) the values of $\bar{n}$ and $S(r)$ are evaluated separately for each mock catalogue using the methods and luminosity function of chapter 3. J_3 is evaluated for each mock catalogue using the simple power law of equation 4.27 with $r_0 = 5.0h^{-1}$Mpc, $\gamma = 1.8$ and a maximum possible value of $4\pi J_3(r_c) = 5000h^{-3}\text{Mpc}^3$ (see section 3.3.4). However, the estimates from this weighting scheme are relatively insensitive to the exact values of these parameters used.

The following figures show the mean and 1σ error on ξ assuming that each mock catalogue is a statistically independent estimate of ξ, the error on a single mock catalogue would have to be multiplied by a $\sqrt{n}$ factor (where n is the number of mock catalogues averaged over). For consistency, the mock catalogues from one of the SCDM simulations was left out of this analysis (see section 4.5.1).

For reasons of brevity, only the *redshift* space catalogues are presented here, very similar results were found for the real space catalogues. Therefore, the conclusions of this analysis are **independent** of any real/redshift space effects.

Also, only the results from the *non-uniformly* selected mock catalogues are shown. Again, very similar results were found for the *uniformly* selected mock catalogues. Therefore, constructing the random catalogue according to sampling rate and magnitude limit **does** account for these observational constraints. This will not be discussed further and the *uniformly* selected mock catalogues are no longer considered.

Redshift Space : SCDM Mock Catalogues

The solid line on each of the following plots of ξ shows the actual SCDM redshift space correlation function from figures 4.9 and 4.10. Also, for reasons of graphical clarity the error bars shown are alternately those from the DD/DR, $DD.RR/DR^2$ and $(DD - 2DR + RR)/RR$ estimators.

1. Figures 4.13 and 4.14 show the unweighted ($w = 1$) ξ's calculated using the 3 different estimators on small ($< 10h^{-1}$Mpc) and large ($> 10h^{-1}$Mpc) scales, respectively.

   On small scales, there are no significant differences between the estimates although they are all higher than the actual correlation function by $\sim 1\sigma$. This does not appear to be a significant bias. On large scales, there are no significant differences between the estimates but they are all lower than the actual correlation function by $\sim 2\sigma$. This is tentative evidence for a bias in the unweighted estimates.

2. Figures 4.15 and 4.16 show the weighted ($w = 1/(1 + 4\pi n J_3)$) ξ's calculated using the 3 different estimators on small and large scales, respectively.

   On small scales, there are no significant differences between the estimates and the agreement with the actual correlation function is impressive. On large scales, all the estimates, bar the DD/DR one, agree well with themselves and the actual correlation function. The DD/DR estimate appears biased lower by $\sim 2\sigma$ at every point on large scales.

3. Figures 4.17 and 4.18 show the standard deviation in ξ ($\Delta\xi$) vs s from the 3 unweighted and weighted estimators, respectively. Note that these errors are the standard deviation on an *individual* mock catalogue (ie. $\sqrt{18}$ larger than figures 4.13-4.16).

   These error plots show that the weighted $DD.RR/DR^2$ and $(DD - 2DR + RR)/RR$ estimates have the minimum variance associated with them on large scales. However, on the very large scales, $\sim 100h^{-1}$Mpc, the unweighted $DD.RR/DR^2$ and $(DD - 2DR + RR)/RR$ estimates also have similar errors. It is interesting to note that the DD/DR estimator gives the largest measured variance, with the weighted estimate being worse than the unweighted one on scales larger than $\sim 30h^{-1}$Mpc.

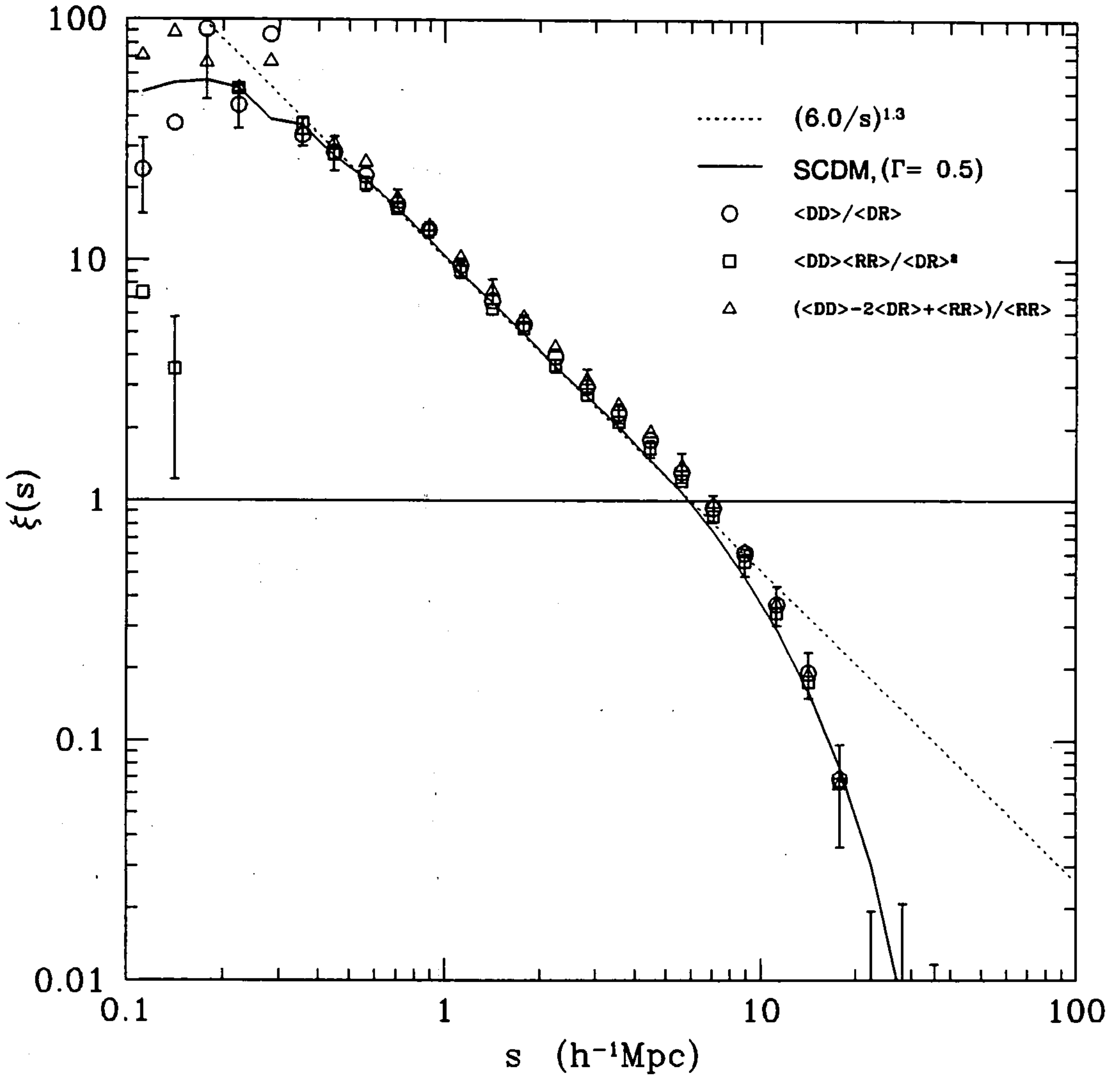

Figure 4.13: The unweighted *redshift* space $\xi(s)$ evaluated from the SCDM mock catalogues using 3 estimators on a log-log plot.

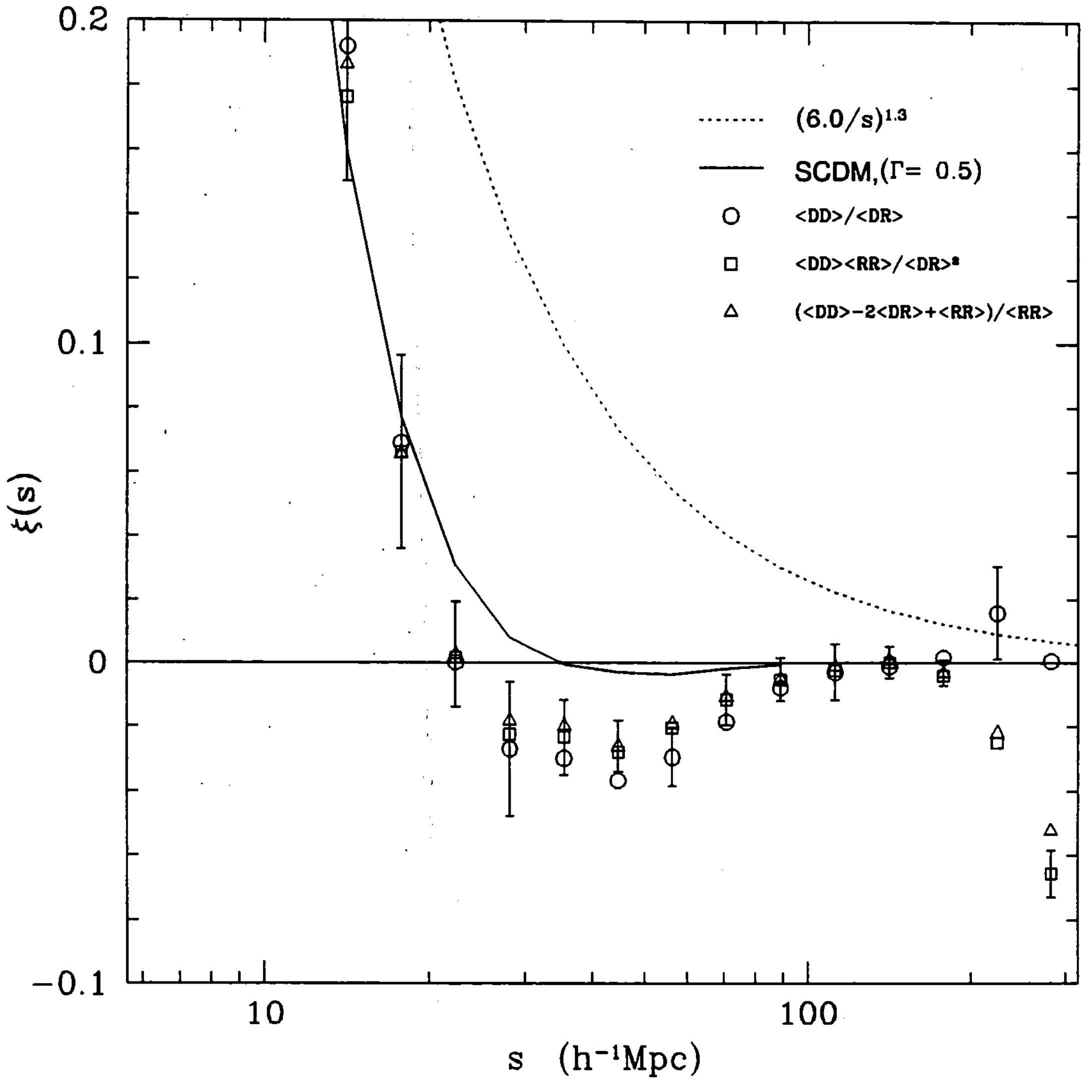

Figure 4.14: The unweighted *redshift* space $\xi(s)$ evaluated from the SCDM mock catalogues using 3 estimators on a log-linear plot.

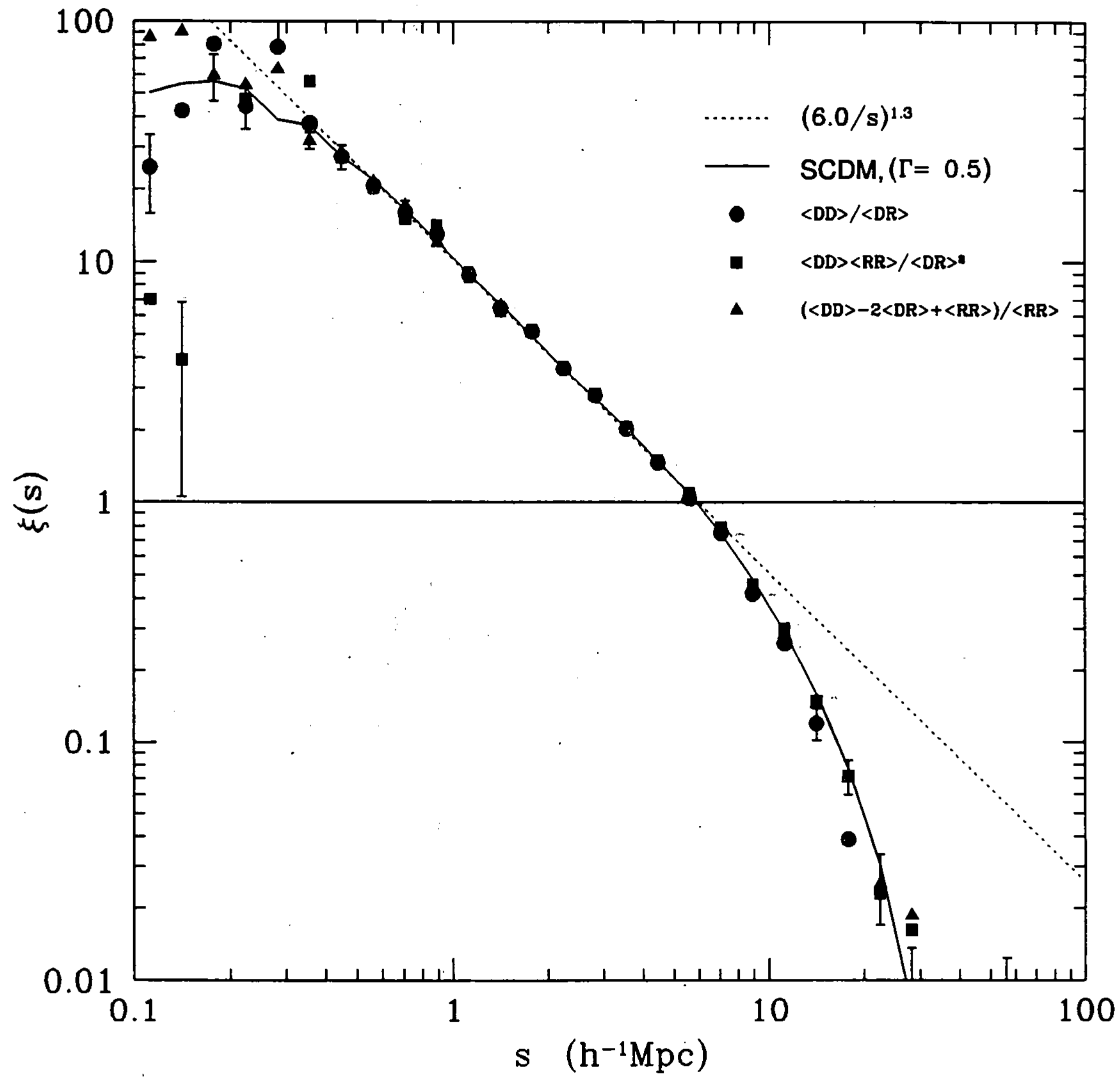

Figure 4.15: The weighted *redshift* space $\xi(s)$ evaluated from the SCDM mock catalogues using 3 estimators on a log-log plot.

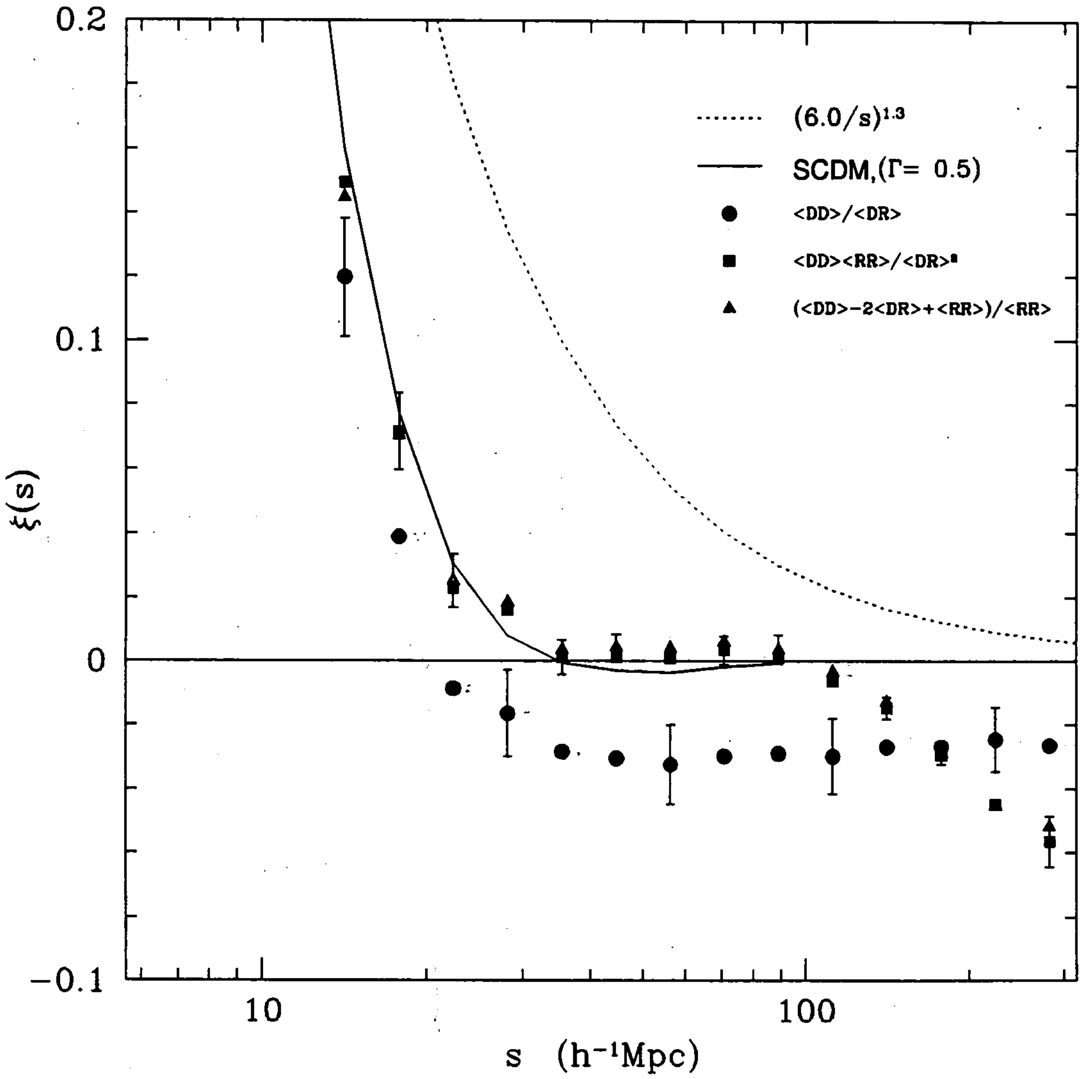

Figure 4.16: The weighted *redshift* space $\xi(s)$ evaluated from the SCDM mock catalogues using 3 estimators on a log-linear plot.

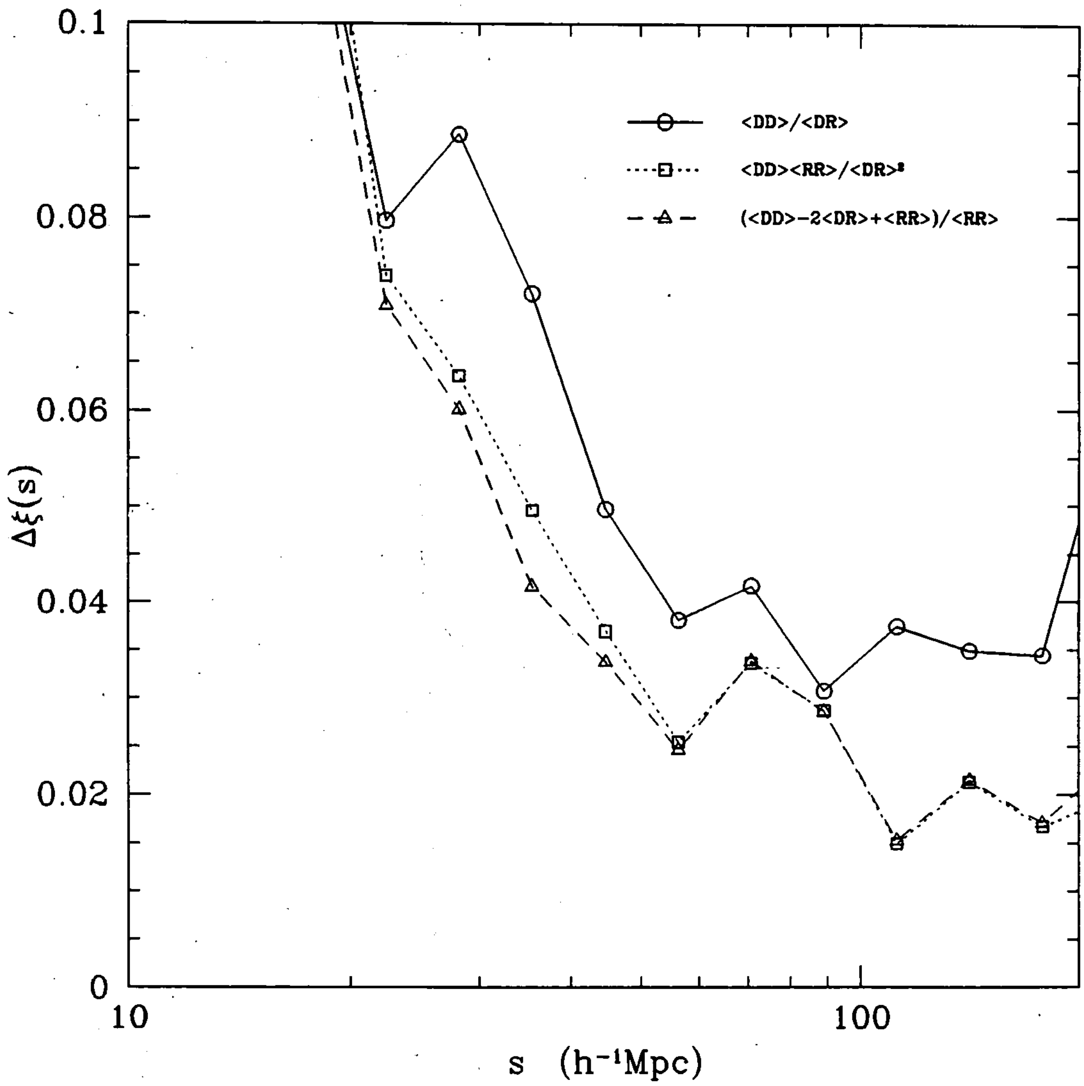

Figure 4.17: The unweighted *redshift* space error estimates, $\Delta\xi(s)$, evaluated from the SCDM mock catalogues using 3 estimators.

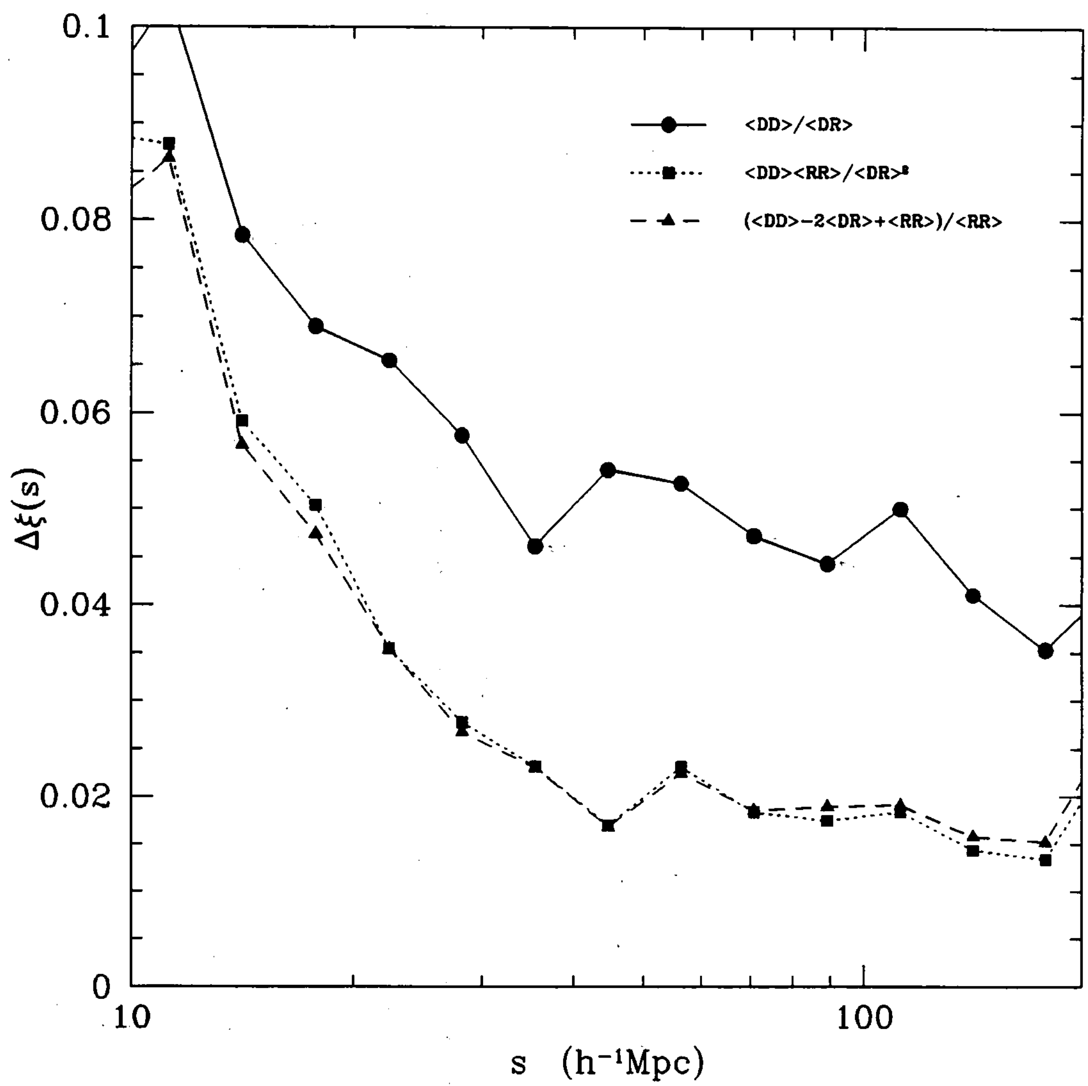

Figure 4.18: The weighted *redshift* space error estimates, $\Delta\xi(s)$, evaluated from the SCDM mock catalogues using 3 estimators.

Redshift Space : LCDM Mock Catalogues

The solid line on each of the following plots of ξ shows the actual LCDM redshift space correlation function from figures 4.11 and 4.12. Again, for reasons of graphical clarity the error bars shown are alternately those from the DD/DR, $DD.RR/DR^2$ and $(DD - 2DR + RR)/RR$ estimators.

1. Figures 4.19 and 4.20 show the unweighted ($w = 1$) ξ's calculated using the 3 different estimators on small ($< 10h^{-1}$Mpc) and large ($> 10h^{-1}$Mpc) scales, respectively.

   On small scales, there are no significant differences between the estimates although they are all lower than the actual correlation function by $\sim 1\sigma$. Again, this does not appear to be a significant bias. On large scales, there are no significant differences between the estimates but they are all biased low by 3-4 σ. This is stronger evidence for a bias in the unweighted estimates.

2. Figures 4.21 and 4.22 show the weighted ($w = 1/(1 + 4\pi n J_3)$) ξ's calculated using the 3 different estimators on small and large scales, respectively.

   On small scales, there are no significant differences between the estimates and the agreement with the actual correlation function is again impressive. On large scales, the DD/DR and $(DD - 2DR + RR)/RR$ estimates are $\sim 1\sigma$ lower and higher, respectively, than the actual correlation function. However, the $DD.RR/DR^2$ estimate is particularly impressive in its agreement with the actual correlation function.

3. Figures 4.23 and 4.24 show the standard deviation in ξ ($\Delta\xi$) vs s from the 3 unweighted and weighted estimators, respectively. Again, these errors are on an *individual* mock catalogue (ie. $\sqrt{15}$ larger than figures 4.19-4.22).

   These error plots show that the weighted $DD.RR/DR^2$ and $(DD - 2DR + RR)/RR$ estimates have the minimum variance associated with them on large scales. These are closely followed by the corresponding unweighted estimates. In fact, on the very large scales, $\sim 100h^{-1}$Mpc, these 2 unweighted estimates have comparable errors to the weighted ones. Overall, the weighted $DD.RR/DR^2$ estimate gives marginally smaller errors than the other weighting/estimator combinations. Also, it is interesting to note that the DD/DR estimator gives the largest measured variance, with the weighted estimate being *far* worse than the unweighted one.

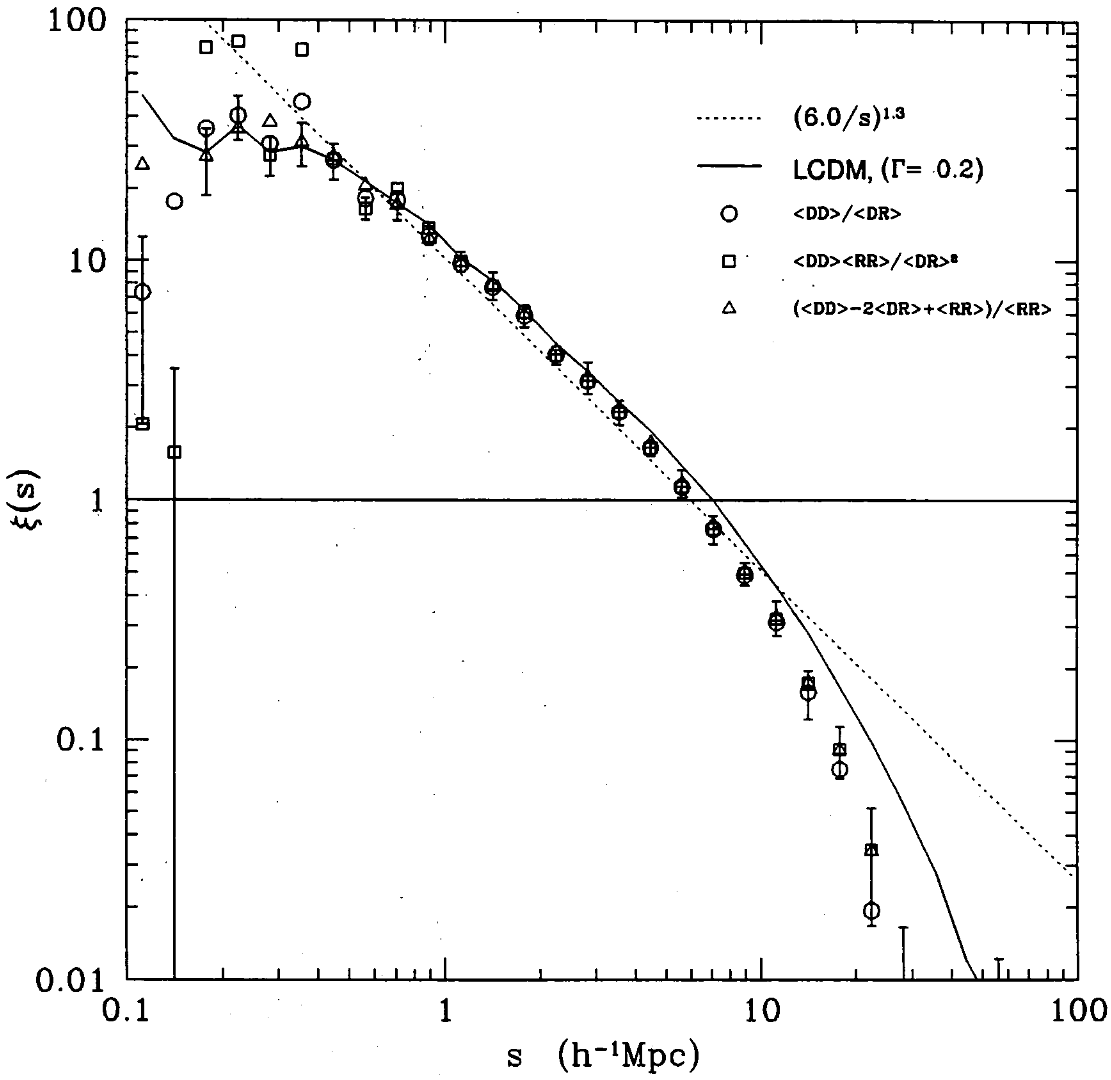

Figure 4.19: The unweighted *redshift* space $\xi(s)$ evaluated from the LCDM mock catalogues using 3 estimators on a log-log plot.

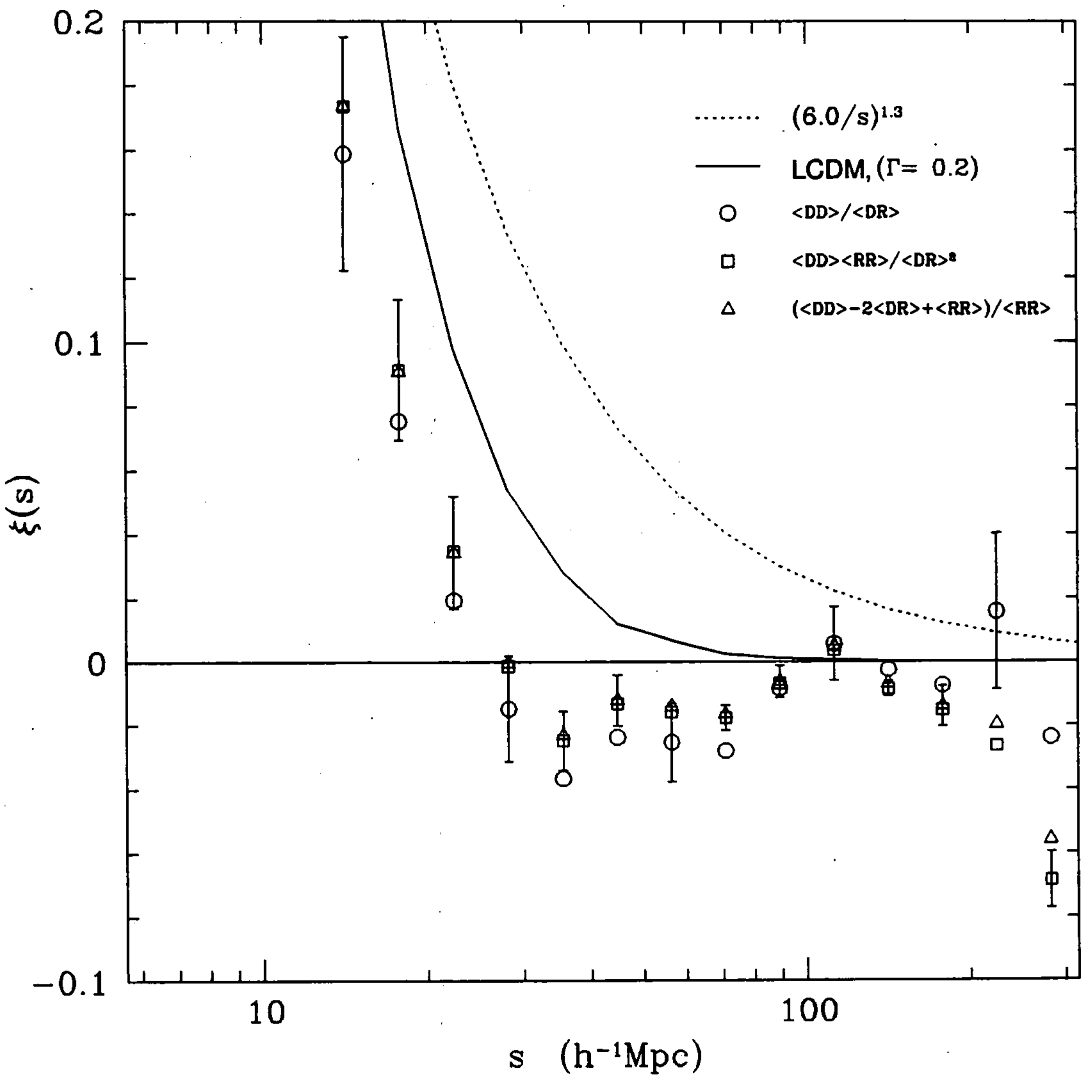

Figure 4.20: The unweighted *redshift* space $\xi(s)$ evaluated from the LCDM mock catalogues using 3 estimators on a log-linear plot.

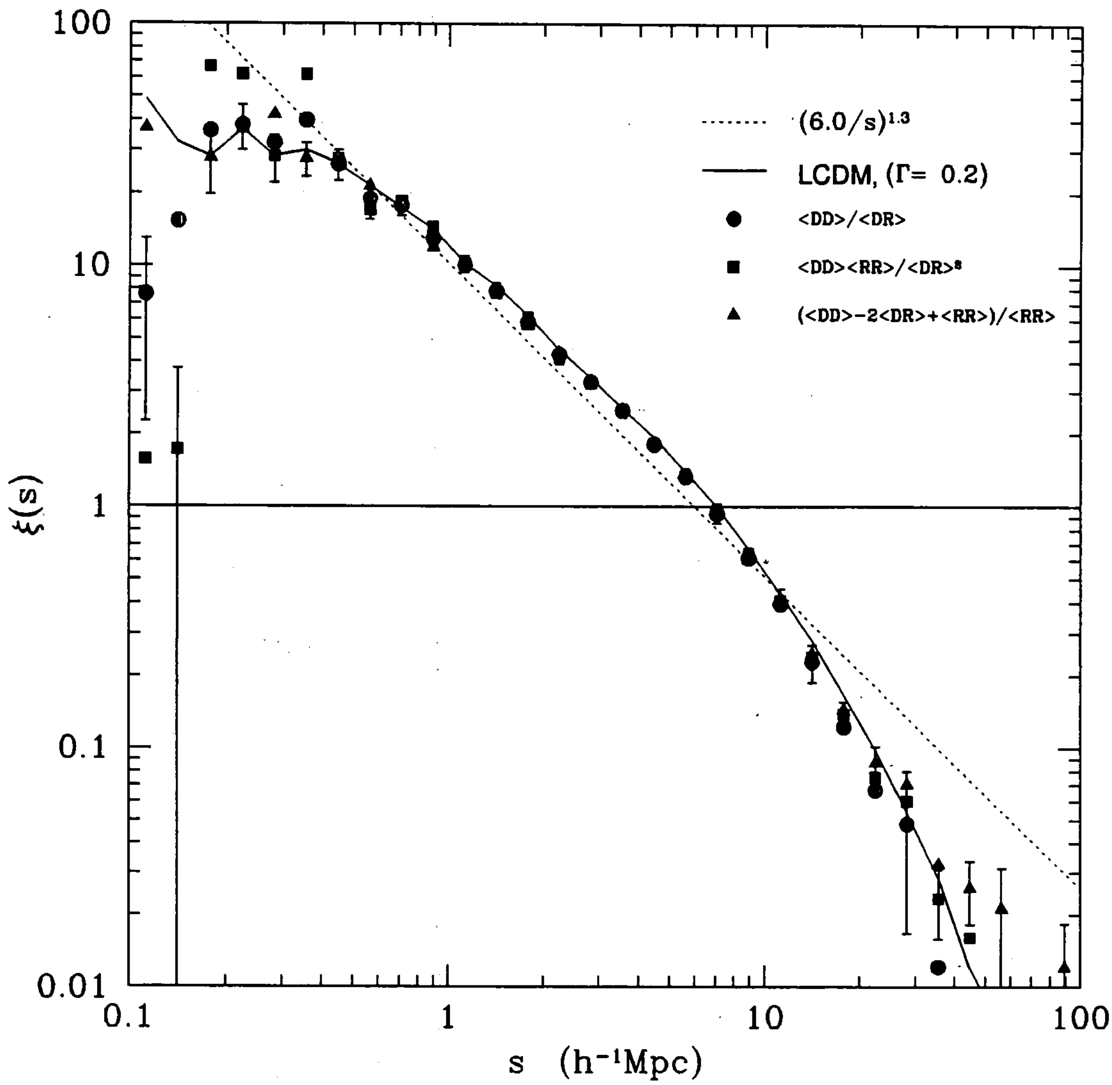

Figure 4.21: The weighted *redshift* space $\xi(s)$ evaluated from the LCDM mock catalogues using 3 estimators on a log-log plot.

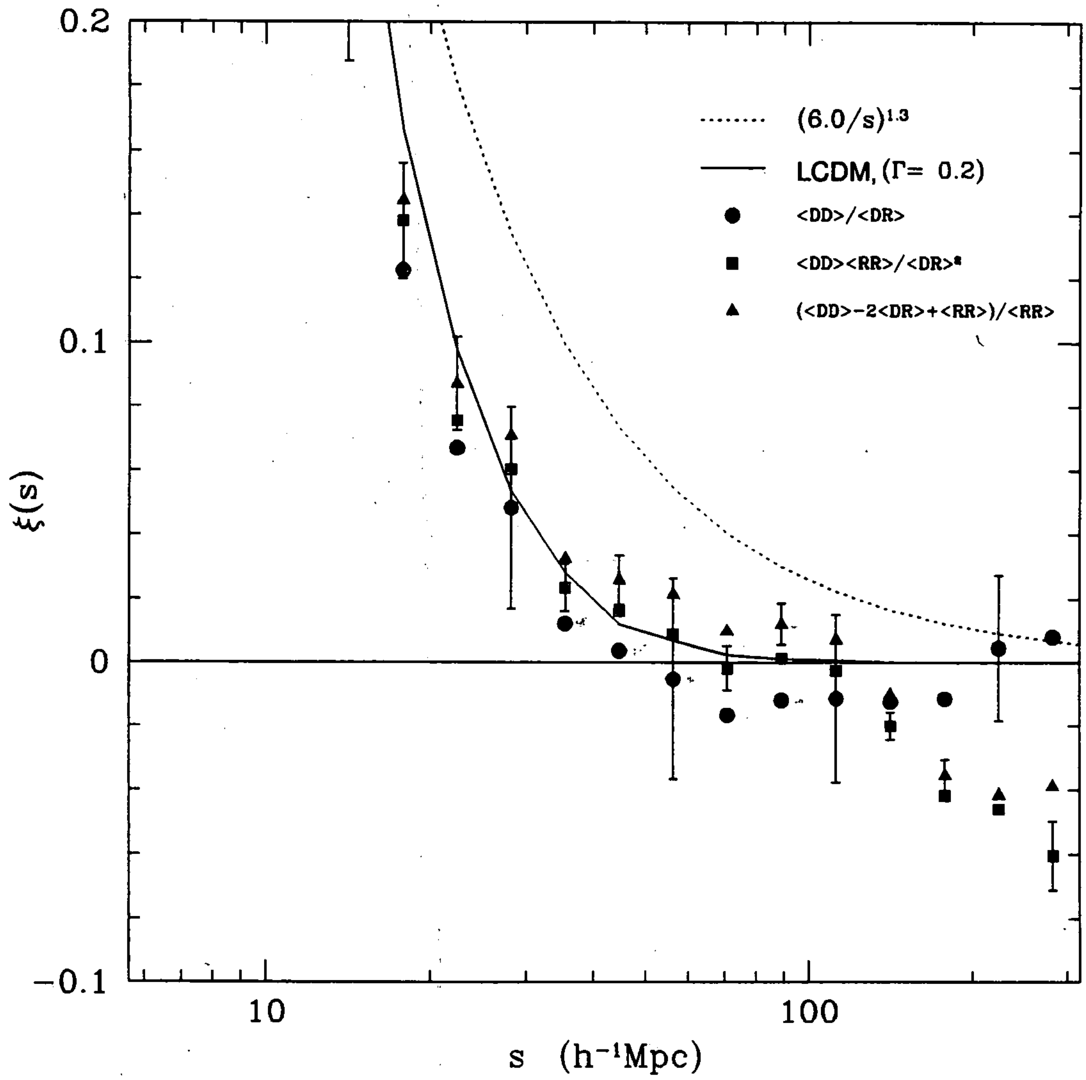

Figure 4.22: The weighted *redshift* space $\xi(s)$ evaluated from the LCDM mock catalogues using 3 estimators on a log-linear plot.

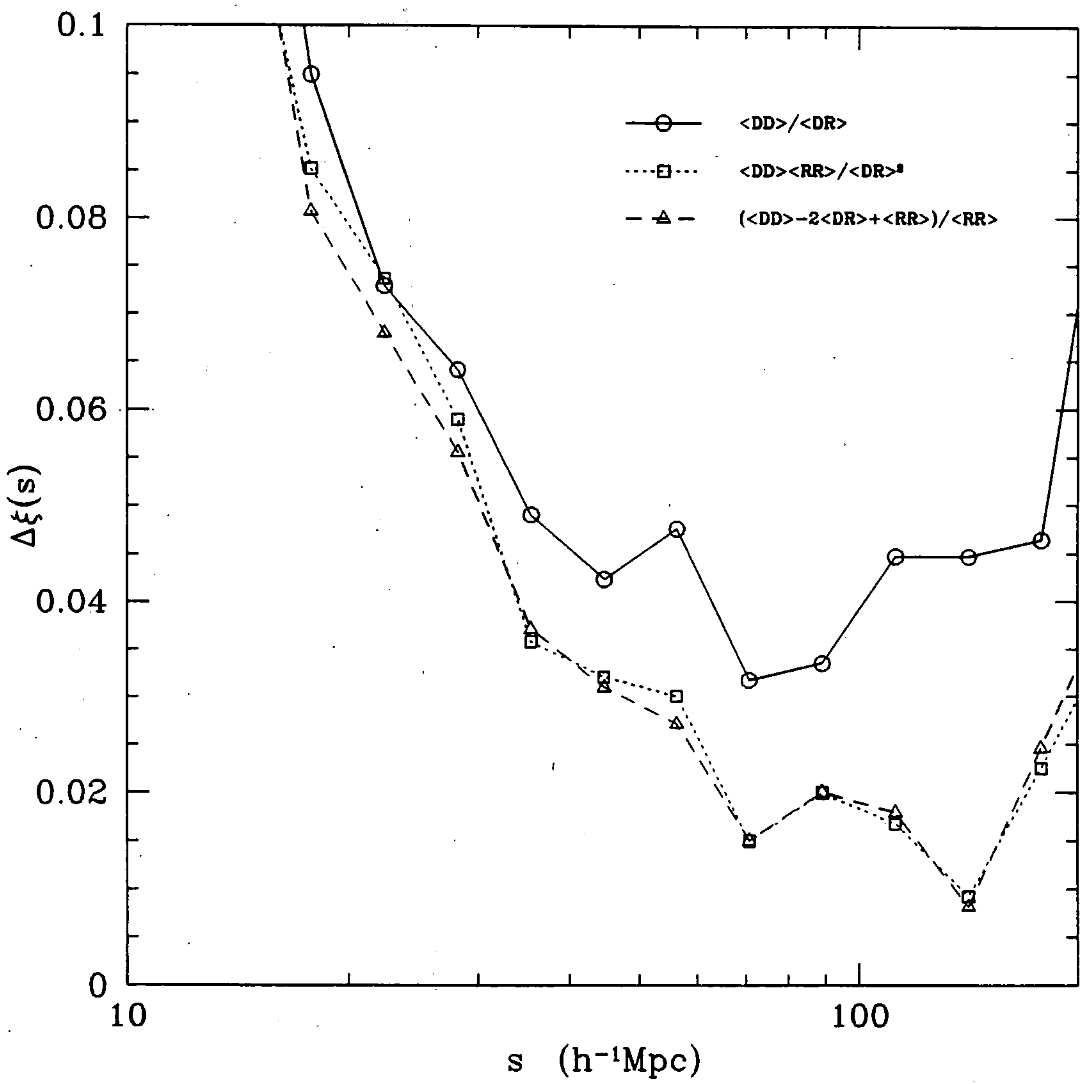

Figure 4.23: The unweighted *redshift* space error estimates, $\Delta\xi(s)$, evaluated from the LCDM mock catalogues using 3 estimators.

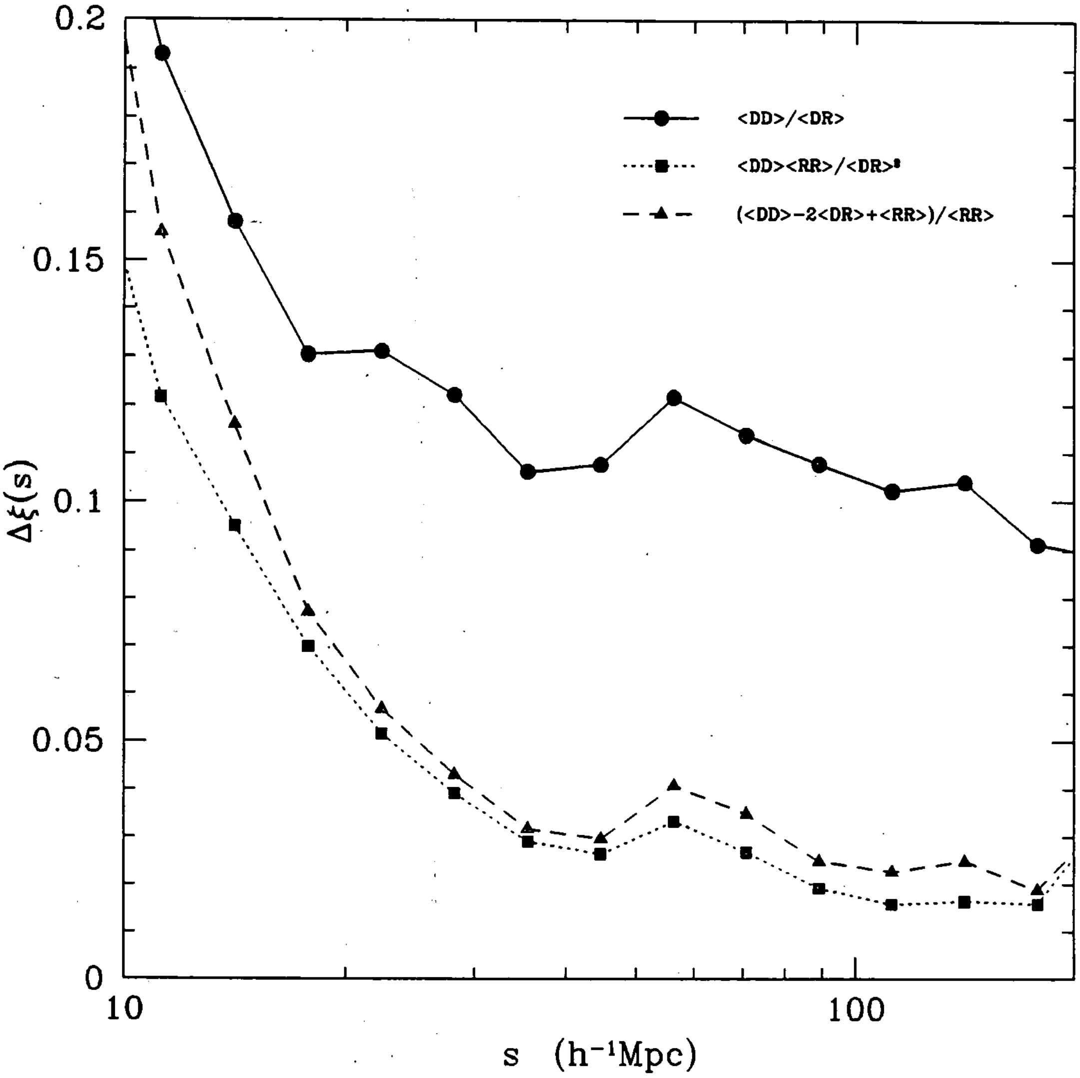

Figure 4.24: The weighted *redshift* space error estimates, $\Delta\xi(s)$, evaluated from the LCDM mock catalogues using 3 estimators.

4.5.3 The Theoretical Error on the 2-Point Correlation Function

The theoretical limit on the errors in the 2-point correlation function was estimated by Peebles (1973) (also see Kaiser, 1986) and is now quoted here. Let the total galaxy number in the survey be n_{gal} and the volume integral of the 2-point correlation function be $J_3(s)$. Now consider a single radial shell with observed galaxy number density $n(r)$, the error in $\xi(s)$ in a wide bin containing N_p galaxy pairs is given by (Peebles, 1973)

$$\Delta\xi(s) = \frac{1 + 4\pi n(r) J_3(s)}{\sqrt{N_p}}, \tag{4.30}$$

assuming that ξ is small ($\ll 1$). This is essentially a $\sqrt{N}$ poisson error taking into account the clustering in the sample. Clustering reduces the amount of independent information available which in turn increases the estimated error. This can be illustrated using the "cluster model" of Peebles (1980) where galaxies are distributed in tight clusters, with n_c members in each cluster, and these clusters are then distributed at random in the survey. In this case, when J_3 reaches its maximum, the $(1 + 4\pi n(r) J_3(s))$ factor is simply the number of galaxies in a cluster (eg. Peebles, 1980) and so the assumption is that, for a large bin, each *cluster* contributes an independent signal and not each *galaxy.*

The maximum values of $4\pi J_3$ seen in the SCDM and LCDM simulations are ~ 7000 and $17000 h^{-3}\mathrm{Mpc}^3$, respectively (see chapter 6). Given that there are $n_{gal} \simeq 2000$ galaxies in each mock catalogue one can estimate the minimum theoretical error to be $\Delta\xi \simeq 0.002$ and 0.007 for the SCDM and LCDM mock catalogues, respectively. These errors assume that $N_p \simeq n_{gal}^2$, namely that the bin is of order the size of the survey, ie. very large indeed ! Experience with the SCDM/LCDM mock catalogues shows that the pair count in the (0.1 lg) bins at large scales is at least a factor of 5 fewer than n_{gal}^2 and more likely to be a factor of 10 in most bins. This implies that a more realistic minimum error is $\Delta\xi \simeq 0.005$ and 0.015 for the SCDM and LCDM mock catalogues, respectively. However, in studies of QSO clustering Shanks and Boyle (1994) have empirically shown that the above approximate $\sqrt{N}$ error works well on scales where $N_p < n_{gal}$. However, when $N_p > n_{gal}$ a more realistic estimate of the error is given by a $\sqrt{n_{gal}}$ type error. In this case both the SCDM and LCDM mock catalogues are limited by n_{gal} and the estimated minimum error is $\Delta\xi \simeq 0.02$. The scale on which N_p reaches n_{gal} is seen to be 5-10h^{-1}Mpc for both sets of mock catalogues and therefore this error should be the limit for scales larger than this.

4.5.4 The Integral Constraint on the 2-Point Correlation Function

The integral constraint (eg. Peebles, 1980) is a systematic error in ξ which is due to the fact that one estimates both the mean density and the pair counts from the same survey. Imagine that one normalises the random catalogue to the have the mean density of the survey, ξ is then constrained to be zero over the whole survey if the weighting scheme used in the pair counting preserves the total pair count in the survey. This would occur when one uses the single pair weighting, $w = 1$, but not necessarily with the "minimum variance" weighting, $w = 1/(1 + 4\pi n(r) J_3)$.

The size of this constraint can be demonstrated with the "cluster model" of Peebles (1980). Consider ξ on separations larger than the size of a cluster but smaller than the size of the survey. Let ΔV be the volume of the spherical shell in question and $\bar{n}$ $(= n_{gal}/V)$ be the mean galaxy density, where V is the volume of the survey. The observed number of DD pairs is then given by

$$DD = n_{gal}\Delta V \left(\frac{n_{gal} - n_c}{V}\right), \tag{4.31}$$

$$= n_{gal}\Delta V \left(\bar{n} - \frac{n_c}{V}\right). \tag{4.32}$$

Basically, starting from a galaxy (and hence a cluster) center has biased this pair count low because the galaxies in this starting cluster cannot be included in the pair count. The RR pair count (or similarly DR) will be

$$RR = n_{gal}\Delta V \bar{n}, \tag{4.33}$$

where the random and data catalogues are assumed to have the same mean densities. Therefore, $\xi = DD/RR - 1$ will be biased low by a constant amount of

$$I_c = n_c/n_{gal}. \tag{4.34}$$

One can derive a more general relation for I_c from the following arguments. Assume that one has an ensemble of surveys to choose from. First consider the relation between the total number of pairs in any one survey and the volume integral over the estimated ξ from that survey. This is simply the total pair constraint on the estimated ξ. Then derive another relation by considering the ensemble variance in the total number of galaxies in each survey and its relation to the true ξ of the ensemble. One can then find the difference between the ensemble average of the ξ's and the true ξ of the ensemble. This is the integral constraint (eg. Peebles, 1980 or Hale-Sutton, 1990)

$$I_c \simeq \frac{(1 + 4\pi n(r) J_3^{\max})}{n_{gal}}, \tag{4.35}$$

and should be added to ξ from an ensemble of surveys.

One can further simplify this formula and its interpretation. Consider the approximation

$$n(r) \simeq n_{gal}/V_{eff}, \tag{4.36}$$

where V_{eff} is the effective volume of the survey

$$V_{eff} = \int_V f(r)dV, \tag{4.37}$$

and $f(r)$ is a function which depends on how the galaxies are weighted. For example, single pair weighting, $w = 1$, will have $f(r) = S(r)$, whereas volume weighting, $w = 1/S(r)$, will have $f(r) = 1$. Equation 4.35 then becomes

$$I_c \simeq \frac{1 + 4\pi(n_{gal}/V_{eff})J_3^{\max}}{n_{gal}}, \tag{4.38}$$

$$\simeq \frac{4\pi J_3^{\max}}{V_{eff}}, \tag{4.39}$$

where the second approximation assumes that $4\pi n(r) J_3^{\max} \gg 1$. For a typical mock catalogue one calculates $V_{eff} \sim 2 \times 10^5 h^{-3}\mathrm{Mpc}^3$ for $w = 1$ and $4 \times 10^6 h^{-3}\mathrm{Mpc}^3$ for $w = 1/S(r)$. Recalling the maximum values of $4\pi J_3$ quoted in section 4.5.3 one finds that for volume weighting of galaxies $I_c \simeq 0.002$ and 0.004 for the SCDM and LCDM mock catalogues, respectively. However, for single pair weighting of galaxies $I_c \simeq 0.035$ and 0.085 for the SCDM and LCDM mock catalogues, respectively. Therefore, the integral constraint is not thought to be a problem (for surveys of similar size and clustering characteristics to the SCDM/LCDM mock catalogues) on scales much larger than those where J_3 converges or reaches a maximum if one weights volumes equally. However, a significant bias could occur on these scales if a single pair weighting is used. This is dicussed further in section 4.5.5.

4.5.5 The Optimal Estimate of the 2-Point Correlation Function and General Discussion of the Estimates

Section 4.5.3 showed that, from a theoretical point of view, due to the relative amounts of clustering, the SCDM mock catalogues should have smaller errors than the LCDM mock catalogues at large scales, $> 10h^{-1}$Mpc. Also, it was seen that this minimum theoretical error was more than likely to be an underestimate of the minimum observed error. These two features can be tested by comparing figures 4.17 and 4.18 (SCDM errors) with figures 4.23 and 4.24 (LCDM errors). For the unweighted estimates $\Delta\xi_{LCDM} \simeq \Delta\xi_{SCDM}$, contrary to the above statement. However, for the weighted estimates this prediction is correct and $\Delta\xi_{LCDM} > \Delta\xi_{SCDM}$ until very large scales, $> 100h^{-1}$Mpc. In general these figures also show that all the errors asymptote towards $\Delta\xi \simeq 0.02$ on large scales, in good agreement with the $\sqrt{n_{gal}}$ error.

Similarly, section 4.5.4 described how the relative amounts of clustering and effective volume of space surveyed (which depends on the weighting scheme in the calculation of ξ) all affect the magnitude of the estimated integral constraint. It was shown that while I_c can be neglected for a weighting scheme which treats volumes equally it could cause a significant bias in a weighting scheme which weights galaxies equally. This bias was also shown to be larger for the LCDM mock catalogues than for the SCDM mock catalogues because the J_3^{max} value is higher for LCDM than for SCDM. The first of these predictions can be tested by looking at figures 4.16 (weighted SCDM) and 4.22 (weighted LCDM). One immediately sees that these weighted estimates are not significantly biased on large scales (bar the DD/DR one, see below) and hence the first prediction is correct. To check the second prediction one can compare figures 4.14 (unweighted SCDM) and 4.20 (unweighted LCDM). On large scales, $> 10h^{-1}$Mpc, the SCDM mock catalogues lie 0.02-0.03 below the actual ξ for this model. Similarly, the LCDM mock catalogues are 0.05-0.10 below the model ξ. These numbers are in very good agreement with the predictions of ~ 0.035 and 0.085 for the SCDM and LCDM mock catalogues, respectively, from section 4.5.4. Therefore, the second prediction is also correct and the integral constraint does appear to be a problem for the unweighted estimates. Finally, these figures do show that the LCDM mock catalogues have a larger bias than the SCDM mock catalogues.

The question one would like to answer is, "What is the weighting and estimator that produces the minumum variance and bias in ξ ?" First consider the small scales, $< 10h^{-1}$Mpc. All 3 estimators, regardless of weighting, can reproduce the actual correlation function within 1σ (using the corresponding estimator's error). The errors seen in the weighted estimates are all of a similar magnitude but are smaller than the unweighted ones by a factor of 2-3 in this region. Second consider the large scales, $> 10h^{-1}$Mpc. The results are split between the unweighted and weighted estimates. For the SCDM mock catalogues the unweighted estimates show slight evidence for a systematic lowering of ξ by 0.02-0.03, at the 2σ level, on scales ~ 10-$50h^{-1}$Mpc. As discussed above, this is thought to be due to the integral constraint. This bias appears larger (3-4 σ) in the LCDM mock catalogues, which have more large scale power (and consequently a larger J_3^{max}), and ξ is measured low by 0.05-0.10. Again, this is thought to be due to the integral constraint. Considering the weighted estimates from the SCDM mock catalogues one sees that they all accurately trace the actual correlation function within 1σ, bar the DD/DR estimate (see next paragraph). This is confirmed with the LCDM mock catalogues where even the DD/DR estimate is within 1σ, albeit using substantially larger error bars. Finally, the errors in the weighted estimates are smaller than the corresponding ones in the unweighted estimates until very large scales, $> 100h^{-1}$Mpc, where they all asymptote towards $1/\sqrt{n_{gal}}$. Note that the weighted $DD.RR/DR^2$ estimate gives the smallest error of all and also most accurately reproduces the actual correlation function for both the SCDM and LCDM mock catalogues. Therefore, the conclusion must be that the weighted $DD.RR/DR^2$ estimate produces the best results (minimum variance and least bias) on both small and large scales.

The DD/DR estimator deserves a discussion on its own because of its use by many workers for over a decade. Theoretically it has been claimed that the $w = 1/(1 + 4\pi n J_3)$ weighting produces the minimum variance in ξ (Efstathiou, 1988, Peebles, 1973 and Loveday *et al.* 1995b) and is therefore used by the majority of workers in the field (eg. Saunders *et al.* 1991, Loveday *et al.* 1992a and Fisher *et al.* 1994). However, Fong *et al.* (1991) carried out an empirical study of the effects of different weightings on pencil beam galaxy redshift surveys and came to the conclusion that the unweighted estimate produced the minimum variance in ξ. Of course, since the $DD.RR/DR^2$ and $(DD - 2DR + RR)/RR$ estimators were not published until 1993, the Fong *et al.* (1991) study used the simple DD/DR estimator. It is interesting to see that figures 4.17, 4.18, 4.23 and 4.24 confirm this result, namely that, for the DD/DR estimator, the unweighted estimate produces the minimum variance in ξ and arguably the least bias as well. A possible explanation for why the weighted DD/DR errors are larger than the unweighted ones is now suggested. The $w = 1/(1 + 4\pi n J_3)$ weighting produced the minimum variance in ξ for the $DD.RR/DR^2$ and $(DD - 2DR + RR)/RR$ estimators but not the DD/DR estimator. Hamilton (1993) has shown that the DD/DR estimator is sensitive to the error in the mean density whereas the $DD.RR/DR^2$ and $(DD-2DR+RR)/RR$ estimators are sensitive to the square of the error in the mean density. All of the unweighted estimates suffer from the fact that they are constrainted to be zero over the whole survey (because of the normalisation and conservation of pair counts) and therefore must lose some variance due to this fact. This need not happen for the weighted estimates. A possible explanation for the above effect with the DD/DR estimator is that the error in the mean density dominates these DD/DR estimates, with the unweighted one missing some variance compared to the weighted one due to this normalisation technique. Therefore, this would not be seen in the other 2 estimators, which are less sensitive to the error in the mean density, and the $w = 1/(1 + 4\pi n J_3)$ weighting does indeed produce the minimum variance. Unfortunately, this argument cannot explain why the weighted DD/DR estimate appears biased low on large scales, particularly for the SCDM mock catalogues.

4.6 Conclusions

This chapter has attempted to address some of the problems that occur in trying to estimate the 2-point correlation function, ξ, from a magnitude limited survey. Two sets of mock catalogues, drawn from SCDM and LCDM N-body simulations, have been analysed using 6 different weighting/estimator combinations for estimating ξ. The conclusions (which were independent of real/redshift space) are given below :

(a) The non-uniform magnitude limits and sampling rates (due to observational constraints) **are** effectively corrected for using the method of evaluation of the pair counts described in section 4.5.2.

(b) The minimum theoretical error on ξ is estimated to be **smaller** than a realistic minimum error which comes from an empirical relation found by Shanks & Boyle (1994). This realistic minimum error is **confirmed** by almost all of the mock catalogues where $\Delta\xi \rightarrow 1/\sqrt{n_{gal}}$.

(c) The integral constraint is introduced and is then estimated for the mock catalogues. For surveys similar to these mock catalogues the integral constraint should **not** be a problem **if** one volume weights the survey. However, single pair weighting of galaxies **reduces** the effective volume of the survey and is thought to cause the systematic offset seen in the unweighted estimators on scales $\sim$ 10-50h^{-1}Mpc.

(d) On small scales, $< 10h^{-1}$Mpc, all the estimators can reproduce the actual correlation function within 1-2 σ. However, the **weighted**, $w = 1/(1 + 4\pi n J_3)$, estimates (Efstathiou, 1988), especially the estimators of Hamilton (1993) and Landy & Szalay (1993), have **smaller** errors than the corresponding unweighted, $w = 1$, estimates (by a factor of 2-3).

(e) On large scales, $> 10h^{-1}$Mpc, the **unweighted** estimates are biased low because of the integral constraint. This effect is larger for models with larger values of J_3^{max}. Therefore, this will be important if one is trying to detect power in the 2-point correlation function on large scales using unweighted estimates. However, the **weighted** estimates do **not** suffer from any such problems, bar the standard estimator, and the $DD.RR/DR^2$ estimator proposed by Hamilton (1993) is the **most** reliable and also has the **least** scatter associated with it. Contrary to what might have been expected, the standard estimator shows more scatter with a weighting than without, this **could** be due to a combination of errors in the mean density and the normalisation used.

Chapter 5

Galaxy Clustering via the 2-Point Correlation Function

5.1 Introduction

The 2-point correlation function, $\xi(x)$, was introduced in chapter 4 as a statistical measure of clustering. The optimal method of estimating ξ was empirically determined for a magnitude limited survey using mock catalogues of the Durham/UKST galaxy redshift survey constructed from N-body simulations. These methods are now applied to the Durham/UKST galaxy redshift survey.

The format of the chapter is as follows. The redshift space correlation function is presented and compared with that from other data sets as well as two theoretical models of structure formation. Various checks of possible systematic errors in this estimate are also shown. The projected correlation function is then presented, modelled and inverted to obtain the real space correlation function using a new application of the Richardson-Lucy algorithm. The forms of the real and redshift space correlation function are then briefly discussed. The chapter ends with the main conclusions obtained from this analysis of the Durham/UKST survey.

5.2 The Redshift Space Correlation Function

Any catalogue which uses redshifts to estimate distances will suffer from the effects of galaxy peculiar velocities. The *real* space correlation function of the galaxy distribution, $\xi(r)$, is the object that is directly predicted from theories of structure formation. However, only the *redshift* space correlation function, $\xi(s)$, is directly observable from a redshift survey. It is known that the distortions produced in redshift space can be used to determine certain important cosmological parameters; this will be expanded on in chapter 6. In calculating the *redshift* space correlation function, $\xi(s)$, the redshift space separation, s, between two galaxies is used. This is defined by the redshift distances s_i and s_j and angular separation on the sky, θ, namely

$$s = \sqrt{s_i^2 + s_j^2 - 2s_i s_j \cos\theta}. \tag{5.1}$$

This therefore assumes a spatially flat ($k = 0$) cosmological model with Euclidean geometry ($\Lambda = 0$), consistent with sections 2.9 and 3.3.

5.2.1 Method of Calculation

In this chapter all correlation functions were estimated using the techniques described in chapter 4, ie. the radial and angular selection functions were used to produce a random catalogue which was then used for cross correlation with the data catalogue. Also, the estimator which produced the most accurate and consistent results, namely that of Hamilton (1993), was used to determine ξ but the estimates with both weighted ($w = 1/(1+4\pi\bar{n}S(x)J_3(s))$) and unweighted ($w = 1$) pair counts are shown for absolute clarity.

5.2.2 Results from the Durham/UKST Galaxy Redshift Survey

Figures 5.1 and 5.2 show the results of the Hamilton (1993) estimator for ξ (with and without a weighting) on small and large scales, respectively. The error bars come from splitting the survey into 4 roughly equal quadrants and assume that each quadrant provides an independent estimate of the correlation function. This assumption should be valid on all but the largest scales where the wavelength of the perturbation becomes comparable to the size of the quadrant itself.

On small scales, $< 10h^{-1}$Mpc, figure 5.1 shows that the unweighted estimate is systematically $\sim 30\%$ below the weighted estimate. As will be discussed in section 5.2.5 this inconsistency could not be traced to a systematic problem in the survey, quite simply it is due to the different weighting used. Therefore, the cause of this effect remains unknown but statistical fluctuations could be partially responsible. On large scales, $> 10h^{-1}$Mpc, figure 5.2 shows that the unweighted estimate is consistent with zero by scales of $\sim 20h^{-1}$Mpc while the weighted estimate continues its approximate power law form out to $\sim 40h^{-1}$Mpc. The unweighted estimate is again systematically low, this time by 0.1-0.3 in ξ until $\sim 40h^{-1}$Mpc. Again, this is could not be traced to any systematic problem in the survey. It is more than likely that this effect is a combination of the integral constraint and statistical fluctuations. It was shown in chapter 4 that the integral constraint could cause a systematic lowering of ξ. Using equation 4.39 and the estimate of J_3^{max} from chapter 6 one finds that the integral constraint could be as large as ~ 0.2 for the Durham/UKST survey when using a unweighted estimate. Such a number could explain almost all of the

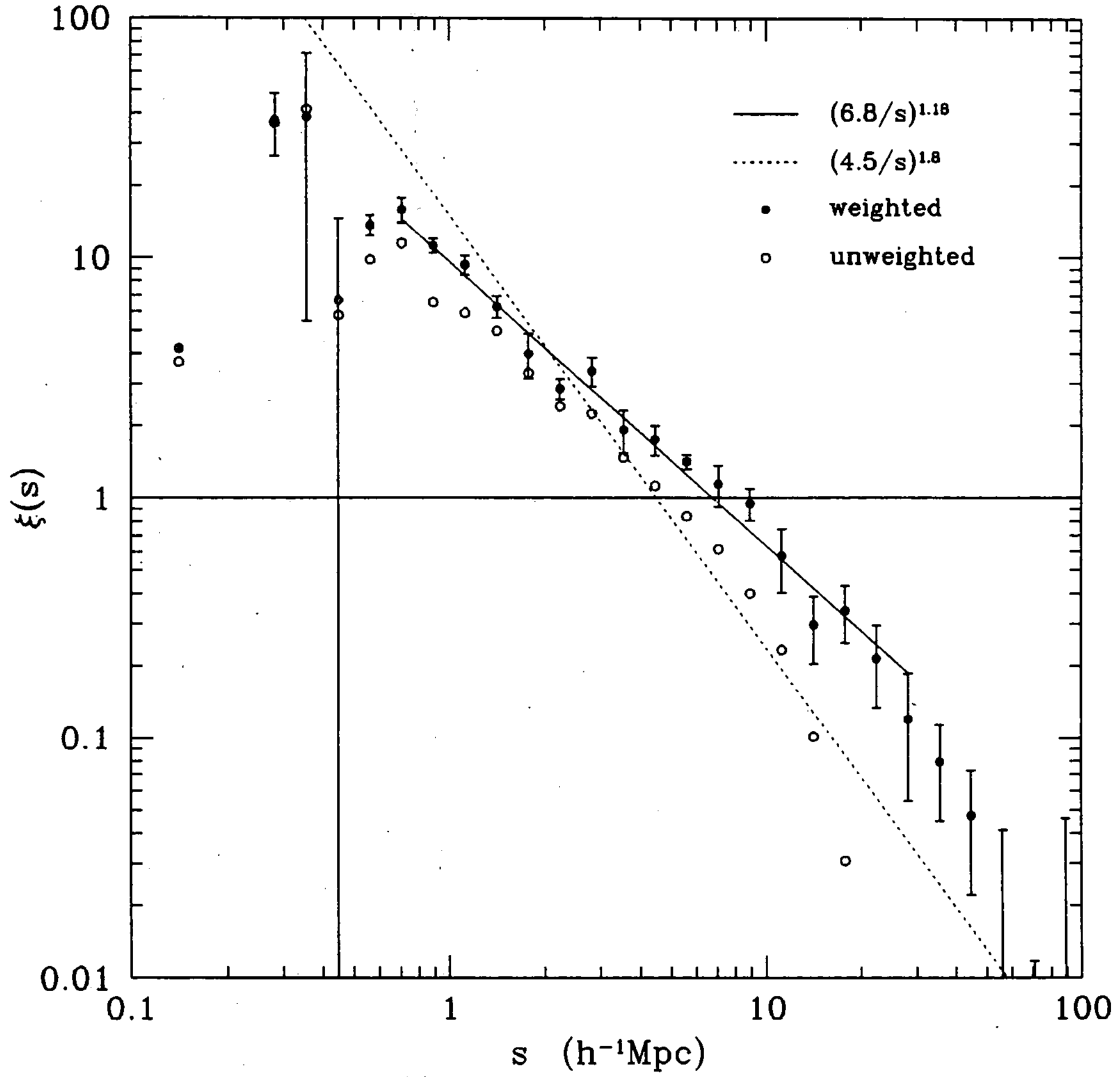

Figure 5.1: The *redshift* space $\xi(s)$ evaluated directly from the Durham/UKST survey using the estimator of Hamilton (1993) on a log-log plot.

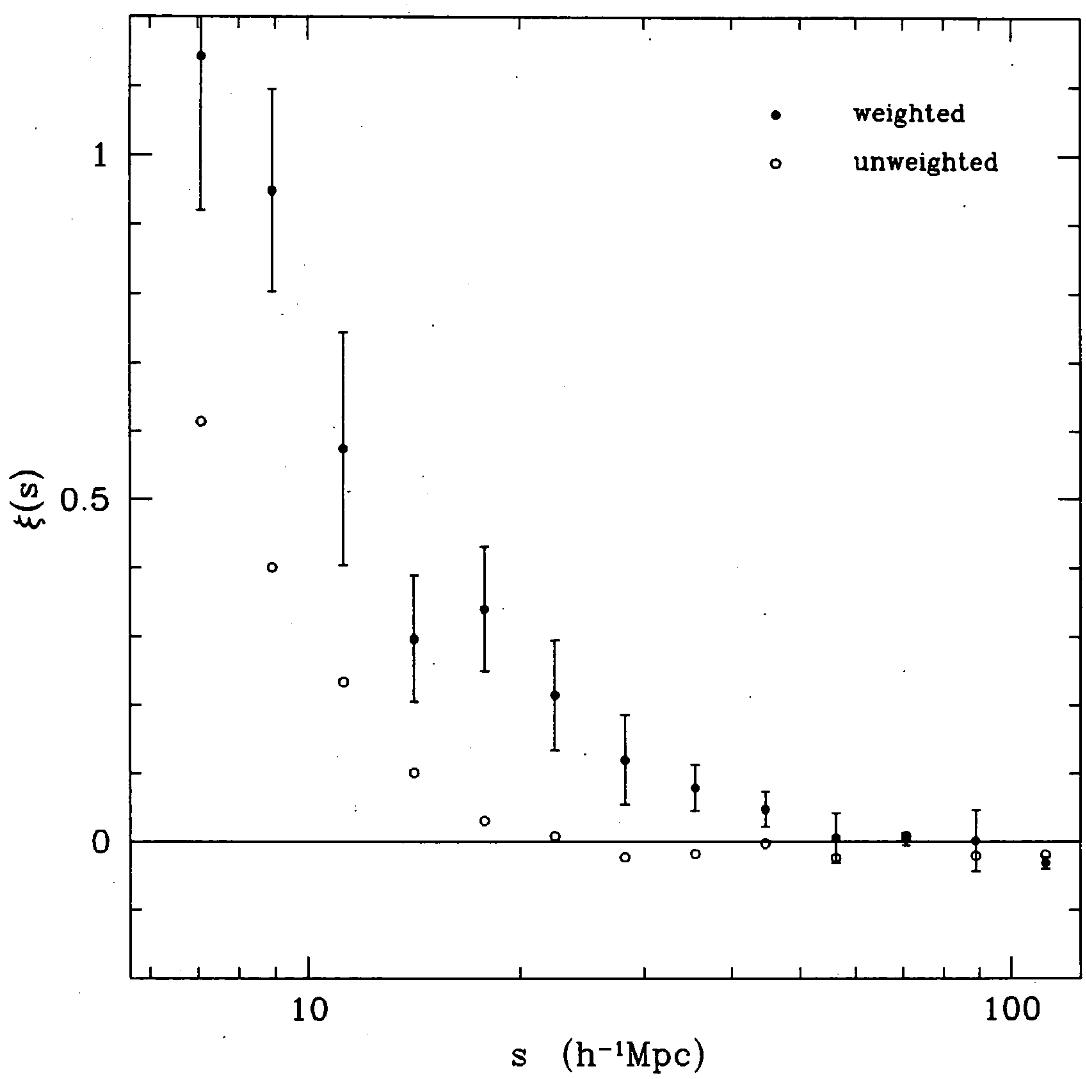

Figure 5.2: The *redshift* space $\xi(s)$ evaluated directly from the Durham/UKST survey using the estimator of Hamilton (1993) on a log-linear plot.

N	χ^2	Prob.	s_0 (h^{-1}Mpc)	γ
16	23.1	0.11	$6.8 \pm 0.3 h^{-1}$Mpc	1.18 ± 0.04

Table 5.1: Minimum χ^2 fit to a single power law model for the Durham/UKST survey $\xi(s)$.

observed difference between the weightings on large scales. On the very large scales, $> 50h^{-1}$Mpc, both estimates are consistent with zero.

The weighted estimate is relatively insensitive to the absolute value of the weighting used as halving or doubling the value of the mean density ($\bar{n}$) used in the $w = 1/(1 + 4\pi\bar{n}S(x)J_3(s))$ weighting makes little difference to the estimate itself. This may have been expected given that Fong *et al.* (1991) found that only small values of m (≤ 10), where $w = 1/(1 + mS(x))$, produced any significant effect on ξ or its variance. The $w = 1/(1 + 4\pi\bar{n}S(x)J_3(s))$ weighting has an effective value of $m \sim 500$ on large scales, when J_3 has reached a maximum ($\sim 5000h^{-3}\mathrm{Mpc}^3$), and therefore halving or doubling this number makes little difference.

To aid a comparison with other surveys a power law fit has been calculated for the weighted estimate of ξ where

$$\xi(s) = \left(\frac{s_0}{s}\right)^{\gamma}. \tag{5.2}$$

A minimum χ^2 fit is attempted in the region $[0.7, 30.0]h^{-1}$Mpc and the results of this fit are relatively insensitive to the scales one fits over. One should sound a word of caution about the significance of these fits due to the non-independent nature of the $\xi(s)$ points. A principal component analysis (eg. Kendall, 1975) was considered but not deemed necessary for such a simple first analysis as this.

Table 5.1 shows the best fit values for s_0 and γ along with the individual 1σ error estimates in each parameter. These errors come from the $\Delta\chi^2 = 1.0$ contour in the individual confidence regions of each parameters. As can be seen in table 5.1 and figure 5.1 a single power law does not give a particularly good fit to the finer details of ξ (see section 5.5). However, $\xi(s)$ does appear to be an approximate power law in this regime. Also shown in figure 5.1 is a power law with the canonical values of $r_0 = 4.5h^{-1}$Mpc and $\gamma = 1.8$ (eg. Peebles, 1980). It is quite obvious that this is a very poor fit to the observed redshift space $\xi(s)$.

It is worth stating again that the weighting of Efstathiou (1988) and estimator of Hamilton (1993) gave the minimum variance and least bias in the estimate of $\xi(s)$ from chapter 4 and is therefore prefered here as well.

5.2.3 Comparison with other Redshift Surveys

The results of the weighted Durham/UKST $\xi(s)$ from section 5.2.2 are compared with the APM-Stromlo redshift survey of Loveday *et al.* (1992a) (also see Loveday

Survey	Durham/UKST	APM-Stromlo	Las Campanas	DARS/SAAO
s_0 (h^{-1}Mpc)	6.8 ± 0.3	5.9 ± 0.3	6.8 ± 1.1	6.5 ± 0.5
γ	1.18 ± 0.04	1.47 ± 0.12	1.70 ± 0.11	(1.8)

Table 5.2: Comparison of *redshift* space $\xi(s)$ single power law fits for different surveys.

et al. 1995b), the Las Campanas redshift survey of Tucker *et al.* (1995) (also see Lin *et al.* 1995a), and the previous Durham redshift surveys of Shanks *et al.* (1983) and Shanks *et al.* (1989) (DARS/SAAO).

Figures 5.3 and 5.4 show the comparison on small and large scales, respectively. The error bars on the Durham/UKST ξ again come from splitting the survey into 4 roughly equal quadrants as before. On small scales, $< 10h^{-1}$Mpc, the weighted Durham/UKST ξ agrees very well with the other estimates (given the errors involved). On large scales, $> 10h^{-1}$Mpc, the weighted Durham/UKST ξ is also consistent with the previously claimed detections of large scale structure out to $\sim 40h^{-1}$Mpc, albeit $\sim 1\sigma$ higher in the 10-20h^{-1}Mpc range.

This detection of power on scales 10-40h^{-1}Mpc is in disagreement with the previous Durham redshift survey results (DARS/SAAO). This inconsistency is probably partly statistical but also partly due to the weighting and estimator the DARS/SAAO surveys used. The DARS/SAAO $\xi(s)$ used the $w = 1$ weighting and the standard DD/DR estimator. (Note that the relatively new estimators of Hamilton (1993) and Landy & Szalay (1993) did not exist at the time the DARS/SAAO results were published.) It was shown in chapter 4 (see also Fong *et al.* 1991) that the $w = 1$ unweighted DD/DR estimator gave a smaller variance than the corresponding $w = 1/(1 + 4\pi\bar{n}S(x)J_3(s))$ weighted one. Therefore, at that time it was logical to use the unweighted estimates. However, the integral constraint appears to systematically bias the unweighted DD/DR estimate low on scales 10-50h^{-1}Mpc by 0.1-0.2 in ξ for a survey like the Durham/UKST one. For 1-D pencil beam surveys like DARS/SAAO (with a smaller volume and number of galaxies) the integral constraint would be larger and could explain the observed differences.

The best fit power law parameters from the above surveys are compared in table 5.2. It can be seen that the amplitudes, s_0, agree quite well to a value in the range $[6.0, 7.0]h^{-1}$Mpc. However, the slopes, γ, all differ significantly given the quoted errors. (Note that the Durham/UKST errors are likely to be an underestimate due to the simplistic χ^2 fitting procedure and also that the DARS/SAAO slope was fixed to be 1.8 before fitting for s_0.) Therefore, while $\xi(s)$ can be approximated by a single power law, there is considerable scatter in the best fit parameters obtained from the currently available data sets.

Overall, figures 5.3, 5.4 and table 5.2 show that the agreement between the different surveys is good. However, it appears that a simple one power law model does not give a good fit to the data sets.

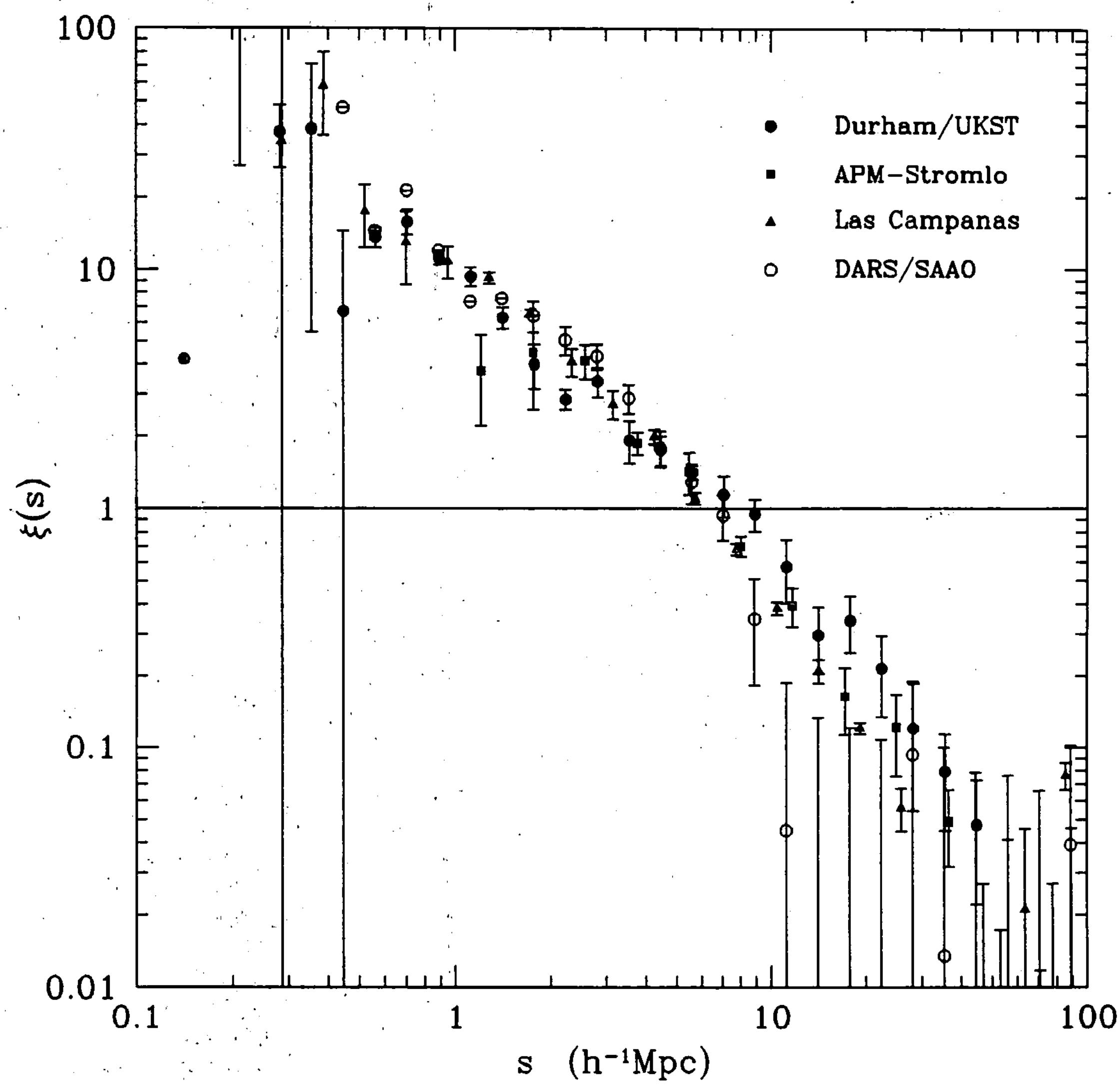

Figure 5.3: Comparison of the Durham/UKST survey $\xi(s)$ with those from other redshift surveys on a log-log plot.

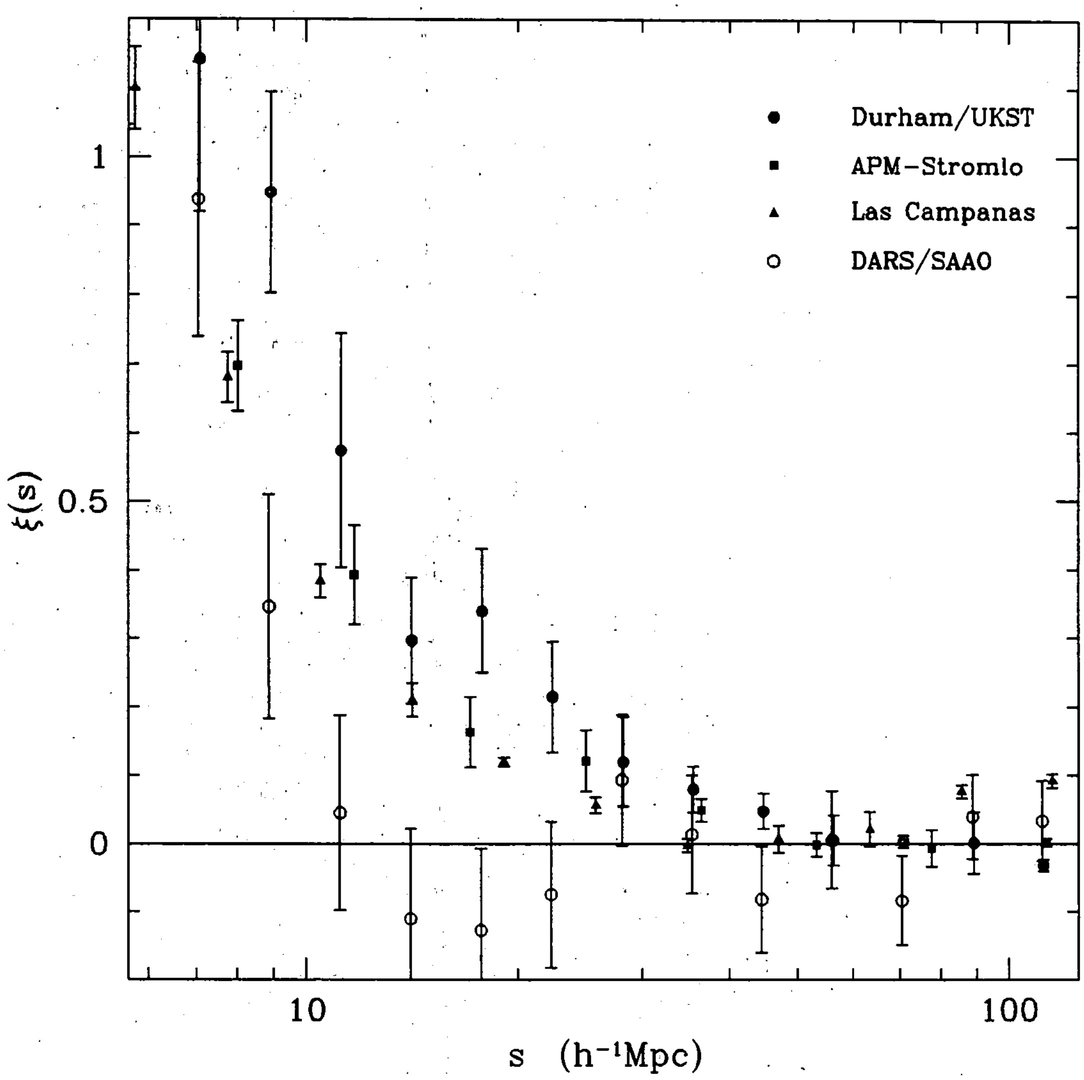

Figure 5.4: Comparison of the Durham/UKST survey $\xi(s)$ with those from other redshift surveys on a log-linear plot.

5.2.4 Comparison with the Simulations

Figures 5.5 and 5.6 show the comparison between the Durham/UKST survey and the SCDM & LCDM mock catalogues on small and large scales, respectively. The mean and standard deviation of the ξ's estimated from each set of mock catalogues can be used to denote a region in ξ. The shaded areas in figures 5.5 and 5.6 denote the 68% confidence regions on an *individual* mock catalogue. The test is to see if the model is consistent with the data and one can ask the question, "How often can the SCDM/LCDM mock catalogues produce the ξ seen in the Durham/UKST survey ?" Therefore, there is no need to plot the Durham/UKST error bars because the interest lies in the scatter seen in the mock catalogues and the difference between them and the data. For consistency, these confidence regions were calculated using the same weighting/estimator combination as the data, namely the estimator of Hamilton (1993) and weighting of Efstathiou (1988) (see figures 4.15, 4.16, 4.21 and 4.22).

On small scales, $< 10h^{-1}$Mpc, both models of CDM give good agreement with the Durham/UKST correlation function (within the errors). On large scales, $> 10h^{-1}$Mpc, the SCDM model shows no significant power above $\sim 20h^{-1}$Mpc whereas the LCDM model shows significant power out to $\sim 30h^{-1}$Mpc. The Durham/UKST correlation function shows power **above and beyond** that of SCDM up to $\sim 40h^{-1}$Mpc at the $> 3\sigma$ level but is more consistent with the LCDM, although even this model produces too little power at the 1-2σ level.

5.2.5 Checking for Systematic Errors

Obviously, any observational result is only as good as the accompanying error analysis. A method such as splitting the survey into quadrants will give a measure of the combined variance from the sample itself and the fluctuations inherent in the Universe (the so-called "Cosmic" variance). However, this does not take into account the possibility of systematic errors occuring. The three systematic errors tested here, when trying to estimate $\xi(s)$, are errors in the photometry zero-points, random errors in the measured redshifts and the variable completeness rates in the survey. Due to lack of space the results of these tests are not shown in graphical form and are simply described.

(i) The photometry for the Durham/UKST survey comes from the Collins *et al.* (1988) EDSGC which is derived from COSMOS scans of UKST plates (see section 2.2). A relatively crude correction in each field is applied, scaling the photometry zero-points to agree with those of the Maddox *et al.* (1990a) APM survey (see section 2.3). Systematic effects are tested for by estimating $\xi(s)$ without any correction and also with twice the correction. On small scales, $< 10h^{-1}$Mpc, the photometry correction makes virtually no difference ($\pm 0.5\sigma$) to either estimate, weighted or unweighted. On large scales, $> 10h^{-1}$Mpc, the photometry correction makes no difference to the unweighted estimate.

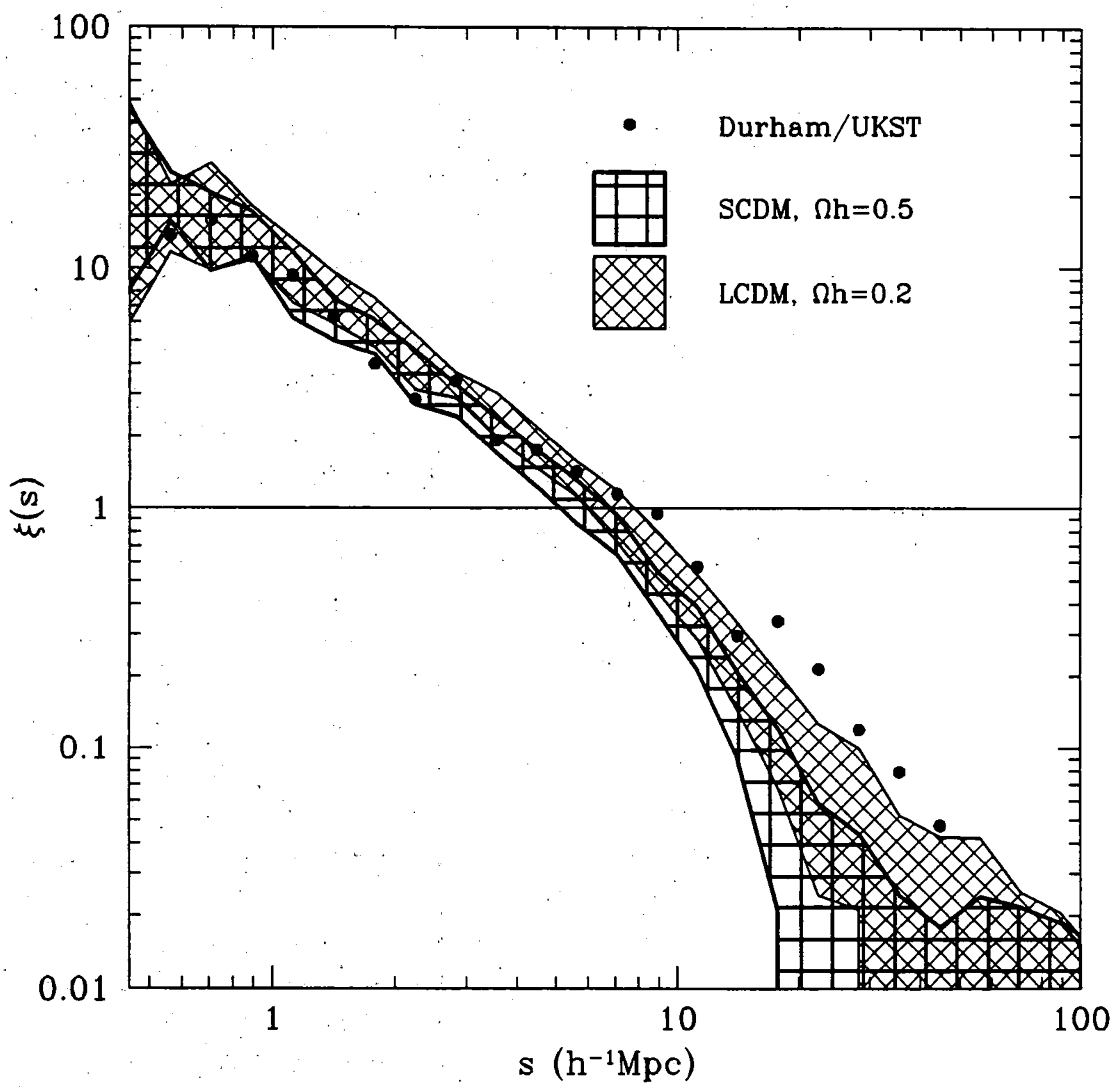

Figure 5.5: Comparison of the Durham/UKST survey $\xi(s)$ with those from the CDM mock catalogues on a log-log plot.

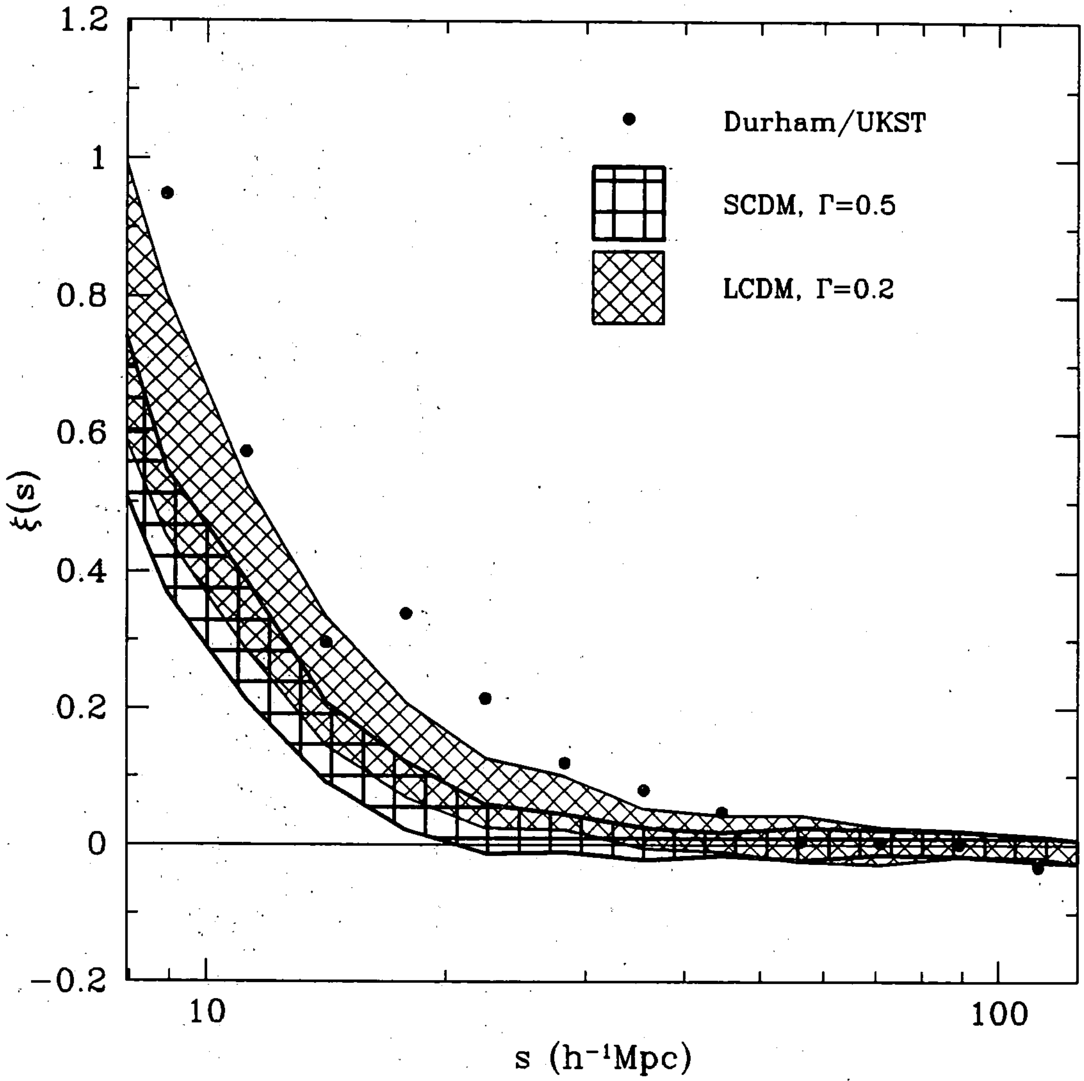

Figure 5.6: Comparison of the Durham/UKST survey $\xi(s)$ with those from the CDM mock catalogues on a log-linear plot.

However, the weighted estimates with the "wrong" correction (either when not applied or applied twice) are systematically higher than the weighted estimate with the "right" correction by $\sim 1\sigma$ at all scales.

(ii) Section 2.6.2 showed that the measured redshifts from the Durham/UKST survey should be correct to $\sim \pm 150$ kms^{-1} with a negligible offset. Systematic effects are tested for by adding a random velocity (from a Gaussian with $\bar{x} = 0$ kms^{-1} and $\sigma_x = 300$ kms^{-1}) to each galaxy and ξ is re-evaluated. These random velocities should overestimate any real effects due to measurement errors. On very small scales, $< 1h^{-1}$Mpc, any power law form is completely smoothed out by the random velocities. On scales 1-6h^{-1}Mpc the power law is flattened slightly ($\gamma \simeq 1.2 \rightarrow 1.1$). On larger scales, $> 6h^{-1}$Mpc, the random velocities have virtually no effect on ξ.

(iii) The completeness rate of the Durham/UKST survey varies as a function of field number and apparent magnitude. Therefore, when calculating the pair counts for estimating ξ, one should ideally weight by the inverse of the completeness rate in each field and apparent magnitude interval. As this is not explicitly accounted for in previously estimates of ξ it is a possible source of systematic error. On small scales, $< 10h^{-1}$Mpc, this correction to the estimation technique makes almost no difference to either estimate, weighted or unweighted. On large scales, $> 10h^{-1}$Mpc, this correction again makes almost no difference to either estimate.

Therefore, the three possible systematic errors considered here appear small and may only affect the results at the 1σ level (at worst). Also, none of these systematic errors were at a level where they can account for the systematic difference seen between the weighted and unweighted estimates.

5.3 The Projected Correlation Function

In section 5.2 the 2-point correlation function was evaluated as a function of one variable – the separation between two galaxies, s. However, one could evaluate ξ as a function of two variables – the separations perpendicular and parallel to the line of sight, σ and π, respectively. Such an object, $\xi(\sigma, \pi)$, will be very useful when studying the distortions which come from using redshifts as distances.

Following Peebles (1980), for example, define a projected correlation function, $w_v(\sigma)$, as follows

$$w_v(\sigma) = \int_{-\infty}^{\infty} \xi(\sigma, \pi) d\pi, \quad (5.3)$$

$$= 2\int_{0}^{\infty} \xi(\sigma, \pi) d\pi. \quad (5.4)$$

As will be shown in section 5.4, this projected correlation function can be used to estimate the real space correlation function.

5.3.1 Modelling the Projected Correlation Function

Due to the projection/integration in equation 5.4 it is possible to write

$$w_v(\sigma) = 2\int_0^{\infty} \xi(\sqrt{\sigma^2+\pi^2})d\pi, \tag{5.5}$$

where $\xi(\sqrt{\sigma^2+\pi^2})$ is the *real* space correlation function. Assuming a power law form of $\xi(r) = (r_0/r)^\gamma$ with $r^2 = \sigma^2 + \pi^2$ the integral in equation 5.5 becomes

$$w_v(\sigma) = r_0^\gamma \left[\frac{\Gamma\left(\frac{1}{2}\right)\Gamma\left(\frac{\gamma-1}{2}\right)}{\Gamma\left(\frac{\gamma}{2}\right)}\right]\sigma^{(1-\gamma)}, \tag{5.6}$$

where $\Gamma(x)$ is the usual Gamma function and $\gamma > 1$ is assumed.

5.3.2 Method of Calculation

Our method of estimating $\xi(\sigma,\pi)$ is the same as the method of section 5.2 but here binning is done as a function of two variables instead of just one. This is described in more detail in chapter 6 which concentrates specifically on redshift space distortions. Figure 5.7 shows a schematic diagram of how σ and π are defined. The mathematical definitions of these variables are given in section 6.2 but the results are fairly insensitive to their exact nature and even the small angle approximation gives quite consistent results.

The estimate of $\xi(\sigma,\pi)$ will become noisy at large scales, therefore for the purpose of evaluating equation 5.4 the integral is truncated at some upper limit, π_{cut}

$$w_v(\sigma) = 2\int_0^{\pi_{cut}} \xi_v(\sigma,\pi)d\pi. \tag{5.7}$$

In practice π_{cut}'s of 20, 30 and $40h^{-1}$Mpc are used. The results are relatively insensitive to the value of π_{cut} chosen. This is not too surprising given that the integral in equation 5.7 weights all separations equally and is therefore sensitive to ξ on small scales where it is very large with respect to its value on other scales. The integral in equation 5.7 is carried out using a simple midpoint integration scheme which is quite adequate given the uncertainties present in $\xi(\sigma,\pi)$.

5.3.3 Tests of the Method

The SCDM mock catalogues are used to test this method. This set of mock catalogues have less large scale power than the LCDM ones, therefore they should provide a more stringent test of the method because on large scales the relative level of signal to noise is lower than that of the LCDM case. In chapter 4 it was seen that the *real* space correlation function for the SCDM simulations could be approximated

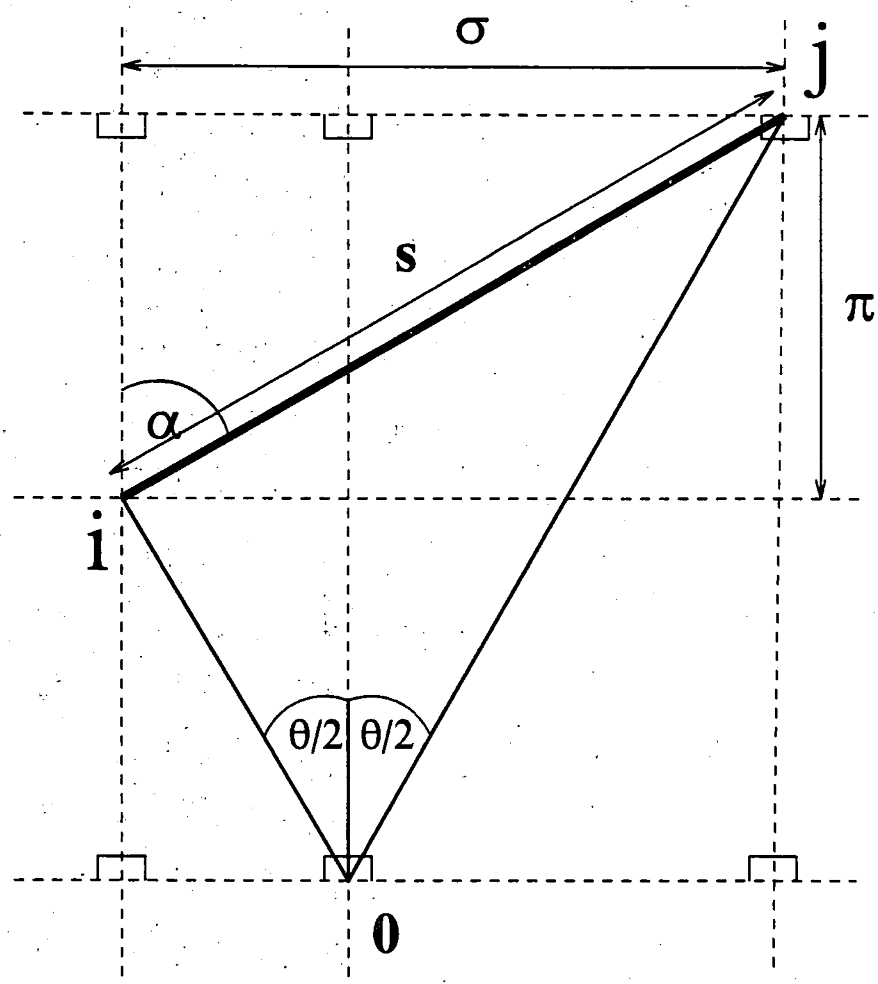

Figure 5.7: Schematic diagram to show the definitions of σ and π.

by a power law with slope $\gamma \simeq 2.2$ and amplitude $r_0 \simeq 5.0h^{-1}$Mpc. This was a very good approximation up to $\sim 10h^{-1}$Mpc and in equation 5.6 it predicts

$$w_v(\sigma) \simeq 95.7\,\sigma^{-1.2}. \tag{5.8}$$

Figure 5.8 shows the mean and 1σ error on $w_v(\sigma)$ assuming that each mock catalogue is statistically independent. These were evaluated using equation 5.7 with a π_{cut} of $20h^{-1}$Mpc and unweighted & weighted estimators for the determination of $\xi(\sigma,\pi)$. The solid line is the result from equation 5.7 (again $\pi_{cut} = 20h^{-1}$Mpc) using the average of the $\xi(\sigma,\pi)$'s from the full N-body SCDM simulations. The dotted line is the model prediction from equation 5.8. Given that the SCDM simulations have little or no power in ξ above 10-$20h^{-1}$Mpc raising π_{cut} makes very little difference to $w_v(\sigma)$ other than to increase the noise.

The agreement between the solid SCDM line and the dotted model prediction line is good everywhere apart from on large scales ($> 10h^{-1}$Mpc). This is where the SCDM model falls off steeper than a pure power law and the model prediction of equation 5.6 will be an overestimate of the SCDM $w_v(\sigma)$. Looking at the results from the SCDM mock catalogues themselves figure 5.8 shows that both weighted and unweighted estimators can reproduce the SCDM prediction, easily consistent within 1σ. The slight systematic bias seen (on large scales) when using unweighted estimators (probably due to the integral constraint) is not apparent here. This is because this bias was small for the SCDM mock catalogues, ~ 0.03 in ξ, and therefore makes little difference in the integral of equation 5.7.

In conclusion, this method can self-consistently reproduce the power law form of $\xi(r)$ from $\xi(\sigma,\pi)$ via $w_v(\sigma)$. Since the small scale redshift space distortions should be larger in the SCDM simulations than in the real Universe (the higher velocity dispersion dominates, see chapter 6) this gives confidence in applying this method to the Durham/UKST survey. However, one should sound a word of caution about the error bars in figure 5.8 because the errors on a individual mock catalogue would be $\sqrt{18}$ larger and hence become quite noisy on large scales, $> 10h^{-1}$Mpc.

5.3.4 Results from the Durham/UKST Galaxy Redshift Survey

Figure 5.9 shows the $w_v(\sigma)$ estimates calculated from equation 5.7 for $\xi(\sigma,\pi)$ (with and without a weighting) and a π_{cut} of $20h^{-1}$Mpc. For comparison figure 5.10 shows the corresponding plot with $\pi_{cut} = 30h^{-1}$Mpc. It can be seen that the unweighted estimate appears smoother than the weighted one although the weighted one has the smaller error bars. This is because the $\xi(\sigma,\pi)$ contour plot is noisier for the weighted estimator than for the unweighted one, see chapter 6. The error bars come from the scatter between the 4 quadrants and assume that each quadrant provides an independent estimate of the correlation function. On small scales, $< 10h^{-1}$Mpc, both estimates have an approximate power law form. On large scales, $> 10h^{-1}$Mpc, the unweighted estimate loses its power law shape whereas the weighted estimate retains a power law form.

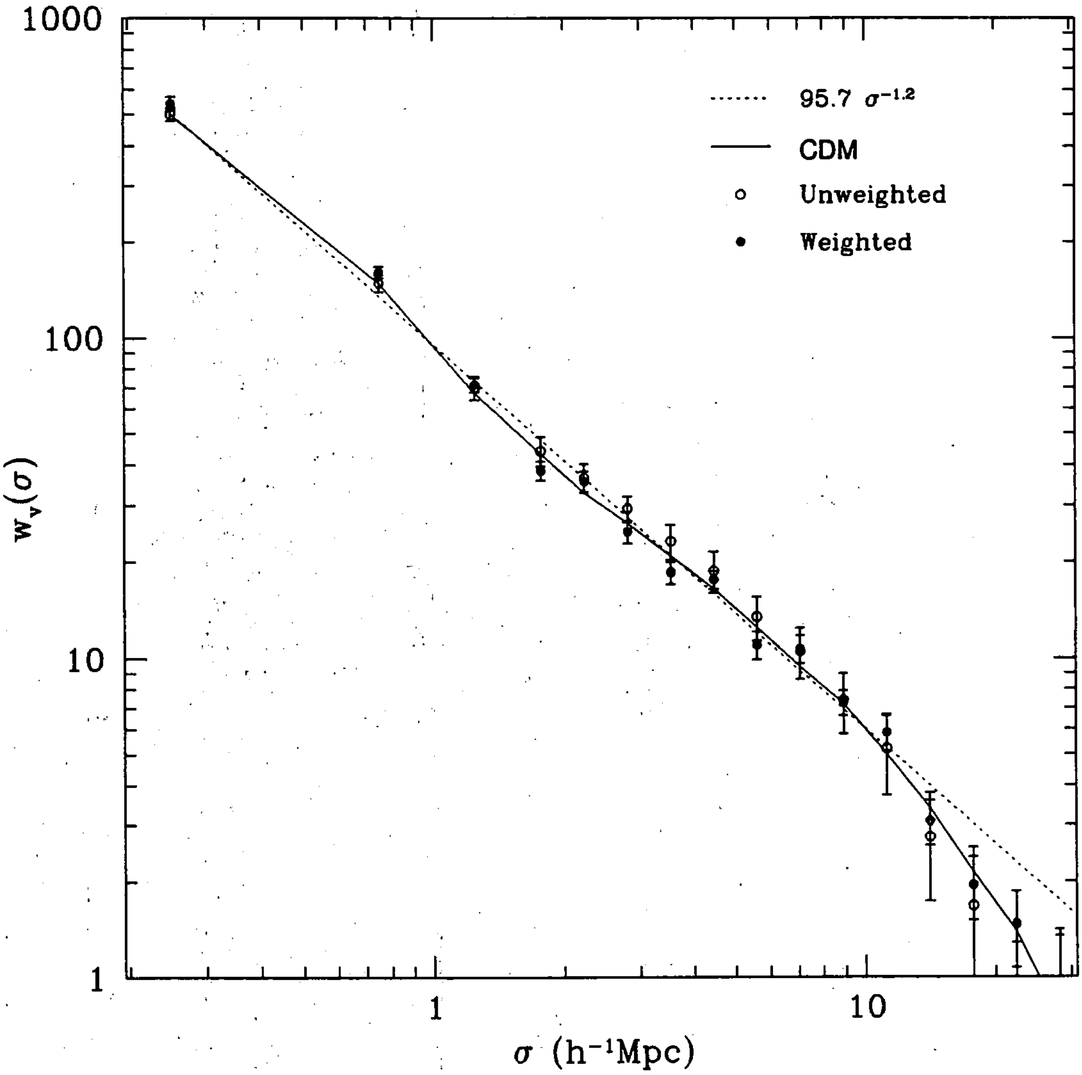

Figure 5.8: $w_v(\sigma)$ as evaluated from the SCDM mock catalogues using weighted and unweighted estimators.

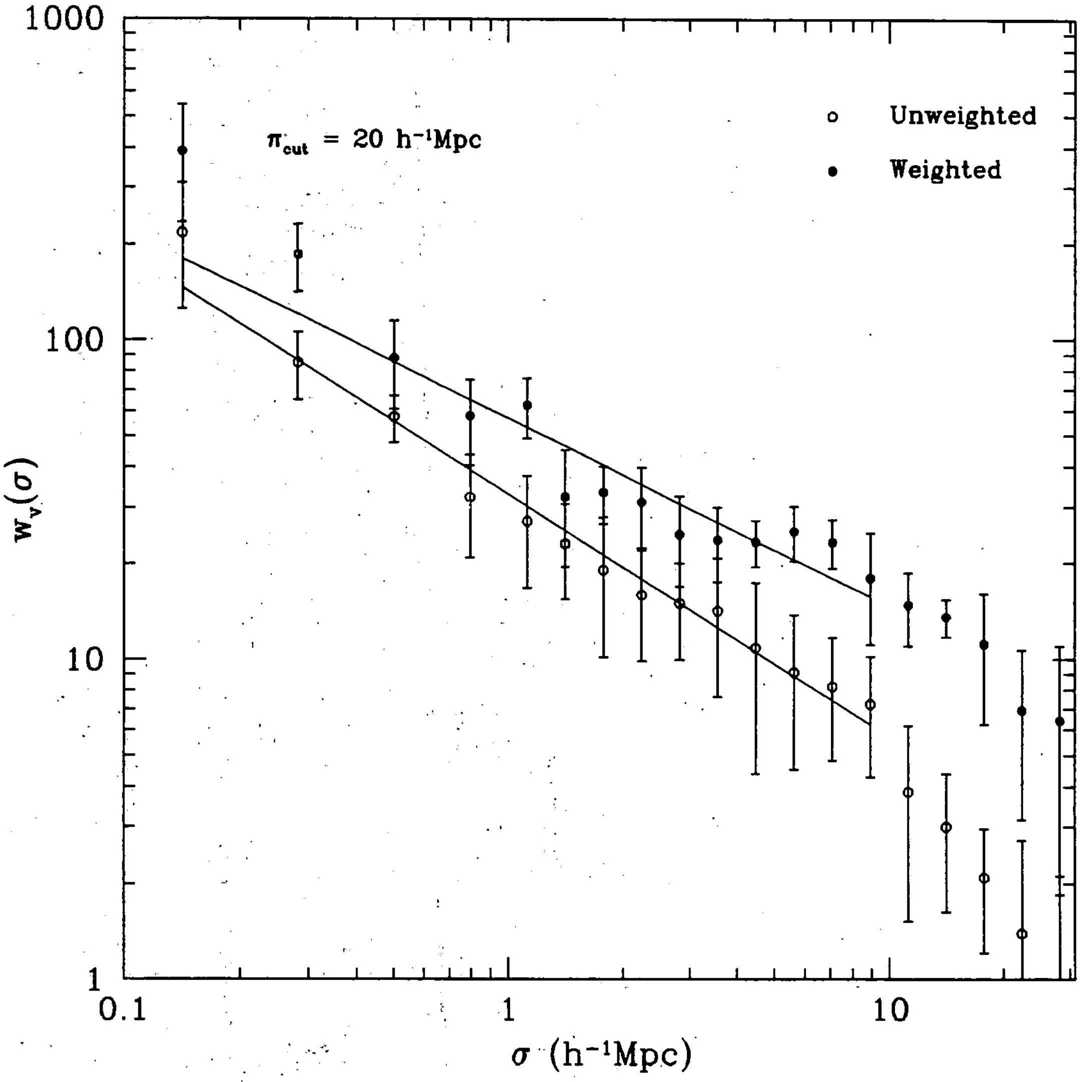

Figure 5.9: $w_v(\sigma)$ as evaluated from the Durham/UKST survey using unweighted and weighted estimators with a π_{cut} of $20h^{-1}$Mpc.

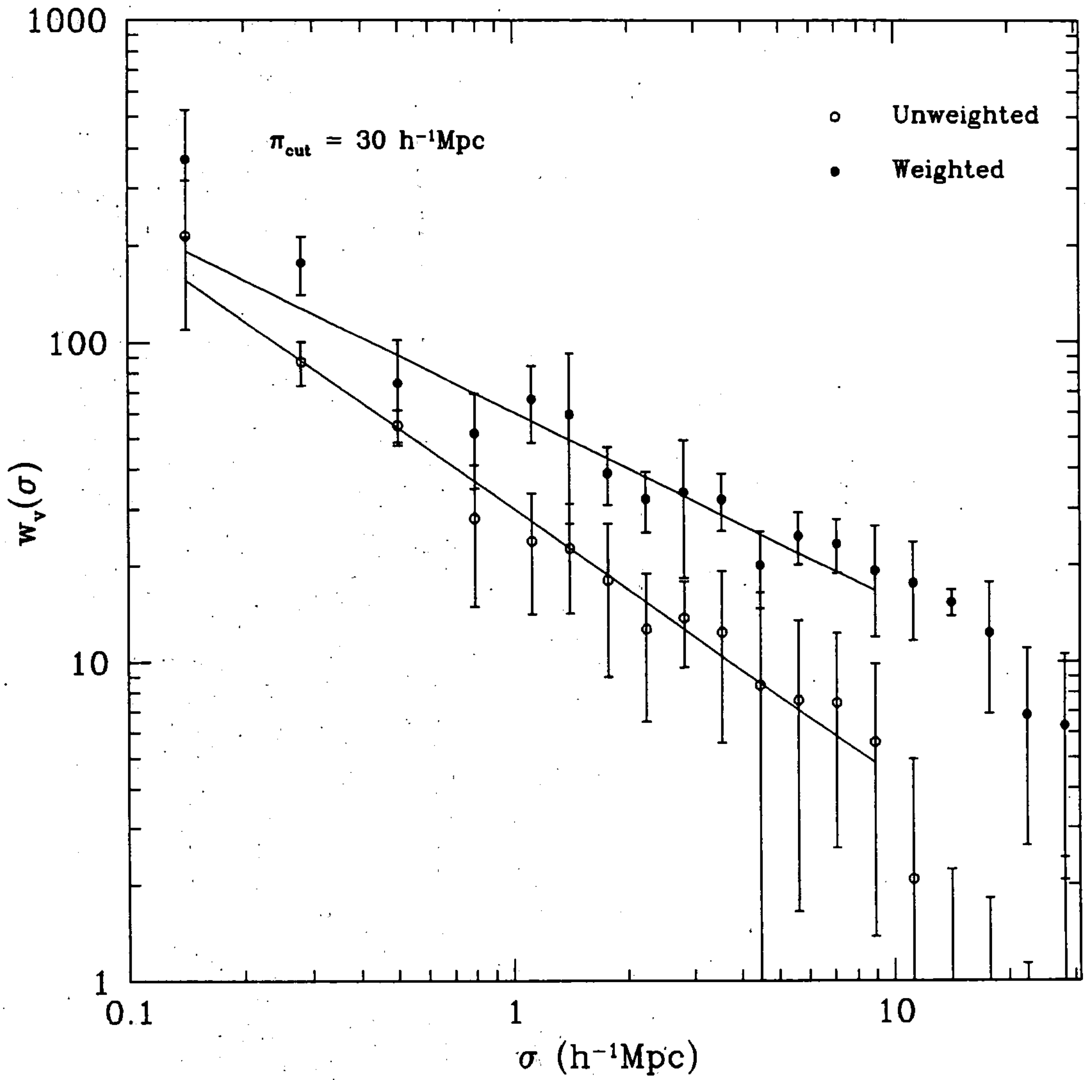

Figure 5.10: $w_v(\sigma)$ as evaluated from the Durham/UKST survey using unweighted and weighted estimators with a π_{cut} of $30h^{-1}$Mpc.

Weighting	π_{cut} (h^{-1}Mpc)	N	χ^2	Prob.	r_0 (h^{-1}Mpc)	γ
N	20	14	1.58	1.000	3.4 ± 0.2	1.76 ± 0.10
	30	14	1.41	1.000	3.2 ± 0.2	1.84 ± 0.12
	40	14	3.96	0.995	3.3 ± 0.2	1.81 ± 0.08
Y	20	14	10.91	0.686	4.8 ± 0.3	1.59 ± 0.10
	30	14	8.39	0.867	5.1 ± 0.3	1.59 ± 0.09
	40	14	7.25	0.927	5.0 ± 0.3	1.61 ± 0.12

Table 5.3: Minimum χ^2 fits to a power law model for $w_v(\sigma)$ from the Durham/UKST survey.

Survey	Durham/UKST	APM-Stromlo	Las Campanas	DARS/SAAO
r_0 (h^{-1}Mpc)	5.1 ± 0.3	5.1 ± 0.2	5.0 ± 0.14	4.7 ± 0.4
γ	1.59 ± 0.09	1.71 ± 0.05	1.79 ± 0.04	(1.8)

Table 5.4: Comparison of *real* space 2-point correlation function power law fits to the modelled projected correlation function for different surveys.

A minimum χ^2 fit is calculated assuming the power law model of equation 5.6 in the region $[0.1, 10.0]h^{-1}$Mpc. Table 5.3 shows the results of this fit for $\pi_{cut} = 20$, 30 and $40h^{-1}$Mpc along with the individual 1σ error bars in each parameter estimated from $\Delta\chi^2 = 1$. It can be seen that the value of π_{cut} does not significantly alter these minimum χ^2 fits. Figure 5.11 shows an example of the $\Delta\chi^2$ contours (for $\pi_{cut} = 20h^{-1}$Mpc) which correspond to the 68% and 96% joint confidence regions in both parameters. Again, a word of caution is necessary as to the significance of the error bars quoted here due to the non-independent nature of these points.

Table 5.3 and figure 5.11 show that the results of the fits to the unweighted and weighted estimates are consistent in slope, γ, but differ at the $\sim 5\sigma$ level in amplitude, r_0 (although this significance level is not concrete due to the simplistic χ^2 fit used). The difference seen between the weighted and unweighted power law amplitudes is a direct result of the difference seen between the weighted and unweighted redshift space ξ's (see figure 5.1). Therefore, for the purpose of comparison with other redshift surveys the weighted estimate is preferred, with $\pi_{cut} = 30h^{-1}$Mpc.

5.3.5 Comparison with other Redshift Surveys

Table 5.4 shows a comparison between the best fit parameters for $\xi(r)$ to the power law model of equation 5.6 for the optical redshift surveys mentioned in section 5.2.3. The weighted estimate from the Durham/UKST survey is used here. Once again the DARS/SAAO slope was fixed at 1.8 before fitting for r_0. It can be seen that all of the amplitudes agree well with the value $r_0 \simeq 5.0h^{-1}$Mpc. It is also seen that all of the slopes agree well with the value $\gamma \simeq 1.75$, bar the Durham/UKST one (1-2σ low). Consistent results are found when comparing these values with the $r_0 = 4.5h^{-1}$Mpc

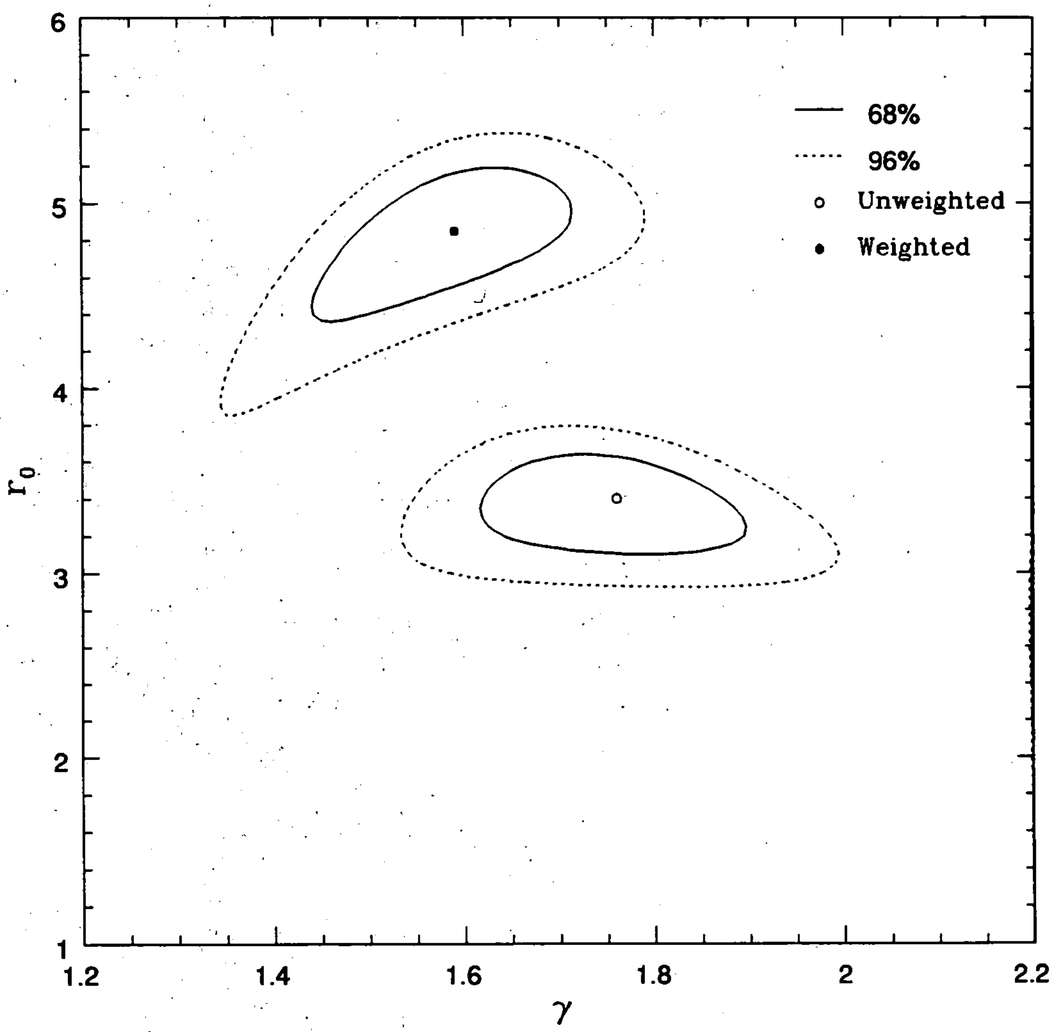

Figure 5.11: $\Delta\chi^2$ contours denoting the 68% and 96% joint confidence regions in model power law fits to the Durham/UKST $w_v(\sigma)$ with $\pi_{cut} = 20h^{-1}$Mpc.

and $\gamma = 1.7$ obtained for $\xi(r)$ by Baugh (1996) from numerically inverting the APM angular correlation function, $w(\theta)$. These estimates are discussed further in section 5.5. In conclusion, all of the *real* space parameters appear consistent with each other.

5.4 Inversion to find the Real Space Correlation function

In section 5.3 the projected correlation function, $w_v(\sigma)$, was studied by comparison with a model deduced from the real space correlation, $\xi(r)$. The model assumed a pure power law for $\xi(r)$ and a fit was done to the amplitude and slope of this power law. However, $\xi(r)$ is unlikely to be a pure power law other than in a limited spatial region so the model will never be able to fully reproduce $\xi(r)$ and any features in it. There exists the possibility that one can mathematically or numerically invert equation 5.5 for $w_v(\sigma)$ to determine $\xi(r)$ directly. In sections 5.4.1 and 5.4.2 two methods of inversion are investigated ; (i) by direct Abel inversion of the integral equation, (ii) by Richardson-Lucy iteration. The immediate aim of this study is to see if it is possible to successfully invert equation 5.5 before considering the results from the Durham/UKST survey.

5.4.1 Direct Abel Inversion of the Integral Equation

Equation 5.5 can be mathematically inverted using the generalized Abel equation to give

$$\xi(r) = -\frac{1}{\pi}\frac{d}{dr}\left(\int_r^\infty \frac{w_v(\sigma)}{\sqrt{\sigma^2 - r^2}}\frac{r}{\sigma}d\sigma\right), \tag{5.9}$$

which can be written in a slightly more "user friendly" form as

$$\xi(r) = -\frac{1}{\pi}\int_r^\infty \frac{d\left[w_v(\sigma)\right]}{d\sigma}\frac{d\sigma}{\sqrt{\sigma^2 - r^2}}. \tag{5.10}$$

Saunders *et al.* (1992) consider the case when the data is logarithmically binned. $w_v(\sigma)$ then takes the form of a series of step functions with logarithmic spacing, $w_v(\sigma) = w_v(\sigma_i) = w_i$ for σ in the logarithmic interval centered on σ_i. They then approximate $w_v(\sigma)$ by linearly interpolating between each w_v point to get around singularities in the integral. This simplifies the expression for $d[w_v(\sigma)]/d\sigma$ which becomes a constant value between each pair of σ spacings. The remaining part of the integral can be evaluated to give the real space correlation function at $r = \sigma_i$

$$\xi(\sigma_i) = -\frac{1}{\pi}\sum_{j\geq i}\left[\frac{w_{j+1} - w_j}{\sigma_{j+1} - \sigma_j}\right]\ln\left(\frac{\sigma_{j+1} + \sqrt{\sigma_{j+1}^2 - \sigma_i^2}}{\sigma_j + \sqrt{\sigma_j^2 - \sigma_i^2}}\right). \tag{5.11}$$

5.4.2 Inversion by Richardson-Lucy Iteration

A simple technique for numerical inversion of Fredholm integral equations of the first kind was developed independently by Richardson (1972) and Lucy (1974). This method has recently become popular for inversion applications in the field of large scale structure, see Baugh & Efstathiou (1993). In one dimension the general form is

$$\phi(x) = \int_a^b \psi(t) P(x|t) dt, n \tag{5.12}$$

where $\phi(x)$ is the known (or observed) function, $\psi(t)$ is the unknown function and $P(x|t)$ is the kernel of the integral equation. Richardson-Lucy iteration (or deconvolution) uses Bayes' theorem for conditional probabilities which makes a "guess" to estimate the form of the unknown function, $\psi(t)$, and then generate an estimate of the known function, $\phi(x)$. From this new estimate of $\phi(x)$ a better estimate of $\psi(t)$ is then generated. This cycling between unknown and known functions continues and after n iterations gives

$$\phi^n(x) = \int_a^b \psi^n(t) P(x|t) dt, \tag{5.13}$$

and the next iterate of $\psi(t)$ is

$$\psi^{n+1}(t) = \psi^n(t) \frac{\int_a^b \frac{\tilde{\phi}(x)}{\phi^n(x)} P(x|t) dx}{\int_a^b P(x|t) dx}, \tag{5.14}$$

where $\tilde{\phi}(x)$ is the actual observed function.

Equation 5.4 can be re-written as

$$w_v(\sigma) = \int_\sigma^\infty \xi(r) \left(\frac{2r}{\sqrt{r^2 - \sigma^2}} \right) dr, \tag{5.15}$$

by changing the variable of integration from π to r. This is not quite in the form specified by equation 5.12 but by suitable extension of the kernel into the region $[0, \sigma]$ one can write

$$w_v(\sigma) = \int_0^\infty \xi(r) K(\sigma, r) dr, \tag{5.16}$$

where

$$K(\sigma, r) = 0 \quad \text{for} \quad 0 < r < \sigma, \tag{5.17}$$

$$= \frac{2r}{\sqrt{r^2 - \sigma^2}} \quad \text{for} \quad \sigma < r < \infty. \tag{5.18}$$

To apply this method to the logarithmically binned $w_v(\sigma)$ data the integrals in equations 5.13 and 5.14 are approximated by the following summations

$$w_v^n(\sigma_j) = \sum_{i=1}^{N} \xi^n(r_i) K(\sigma_j, r_i) r_i \Delta \ln r, \tag{5.19}$$

$$\xi^{n+1}(r_i) = \xi^n(r_i) \frac{\sum_{j=1}^{M} \frac{\tilde{w}_v(\sigma_j)}{w_v^n(\sigma_j)} K(\sigma_j, r_i) \sigma_j \Delta \ln \sigma}{\sum_{j=1}^{M} K(\sigma_j, r_i) \sigma_j \Delta \ln \sigma}, \tag{5.20}$$

where M is the number of $w_v(\sigma)$ bins and $N = M/2$ is the number of $\xi(r)$ bins. The spacing in σ is $\Delta \lg \sigma = 0.1$ and hence the spacing in r is $\Delta \lg r = 0.2$. Obviously one cannot get back more data points than are put in and $N \leq M$. In general, the choice of $N = M/2$ should assure a fairly smooth answer.

There are two points worth noting about Richardson-Lucy algorithms. Firstly, there is no constraint on how many iterations are required for convergence to a stable answer. Therefore, there is no specific rule to know when to stop iterating. Experience with Richardson-Lucy techniques shows that ~ 10 iterations are generally required (eg. Lucy, 1994). Secondly, this method assumes that the function $\psi(t) \geq 0$. This is not always the case for our function $\xi(r)$. However, this is not too worrying as $\xi(r)$ is only likely to go negative on large scales when it is very near zero, this is where our inversion process will be least believable anyway (see section 5.4.3). Also, Baugh & Efstathiou (1993) and Baugh (1996) have applied similar inversion techniques to the angular correlation function to estimate the power spectrum (always positive) and real space correlation function (negative tail) and find very consistent results.

5.4.3. Testing the Methods of Inversion - Fake Data

These two methods of inversion are tested by making a "fake" data set. Consider a pure power law of $\xi(r) = (6.0/r)^{1.7}$ in the region $[0.1, 100.0]h^{-1}$Mpc (adding noise later). $\xi(\sigma, \pi)$ is first produced using this power law, where $r = \sqrt{\sigma^2 + \pi^2}$, and then the integral of equation 5.4 is carried out to give $w_v(\sigma)$. This $w_v(\sigma)$ is then inverted using the two techniques to give an estimate of the initial $\xi(r)$. $\Delta \lg = 0.1$ bins are chosen for r, σ and π and therefore there are 30 bins of $w_v(\sigma)$ to invert in this case.

Figure 5.12 shows the results of equation 5.11 and equations 5.19 & 5.20 on this pure power law. The Richardson-Lucy method converges after only a few iterations (independent of the initial guess for $\xi(r)$) and is stable thereafter. It can be seen that both methods can reproduce the original $\xi(r)$ very well in the region $[1.0, \sim 40]h^{-1}$Mpc. In this region the Abel equation method gives an answer which is systematically $\sim 6\%$ too low and the Richardson-Lucy method is systematically $\sim 12\%$ too low. These are probably due to the finite binning which is used. As will be seen in section 5.4.5 these systematics are acceptable compared to the other uncertainties present in the actual data set.

On the very small and the very large scales both methods underestimate the actual power law (apart from the Richardson-Lucy method on large scales which overestimates the power law). This is simply due to the small and large scale cut-offs used in the power law and hence the summations of equations 5.11, 5.19 and 5.20. Although it is not actually shown, the region of the power law was increased by an order of magnitude in either direction to $[0.01, 1000.0]h^{-1}$Mpc and a reliable inversion was then obtained in the $[0.1, \sim 400]h^{-1}$Mpc range.

Obviously the actual data has uncertainties in it and noise is now added to $\xi(\sigma, \pi)$

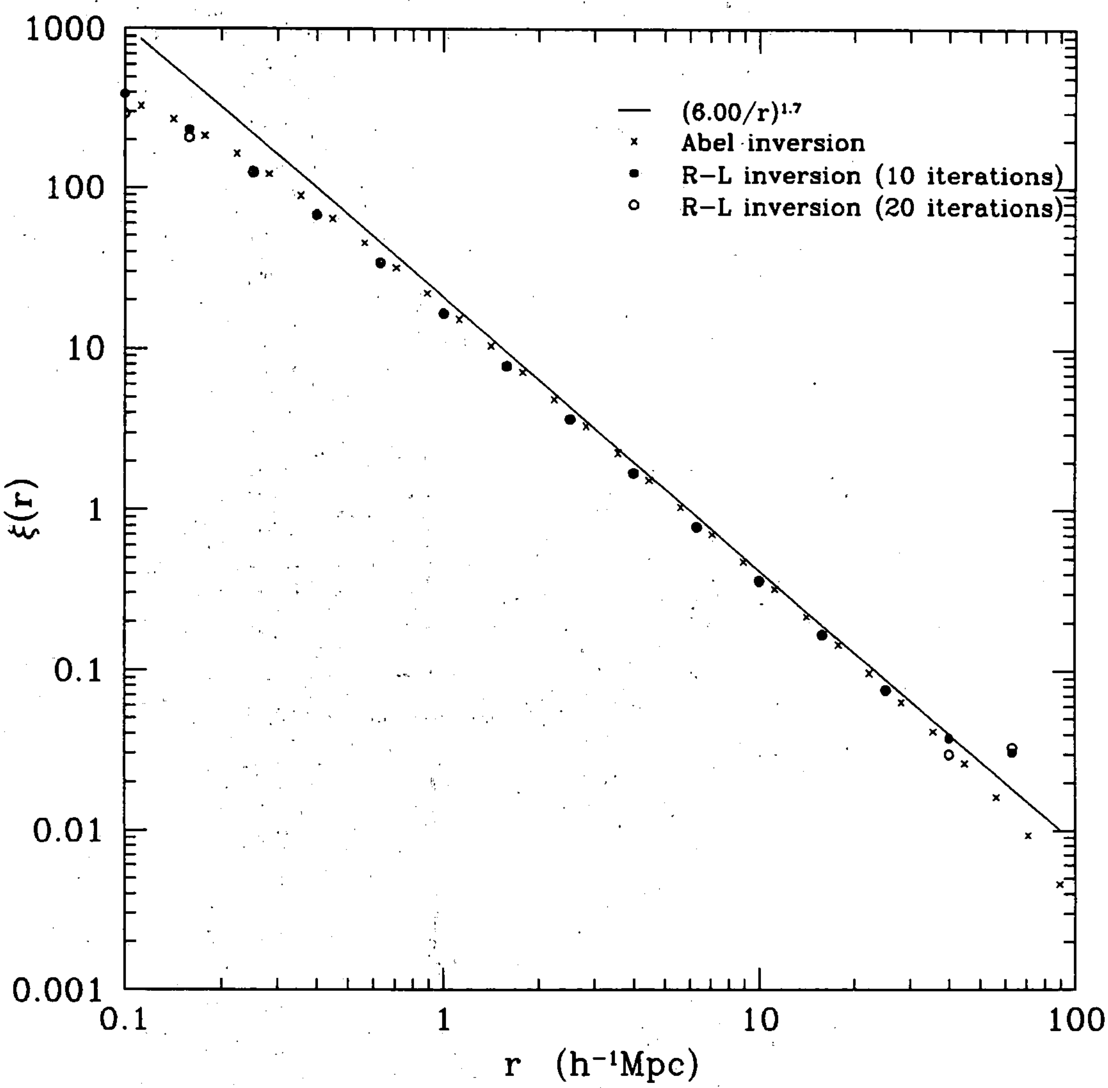

Figure 5.12: Testing the methods of inverting $w_v(\sigma)$ to give $\xi(r)$ using a pure power law model.

in an attempt to model this. The noise model is quite simple, $\xi(\sigma, \pi)$ is calculated using the power law for $\xi(r)$ as before, numbers from a gaussian distribution with zero mean and a standard deviation dependent on r are selected and then added to $\xi(\sigma, \pi)$. The results from the SCDM mock catalogues give indicative values of the dependence of these standard deviations with r, for example $r \in [1.0, 3.5]h^{-1}$Mpc $\Rightarrow$ s.d. $\simeq 1$.

Figure 5.13 shows the results of the inversions on this noisy power law. It can be seen that the method which best reproduces the original power law is the Richardson-Lucy technique when stopped after 10 iterations. The direct inversion using Abel's equation is very noisy but does get the general form correct. A similar comment can be made if the Richardson-Lucy iterations are allowed to continue further. Therefore, 10 iterations are found to give a reasonable compromise between convergence to the large scale features and overfitting the small scale noise.

As a final test on "fake" data a two power law model is inverted. Figures 5.14 and 5.15 show the results from the inversions of $\xi(r)$ without and with noise, respectively. The model power laws are $(6.0/r)^{1.7}$ for $r < 10h^{-1}$Mpc and $(7.62/r)^{3.2}$ for $r > 10h^{-1}$Mpc. The noise was generated exactly as above. It can be seen that both methods can easily deal with this input $\xi(r)$ in the case of no noise. When noise is added the general power law features are reproduced out to $\sim$ 10-20h^{-1}Mpc. The Richardson-Lucy method after 10 iterations again gives the smoothest and most accurate answer, reliable to at least $20h^{-1}$Mpc.

Some general comments can be made about the results from these different inversion techniques. The finite binning scheme used here (for approximating integrals with summations) appears to lower the inverted answer by 5-10% from the real answer. This is not thought to be a major problem. As the direct Abel inversion process is a point by point method the noise in the original $w_v(\sigma)$ will also be inverted. This effect is clearly seen in figures 5.13 and 5.15 where the Abel method is arguably the most noisy inversion process. These figures also show that the Richardson-Lucy method produces the most accurate inversion after 10 iterations. Letting the iteration continue gives a worse answer as the inversion process converges to the noise in the data, eg. 20 iterations. Although not shown the Richardson-Lucy method was allowed to continue until $\sim$ 100 iterations with the result that the inversion process does not appear to become unstable. This is interesting because after a large number of iterates Richardson-Lucy answers usually "flip" from one permitted solution to another because of the freedom allowed due to the noise. This does not appear to be the case here. This is probably due to the large bin size used in the summations (ie. the small number of bins) which restricts the number of permitted solutions. In conclusion, the Richardson-Lucy method produces the best inversion, generally taking $\sim$ 10 iterations to converge. However, this method only produces estimates of $\xi(r)$ at half the number of original bins unless some sort of interpolation of $w_v(\sigma)$ is carried out.

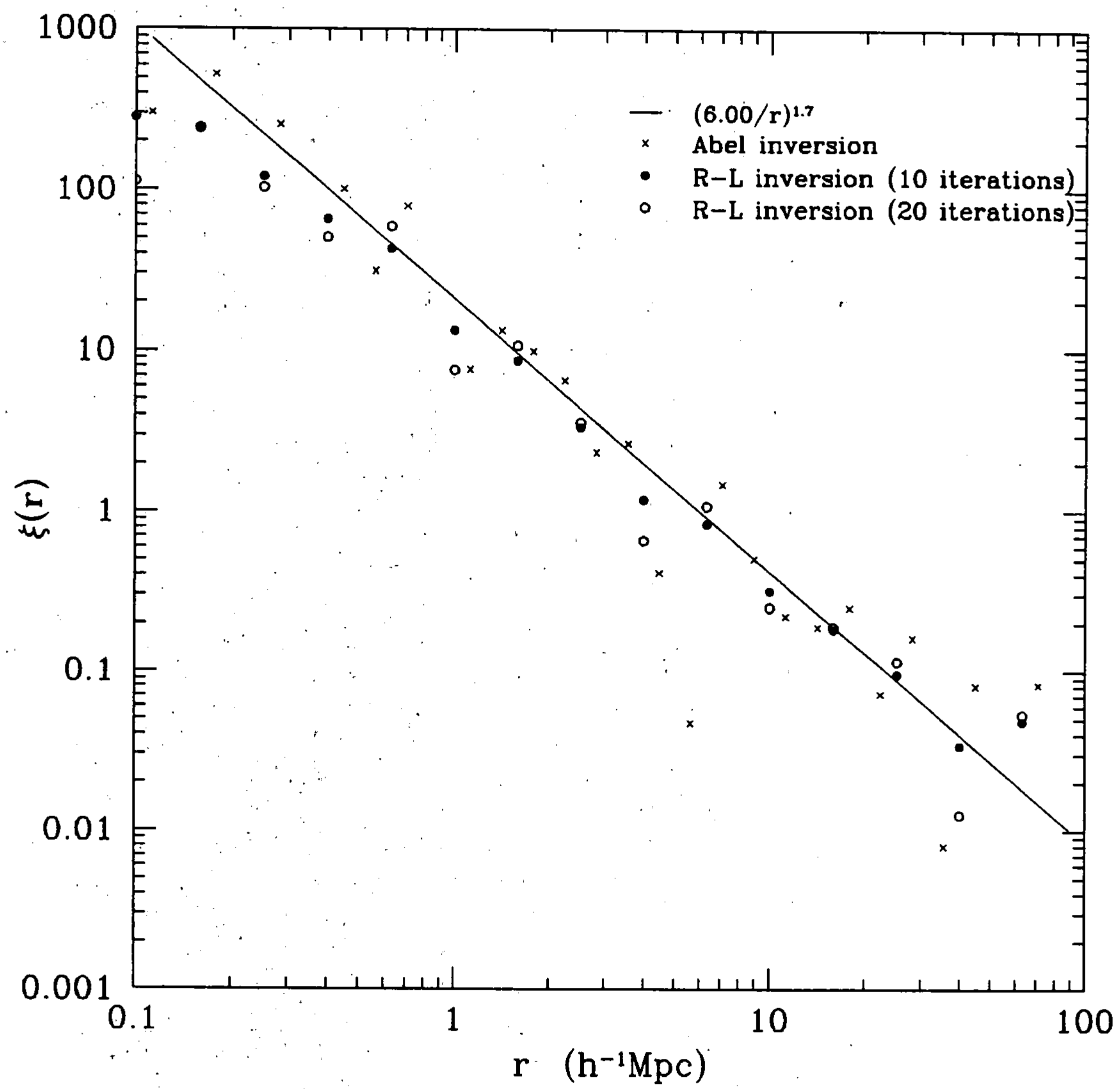

Figure 5.13: Testing the methods of inverting $w_v(\sigma)$ to give $\xi(r)$ using a noisy power law model.

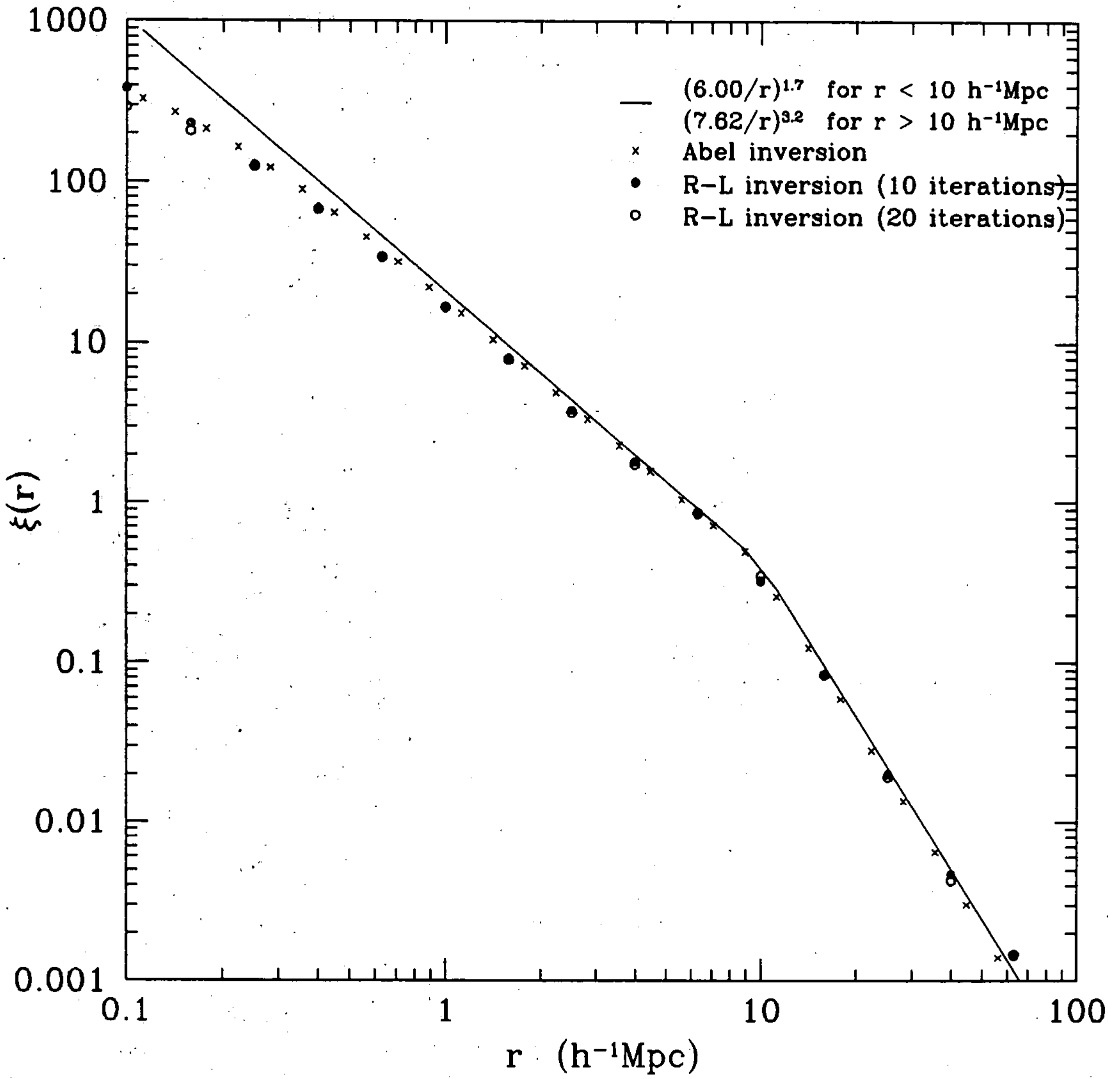

Figure 5.14: Testing the methods of inverting $w_v(\sigma)$ to give $\xi(r)$ using a pure two power law model.

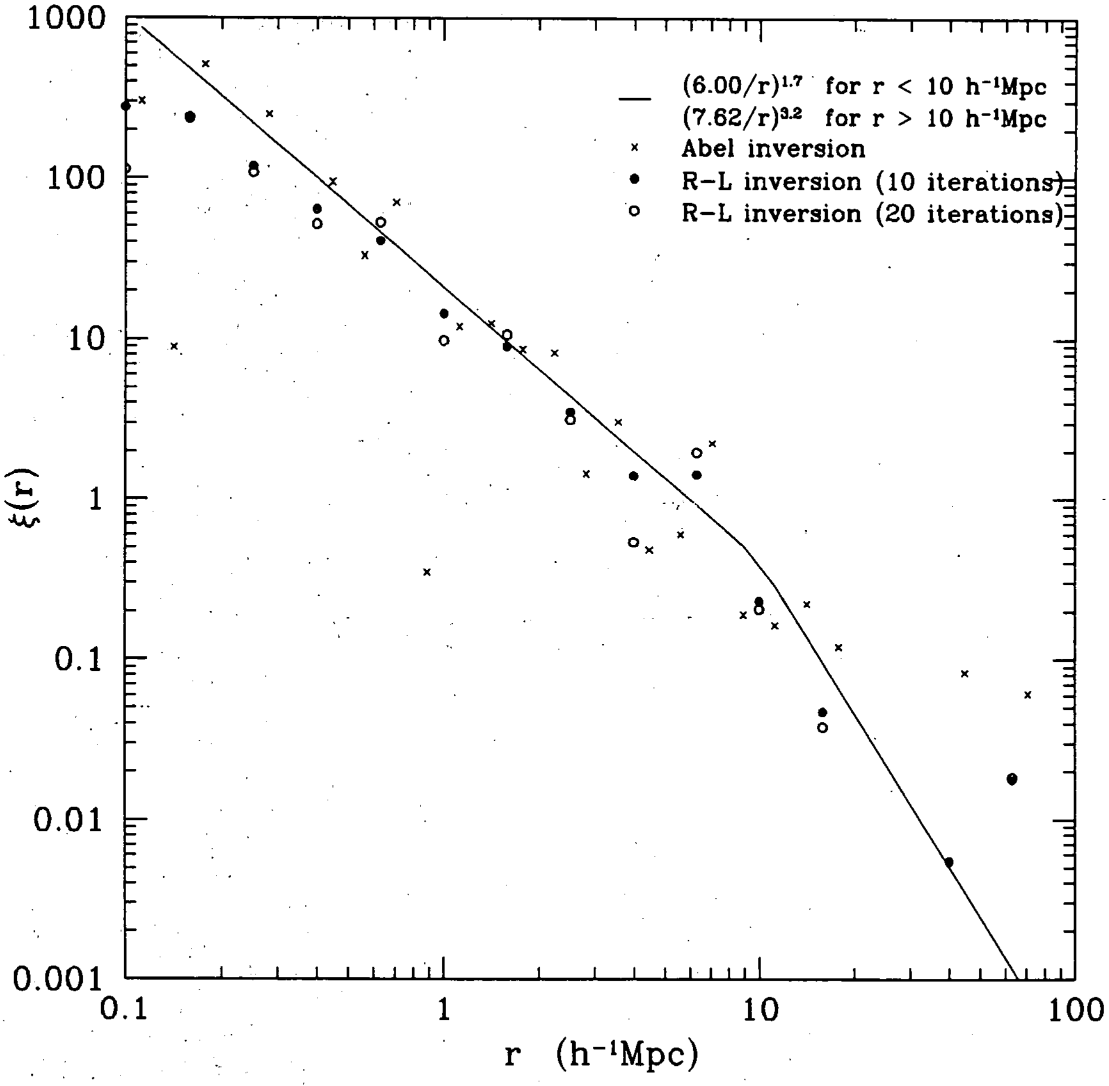

Figure 5.15: Testing the methods of inverting $w_v(\sigma)$ to give $\xi(r)$ using a noisy two power law model.

5.4.4 Testing the Methods of Inversion - SCDM Mock Catalogues

These inversion techniques are also tested on the SCDM mock catalogues which should have similar uncertainties in them as the Durham/UKST survey. Figures 5.16 and 5.17 show the mean and 1σ error on the recovered $\xi(r)$ using equation 5.11 (direct Abel method) and equations 5.19 & 5.20 (Richardson-Lucy iteration), respectively, with a π_{cut} of $20h^{-1}$Mpc. These results are insensitive to raising the value of π_{cut} given that the SCDM model does not have any power above $\sim 20h^{-1}$Mpc. The error bars assume that each SCDM mock catalogue is statistically independent. Both unweighted and weighted estimators are shown. In figure 5.17 circles show the results after 10 iterations, triangles denote 20 iterations, although error bars are only given on the former. The solid line is the result of the average $\xi(r)$ from the full N-body SCDM simulations as estimated in section 4.5.1.

For the direct Abel method both unweighted and weighted estimates reproduce the original $\xi(r)$ out to $\sim 20h^{-1}$Mpc, with the weighted estimate being arguably the more noisier. However, both estimates become noisy and overestimate $\xi(r)$ on $> 30h^{-1}$Mpc scales and therefore the method cannot be trusted in this region.

For the Richardson-Lucy iteration both unweighted and weighted estimates reproduce the original $\xi(r)$ out to $\sim 30h^{-1}$Mpc and this is the scale out to which the inversion process in believable. In general, the error bars are smaller for this method than for the direct Abel inversion. However, this is offset by only having an estimate at half the number of points. As mentioned previously one could interpolate or fit a specific functional form to $w_v(\sigma)$ and then invert this given that one could estimate it at many points. This is not attempted here given the size of the error bars in $w_v(\sigma)$ and the fact that this is a merely an initial attempt of this inversion technique.

Finally, one should note that the weighted and unweighted estimates agree within 1σ with no systematic bias seen. This agrees with what was previously found in section 5.3.3 and is because this bias (probably integral constraint) was small for the SCDM mock catalogues of chapter 4.

5.4.5 Applying the Methods of Inversion to the Durham/UKST Survey

The real space estimates of $\xi(r)$ for the Durham/UKST survey are now presented using these two methods of inversion. Figures 5.18 and 5.19 show $\xi(r)$ as evaluated from equation 5.11 (direct Abel method) and equation 5.20 (Richardson-Lucy iteration), respectively, with a π_{cut} of $30h^{-1}$Mpc. The Richardson-Lucy process is stopped after 10 iterations although the answer does not change a great deal with further iteration. Figure 5.20 gives a comparison of the $w_v(\sigma)$ evaluated from equation 5.19 (Richardson-Lucy iteration) with the original $w_v(\sigma)$ in figure 5.10. The

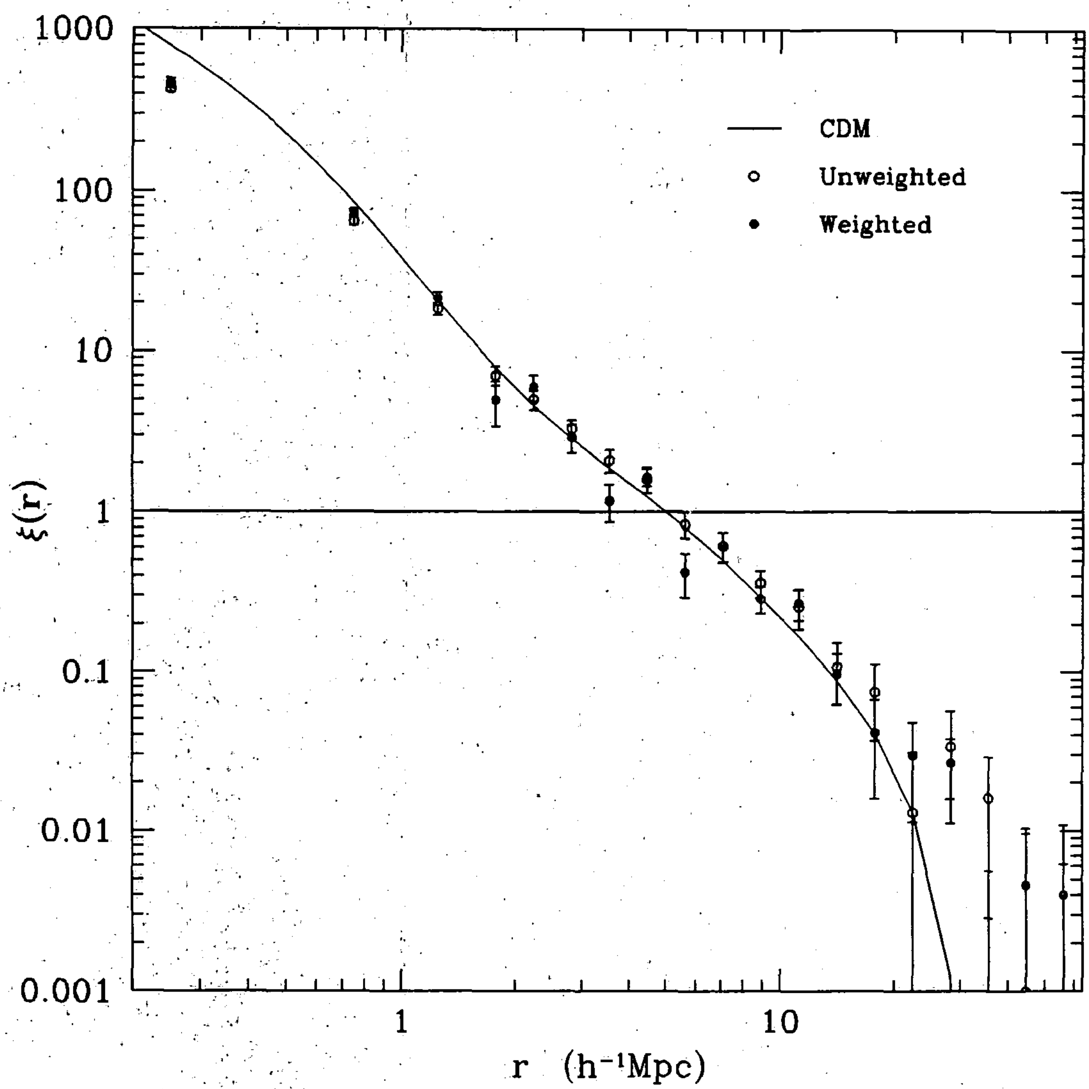

Figure 5.16: $\xi(r)$ as evaluated via direct Abel inversion from the SCDM mock catalogues.

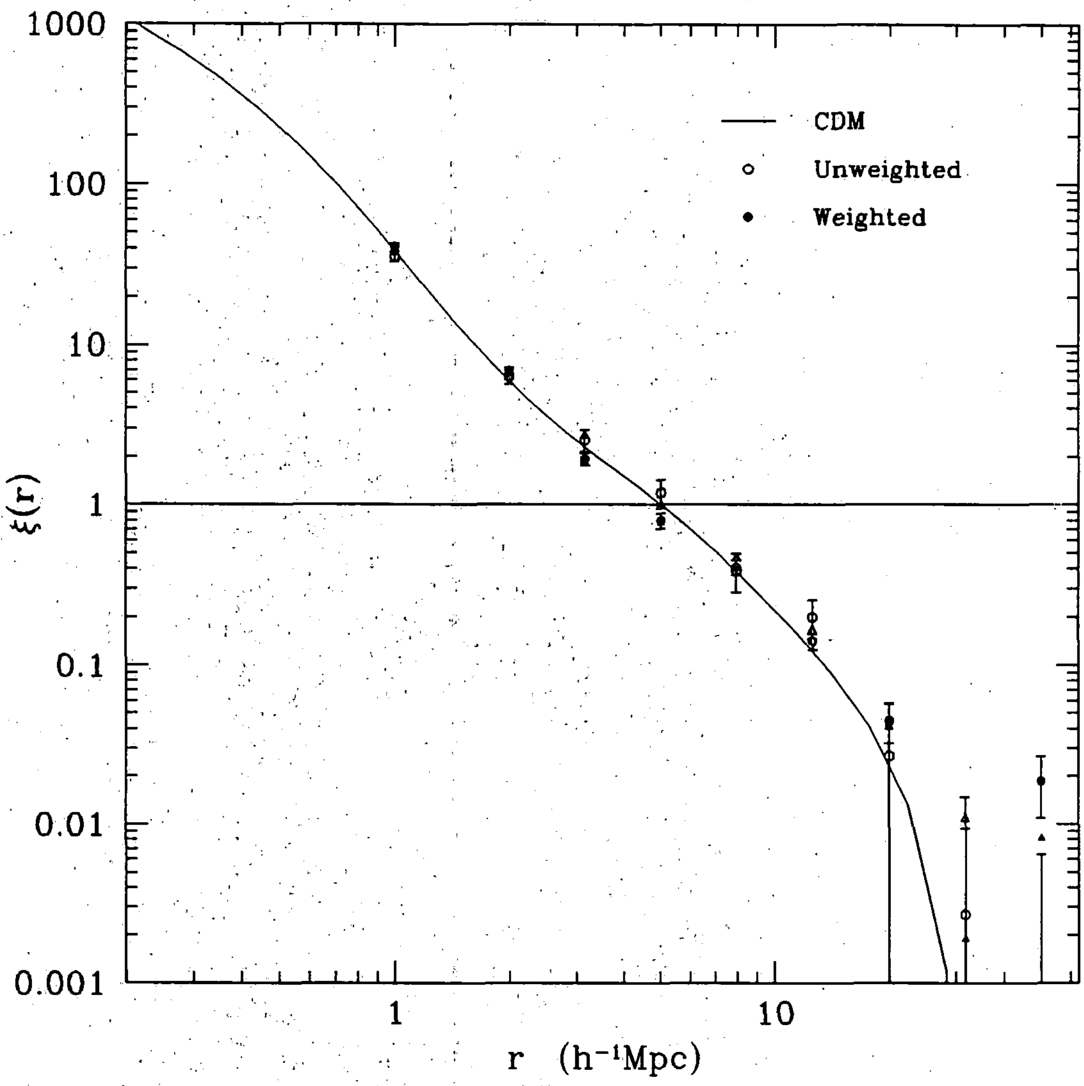

Figure 5.17: $\xi(r)$ as evaluated via Richardson-Lucy iteration from the SCDM mock catalogues.

Weighting	π_{cut} (h^{-1}Mpc)	N	χ^2	Prob.	r_0 (h^{-1}Mpc)	γ
N	20	17	9.27	0.900	3.2 ± 0.2	1.80 ± 0.12
	30	17	12.33	0.726	3.2 ± 0.3	1.79 ± 0.10
	40	17	28.13	0.031	3.3 ± 0.3	1.77 ± 0.10
Y	20	16	8.21	0.916	4.5 ± 0.9	1.7 ± 0.4
	30	16	8.02	0.924	4.8 ± 0.5	1.6 ± 0.3
	40	16	10.67	0.787	5.6 ± 0.9	1.5 ± 0.2

Table 5.5: Minimum χ^2 fits to a power law model for the Durham/UKST $\xi(r)$.

Weighting	π_{cut} (h^{-1}Mpc)	N	χ^2	Prob.	r_0 (h^{-1}Mpc)	γ
N	20	9	1.48	0.993	3.1 ± 0.3	1.70 ± 0.12
	30	9	1.73	0.988	3.0 ± 0.5	1.74 ± 0.15
	40	9	14.22	0.083	2.6 ± 0.6	1.72 ± 0.23
Y	20	9	12.12	0.151	4.1 ± 0.4	1.72 ± 0.10
	30	9	2.09	0.978	4.6 ± 0.6	1.61 ± 0.12
	40	9	4.22	0.839	4.2 ± 0.6	1.64 ± 0.12

Table 5.6: Minimum χ^2 fits to a power law model for the Durham/UKST $\xi(r)$.

error bars come from splitting the survey into 4 roughly equal quadrants and assuming that each quadrant provides an independent estimate of the correlation function. Table 5.5 shows the results and individual 1σ errors in each parameter from minimum χ^2 power law fits to the Abel inverted $\xi(r)$ in the $\sim$ 0.1-17h^{-1}Mpc region using these error bars and the $\Delta\chi^2 = 1$ contour. Table 5.6 shows the corresponding results for the Richardson-Lucy inverted $\xi(r)$. The solid lines on figures 5.18 and 5.19 are the best fits to the weighted and unweighted estimates with a π_{cut} of $30h^{-1}$Mpc. Note that for the weighted Abel inverted $\xi(r)$ the negative point at $r \sim 4.5h^{-1}$Mpc has been deleted in the minimum χ^2 fit. If included this point can bias the estimated value of r_0 low by 2-3σ !. Also, a word of caution is sounded about the significance levels of these χ^2 fits due to the non-independent nature of these points.

Comparing tables 5.5 and 5.6 shows that the two different methods of inversion produce consistent results. However, the effect of using an unweighted estimate again causes a lower value of r_0 to be estimated. This is in agreement with the results of section 5.3.4. Also, it can be seen that the value of π_{cut} does not significantly alter these minumum χ^2 fits, again consistent with section 5.3.4. The Richardson-Lucy method gives a slightly smoother $\xi(r)$ than the direct Abel method. This may have been expected given that the iteration was (hopefully) stopped before convergence to the small scale noise occurs. The Abel method, because it is a point by point inversion, does appear to suffer from this problem. The unweighted $\xi(r)$ is consistent with a power law with $r_0 \simeq 3.1h^{-1}$Mpc and $\gamma \simeq 1.75$, whereas the weighted $\xi(r)$ has $r_0 \simeq 4.6h^{-1}$Mpc and $\gamma \simeq 1.6$. Given that chapter 4 showed that the weighted estimate does not suffer from any systematic bias this estimate of $\xi(r)$ is preferred here. Finally, figure 5.20 shows that the original $w_v(\sigma)$'s are well reproduced by the inverted $\xi(r)$'s. Error bars on this figure come from the quadrants of the survey.

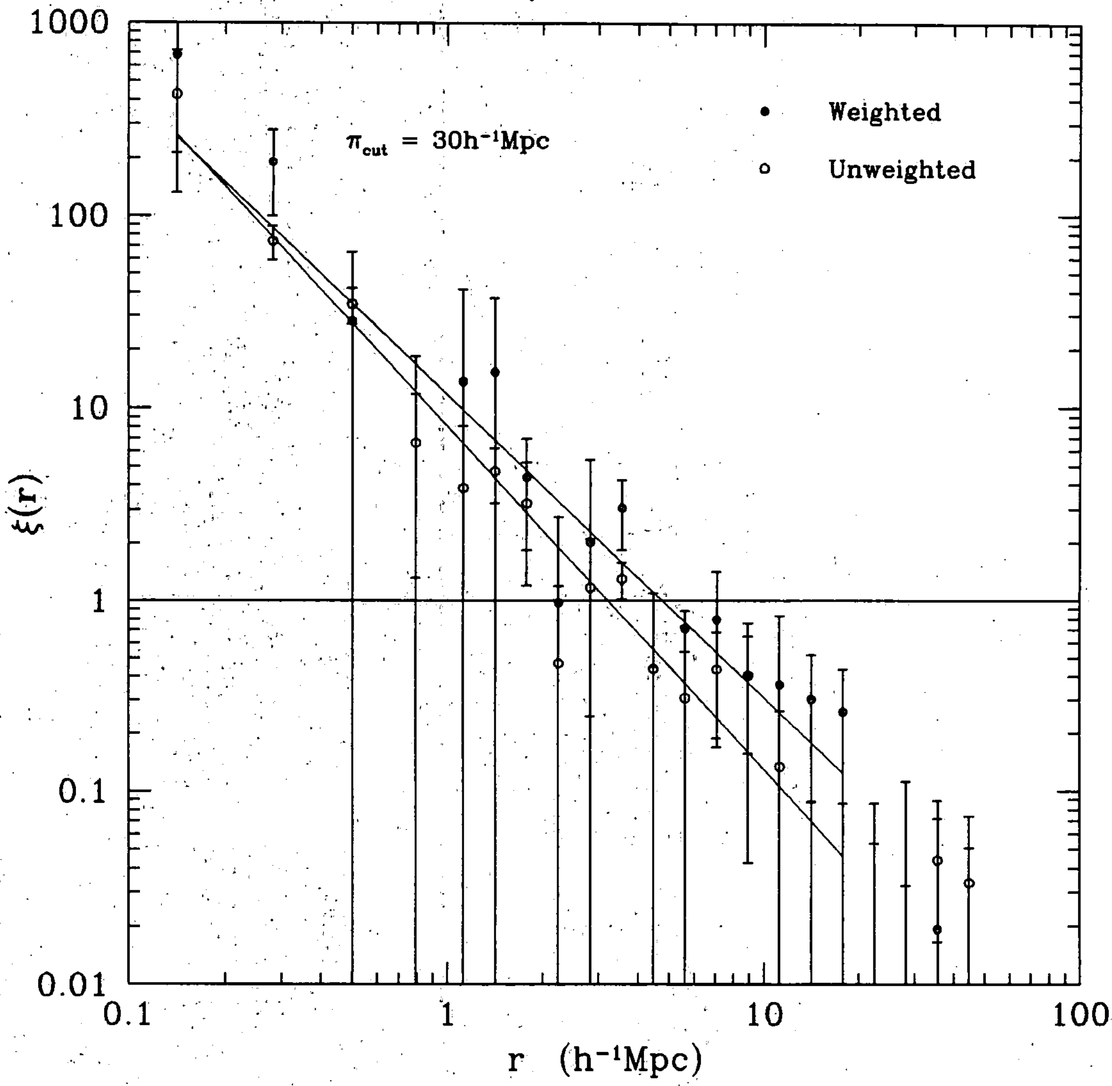

Figure 5.18: $\xi(r)$ as evaluated via direct Abel inversion of an integral equation involving $w_v(\sigma)$ for the Durham/UKST survey with $\pi_{cut} = 30h^{-1}$Mpc.

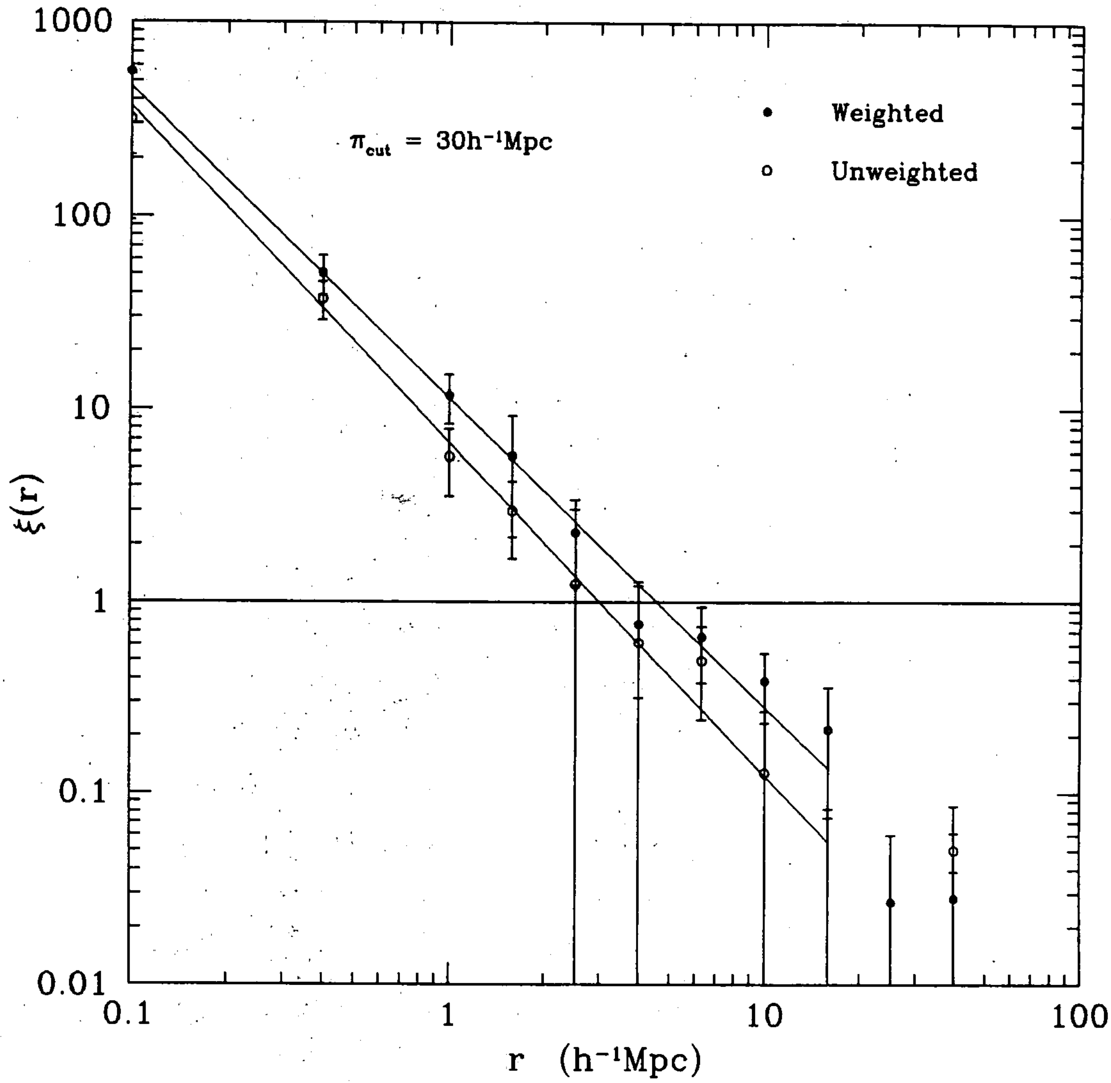

Figure 5.19: $\xi(r)$ as evaluated via Richardson-Lucy iterative inversion of an integral equation involving $w_v(\sigma)$ for the Durham/UKST survey with $\pi_{cut} = 30h^{-1}$Mpc.

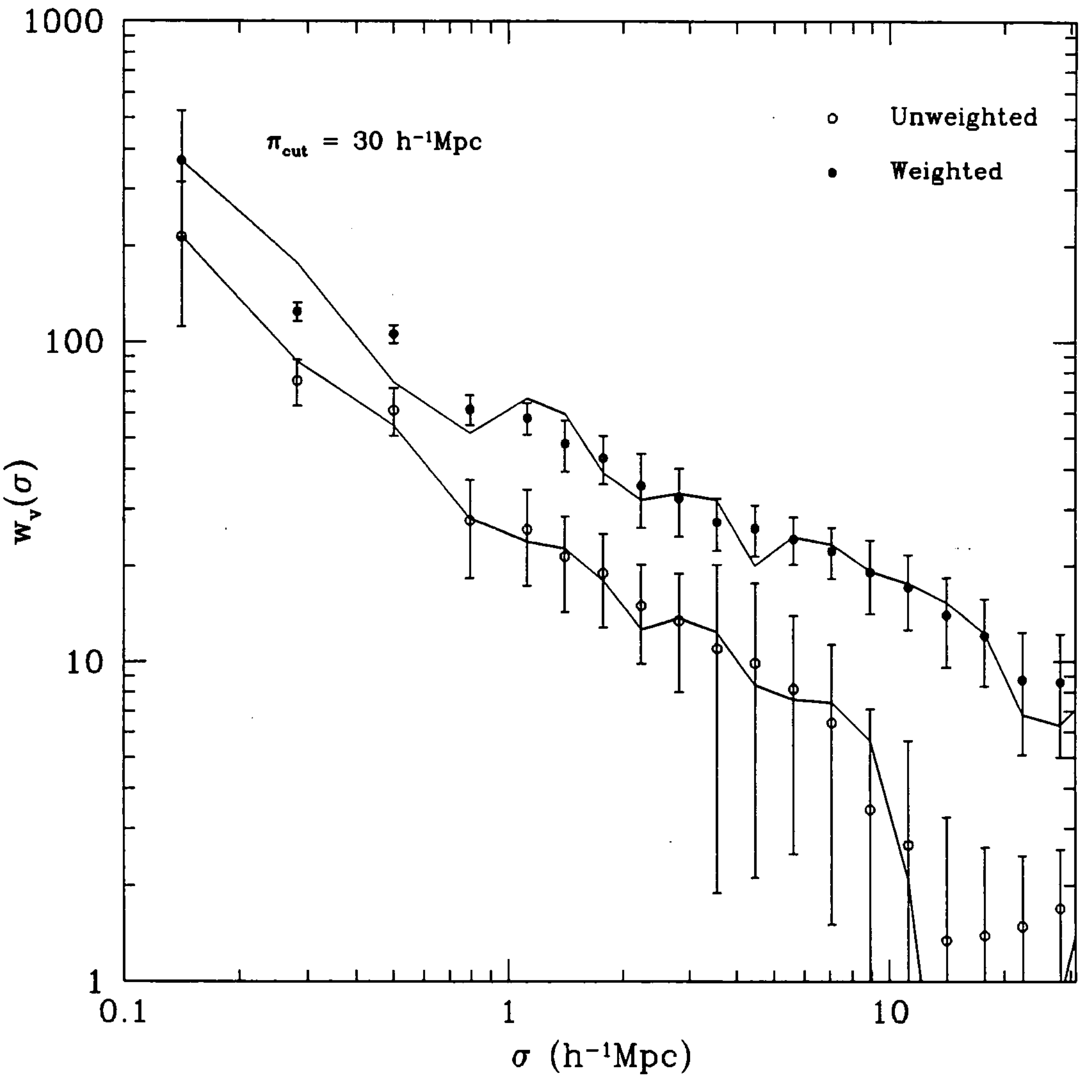

Figure 5.20: The predicted $w_v(\sigma)$ from the Richardson-Lucy inversion for the Durham/UKST survey with $\pi_{cut} = 30h^{-1}$Mpc. The solid lines are the measured $w_v(\sigma)$'s from figure 5.10, while the points are the $w_v(\sigma)$'s calculated from the inverted $\xi(r)$.

5.5 Discussion

In an effort to determine the best estimate of the *redshift* space correlation function the weighted estimates of $\xi(s)$ from figure 5.3 for the Durham/UKST survey, the APM-Stromlo survey (Loveday *et al.* 1992a) and the Las Campanas survey (Tucker *et al.* 1995) are combined. Similarly, the *real* space correlation functions of these surveys have also been combined (Loveday *et al.* 1995b and Lin *et al.* 1995a) using the weighted Abel inversions of $\xi(r)$ (from equation 5.11). Figure 5.21 shows these *real* and *redshift* space correlation functions. The plotted points are an error weighted mean of the 3 surveys and the error bars themselves assume that each survey provides a statistically independent estimate of ξ. The thick solid line is the *real* space $\xi(r)$ estimated from inversion of the APM $w(\theta)$ by Baugh (1996). The thin lines drawn are not formal fits to the data but are merely shown to guide the eye.

The *real* space $\xi(r)$ appears well modelled by an almost featureless single power law in the $\sim$ 0.5-25h^{-1}Mpc regime, with approximate parameters $r_0 \simeq 5.0h^{-1}$Mpc and $\gamma \simeq 1.8$. The high point seen at $\sim 30h^{-1}$Mpc is in the region where it was previously shown that the Abel inversion technique overestimates ξ (see figure 5.16) and therefore this point is not to be trusted. This estimate of $\xi(r)$ agrees quite well with one inverted from the APM $w(\theta)$ by Baugh (1996). However, Baugh's (1996) $\xi(r)$ has a slight "shoulder" feature on 5-25h^{-1}Mpc scales which is not immediately apparent in the data presented here.

The *redshift* space $\xi(s)$ can be approximated by a single power law but appears better modelled with two power laws. The regime where $\xi(s)$ appears to change shape is 4-7h^{-1}Mpc, namely where $\xi \sim 1$. Below these scales the slope is considerably flatter, while on larger scales it is similar to that found in real space.

One can make a few comments about the relative shapes of the *real* and *redshift* space correlation functions. Firstly, $\xi(s)$ appears flattened below $\xi(r)$ on scales $\leq 3h^{-1}$Mpc, altering both the slope and amplitude of ξ. Secondly, on scales $\geq 6h^{-1}$Mpc, $\xi(s)$ appears enhanced over $\xi(r)$ but only the amplitude is altered while the slope remains the same. Thirdly, there is no compelling evidence of the "shoulder" feature seen in $\xi(s)$ by Shanks *et al.* (1983) and Shanks *et al.* (1989) on scales 2-7h^{-1}Mpc, although this is the regime where $\xi(s)$ appears to change shape. Similarly, the slight "shoulder" seen in Baugh's (1996) $\xi(r)$ does not appear to be reproduced, although it does cross the 1σ error bars on the $\xi(r)$ presented here. Finally, this enhancement on larger scales is very pleasing to see as such an effect was predicted from linear theory (Kaiser, 1987) and will be used in chapter 6 to measure $\Omega^{0.6}/b$.

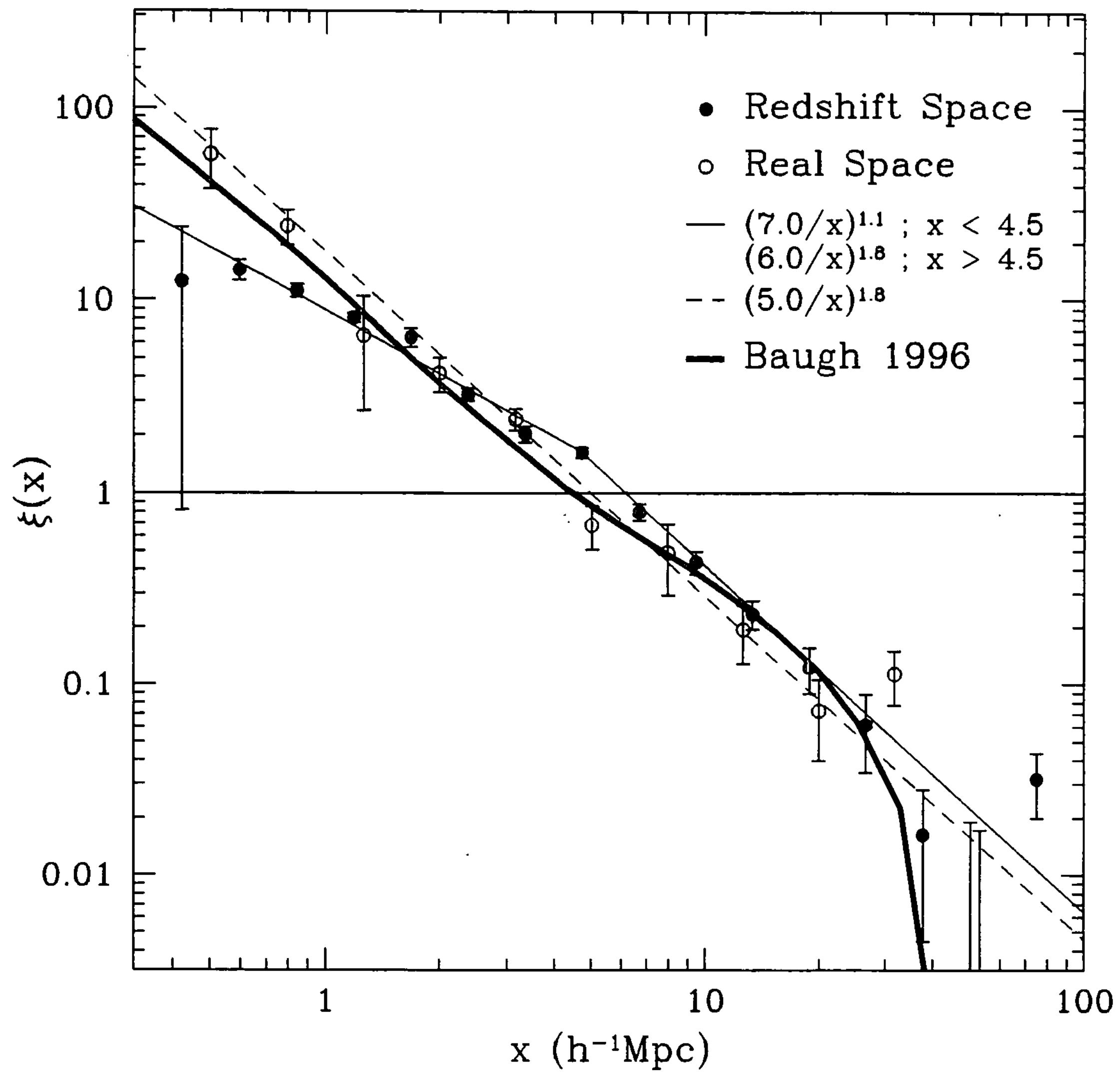

Figure 5.21: The best estimates of the *real* and *redshift* space correlation functions as combined from the Durham/UKST, the APM-Stromlo and the Las Campanas galaxy redshift surveys to produce an error weighted mean.

5.6 Conclusions

The *redshift* space 2-point correlation function, $\xi(s)$, has been estimated from the Durham/UKST galaxy redshift survey and agrees well with other optical estimates of $\xi(s)$ on both small ($< 10h^{-1}$Mpc) and large ($> 10h^{-1}$Mpc) scales. In comparison with two models of structure formation in the Universe, namely SCDM and LCDM, the agreement is also good on small scales. However, on large scales the Durham/UKST survey $\xi(s)$ shows a significant detection of large scale power **above and beyond** that of SCDM. The LCDM model is more consistent with the data but still produces too little large scale power at the 1-2σ level. Also, systematic errors do **not** appear to dominate the estimate of $\xi(s)$ from the Durham/UKST survey and cannot account for the systematic difference seen between the weighted and unweighted estimates which is probably a combination of statistics and a possible systematic bias in the unweighted estimate, thought to be the integral constraint, see chapter 4.

The projected correlation function, $w_v(\sigma)$, has been estimated from the Durham/ UKST galaxy redshift survey. Using a power law model for the *real* space correlation function, $\xi(r)$, the best fit amplitude $r_0 = 5.1 \pm 0.3h^{-1}$Mpc and slope $\gamma = 1.59 \pm 0.09$ are found. These values are consistent with those estimated from other optical surveys. A method of estimating $\xi(r)$ from $w_v(\sigma)$ using an application of the Richardson-Lucy inversion technique is developed and then tested. This method (and another) are then applied to the Durham/UKST survey to give consistent results to the above $\xi(r)$.

Finally, the *real* and *redshift* space correlation functions are combined from the Durham/UKST, APM-Stromlo and Las Campanas galaxy redshift surveys. This shows that $\xi(r)$ appears to have the shape of a single power law, while $\xi(s)$ is better modelled by two power laws. $\xi(s)$ is flattened with respect to $\xi(r)$ on scales $\leq 3h^{-1}$Mpc yet has a similar slope and higher amplitude on scales $\geq 6h^{-1}$Mpc.

Chapter 6

Redshift Space Distortions via the 2-Point Correlation Function

6.1 Introduction

Chapter 5 concentrated on the *redshift* space correlation function, $\xi(s)$, and methods of estimating the *real* space correlation function, $\xi(r)$, from the projected correlation function, $w_v(\sigma)$. This projected correlation function was estimated from the correlation function perpendicular and parallel to the line of sight, $\xi(\sigma, \pi)$, which is affected by the peculiar velocities of galaxies. In this chapter these redshift space distortions are used to estimate some important cosmological parameters.

Throughout this chapter a slightly naive approach is taken in that the analysis is segregated to the non-linear and linear regimes, namely the small and large scales, respectively. The transition between the linear and non-linear regimes can be traced (using numerical simulations) and the accuracy of the modelling determined. It may be better to model simultaneously both regimes at the same time but in this first analysis the simpler approach is taken.

The format of the chapter is as follows. The estimates of $\xi(\sigma, \pi)$ for the Durham/UKST galaxy redshift survey (which were used in chapter 5) are formally presented. These are followed by the analysis of $\xi(\sigma, \pi)$ in the non-linear regime where an estimate of the 1-D pairwise velocity dispersion of galaxies is found. Finally, the analysis of $\xi(\sigma, \pi)$ in the linear regime is shown. This is where the quantity $\beta \simeq \Omega^{0.6}/b$ is estimated, where Ω is the mean mass density of the Universe and b is the linear bias factor relating the matter and galaxy distributions. The chapter ends with the main conclusions from this analysis of the Durham/UKST survey.

6.2 Method of Calculation

$\xi(\sigma, \pi)$ is estimated as follows. A random catalogue is distributed exactly as for the previous estimates of ξ, see chapters 4 and 5. Then the DD, DR and RR pair counts are calculated with and without a weighting. However, binning is now done as a function of two variables, σ and π, perpendicular and parallel to the line of sight, respectively. These two variables were shown in the schematic diagram of figure 5.7 and are now mathematically defined. The line of sight unit vector, $\vec{\mathbf{n}}$, is defined by the bisector of the angular separation of the i'th and j'th points on the sky, θ, and the vector of pair separation, $\vec{\mathbf{s}}$, where

$$\cos\theta = \frac{\vec{\mathbf{r}}_i . \vec{\mathbf{r}}_j}{r_i r_j}, \tag{6.1}$$

$$\vec{\mathbf{s}} = \vec{\mathbf{r}}_i - \vec{\mathbf{r}}_j, \tag{6.2}$$

and $\vec{\mathbf{r}}_i$ and $\vec{\mathbf{r}}_j$ are the position vectors of the i'th and j'th points respectively. π and σ are then naturally defined as the components of $\vec{\mathbf{s}}$ parallel and perpendicular to $\vec{\mathbf{n}}$

$$\pi = \left|\vec{\mathbf{r}}_i . \vec{\mathbf{n}} - \vec{\mathbf{r}}_j . \vec{\mathbf{n}}\right|, \tag{6.3}$$

$$\sigma = \sqrt{r_i^2 - \left(\vec{\mathbf{r}}_i . \vec{\mathbf{n}}\right)^2} + \sqrt{r_j^2 - \left(\vec{\mathbf{r}}_j . \vec{\mathbf{n}}\right)^2}. \tag{6.4}$$

The result is a 2-dimensional array in DD, DR and RR and ξ is then calculated using the estimator of Hamilton (1993). The results of $\xi(\sigma, \pi)$ are relatively insensitive to the specific definitions of σ and π used. Very similar results are found when one uses the definitions of Fisher *et al.* (1994). Even the small angle approximations of σ and π (eg. Hale-Sutton, 1990) give reasonably consistent results for $\xi(\sigma, \pi)$.

6.3 Results from the Durham/UKST Galaxy Redshift Survey

Figures 6.1 and 6.2 show contour plots of constant ξ as a function of σ and π without and with a weighting, respectively. The bin sizes are 0.2 *dex* in pair separation and no smoothing has been applied. Solid contours are for $\xi > 1$ and have $\Delta\xi = 1.0$, dotted contours are for $0 < \xi < 1$ and have $\Delta\xi = 0.1$ and dashed contours are for $\xi < 0$ and have $\Delta\xi = 0.1$. For clarity, the two contours in bold denote $\xi = 1$ and $\xi = 0$ and to help the eye determine the significance of the elongation/compression of the ξ contours, an isotropic model of ξ is plotted as the 4 smooth curves. These two figures show the larger scale features more clearly than the smaller scale ones. Therefore, as a visual aid, figure 6.1 is recalculated with linear binning. This is shown in figure 6.3 where the contours are the same as in figure 6.1 but $0.5h^{-1}$Mpc bins are used. Again, no smoothing has been applied.

It is seen that the unweighted estimate is biased low with respect to the weighted estimate. This is very similar to what was seen in chapter 5. The shape of the

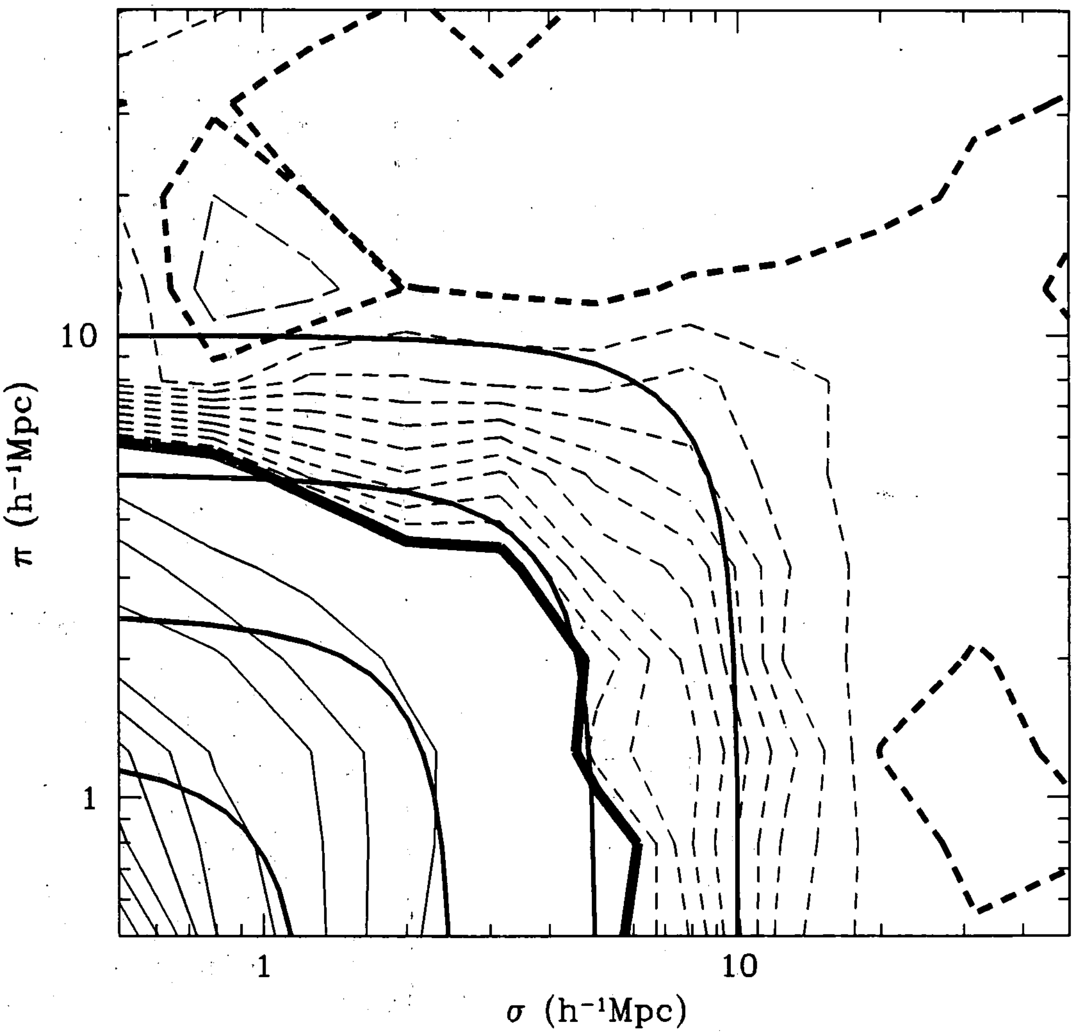

Figure 6.1: $\xi(\sigma, \pi)$ evaluated from the Durham/UKST survey using an *unweighted* estimator on a log-log plot.

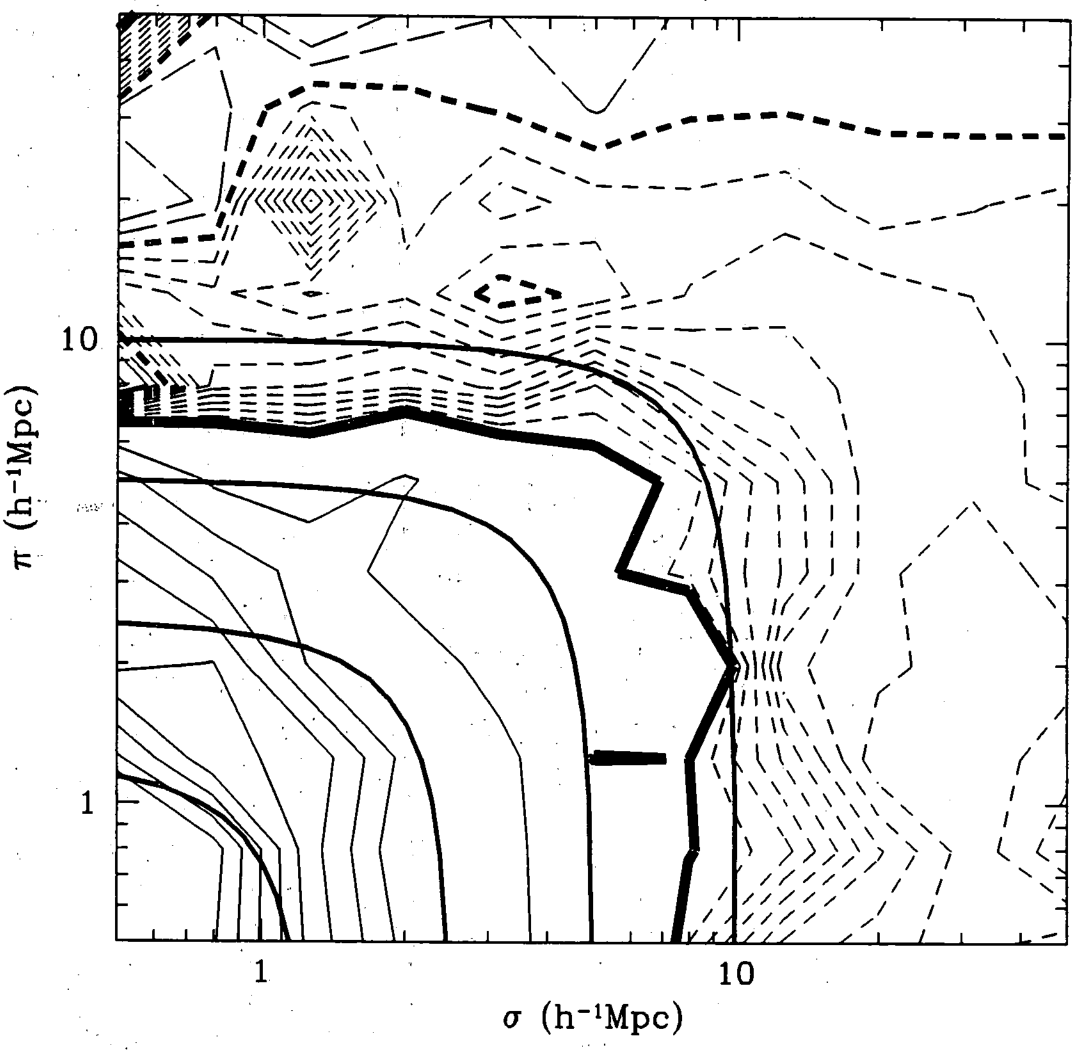

Figure 6.2: $\xi(\sigma, \pi)$ evaluated from the Durham/UKST survey using a *weighted* estimator on a log-log plot.

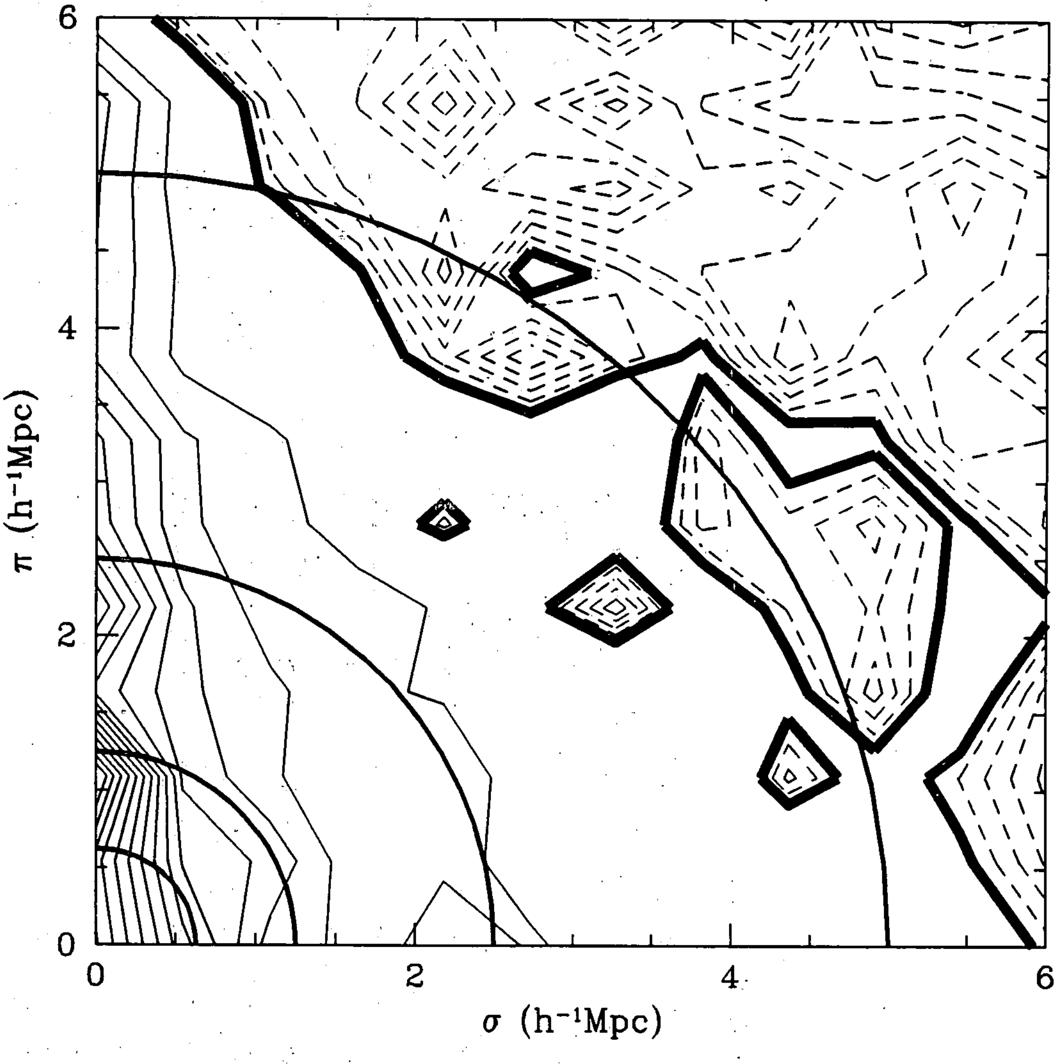

Figure 6.3: $\xi(\sigma, \pi)$ evaluated from the Durham/UKST survey using an *unweighted* estimator on a linear-linear plot.

contours are important because in *real* space they should be circles centered on the origin but in *redshift* space galaxy peculiar velocities distort their shape. On very small scales ($\leq 2h^{-1}$Mpc) the contours are elongated along the line of sight direction (π). This is due to the rms velocity dispersion of galaxies in virialised regions such as clusters and is the well known "finger of God" effect (eg. Peebles, 1980). On larger scales ($> 7h^{-1}$Mpc) the contours are compressed along the line of sight direction (π). This is due to infall (outfall) of galaxies into overdense (underdense) regions. As will be shown in sections 6.5 and 6.6 these two effects can be used to imply information about the dynamics of the Universe.

Viewing these figures by eye gives the impression that the unweighted estimate has less noise associated with it than the weighted one. This is confusing as the weighting used was supposed to produce the minumum variance in ξ. It is possible that the $w = 1/(1 + 4\pi\bar{n}S(x)J_3(s))$ weighting is no longer optimal in terms of producing the minimum variance in ξ. Basically, in $\xi(s)$ the s variable defines bins which are spherical shells and the above weighting is optimal in this case (eg. Efstathiou, 1988 or Loveday *et al.* 1995b). However, in $\xi(\sigma,\pi)$ the σ and π variables define bins which are cylindrical shells and this change in geometrical shape could imply that the above weighting is no longer optimal. However, despite the visual impression which favours the unweighted estimate of $\xi(\sigma,\pi)$, the weighted estimate is again preferred (similar to chapters 4 and 5) because this estimate does not suffer from the systematic bias which lowers the unweighted estimate.

6.4 Comparison with the CDM Simulations

6.4.1 The N-Body Simulations

ξ was calculated from the SCDM & LCDM simulations (as described in chapters 4 and 5) assuming the distant observer approximation, namely that the N-body cube was at a large distance away from the observer such that the line of sight direction can simply be assumed to be the z-direction. Binning was then done in the σ and π variables which (in the distant observer approximation) define cylindrical shells in $\sqrt{x^2+y^2}$ and z, respectively.

Figure 6.4 shows the mean contour plot of constant ξ as a function of σ and π for the 9 full SCDM N-body simulations. It is clear that the small scale ($\pi < 10h^{-1}$Mpc) rms velocity dispersion dominates the whole plot, elongating the contours drastically in the π direction. This elongation is seen even on large scales ($\pi > 10h^{-1}$Mpc) where it was hoped that the compression in the π direction from dynamical infall would be prominent. The $\xi = 1$ contour cuts the σ axis between 4.5-5.0h^{-1}Mpc which agrees well with the real space amplitude for these simulations (5.0h^{-1}Mpc).

Figure 6.5 shows a similar plot for the 5 full LCDM N-body simulations. Even in these simulations the small scale ($\pi < 10h^{-1}$Mpc) rms velocity dispersion is significant although less so than for the SCDM simulations. There is possible evidence

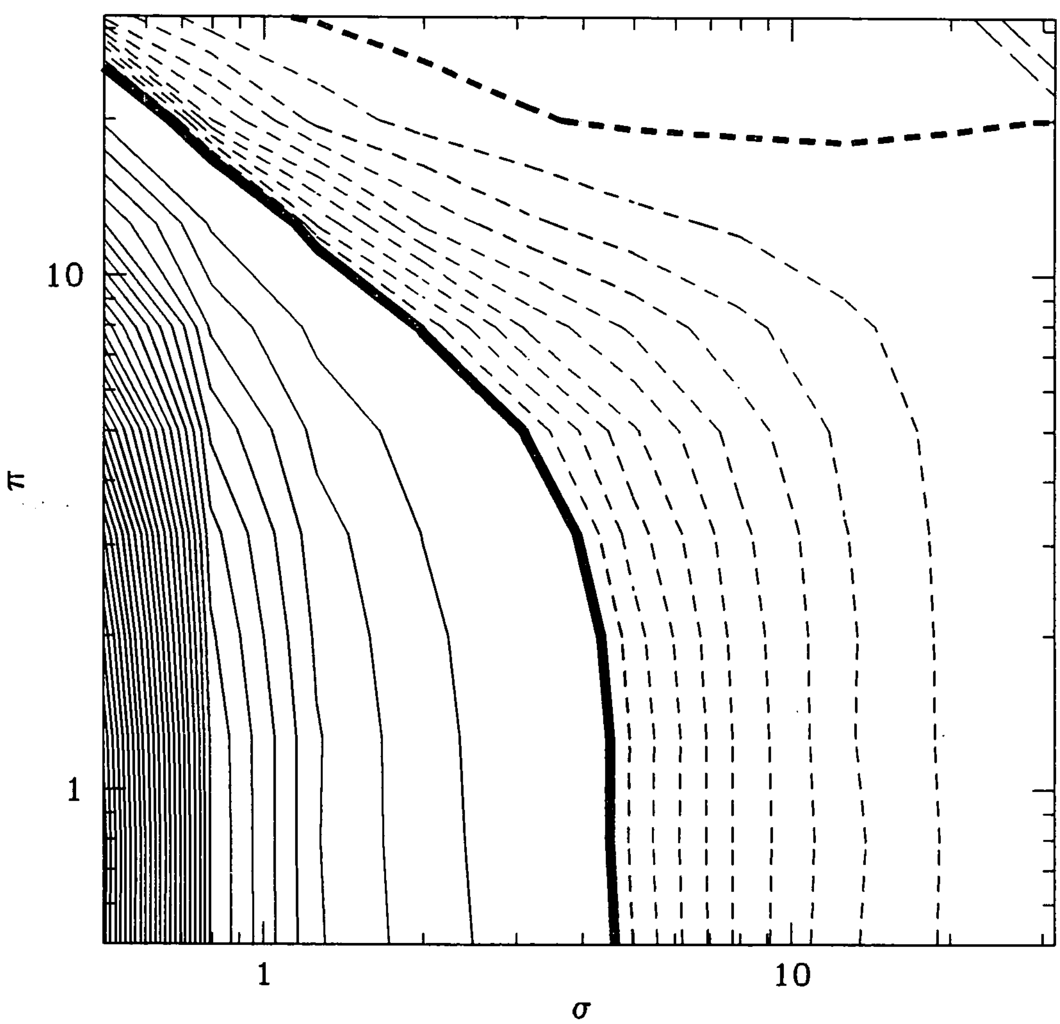

Figure 6.4: The mean $\xi(\sigma, \pi)$ evaluated from the 9 full SCDM N-body simulations on a log-log plot.

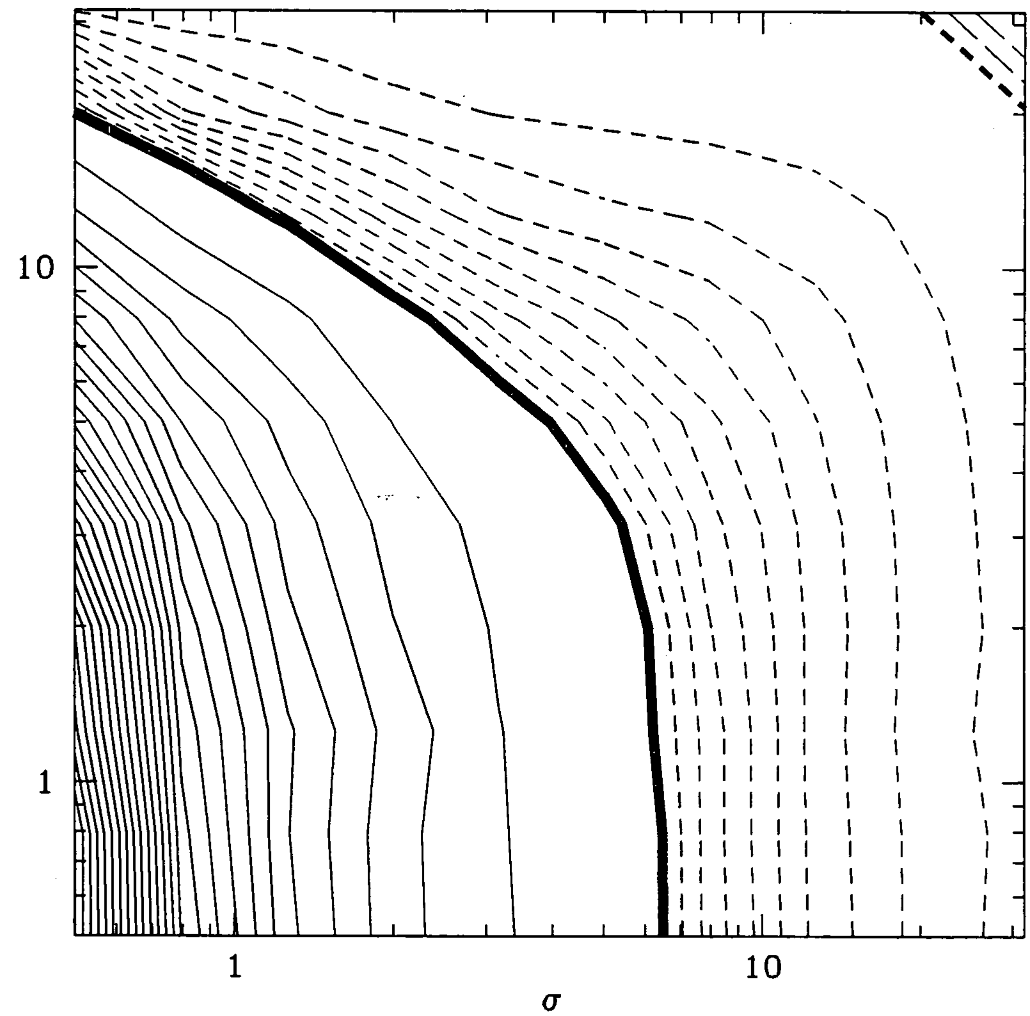

Figure 6.5: The mean $\xi(\sigma, \pi)$ evaluated from the 5 full LCDM N-body simulations on a log-log plot.

of a compression in the π direction near $\pi \sim 20h^{-1}$Mpc, this will be investigated in section 6.6. The extra large scale power in this model can be seen as the $\xi = 1$ contour now cuts the σ axis at $\sim 6.5h^{-1}$Mpc. Again this agrees well with the real space amplitude for these simulations ($6.0h^{-1}$Mpc).

6.4.2 The Mock Catalogues

ξ was calculated from these mock catalogues in exactly the same way as the Durham/UKST data (as outlined in section 6.2). Only one example of $\xi(\sigma, \pi)$ from the set of SCDM/LCDM mock catalogues is shown so that a direct comparison of the relative noise levels in the mock catalogues and Durham/UKST survey can be made.

Figures 6.6 and 6.7 show the contour plots of constant ξ as functions of σ and π for the first mock catalogue drawn from the SCDM simulations with ξ calculated without and with a weighting, respectively. Comparison with figure 6.4 shows that the mock catalogues do reproduce the same features seen in the $\xi(\sigma, \pi)$ from the SCDM simulations. The noise levels are similar to those seen in the Durham/UKST data for both plots with the weighted estimate being slightly worse, see section 6.3 for a possible explanation. The systematic bias which lowers the unweighted estimate on large scales is not immediately apparent in figure 6.6. This is because the bias in these mock catalogues was quite small, ~ 0.03 in ξ, and should only really be added for an ensemble of surveys, not just the one shown here.

Figures 6.8 and 6.9 show the corresponding plots for the first mock catalogue drawn from the LCDM simulations. One can make similar qualitative statements (to those for the SCDM mock catalogues) regarding the noise levels in $\xi(\sigma, \pi)$, the systematic bias seen in the unweighted estimate and the ability of the mock catalogues to reproduce the same features as the simulations.

6.5 Non-linear Effects – Small Scales

6.5.1 Modelling the Pairwise Velocity Dispersion

Following the modelling of Peebles (1980) define $\vec{\mathbf{v}}$ to be the peculiar velocity of a galaxy above the Hubble flow, therefore $\vec{\mathbf{w}} = \vec{\mathbf{v}}_i - \vec{\mathbf{v}}_j$ is the peculiar velocity difference of two galaxies separated by a vector $\vec{\mathbf{r}}$. Now let $g(\vec{\mathbf{r}}, \vec{\mathbf{w}})$ be the distribution function of $\vec{\mathbf{w}}$. The correlation function in *real* space is convolved with this distribution function to give the *redshift* correlation function in σ and π space

$$1 + \xi(\sigma, \pi) = \int [1 + \xi(r)]\, g(\vec{\mathbf{r}}, \vec{\mathbf{w}}) d^3 w, \tag{6.5}$$

where

$$r^2 = \sigma^2 + r_z^2 \quad , \quad r_z = \pi - \frac{w_z}{H_0}, \tag{6.6}$$

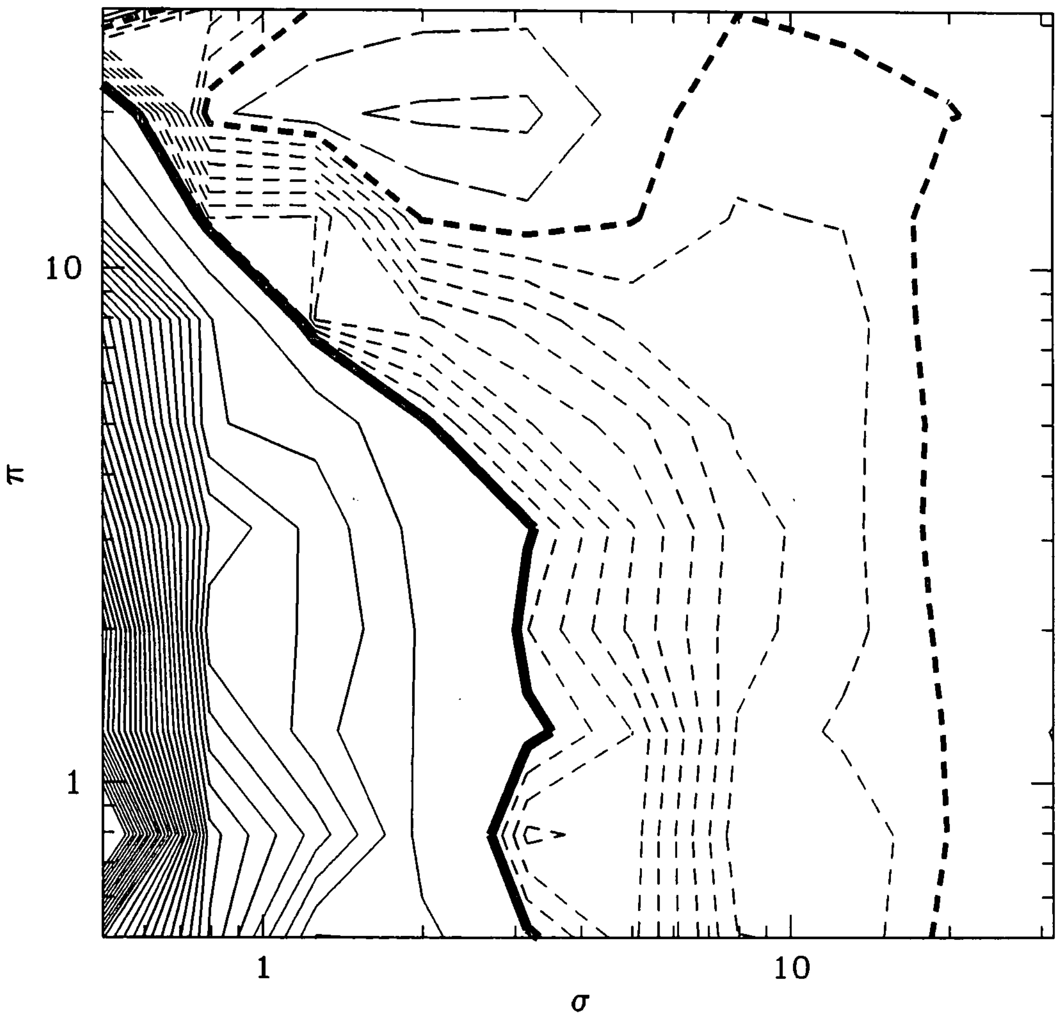

Figure 6.6: $\xi(\sigma, \pi)$ evaluated using an *unweighted* estimate from the first mock catalogue selected from the SCDM simulations on a log-log plot.

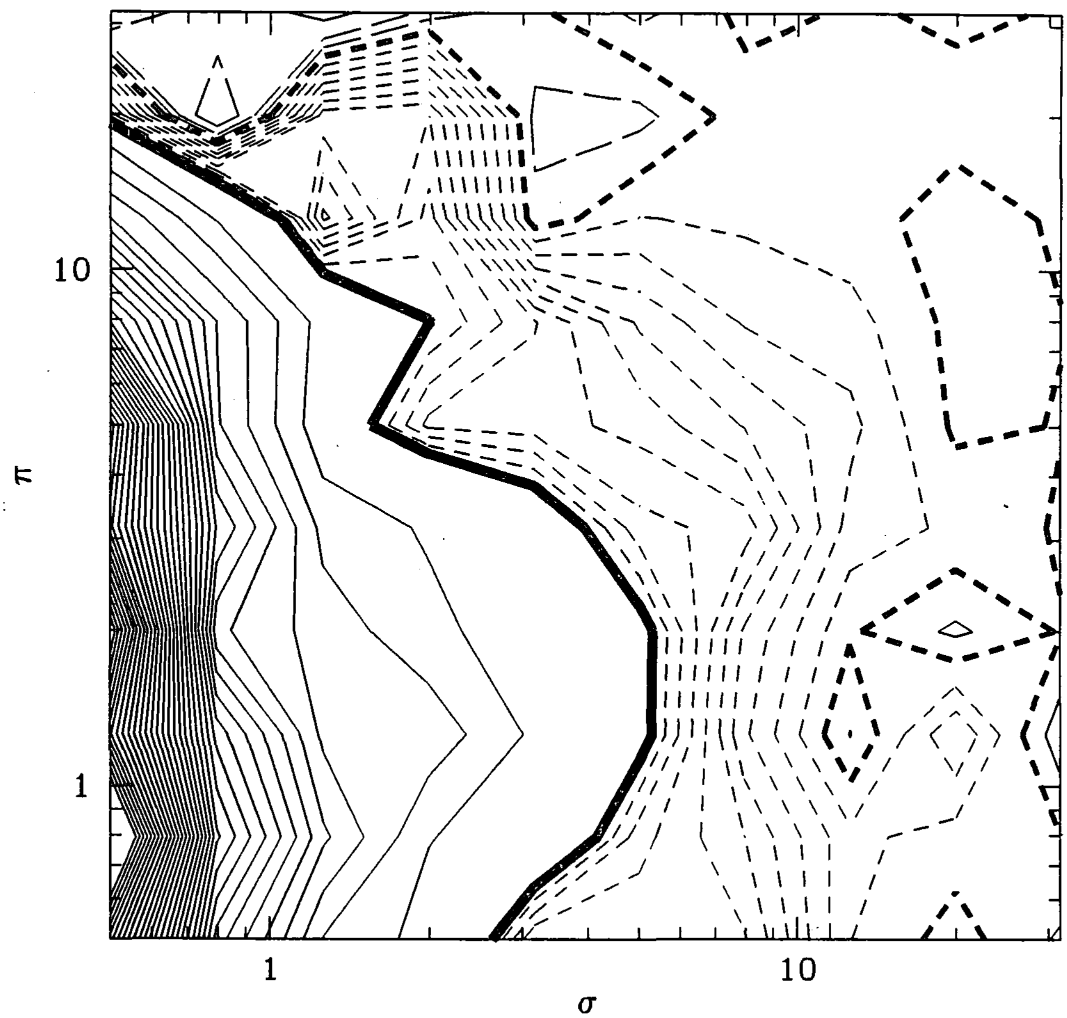

Figure 6.7: $\xi(\sigma, \pi)$ evaluated using a *weighted* estimate from the first mock catalogue selected from the SCDM simulations on a log-log plot.

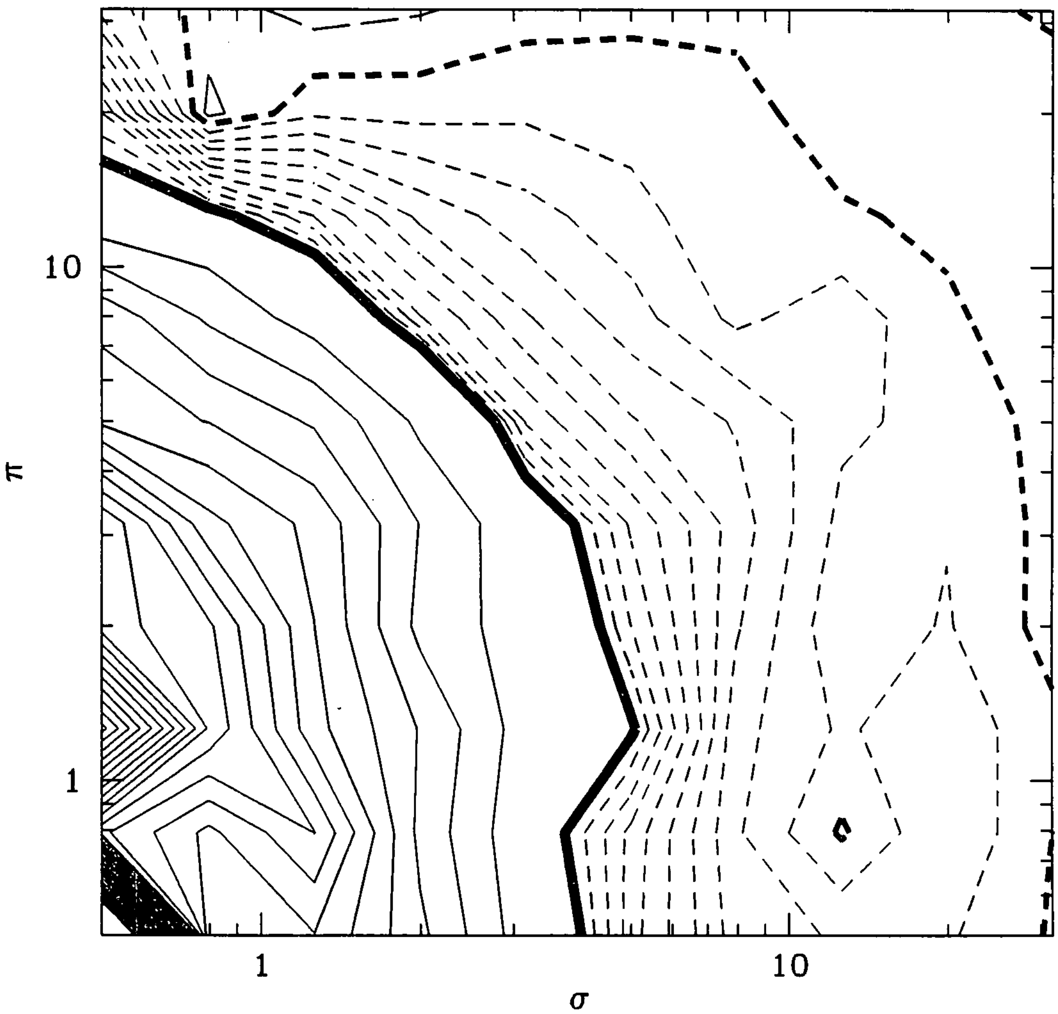

Figure 6.8: $\xi(\sigma, \pi)$ evaluated using an *unweighted* estimate from the first mock catalogue selected from the LCDM simulations on a log-log plot.

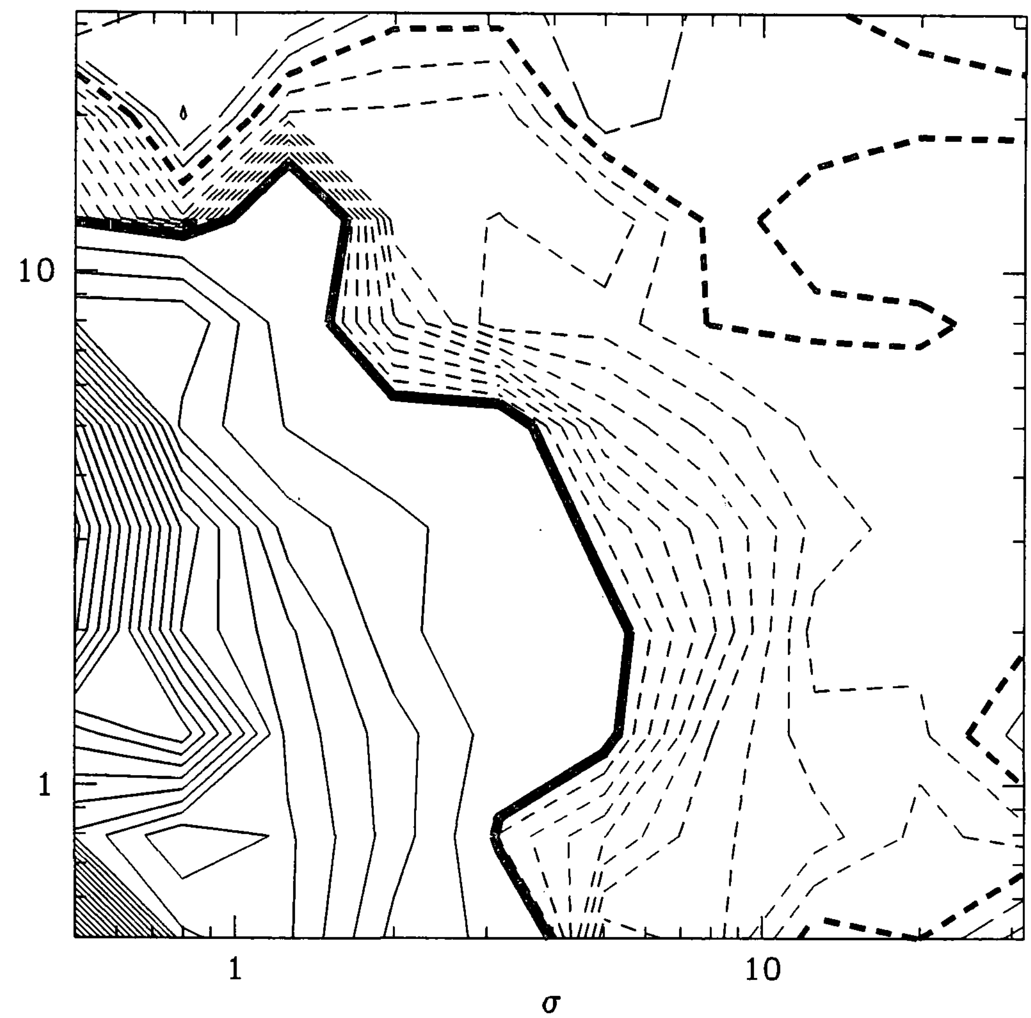

Figure 6.9: $\xi(\sigma, \pi)$ evaluated using a *weighted* estimate from the first mock catalogue selected from the LCDM simulations on a log-log plot.

and w_z is the component of $\vec{\mathbf{w}}$ parallel to the line of sight, which for simplicity is called the z direction. Note that $(1+\xi)$ is convolved (and not simply ξ) because it is the data pair counts that are actually altered by the convolution and this transfers itself to ξ since $DD \sim (1+\xi)$. It is common to assume that g is a slowly varing function of $\vec{\mathbf{r}}$ such that $g(\vec{\mathbf{r}}, \vec{\mathbf{w}}) = g(\vec{\mathbf{w}})$ and therefore it is possible to make the approximation

$$\int dw_x \int dw_y \; g(\vec{\mathbf{w}}) = f(w_z). \tag{6.7}$$

Equation 6.5 then becomes

$$1 + \xi(\sigma, \pi) = \int [1 + \xi(r)] \, f(w_z) dw_z, \tag{6.8}$$

which further reduces to

$$\xi(\sigma, \pi) = \int_{-\infty}^{\infty} \xi(r) f(w_z) dw_z, \tag{6.9}$$

when the normalisation of $f(w_z)$ is considered, namely that $\int f(w_z) dw_z = 1$. If it is considered necessary to include a streaming model which describes the relative bulk motion of galaxies towards (or away from) each other then this can be incorporated as follows

$$g(\vec{\mathbf{r}}, \vec{\mathbf{w}}) = g(\vec{\mathbf{w}} - \hat{\mathbf{r}} v(r)), \tag{6.10}$$

where $v(r)$ is the streaming model in question. In equation 6.7 this implies

$$\int dw_x \int dw_y \; g(\vec{\mathbf{w}} - \hat{\mathbf{r}} v(r)) = f(w_z - v(r_z)), \tag{6.11}$$

and equation 6.5 then becomes

$$1 + \xi(\sigma, \pi) = \int [1 + \xi(r)] \, f(w_z - v(r_z)) dw_z, \tag{6.12}$$

$$= \int_{-\infty}^{\infty} \left[1 + \xi\left(\sqrt{\sigma^2 + r_z^2}\right)\right] f\left[w_z - v(r_z)\right] dw_z, \tag{6.13}$$

where again

$$r_z = \left(\pi - \frac{w_z}{H_0}\right). \tag{6.14}$$

Obviously, models for the real space 2-point correlation function, $\xi(r)$, the distribution function, $f(w_z)$, and the streaming motion, $v(r_z)$, are required. The real space 2-point correlation function is simply modelled by a power law (similar to chapters 4 and 5)

$$\xi(r) = \left(\frac{r_0}{r}\right)^{\gamma}, \tag{6.15}$$

and in chapter 5 this was shown to be accurate out to $\sim 20h^{-1}$Mpc. For the distribution function one could assume two possible models which could be used to describe the galaxy velocity dispersion, namely an exponential

$$f(w_z) = \frac{1}{\sqrt{2}\,\langle w_z^2 \rangle^{\frac{1}{2}}} \exp\left[-\sqrt{2}\frac{|w_z|}{\langle w_z^2 \rangle^{\frac{1}{2}}}\right], \tag{6.16}$$

or a Gaussian

$$f(w_z) = \frac{1}{\sqrt{2\pi}\,\langle w_z^2\rangle^{\frac{1}{2}}} \exp\left[-\frac{1}{2}\frac{|w_z|^2}{\langle w_z^2\rangle}\right], \tag{6.17}$$

where $\langle w_z^2\rangle^{\frac{1}{2}}$ is the rms pairwise velocity dispersion, namely the second moment of the distribution function $f(w_z)$

$$\left\langle w_z^2\right\rangle = \int_{-\infty}^{\infty} f(w_z) w_z^2 dw_z. \tag{6.18}$$

N-body simulations done by Efstathiou *et al.* (1988b) show that for a wide set of initial conditions $f(w_z) \sim \exp(-\alpha|w_z|^{3/2})$ gives a good fit to this distribution function and so either the exponential or the gaussian model seem realistic. One might expect a good streaming motion model to depend on the clustering, biasing and the mean mass density of the Universe. The infall model of Bean *et al.* (1983) takes the maximal approach by assuming $\Omega = 1$ and $b = 1$ and uses the second BBGKY equation (eg. Peebles, 1980) to give

$$v(r_z) = -H_0 r_z \left[\frac{\xi(r_z)}{1+\xi(r_z)}\right]. \tag{6.19}$$

6.5.2 Testing the Method with the CDM Simulations

Before testing the modelling of section 6.5.1 it would be advantageous to know the answers one is trying to reproduce. The 2-point correlation functions of these CDM simulations have already been calculated in chapter 4 and therefore need no more description here. The value of $\langle w_z^2\rangle^{\frac{1}{2}}$ for these 2 CDM simulations is now estimated directly from the N-body cubes. Using the SCDM/LCDM subsamples of section 4.5.1 the rms (1-D) difference in peculiar velocities of galaxies is calculated as a function of real space separation r. Figure 6.10 shows the results of the 1-D galaxy pairwise velocity dispersion obtained from averaging over the 9 and 5 simulations of SCDM and LCDM, respectively. It can be seen that $\langle w_z^2\rangle^{\frac{1}{2}} \simeq 950$ and 750 kms^{-1} for the SCDM and LCDM simulations, respectively, on scales $\sim 1h^{-1}$Mpc.

Section 6.5.1 showed that there are 3 parameters which can be estimated in trying to fit these models to the non-linear effects. It is not sensible to try to fit all 3 parameters simultaneously and it is found that the results of the fitting process are insensitive to the value of γ chosen, provided a realistic value is used. In this case (for the CDM simulations) $\gamma = 2.2$. Also, when considering the streaming model a value of $r_0 = 5.0$-$6.0h^{-1}$Mpc is assumed in the ξ used to estimate $v(r_z)$, again the fits are relatively insensitive to the value used. At this stage one might think of using the γ and r_0 estimated from chapter 4 but in practice the results differ little when this is done. The fitting of the other two parameters, $\langle w_z^2\rangle^{\frac{1}{2}}$ and r_0, is done by calculating the minimum value of an approximate χ^2 statistic using the standard deviation seen in the ξ's in the N-body simulations. 40 points in π are fit from

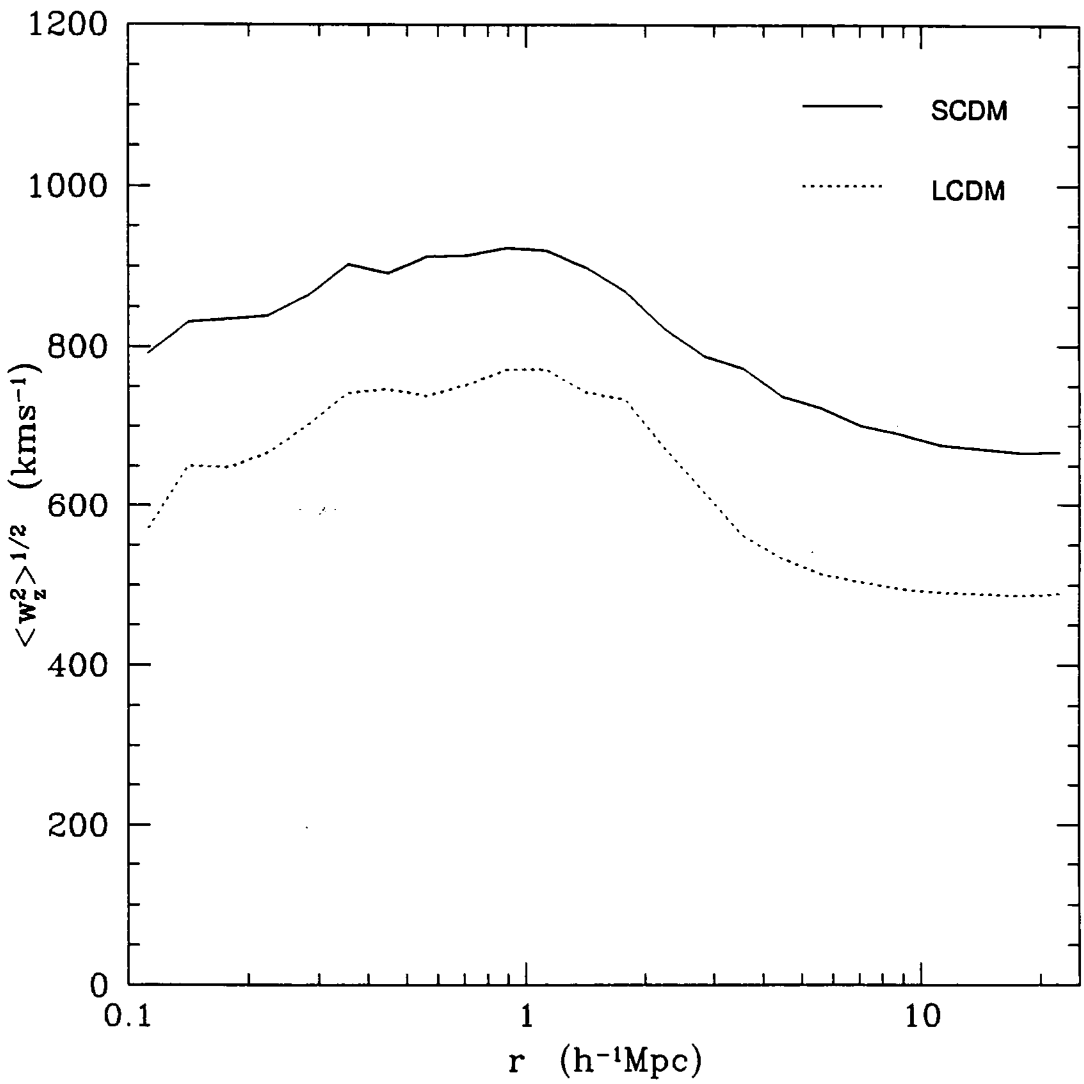

Figure 6.10: The 1-D galaxy pairwise velocity dispersion, $\langle w_z^2 \rangle^{\frac{1}{2}}$, as a function of real space separation, r, for the SCDM and LCDM simulations.

0-20h^{-1}Mpc in linear bins of width 0.5h^{-1}Mpc for four different values of σ. Once again it is important to sound a note of caution about the significance levels of the results in this χ^2 statistic because of the non-independent nature of the points. The results of the χ^2 statistic for the different models are shown in tables 6.1 and 6.2 for the full SCDM and LCDM N-body simulations, respectively. Figures 6.11 and 6.12 show these minimum χ^2 fits to $\xi(\sigma, \pi)$ for the full SCDM N-body simulations with the exponential and gaussian velocity dispersion models, respectively. Figures 6.13 and 6.14 show the corresponding plots for the full LCDM N-body simulations. The histogram denotes the measured $\xi(\sigma, \pi)$, while the solid and dotted lines are the fits with and without the streaming model, respectively.

These tables and figures for the N-body simulations show that the streaming (infall) model only becomes important (in terms of producing consistent results for $\langle w_z^2 \rangle^{\frac{1}{2}}$) when $\sigma >$ 1-2h^{-1}Mpc. This assumes that $\langle w_z^2 \rangle^{\frac{1}{2}}$ does not vary with σ. Also, the exponential distribution function gives a better fit to $\xi(\sigma, \pi)$ regardless of streaming effects, the gaussian one does not quite have the correct shape. This was seen in both the SCDM and LCDM simulations. The best fit model to the N-body simulations, namely exponential with infall, had $\langle w_z^2 \rangle^{\frac{1}{2}} = 980 \pm 22$ kms^{-1} and $r_0 = 5.00 \pm 0.24h^{-1}$Mpc for the SCDM simulations and $\langle w_z^2 \rangle^{\frac{1}{2}} = 835 \pm 60$ kms^{-1} and $r_0 = 5.12 \pm 0.69h^{-1}$Mpc for the LCDM simulations (where the errors come from the scatter in the best fit points in tables 6.1 and 6.2). The values of the velocity dispersion can be compared with those estimated from figure 6.10 on 1h^{-1}Mpc scales, namely 950 and 750 kms^{-1} for the SCDM and LCDM simulations, respectively. This agreement is adequate given that the exponential model was an assumption. The values of r_0 can be compared with the approximate *real* space values estimated from figures 4.9 and 4.11, namely 5.0h^{-1}Mpc and 6.0h^{-1}Mpc for the SCDM and LCDM simulations, respectively. Again, the agreement is adequate in both cases although slightly small for the LCDM model. However, closer inspection of figure 4.11 shows that $r_0 \simeq 5.0h^{-1}$Mpc on scales $r \leq 3h^{-1}$Mpc, this probably explains the lower r_0 seen for the LCDM model.

Tables 6.3 and 6.4 show the results of fitting the exponential model to the unweighted $\xi(\sigma, \pi)$ estimates from the SCDM and LCDM mock catalogues, respectively. The corresponding results for the weighted $\xi(\sigma, \pi)$ estimates are given in tables 6.5 and 6.6. The standard deviations from the SCDM/LCDM mock catalogues are used in these χ^2 fits. The error bars quoted are simply the 1σ standard deviations seen between the mock catalogues themselves and therefore reflect the errors in an individual mock catalogue. All of the $\langle w_z^2 \rangle^{\frac{1}{2}}$ values in tables 6.3, 6.4, 6.5 and 6.6 are consistent, given the quoted errors, with the corresponding results from the full N-body simulations. The SCDM mock catalogue r_0's in table 6.3 and 6.5 are consistent with the value of 5.0h^{-1}Mpc, agreeing well with the SCDM N-body simulations regardless of weighting. The LCDM mock catalogue unweighted r_0's of table 6.4 are slightly lower than expected, 4.5h^{-1}Mpc compared with 6.0h^{-1}Mpc. This is probably a combination of the smaller r_0 on small scales and the slight systematic bias seen in these unweighted estimates. The weighted r_0's of table 6.4 are higher, $\sim 5.3h^{-1}$Mpc, which is expected given the the weighted/unweighted results of chapter 4 for the LCDM mock catalogues.

σ (h^{-1}Mpc)	$\langle w_z^2 \rangle^{\frac{1}{2}}$ (kms^{-1})	r_0 (h^{-1}Mpc)	χ^2 ($N_{bin} = 40$)
Exponential & Infall			
[0,0.5]	990	5.1	39.95
[0.5,1]	1000	5.3	24.67
[1,2]	980	4.8	21.17
[2,4]	950	4.8	34.40
Exponential & No Infall			
[0,0.5]	970	5.1	46.29
[0.5,1]	960	5.4	32.32
[1,2]	800	4.9	28.72
[2,4]	550	5.1	48.20
Gaussian & Infall			
[0,0.5]	750	4.9	152.78
[0.5,1]	740	5.2	76.46
[1,2]	700	4.6	63.08
[2,4]	690	4.6	54.33
Gaussian & No Infall			
[0,0.5]	740	4.9	144.56
[0.5,1]	710	5.3	57.61
[1,2]	610	4.8	28.25
[2,4]	470	5.1	14.94

Table 6.1: Minimum χ^2 results for r_0 and $\langle w_z^2 \rangle^{\frac{1}{2}}$ from the SCDM N-body simulations using two forms for modelling the velocity dispersion, with and without a streaming model.

σ (h^{-1}Mpc)	$\langle w_z^2\rangle^{\frac{1}{2}}$ (kms^{-1})	r_0 (h^{-1}Mpc)	χ^2 ($N_{bin} = 40$)
Exponential & Infall			
[0,0.5]	770	4.1	13.82
[0.5,1]	810	5.3	7.81
[1,2]	850	5.4	16.46
[2,4]	910	5.6	11.07
Exponential & No Infall			
[0,0.5]	780	4.2	14.24
[0.5,1]	760	5.4	8.14
[1,2]	720	5.6	14.02
[2,4]	570	5.9	8.96
Gaussian & Infall			
[0,0.5]	570	4.2	129.39
[0.5,1]	610	5.2	73.79
[1,2]	650	5.3	83.02
[2,4]	620	5.3	124.40
Gaussian & No Infall			
[0,0.5]	560	4.2	118.00
[0.5,1]	580	5.3	58.14
[1,2]	570	5.5	48.48
[2,4]	440	5.8	23.37

Table 6.2: Minimum χ^2 results for r_0 and $\langle w_z^2\rangle^{\frac{1}{2}}$ from the LCDM N-body simulations using two forms for modelling the velocity dispersion, with and without a streaming model.

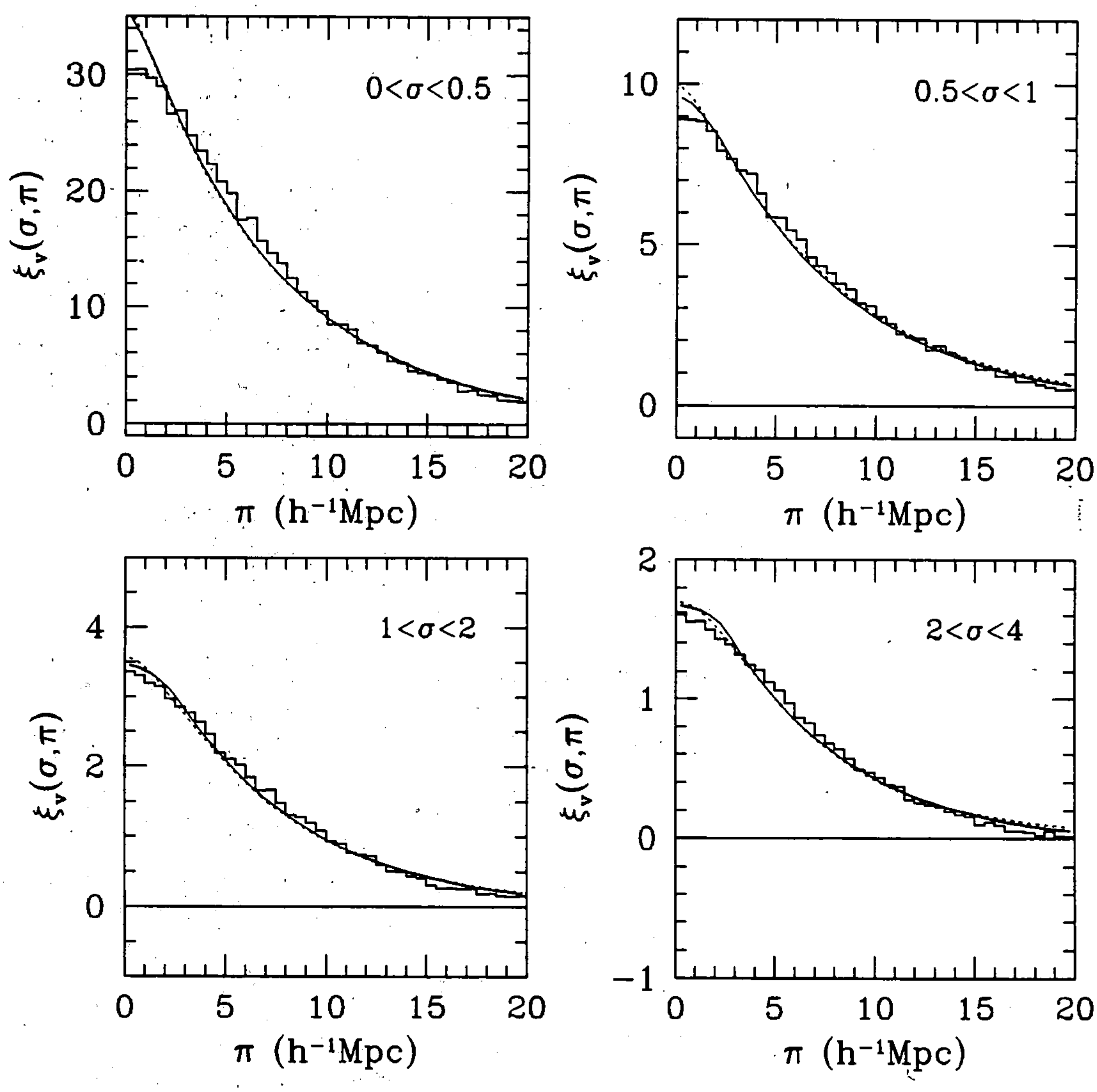

Figure 6.11: Minimum χ^2 fits to $\xi(\sigma, \pi)$ from the full SCDM simulations at different σ separations using an *exponential* model for the velocity dispersion. Solid lines have a streaming model included, dotted lines do not.

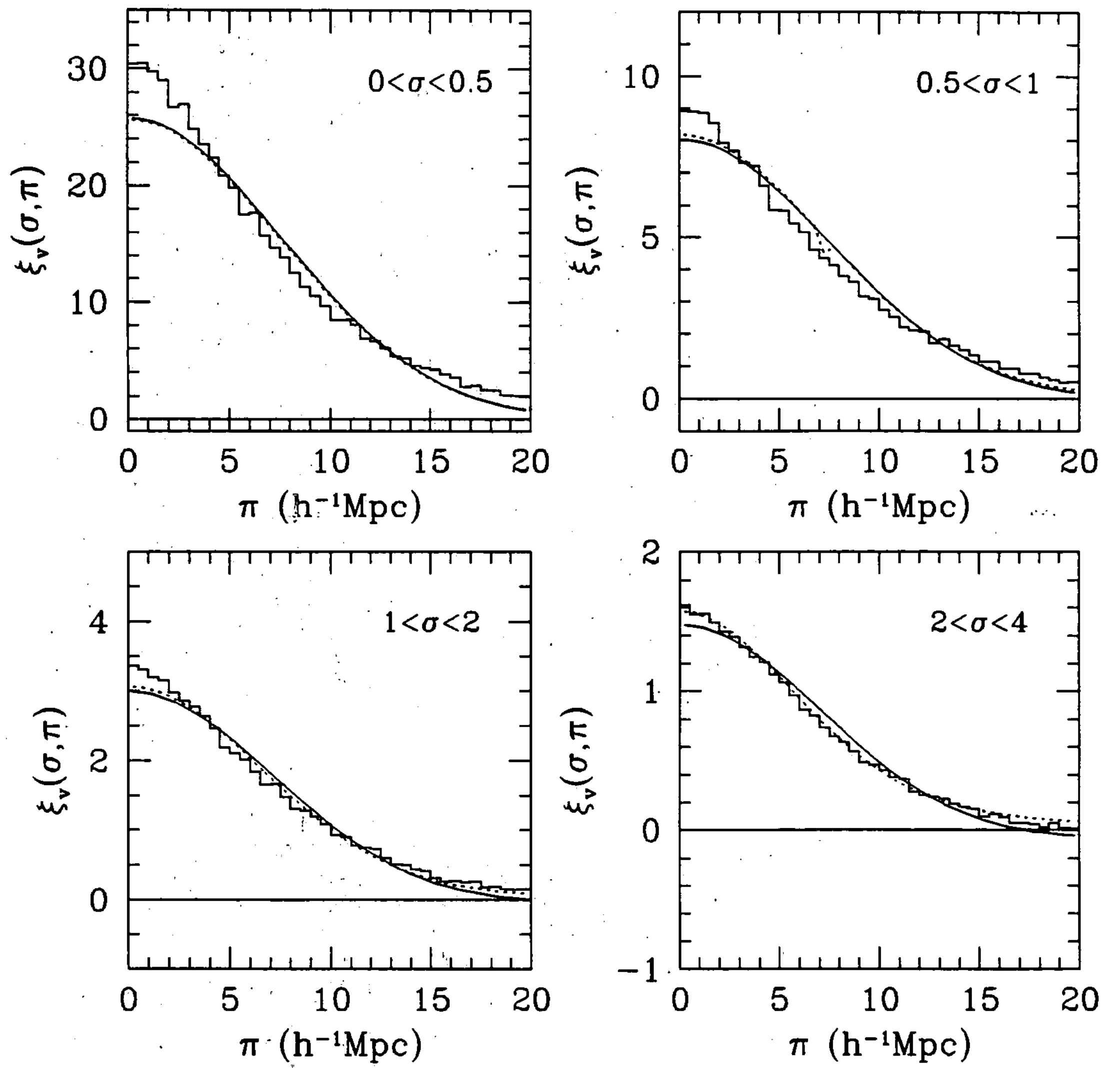

Figure 6.12: Minimum χ^2 fits to $\xi(\sigma, \pi)$ from the full SCDM simulations at different σ separations using a *gaussian* model for the velocity dispersion. Solid lines have a streaming model included, dotted lines do not.

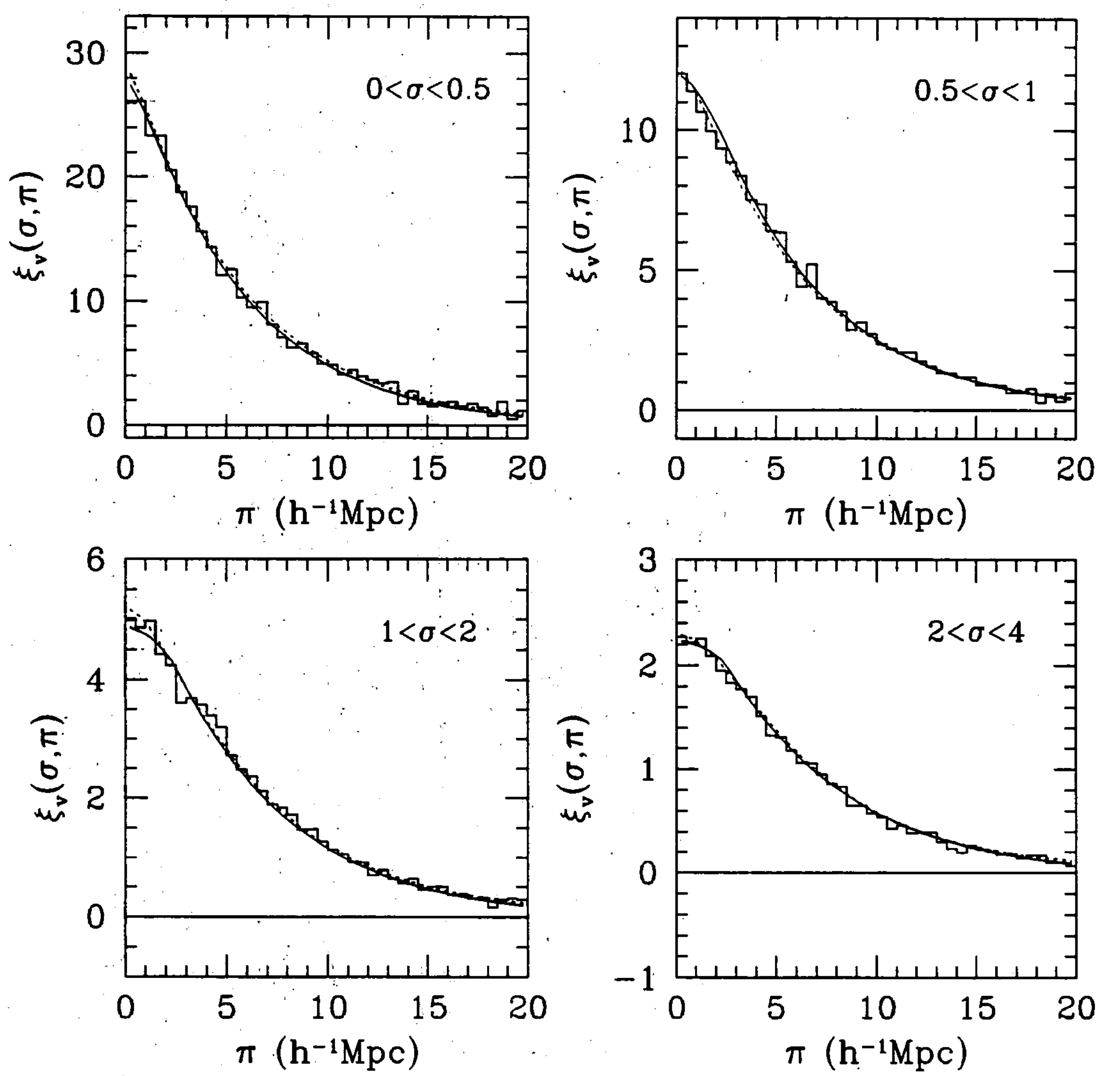

Figure 6.13: Minimum χ^2 fits to $\xi(\sigma, \pi)$ from the full LCDM simulations at different σ separations using an *exponential* model for the velocity dispersion. Solid lines have a streaming model included, dotted lines do not.

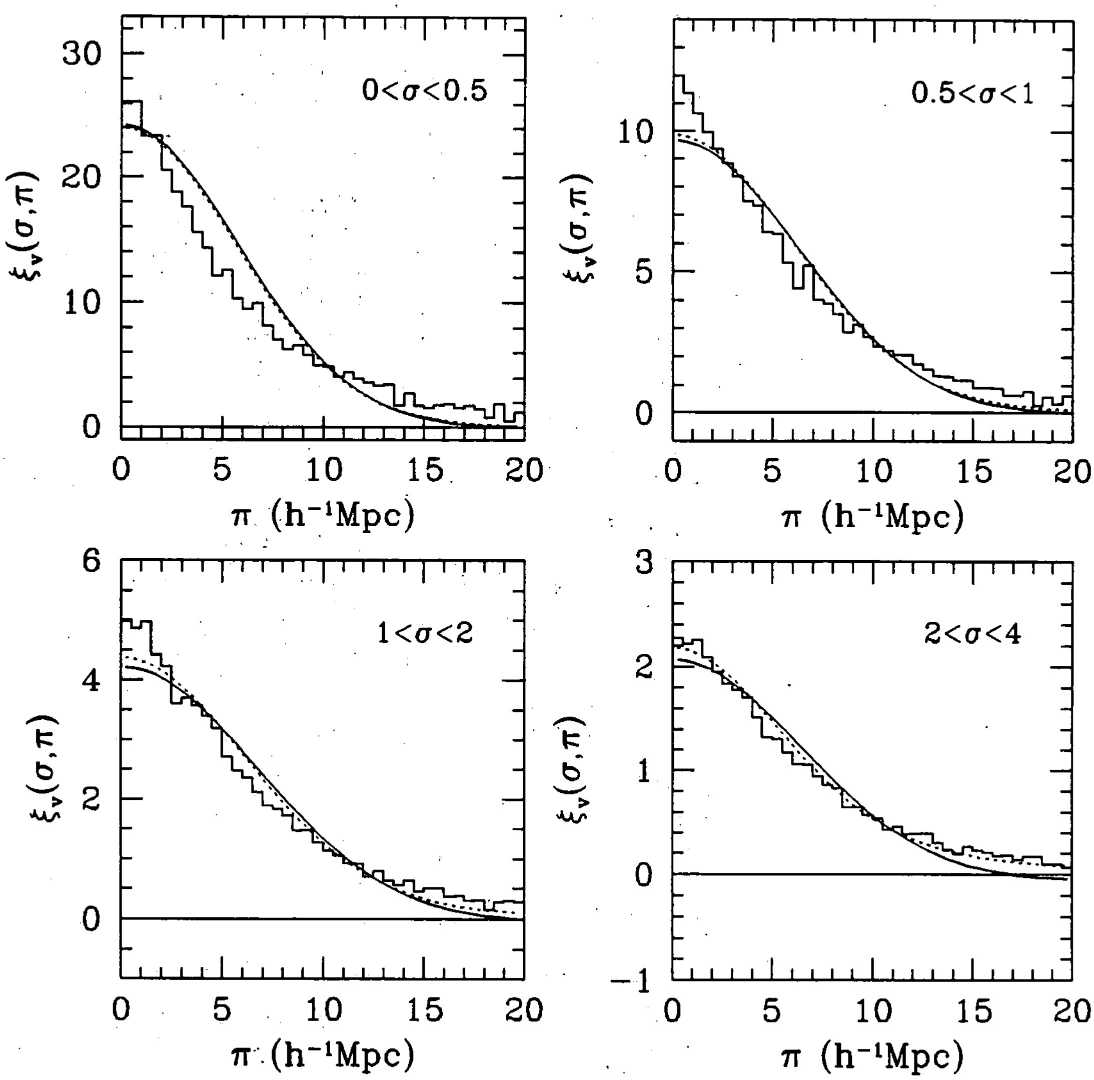

Figure 6.14: Minimum χ^2 fits to $\xi(\sigma, \pi)$ from the full LCDM simulations at different σ separations using a *gaussian* model for the velocity dispersion. Solid lines have a streaming model included, dotted lines do not.

σ (h^{-1}Mpc)	$\langle w_z^2 \rangle^{\frac{1}{2}}$ (kms^{-1})	r_0 (h^{-1}Mpc)
Infall		
[0,0.5]	1055 ± 277	5.14 ± 0.50
[0.5,1]	1017 ± 248	5.30 ± 0.65
[1,2]	1043 ± 270	4.83 ± 0.92
[2,4]	1012 ± 326	4.98 ± 1.20
No Infall		
[0,0.5]	1040 ± 276	5.15 ± 0.50
[0.5,1]	958 ± 237	5.35 ± 0.63
[1,2]	871 ± 265	4.97 ± 0.86
[2,4]	628 ± 298	5.32 ± 1.02

Table 6.3: The mean and 1σ standard deviation of the minimum χ^2 results for r_0 and $\langle w_z^2 \rangle^{\frac{1}{2}}$ from the 18 SCDM mock catalogues using the *unweighted* $\xi(\sigma, \pi)$. An *exponential* form of the velocity dispersion with and without a streaming model was used in the fitting procedure.

σ (h^{-1}Mpc)	$\langle w_z^2 \rangle^{\frac{1}{2}}$ (kms^{-1})	r_0 (h^{-1}Mpc)
Infall		
[0,0.5]	683 ± 157	3.89 ± 0.44
[0.5,1]	703 ± 163	4.72 ± 1.03
[1,2]	691 ± 225	4.67 ± 1.32
[2,4]	804 ± 475	4.73 ± 1.74
No Infall		
[0,0.5]	663 ± 152	3.92 ± 0.42
[0.5,1]	640 ± 170	4.81 ± 0.99
[1,2]	530 ± 241	4.86 ± 1.21
[2,4]	470 ± 532	5.27 ± 1.54

Table 6.4: The mean and 1σ standard deviation of the minimum χ^2 results for r_0 and $\langle w_z^2 \rangle^{\frac{1}{2}}$ from the 15 LCDM mock catalogues using the *unweighted* $\xi(\sigma, \pi)$. An *exponential* form of the velocity dispersion with and without a streaming model was used in the fitting procedure.

σ (h^{-1}Mpc)	$\langle w_z^2 \rangle^{\frac{1}{2}}$ (kms^{-1})	r_0 (h^{-1}Mpc)
Infall		
[0,0.5]	932 ± 190	5.01 ± 0.44
[0.5,1]	966 ± 181	5.26 ± 0.38
[1,2]	917 ± 265	4.57 ± 0.48
[2,4]	812 ± 178	4.49 ± 0.58
No Infall		
[0,0.5]	922 ± 187	5.01 ± 0.44
[0.5,1]	915 ± 167	5.31 ± 0.36
[1,2]	752 ± 225	4.75 ± 0.41
[2,4]	448 ± 131	4.98 ± 0.38

Table 6.5: The mean and 1σ standard deviation of the minimum χ^2 results for r_0 and $\langle w_z^2 \rangle^{\frac{1}{2}}$ from the 18 SCDM mock catalogues using the *weighted* $\xi(\sigma, \pi)$. An *exponential* form of the velocity dispersion with and without a streaming model was used in the fitting procedure.

σ (h^{-1}Mpc)	$\langle w_z^2 \rangle^{\frac{1}{2}}$ (kms^{-1})	r_0 (h^{-1}Mpc)
Infall		
[0,0.5]	608 ± 183	3.83 ± 0.34
[0.5,1]	794 ± 234	5.16 ± 0.69
[1,2]	838 ± 129	5.17 ± 0.69
[2,4]	778 ± 152	5.21 ± 0.68
No Infall		
[0,0.5]	592 ± 168	3.87 ± 0.33
[0.5,1]	750 ± 222	5.24 ± 0.65
[1,2]	689 ± 128	5.31 ± 0.67
[2,4]	441 ± 135	5.59 ± 0.55

Table 6.6: The mean and 1σ standard deviation of the minimum χ^2 results for r_0 and $\langle w_z^2 \rangle^{\frac{1}{2}}$ from the 15 LCDM mock catalogues using the *weighted* $\xi(\sigma, \pi)$. An *exponential* form of the velocity dispersion with and without a streaming model was used in the fitting procedure.

These results confirm that the correct $\langle w_z^2 \rangle^{\frac{1}{2}}$ and r_0 can be reproduced from the mock catalogues. The results from the weighted estimates have slightly smaller errors than those from the unweighted estimates. They also do not suffer from any systematic bias in r_0. Therefore, the weighted estimates are favoured here.

6.5.3 Results from the Durham/UKST Galaxy Redshift Survey

Table 6.7 shows the results for r_0 and $\langle w_z^2 \rangle^{\frac{1}{2}}$ from minimum χ^2 fits to the Durham /UKST survey unweighted $\xi(\sigma,\pi)$. Table 6.8 shows the corresponding results for the weighted $\xi(\sigma,\pi)$. The standard deviations on an individual LCDM mock catalogue are used in the χ^2 fits. Note that these χ^2's are more than likely biased low by the non-independent nature of the points. The error bar quoted in each parameter comes from the $\Delta\chi^2 = 1.0$ contour, namely the 68% confidence interval on an individual parameter. Figures 6.15 and 6.16 show plots of the fits to the unweighted Durham/UKST $\xi(\sigma,\pi)$ data for the exponential and gaussian velocity dispersion models, respectively. Figures 6.17 and 6.18 show the corresponding plots for the weighted $\xi(\sigma,\pi)$ data. As before, the histograms show the measured $\xi(\sigma,\pi)$, while the solid and dotted lines are the fits with and without the streaming model. From these tables and figures one can make 4 comments. Firstly, the streaming model is again required to produce the most consistent fits for $\langle w_z^2 \rangle^{\frac{1}{2}}$ for $\sigma >$ 1-2h^{-1}Mpc (assuming that it is independent of σ). Secondly, the noise in the data does not enable a clear determination between an exponential or a gaussian velocity dispersion (both models produce very similar minimum χ^2 values). Thirdly, better fits (ie. lower χ^2's) are obtained to the unweighted $\xi(\sigma,\pi)$ than the weighted $\xi(\sigma,\pi)$. As discussed in section 6.2 this is because the weighted $\xi(\sigma,\pi)$ is noisier. Finally, the systematic bias in ξ from using an unweighted estimator is also apparent here. Therefore, the best fit unweighted r_0's are again biased low, see chapters 4 and 5.

Assuming that at each σ value an independent estimate of r_0 and $\langle w_z^2 \rangle^{\frac{1}{2}}$ are obtained, one can combine these to produce the best estimate of these two parameters. For the unweighted Durham/UKST $\xi(\sigma,\pi)$, the exponential distribution function with a streaming model gives $r_0 = 3.32 \pm 0.28 h^{-1}$Mpc and $\langle w_z^2 \rangle^{\frac{1}{2}} = 400 \pm 66$ kms^{-1}. The gaussian function with a streaming model gives $r_0 = 3.13 \pm 0.23 h^{-1}$Mpc and $\langle w_z^2 \rangle^{\frac{1}{2}} = 291 \pm 40$ kms^{-1}. For the weighted Durham/UKST $\xi(\sigma,\pi)$, the exponential velocity dispersion with a streaming model gives $r_0 = 4.61 \pm 0.20 h^{-1}$Mpc and $\langle w_z^2 \rangle^{\frac{1}{2}} = 416 \pm 36$ kms^{-1}. The gaussian function with a streaming model gives $r_0 = 4.58 \pm 0.22 h^{-1}$Mpc and $\langle w_z^2 \rangle^{\frac{1}{2}} = 334 \pm 30$ kms^{-1}. These measured values of r_0 can be compared with those estimated in chapter 5 using projected methods involving ξ, namely $r_0 = 3.2 \pm 0.2$ (unweighted) and $r_0 = 5.1 \pm 0.3$ (weighted). The agreement between these weighted/unweighted values of r_0 is good and it is pleasing to see that different methods of analysis on the same data set have produced similar results. Again, one should note that the non-independent nature of $\xi(\sigma,\pi)$ implies that the error bars quoted here are more than likely an underestimate.

σ (h^{-1}Mpc)	$\langle w_z^2\rangle^{\frac{1}{2}}$ (kms^{-1})	r_0 (h^{-1}Mpc)	χ^2 ($N_{bin} = 40$)
Exponential & Infall			
[0,0.5]	400 ± 200	3.7 ± 0.8	1.84
[0.5,1]	330 ± 95	3.4 ± 0.5	3.86
[1,2]	400 ± 105	3.3 ± 0.4	5.81
[2,4]	470 ± 95	3.2 ± 0.4	4.00
Exponential & No Infall			
[0,0.5]	350 ± 190	3.8 ± 0.8	1.73
[0.5,1]	210 ± 85	3.7 ± 0.5	4.53
[1,2]	180 ± 95	3.8 ± 0.3	6.91
[2,4]	10 ± 85	4.2 ± 0.4	8.13
Gaussian & Infall			
[0,0.5]	280 ± 125	3.5 ± 0.7	1.83
[0.5,1]	240 ± 60	3.3 ± 0.4	3.79
[1,2]	280 ± 50	3.0 ± 0.3	4.80
[2,4]	350 ± 55	3.1 ± 0.3	3.38
Gaussian & No Infall			
[0,0.5]	260 ± 130	3.7 ± 0.7	1.74
[0.5,1]	180 ± 75	3.8 ± 0.5	4.51
[1,2]	160 ± 85	3.8 ± 0.3	6.56
[2,4]	10 ± 75	4.2 ± 0.4	8.14

Table 6.7: Minimum χ^2 results of r_0 and $\langle w_z^2\rangle^{\frac{1}{2}}$ for the Durham/UKST survey using two forms for modelling the velocity dispersion, with and without a streaming model. The fits were done to the unweighted $\xi(\sigma, \pi)$.

σ (h^{-1}Mpc)	$\langle w_z^2 \rangle^{\frac{1}{2}}$ (kms^{-1})	r_0 (h^{-1}Mpc)	χ^2 ($N_{bin} = 40$)
Exponential & Infall			
[0,0.5]	510 ± 120	5.1 ± 0.6	18.99
[0.5,1]	300 ± 50	4.7 ± 0.3	23.51
[1,2]	500 ± 65	4.5 ± 0.2	29.56
[2,4]	500 ± 65	4.7 ± 0.4	47.97
Exponential & No Infall			
[0,0.5]	470 ± 130	5.2 ± 0.6	19.10
[0.5,1]	180 ± 70	4.8 ± 0.4	24.01
[1,2]	270 ± 90	4.8 ± 0.3	29.52
[2,4]	180 ± 80	5.5 ± 0.2	56.10
Gaussian & Infall			
[0,0.5]	430 ± 85	5.0 ± 0.6	17.49
[0.5,1]	220 ± 40	4.4 ± 0.4	26.28
[1,2]	350 ± 65	4.2 ± 0.4	30.62
[2,4]	420 ± 40	4.8 ± 0.3	38.41
Gaussian & No Infall			
[0,0.5]	410 ± 85	5.2 ± 0.6	17.83
[0.5,1]	140 ± 60	4.8 ± 0.4	25.06
[1,2]	230 ± 80	4.8 ± 0.3	29.56
[2,4]	190 ± 70	5.5 ± 0.2	55.56

Table 6.8: Minimum χ^2 results of r_0 and $\langle w_z^2 \rangle^{\frac{1}{2}}$ for the Durham/UKST survey using two forms for modelling the velocity dispersion, with and without a streaming model. The fits were done to the weighted $\xi(\sigma, \pi)$.

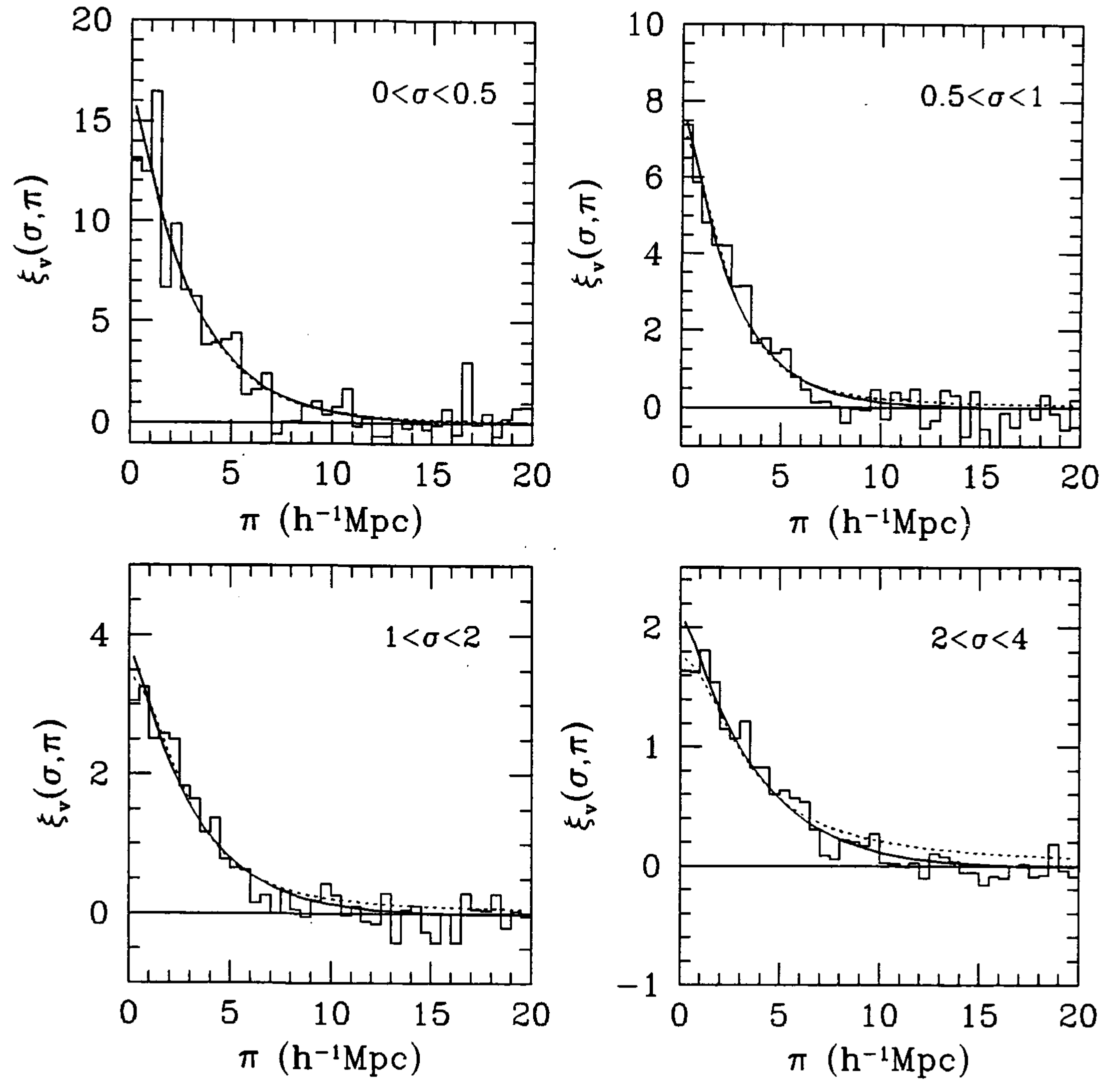

Figure 6.15: Minimum χ^2 fits to the *unweighted* $\xi(\sigma,\pi)$ estimated from the Durham/UKST survey at different σ separations using an *exponential* model for the velocity dispersion. Solid lines have a streaming model included, dotted lines do not.

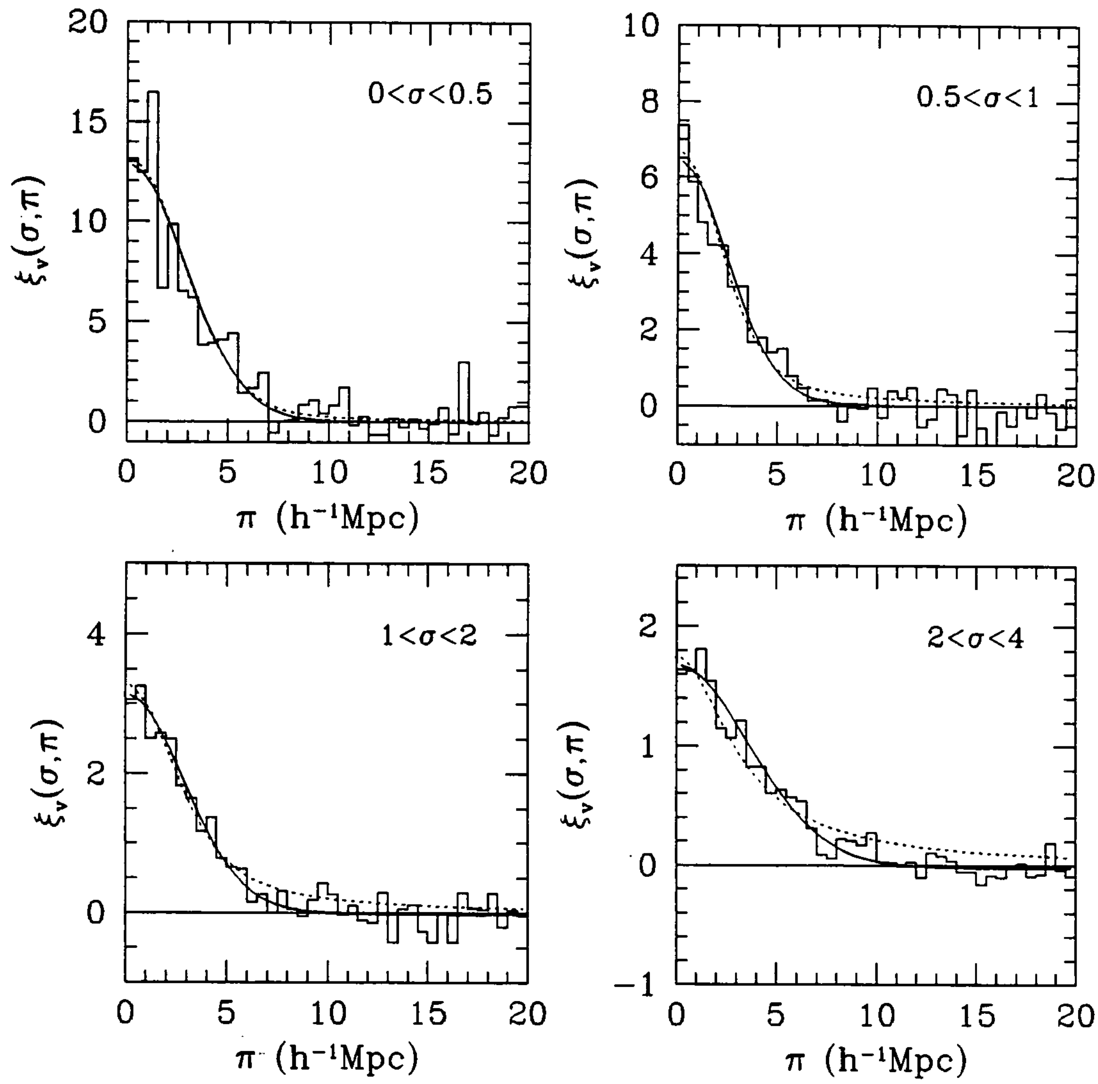

Figure 6.16: Minimum χ^2 fits to the *unweighted* $\xi(\sigma, \pi)$ estimated from the Durham/UKST survey at different σ separations using a *gaussian* model for the velocity dispersion. Solid lines have a streaming model included, dotted lines do not.

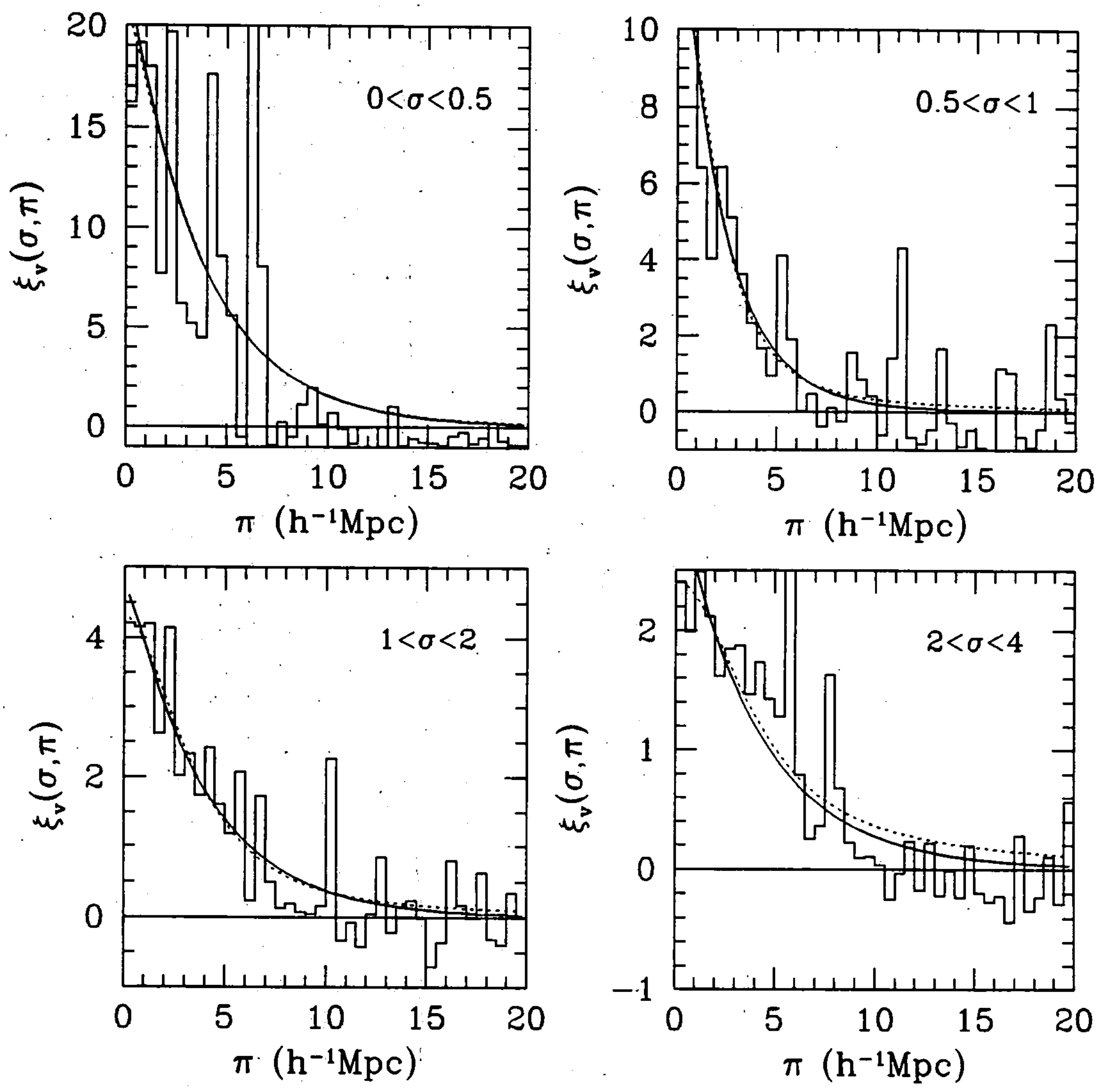

Figure 6.17: Minimum χ^2 fits to the *weighted* $\xi(\sigma, \pi)$ estimated from the Durham/UKST survey at different σ separations using an *exponential* model for the velocity dispersion. Solid lines have a streaming model included, dotted lines do not.

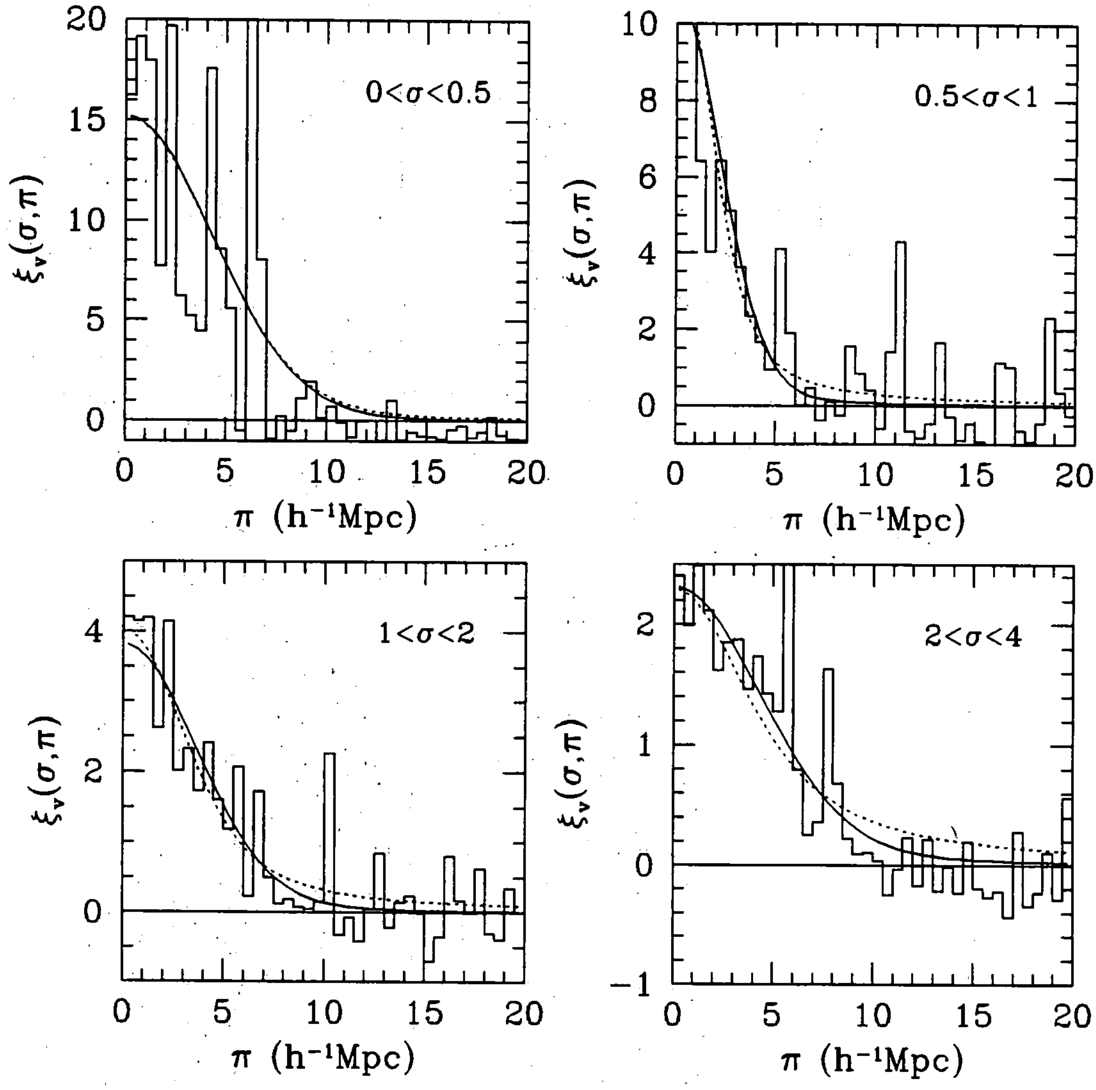

Figure 6.18: Minimum χ^2 fits to the *weighted* $\xi(\sigma, \pi)$ estimated from the Durham/UKST survey at different σ separations using a *gaussian* model for the velocity dispersion. Solid lines have a streaming model included, dotted lines do not.

6.5.4 Comparison with other Data Sets and the Simulations

The minimum χ^2 fit of an exponential distribution function (with a streaming model) to the weighted $\xi(\sigma,\pi)$ from the Durham/UKST survey gave a value of the 1-D pairwise velocity dispersion of 416 ± 36 kms^{-1}. This best fit value is of particular interest as recent estimates from new redshift surveys and the re-analysis of old redshift surveys have been measuring larger 1-D pairwise velocity dispersions than the canonical value of 340 ± 40 kms^{-1} found by Davis & Peebles (1983) from the CfA1 survey. For example, using the CfA2/SSRS2 survey Marzke *et al.* (1995) find 540 ± 180 kms^{-1} and using the Las Campanas survey Lin *et al.* (1995a) find 452 ± 60 kms^{-1}. Mo *et al.* (1993) measured large variations (200-1000 kms^{-1}) in the 1-D pairwise velocity dispersion for a number of samples of similar size to CfA1, they also show that it is sensitive to galaxy sampling, especially dominant clusters the size of Coma. This new estimate from the Durham/UKST survey is still on the low side supporting the old Davis & Peebles (1983) value but is not inconsistent ($> 3\sigma$) with any of these other measured values. When considering these values it is important to note that the Durham/UKST survey covers a volume $\sim 4\times10^6 h^{-3}$Mpc^3, approximately twice that of the CfA2/SSRS2 survey and half that of the Las Campanas survey (see table 3.4). Also, in an unbiased (COBE-normalised) CDM model, Marzke *et al.* (1995) estimated that the velocity dispersion would converge to 10% within a volume $\sim 5\times10^6 h^{-3}$Mpc^3. Therefore, the measurement from the Durham/UKST survey is hopefully believable and representative of the actual value in the Universe. Finally, one notes that the Durham/UKST survey does not contain any extremely dominant clusters (of Coma-like size) and therefore will not be biased high by this.

The best estimates of the 1-D pairwise velocity dispersion from the SCDM and LCDM simulations using the above techniques were 980 and 835 kms^{-1}, respectively. (Note that these values were estimated assuming an exponential distribution function, for consistency one should compare with the Durham/UKST survey exponential value.) These estimates agree well with the actual value of the 1-D pairwise velocity dispersion as measured directly from the N-body simulations. However, these values are inconsistent with the measured value from the Durham/UKST survey at high levels of significance. In fact, even taking the most negative approach possible and using the error bars from the mock catalogues on the Durham/UKST velocity dispersion, namely $\pm\sim 200$ kms^{-1} on an individual independent measurement at a given perpendicular separation and hence $\pm\sim 100$ kms^{-1} overall on the combined measurement, one still finds a significant rejection of both CDM models at the 3-5 σ level. However, it should be noted that a significant velocity bias, b_v, between the matter and galaxy velocity distributions ($b_v \sim 0.4$), see Couchman & Carlberg (1992), would allow consistent results between the models and the data. Also, this rejection of the CDM models assumes that the simple models of linear biasing used here (Bardeen *et al.* 1986) are an adequate description of the galaxy formation process.

6.6 Linear Effects – Large Scales

6.6.1 Modelling the Redshift Space Correlation Function with Linear Theory

On small, non-linear scales it was seen that the velocity dispersion was mainly responsible for the anisotropies in $\xi(\sigma,\pi)$. However, to produce consistent results, it was also necessary to incorporate a model which imitated the streaming motions of galaxies. The model used by Bean *et al.* (1983) appeared to do an adequate job but a slightly different approach can be also taken. This is briefly described here (see Fisher, 1995, for an attempt to combine these two approaches). Kaiser (1987) showed that using the plane-parallel (distant observer) approximation in the linear regime of gravitational instability the strength of an individual plane wave as measured in redshift space is amplified over that measured in real space by a factor

$$\delta^s_{\mathbf{k}} = \delta^r_{\mathbf{k}} \left(1 + \beta\mu^2_{\mathbf{kl}}\right), \tag{6.20}$$

where $\delta^r_{\mathbf{k}}$ and $\delta^s_{\mathbf{k}}$ are the Fourier amplitudes in real (r) and redshift (s) space, respectively, $\mu_{\mathbf{kl}}$ is the cosine of the angle between the wavevector, $\mathbf{k}$, and the line of sight, $\mathbf{l}$, and $\beta = f(\Omega)/b$ where $f(\Omega) \simeq \Omega^{0.6}$ is the logarithmic derivative of the fluctuation growth rate (eg. Peebles, 1980) and b is the linear bias factor relating the mass and galaxy distributions, $(\Delta\rho/\rho)_g = b(\Delta\rho/\rho)_m$. The plane-parallel approximation restricts use of equation 6.20 to angles less than $\sim 50°$ which can cause a systematic effect at the $\sim 5\%$ level in β (Cole *et al.* 1994a). This $(1+\beta\mu^2_{\mathbf{kl}})$ factor propagates through to the power spectrum, $P(k,\mu_{\mathbf{kl}}) \equiv \langle\delta_{\mathbf{k}}\delta^*_{\mathbf{k}}\rangle$

$$P^s(k,\mu_{\mathbf{kl}}) = P^r(k)\left(1+\beta\mu^2_{\mathbf{kl}}\right)^2, \tag{6.21}$$

where the real space $P^r(k)$ is assumed to be an isotropic function of k only. Thus the anisotropy is a strong function of angle between $\mathbf{k}$ and $\mathbf{l}$. It is common to measure the simple angle-averaged $P(k)$ and it is fairly easy to integrate over all angles to determine the amplification in redshift space of the angle-averaged $P(k)$

$$P^s(k) = \frac{\int_{-1}^{1} d\mu_{\mathbf{kl}} P^s(k,\mu_{\mathbf{kl}})}{\int_{-1}^{1} d\mu_{\mathbf{kl}}}, \tag{6.22}$$

$$= P^r(k)\left(1+\frac{2}{3}\beta+\frac{1}{5}\beta^2\right). \tag{6.23}$$

Hamilton (1992) has extended this analysis to the 2-point correlation function, ξ, which is the Fourier transform of the power spectrum. Basically, the cosine factor in Fourier space, $\mu^2_{\mathbf{kl}} \equiv k^2_{\mathbf{l}}/k^2$, becomes a differential operator in real space, $(\partial/\partial|\mathbf{l}|)^2(\nabla^2)^{-1}$, and therefore the Fourier transform of equation 6.21 is

$$\xi^s(r,\mu_{\mathbf{rl}}) = \left(1+\beta(\partial/\partial|\mathbf{l}|)^2(\nabla^2)^{-1}\right)^2 \xi^r(r), \tag{6.24}$$

where $\mu_{\mathbf{rl}}$ is the cosine of the angle between the pair separation, $\mathbf{r}$, and the line of sight, $\mathbf{l}$. Hamilton (1992) then shows that the solution of this can be written in terms of the first 3 even spherical harmonic moments of $\xi^s(r, \mu_{\mathbf{rl}})$ only, all higher moments are zero (odd moments are zero by definition, see equation 6.27)

$$\xi^s(r, \mu_{\mathbf{rl}}) = \xi_0(r) P_0(\mu_{\mathbf{rl}}) + \xi_2(r) P_2(\mu_{\mathbf{rl}}) + \xi_4(r) P_4(\mu_{\mathbf{rl}}), \tag{6.25}$$

where $\xi_l(r)$ are the spherical harmonic moments of $\xi^s(r, \mu_{\mathbf{rl}})$

$$\begin{aligned}
\xi_l(r) &= \frac{2l+1}{2} \int_{-1}^{1} \xi^s(r, \mu_{\mathbf{rl}}) P_l(\mu_{\mathbf{rl}}) d\mu_{\mathbf{rl}}, && (6.26) \\
\xi_0(r) &= \left(1 + \frac{2}{3}\beta + \frac{1}{5}\beta^2\right) \xi^r(r), && (6.27) \\
\xi_2(r) &= \left(\frac{4}{3}\beta + \frac{4}{7}\beta^2\right) \left[\xi^r(r) - \bar{\xi}^r(r)\right], && (6.28) \\
\xi_4(r) &= \frac{8}{35}\beta^2 \left[\xi^r(r) + \frac{5}{2}\bar{\xi}^r(r) - \frac{7}{2}\bar{\bar{\xi}}^r(r)\right], && (6.29)
\end{aligned}$$

$P_l(\mu_{\mathbf{rl}})$ are the usual Legendre polynomials

$$\begin{aligned}
P_0(\mu_{\mathbf{rl}}) &= 1, && (6.30) \\
P_2(\mu_{\mathbf{rl}}) &= (3\mu_{\mathbf{rl}}^2 - 1)/2, && (6.31) \\
P_4(\mu_{\mathbf{rl}}) &= (35\mu_{\mathbf{rl}}^4 - 30\mu_{\mathbf{rl}}^2 + 3)/8, && (6.32)
\end{aligned}$$

and

$$\begin{aligned}
\bar{\xi}^r(r) &\equiv \frac{3}{r^3} \int_0^r \xi(x) x^2 dx, && (6.33) \\
\bar{\bar{\xi}}^r(r) &\equiv \frac{5}{r^5} \int_0^r \xi(x) x^4 dx. && (6.34)
\end{aligned}$$

It is possible to rewrite these equations to give an equation for β involving ξ_0 and ξ_2 only

$$\left(1 + \frac{2}{3}\beta + \frac{1}{5}\beta^2\right) \xi_2(r) = \left(\frac{4}{3}\beta + \frac{4}{7}\beta^2\right) \left[\xi_0(r) - \frac{3}{r^3} \int_0^r \xi_0(s) s^2 ds\right], \tag{6.35}$$

or by defining

$$\begin{aligned}
\tilde{\xi}_0(r) &= -\xi_0(r) + \frac{3}{r^3} \int_0^r \xi_0(s) s^2 ds, && (6.36) \\
\tilde{\xi}_2(r) &= -\xi_2(r), && (6.37)
\end{aligned}$$

equation 6.35 can be written as

$$\frac{\tilde{\xi}_2}{\tilde{\xi}_0} = \frac{\left(\frac{4}{3}\beta + \frac{4}{7}\beta^2\right)}{\left(1 + \frac{2}{3}\beta + \frac{1}{5}\beta^2\right)}. \tag{6.38}$$

By Fourier transforming equation 6.23 (which has no explicit $\mu_{\mathbf{rl}}$ dependence) a somewhat simplier expression relating the angle-averaged $\xi(s)$ to $\xi(r)$ is obtained

$$\xi(s) = \xi(r) \left(1 + \frac{2}{3}\beta + \frac{1}{5}\beta^2\right), \tag{6.39}$$

assuming that $\xi(r)$ is an isotropic function of r only, this follows from a similar assumption made about $P^r(k)$. If the volume integral of ξ is defined as

$$J_3(x) = \int_0^x \xi(y) y^2 dy, \tag{6.40}$$

then it is trivial to produce a similar expression to equation 6.39

$$J_3(s) = J_3(r)\left(1 + \frac{2}{3}\beta + \frac{1}{5}\beta^2\right). \tag{6.41}$$

6.6.2 Testing the Method with the CDM Simulations

In this section the results from the LCDM full simulations and mock catalogues are presented. The SCDM simulations and mock catalogues were not analysed because it was felt that the 1-D pairwise velocity dispersion strongly dominates $\xi(\sigma, \pi)$ and so could not produce accurate results given that only the linear regime is modelled in this first analysis. As will be seen below this is also the case for some aspects of the LCDM simulations. In section 6.6.1 it was noted that equation 6.20 was only strictly correct in the plane parallel approximation and that angles $\leq 50°$ should really only be used. For a survey geometrically similar to the mock catalogues used here this restriction makes a negligible difference to the results for β. It should also be noted that only the weighted estimates of ξ from the mock catalogues are used here. Although the weighted $\xi(\sigma, \pi)$ diagrams appeared noisier than the corresponding unweighted ones they do not suffer from any systematic biases and should therefore produce an unbiased and realistic value of β.

In figures 6.19, 6.20 and 6.21 the dotted line denotes the "theoretical" value of $\beta \simeq \Omega^{0.6}/b = (0.2)^{0.6}/1 \simeq 0.38$, the solid line denotes the results from the average of the ξ's from the 5 LCDM full simulations (ie. take the mean $\xi(\sigma, \pi)$ from the simulations and then manipulate this to get a single value of β), the shaded area denotes the 1σ scatter seen between the 5 LCDM simulations (ie. use $\xi(\sigma, \pi)$ from each simulation, manipulate them to get 5 values of β and then average and standard deviation these) and the points with error bars are the mean and 1σ scatter seen in the LCDM mock catalogues (ie. use $\xi(\sigma, \pi)$ from each mock catalogue, manipulate them to get 15 values of β and then average and standard deviation these). The errors shown are the standard deviations on an *individual* mock catalogue.

The results from equation 6.35 are shown in figure 6.19. This method uses the ratio of the *second* to *zeroth* spherical harmonic moments of ξ to estimate β. The ξ_l's are estimated from

$$\begin{aligned} \xi_l(r) &= \frac{2l+1}{2} \int_{-1}^{1} \xi^s(r, \mu_{\mathbf{rl}}) P_l(\mu_{\mathbf{rl}}) d\mu_{\mathbf{rl}}, & (6.42) \\ &= (2l+1)\Delta\mu_{\mathbf{rl}} \sum_{\mu_{\mathbf{rl}}>0} \xi^s(r, \mu_{\mathbf{rl}}) P_l(\mu_{\mathbf{rl}}), & (6.43) \end{aligned}$$

where in this case the binning is $\Delta\mu_{\mathbf{rl}} = 0.2$. It is clear that the ~ 800 kms^{-1} 1-D pairwise velocity dispersion of these simulations dominates this plot causing a negative value of β to be measured until $\sim 13h^{-1}$Mpc ! Of course, a negative value of β is unphysical and is simply due to the shape of the $\xi(\sigma, \pi)$ contours. In this case the values of β are meaningless. The mock catalogues trace the results of the full simulations adequately apart from on $r < 10h^{-1}$Mpc scales. In this region the mock catalogues, while still giving a negative β, are systematically above the full simulation results. The author could not find any errors in the analysis procedures to explain this result. When considering this method for the Durham/UKST survey one should note that the measured velocity dispersion is approximately half that of the LCDM simulations and therefore the elongation should be less of a problem.

The results from equation 6.39 are shown in figure 6.20. This method uses the ratio of the *redshift* to *real* space ξ's to estimate β. The *redshift* space ξ is estimated directly using the methods described in chapter 4. The *real* space ξ is estimated by Abel inversion of the projected correlation function, $w_v(\sigma)$, with $\pi_{cut} = 30h^{-1}$Mpc, as described in chapter 5. It is clear that this method is not dominated by non-linear effects above $\sim 6h^{-1}$Mpc although they could cause the ~ 0.1 systematic offset in β that is seen out to $> 30h^{-1}$Mpc. Unfortunately, for the full simulations noise begins to dominate the inversion process between 15-20h^{-1}Mpc. For the mock catalogues noise dominates at all scales and the results almost resemble a scatter plot ! While this method is less sensitive to the non-linear velocity dispersion than the spherical harmonic one, the scatter seen in the mock catalogues renders this method almost useless for surveys of this size.

The results from equation 6.41 are shown in figure 6.21. This method uses the ratio of the *redshift* to *real* space J_3's to estimate β. The *redshift* space J_3 is calculated from volume integration of the above *redshift* space ξ while the *real* space J_3 is calculated from volume integration of the above *real* space ξ. It is clear that this method is not dominated by non-linear effects above $\sim 15h^{-1}$Mpc and the value of β obtained is very consistent with the "theoretical" value. The mock catalogues also reproduce the correct answer, albeit with a larger scatter. However, while one would like to combine these points to reduce the errors involved this is not possible because these points are non-independent due to the integration procedure.

These results for the mock catalogues can be summarised as follows. The ratio of the *redshift/real* correlation functions is only weakly affected by the non-linear velocity dispersion above $\sim 6h^{-1}$Mpc scales but gives the noisiest estimate of β by far. The ratio of the *redshift/real* volume integrated correlation functions is only weakly affected by the non-linear velocity dispersion above $\sim 15h^{-1}$Mpc scales and has significantly smaller errors than the simple correlation function method. However, these points are non-independent because of the volume integration process. The ratio of the *second/zeroth* spherical harmonic moments of the correlation functions is severely affected by the large non-linear velocity dispersion in these simulations, but arguably gives the least noisy estimate of β. For a smaller velocity dispersion this could be the most promising method of estimating β.

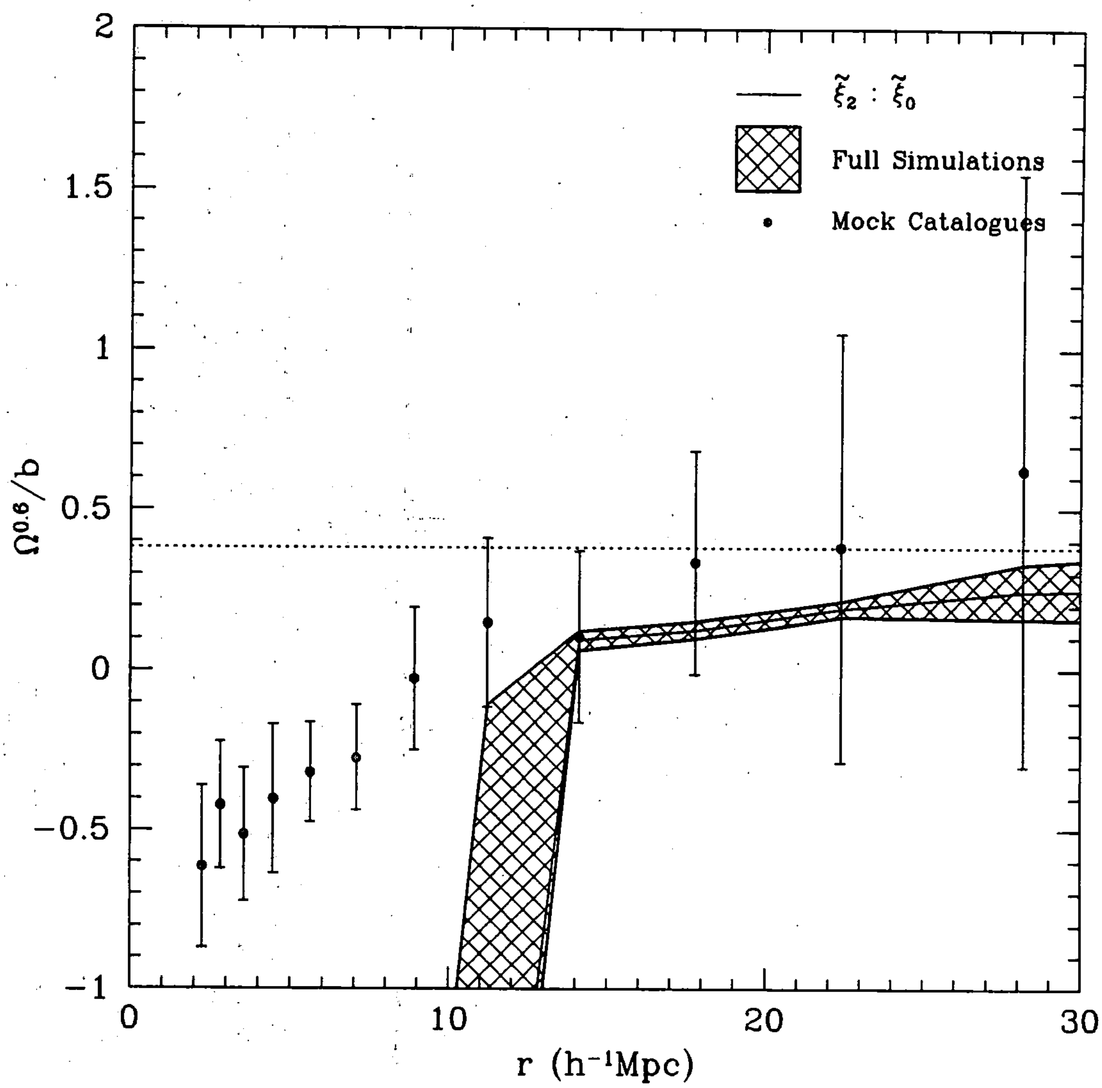

Figure 6.19: Values of $\beta \simeq \Omega^{0.6}/b$ as a function of r using the method which considers the ratio of the *second* to *zeroth* spherical harmonic moments of ξ.

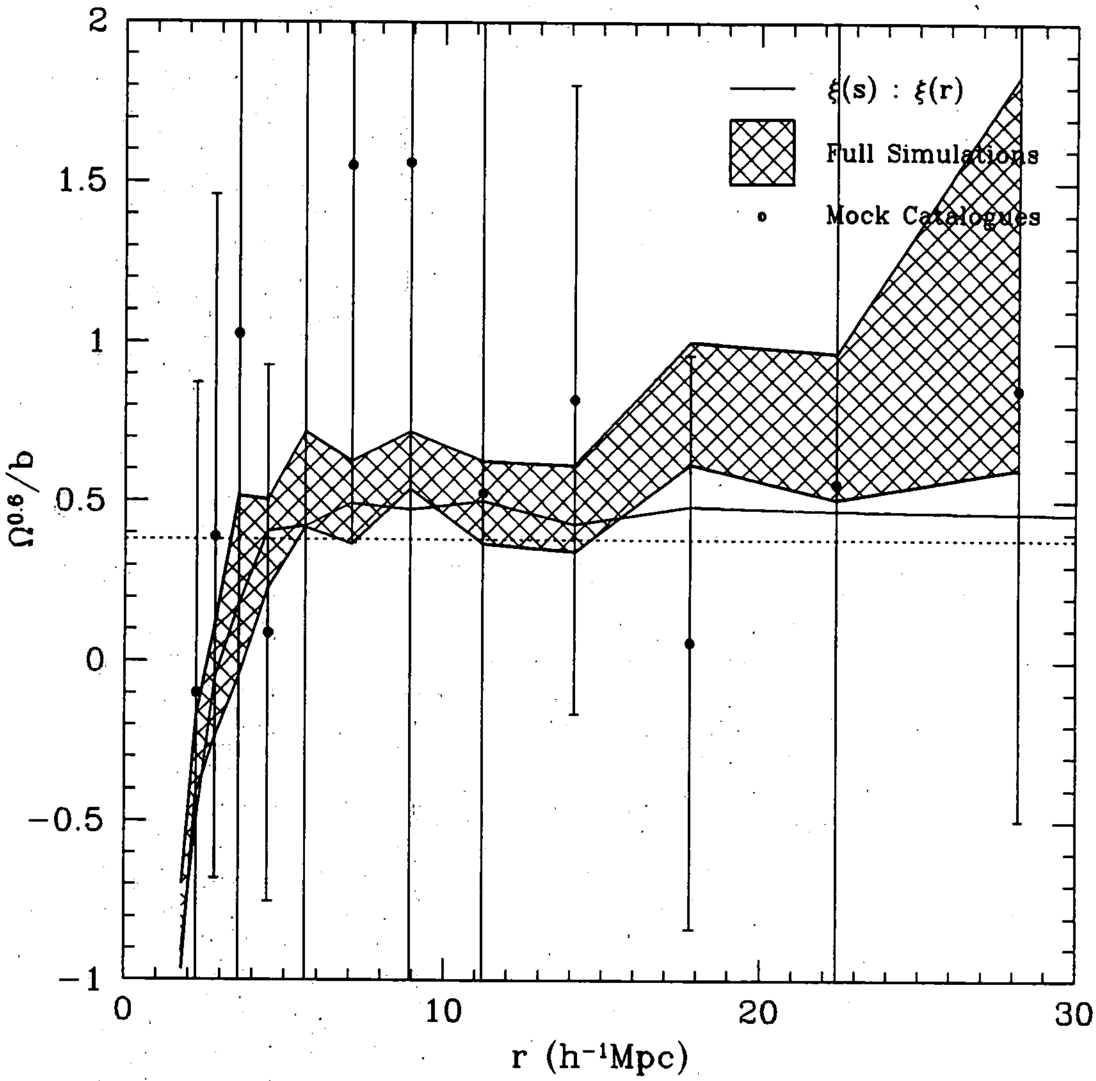

Figure 6.20: Values of $\beta \simeq \Omega^{0.6}/b$ as a function of r using the method which considers the ratio of the *redshift* to the *real* space ξ's.

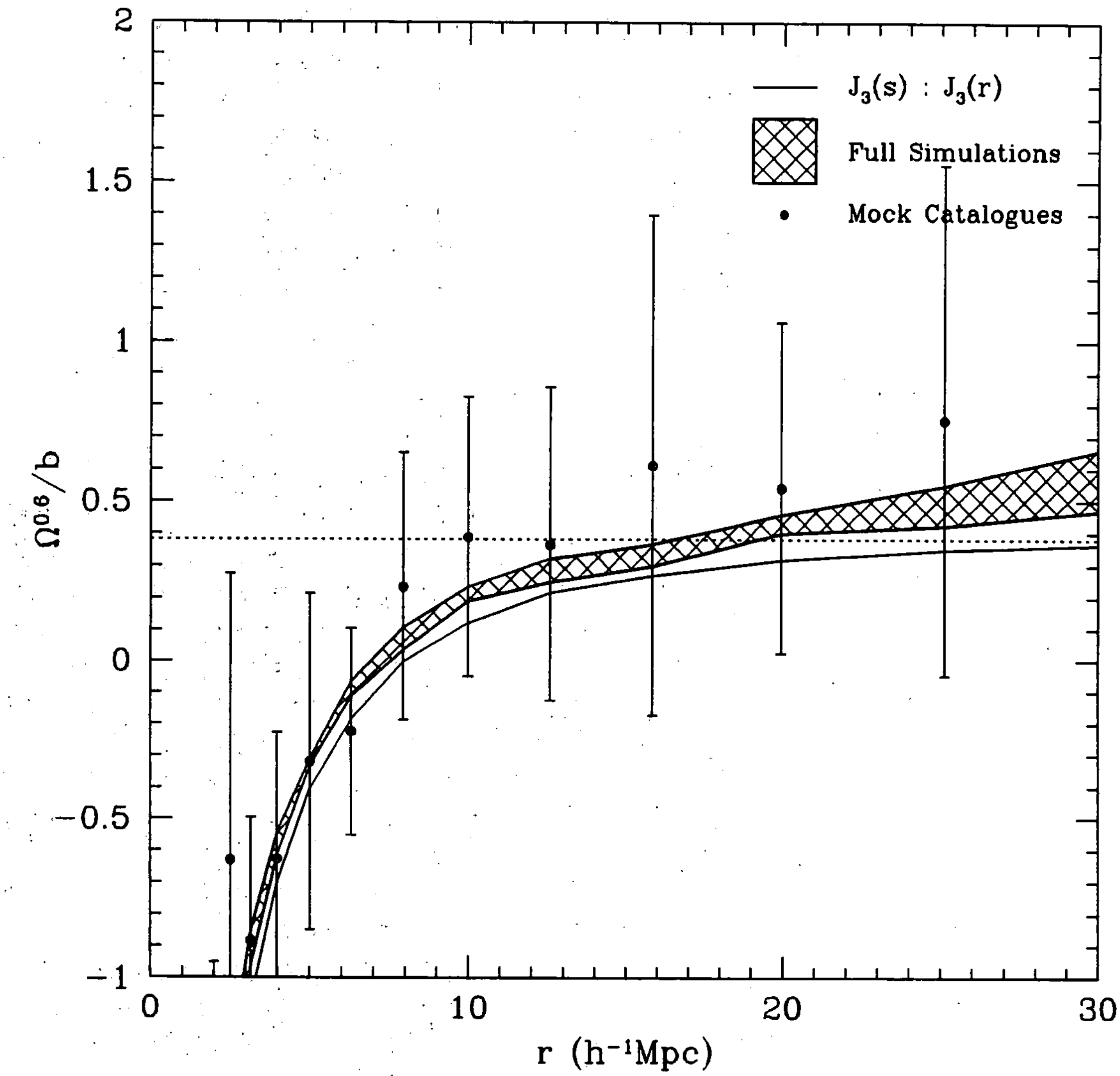

Figure 6.21: Values of $\beta \simeq \Omega^{0.6}/b$ as a function of r using the method which considers the ratio of the *redshift* to the *real* space J_3's.

6.6.3 Results from the Durham/UKST Galaxy Redshift Survey

In this section the results from the Durham/UKST survey are presented. Unless otherwise specified the errors shown are the 1σ standard deviation obtained by splitting the survey into 4 roughly equal quadrants and then assuming that each quadrant provides an independent estimate of β. Again, only the weighted estimate of ξ was used in the analysis for the reasons mentioned in section 6.6.2.

Figure 6.22 shows the *zeroth* and *second* harmonic moments of the 2-point correlation function (note that $-\xi_2$ is actually plotted and not simply ξ_2). These moments were calculated from equation 6.43 using the weighted estimate of ξ. The second harmonic moment is positive until $\sim 8h^{-1}$Mpc which is caused by the elongation of the ξ contours parallel to the line of sight from the non-linear velocity dispersion. On larger separations the second harmonic moment is negative due to the compression of the ξ contours parallel to the line of sight from the linear infall of galaxies.

Figure 6.23 shows the *real* and *redshift* space 2-point correlation functions. The *redshift* space ξ is the weighted estimate of section 5.2.2, while the *real* space ξ is the Abel inverted estimate of the weighted projected correlation function, w_v, with $\pi_{cut} = 30h^{-1}$Mpc (from section 5.3.4). It can be seen that $\xi(r) > \xi(s)$ below $\sim 1h^{-1}$Mpc where $\xi(s)$ is dominated by the non-linear velocity dispersion. Conversely, $\xi(s) > \xi(r)$ above $\sim 1h^{-1}$Mpc. Unfortunately, the noise in these real/redshift space estimates is probably at a level such that it dominates any measurement of β.

Figure 6.24 shows the *real* and *redshift* space volume integrals of the 2-point correlation function. Quite simply these measurements of J_3 are the integrals of figure 6.23 out to the given separation weighted by an r^2 factor. Once again, at small separations $J_3(r) > J_3(s)$, while at larger separations $J_3(s) > J_3(r)$. There is a near constant offset in $\lg J_3$, ie. a constant multiplicative factor in linear J_3, between the *real* and *redshift* space estimates on scales 10-20h^{-1}Mpc. This should give a consistent estimate of β on these scales.

Figure 6.25 shows the results of applying equations 6.38, 6.39 and 6.41 to the data in figures 6.22, 6.23 and 6.24, respectively. For clarity, error bars are not shown for the $\xi(s)/\xi(r)$ method because they are very large and only cause confusion. These points have no systematic trend (other than a large random scatter) and it is probably best to discount them from any further analysis. Concentrating on the other 2 methods, our region of interest is $\sim$ 10-30h^{-1}Mpc due to non-linear effects on smaller scales and noise on larger scales. On these scales one sees that the estimated error bars vary from quite small to quite large, $\pm$ 0.1-1.0. Out of interest to the reader, figure 6.26 plots the points from figure 6.25 but with the error bars from an *individual* LCDM mock catalogue, namely those of figures 6.19 and 6.21.

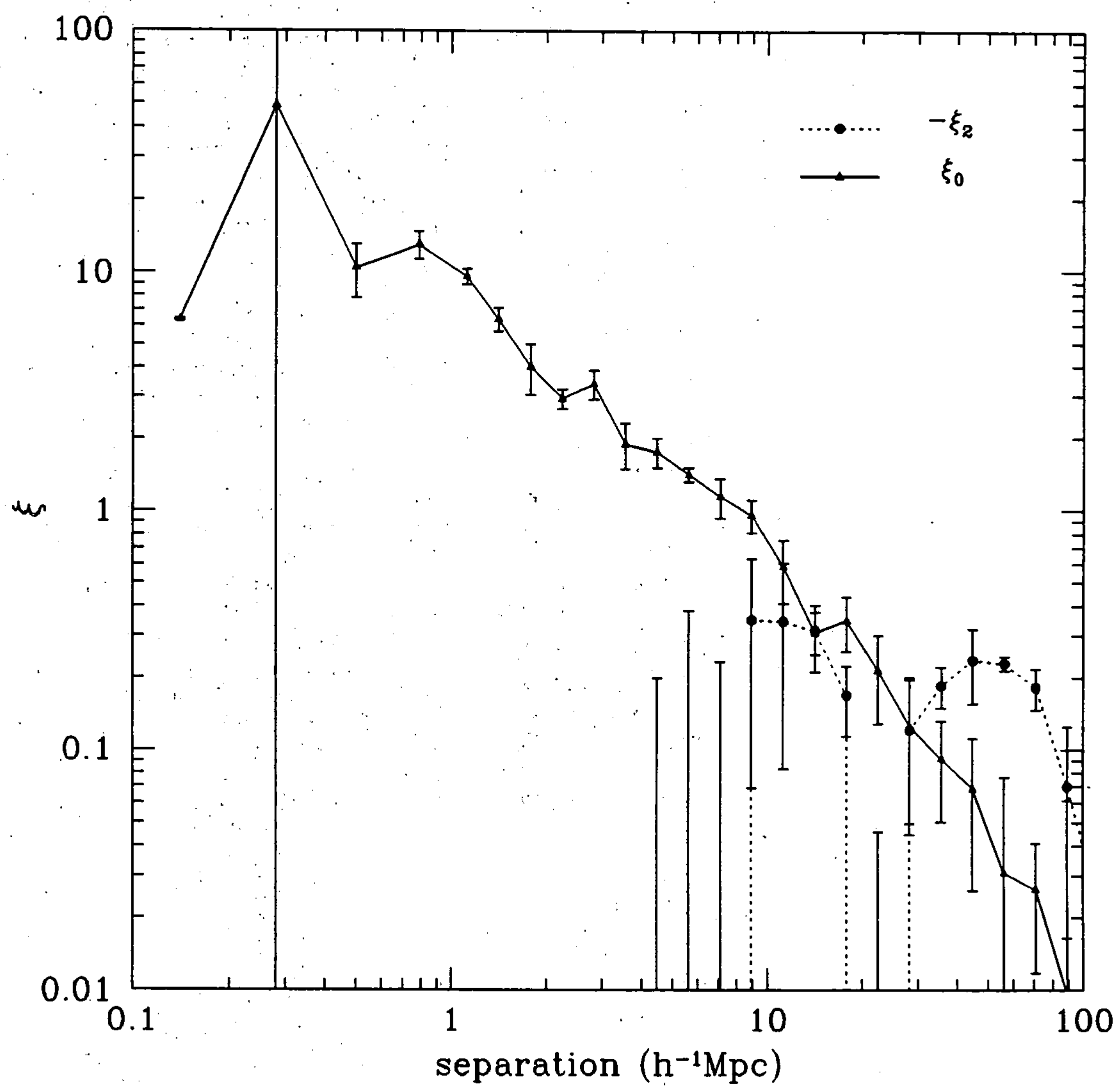

Figure 6.22: The weighted *zeroth* and *second* spherical harmonic moments of ξ from the Durham/UKST survey.

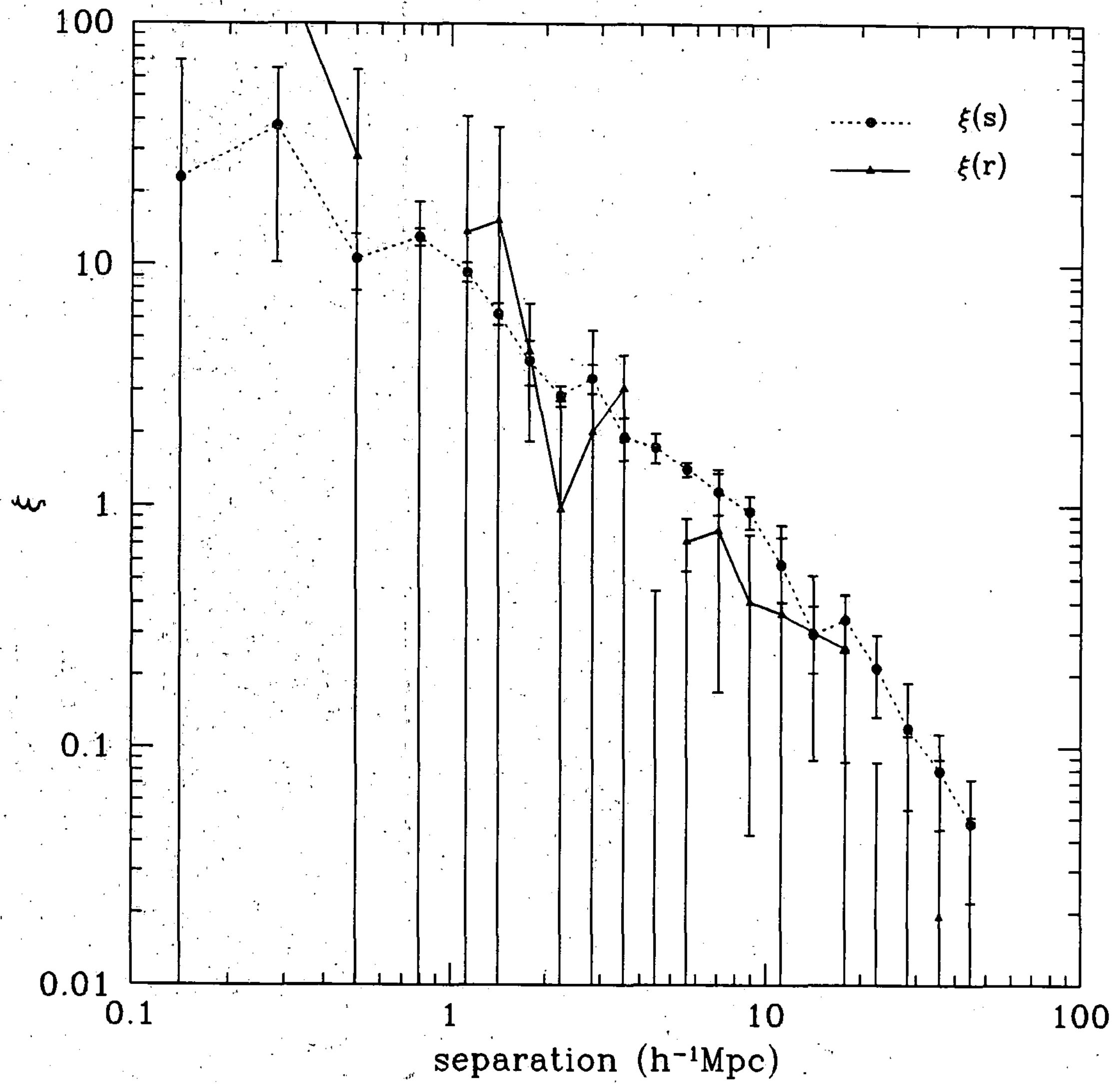

Figure 6.23: The weighted *real* and *redshift* space ξ's from the Durham/UKST survey.

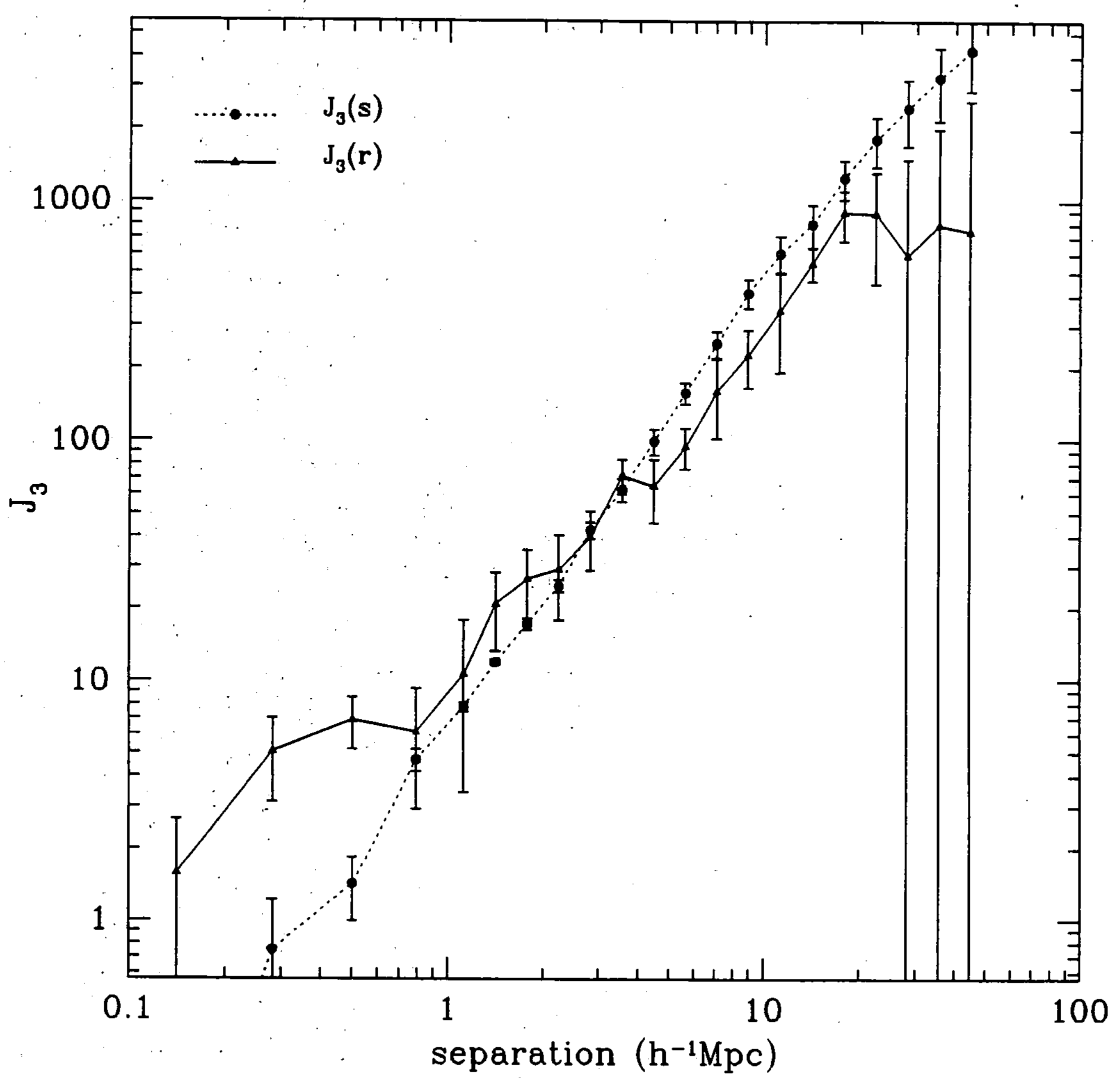

Figure 6.24: The weighted *real* and *redshift* space J_3's from the Durham/UKST survey.

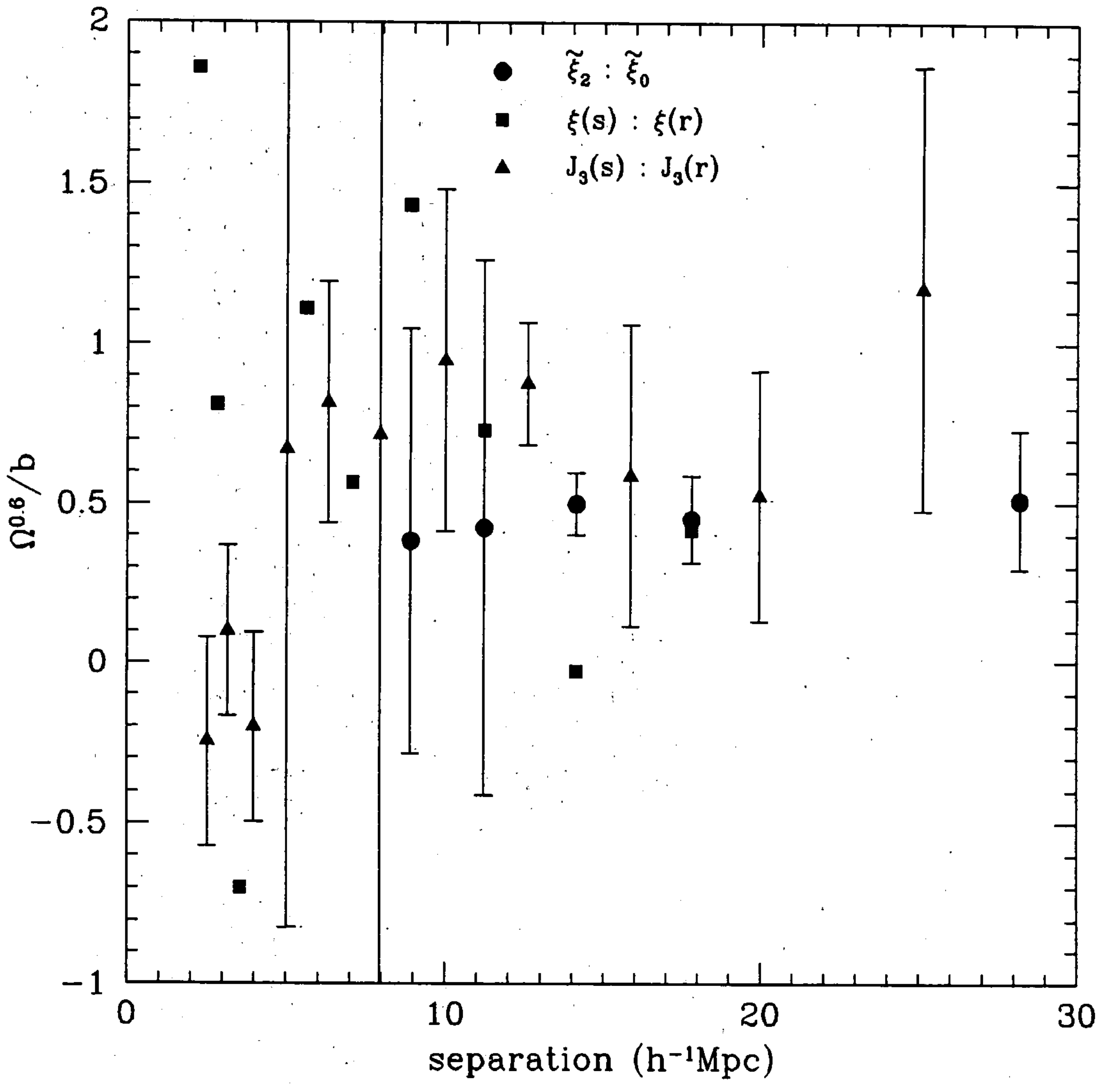

Figure 6.25: Estimates of $\beta \simeq \Omega^{0.6}/b$ from the Durham/UKST survey as a function of spatial separation for 3 methods. The error bars are the variance seen from quadrant to quadrant in the Durham/UKST survey.

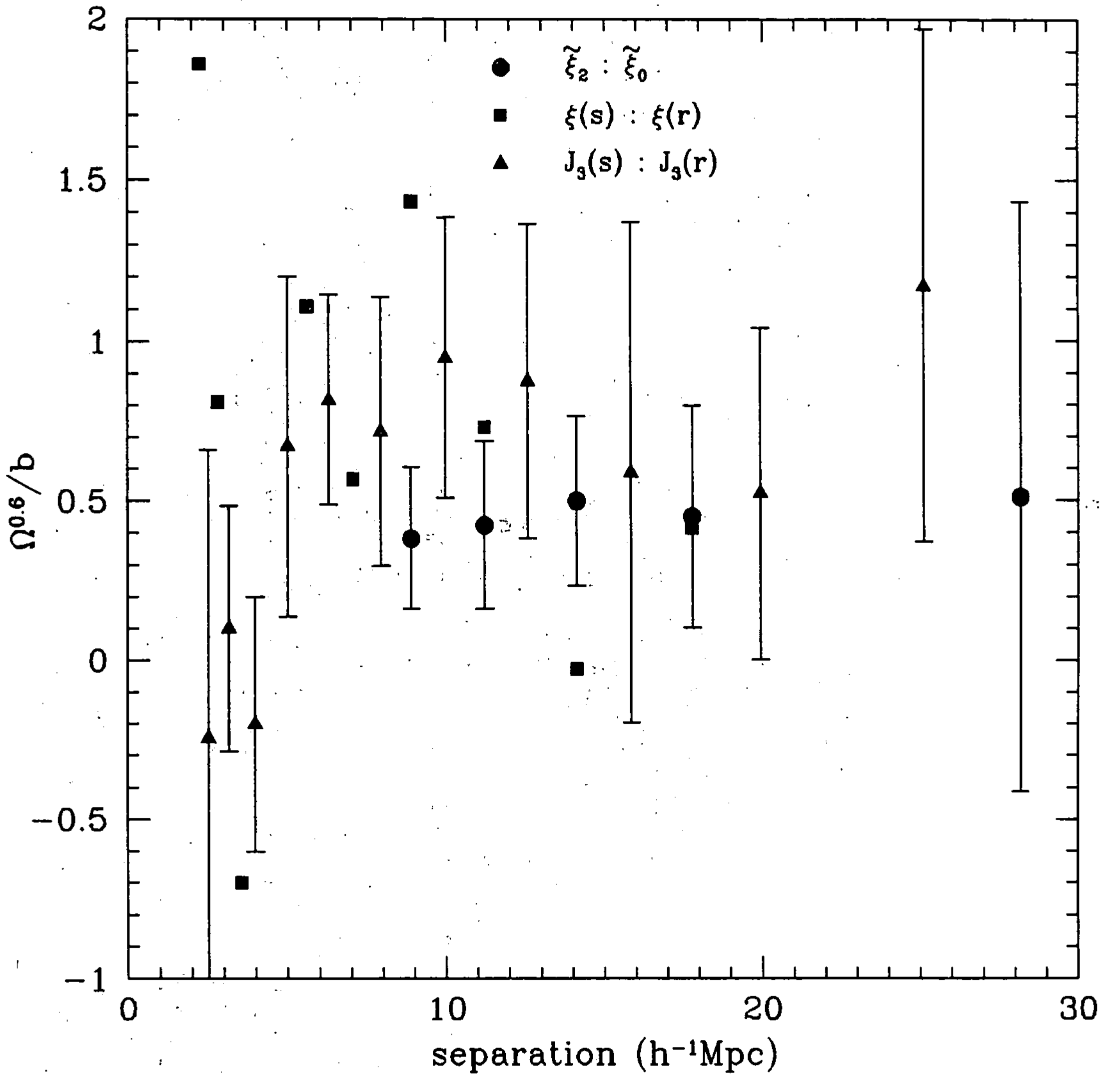

Figure 6.26: The same as figure 6.25 but using the error bars from the LCDM mock catalogues.

In taking a realistic opinion of figures 6.25 and 6.26 one only quotes a single value of β from each of the above methods because of the non-independent nature of the points. Therefore, no formal χ^2 fits are attempted. For the spherical harmonics method the value at $\sim 18h^{-1}$Mpc is quoted, $\beta = 0.45 \pm 0.38$, where the error bar has been estimated by averaging the 5 error bars from this method in the 10-$30h^{-1}$Mpc region. While this error bar is only a rough approximation it does agree well with a typical LCDM mock catalogue error bar (plotted in figure 6.26). For the $J_3(s)/J_3(r)$ method the value at $\sim 16h^{-1}$Mpc is quoted, $\beta = 0.59 \pm 0.46$. This point appears more or less typical of those in the 10-$30h^{-1}$Mpc region and again has the average error bar of the 5 points in this region. Comparison with the LCDM mock catalogue error bars confirms this is a realistic error estimate.

6.6.4 Comparison with other Optical Estimates of β

The best estimate of β from the Durham/UKST survey is $\beta = 0.45 \pm 0.38$. This value can be compared with other optical values of β estimated using similar methods involving redshift space distortions. Peacock & Dodds (1994) used the real and redshift space power spectrum estimates of various cluster, radio, optical and IRAS samples to measure $\beta = 0.77 \pm 0.16$. Loveday *et al.* (1995a) used the method of the ratio of the J_3's to measure $\beta = 0.48 \pm 0.12$ for the APM-Stromlo survey. Lin *et al.* (1995a) used the spherical harmonics of ξ method to measure $\beta = 0.5 \pm 0.25$ for the Las Campanas survey. These values are all consistent with $\beta = 0.57 \pm 0.12$. However, it should be stated that the measurements of β which come from peculiar velocity and density field comparisons do suggest slightly higher values of β, for example $1.28^{+0.38}_{-0.30}$ from Dekel *et al.* (1993) and 0.74 ± 0.13 from Hudson *et al.* (1995).

6.7 Conclusions

Redshift space distortions in the Durham/UKST galaxy redshift survey have been investigated using the 2-point correlation function, $\xi(\sigma, \pi)$, where the non-linear velocity dispersion elongates the ξ contours along the line of sight on small scales, while on larger scales the linear infall compresses the ξ contours in this same direction.

Modelling the velocity dispersion leads to an estimate of the galaxy 1-D pairwise velocity dispersion from the Durham/UKST survey of $\langle w_z^2 \rangle^{\frac{1}{2}} = 416 \pm 36$ kms^{-1}, although this error bar is more than likely an underestimate due to the non-independent nature of the ξ points. This value is consistent with the canonical value (~ 350kms^{-1}) but is slightly smaller than recent measurements and still rules out the SCDM value of ~ 1000 kms^{-1}.

Linear theory gives an expression for the enhancement of the clustering in redshift space as a function of $\beta \simeq \Omega^{0.6}/b$ and different methods of measuring β give consistent results from the Durham/UKST survey, with the best estimate being $\beta = 0.45 \pm 0.38$. This value of β agrees well with previous optical estimates, but cannot discriminate between the SCDM and LCDM models, which predict $\beta \sim 0.4$-0.6. This value of β tends to favour either an unbiased open Universe or (using a fiducial value of $b \simeq 2$) a biased critical density Universe. This value of β is less consistent with an unbiased critical density Universe.

Chapter 7

Conclusions

7.1 The Future of Galaxy Redshift Surveys

7.1.1 The Durham/UKST Survey and FLAIR

While the statistical analysis of the Durham/UKST Galaxy Redshift Survey in this thesis has concentrated on the 2-point correlation function there are other statistics that can be estimated. In particular, the fundamental quantity of interest in the statistical analysis of large scale structure is the power spectrum, $P(k)$, which is the Fourier transform partner of the 2-point correlation function, $\xi(r)$. The Fourier space window function of the Durham/UKST survey is one of the narrowest of any survey currently available (Tegmark, 1995) and since it is this window function that determines the resolution of the estimated power spectrum, the Durham/UKST survey should give one of the best estimates of the power spectrum yet. Also, valuable morphological information can be extracted from the Durham/UKST survey via such methods as the counts-in-cells of Efstathiou *et al.* (1990), the higher order correlations of Baugh & Gaztañaga (1995a), the void probability function of White (1979) and the Minkowski functionals of Mecke *et al.* (1994).

In order for the FLAIR system on the UKST to survive, there are three changes which must occur. Firstly, the UKST still has a large advantage in terms of field of view, $\sim$ 25 sq. degrees compared with $\sim$ 3 for the 2dF, this must be used effectively and projects designed with this in mind. Secondly, the CCD system on the UKST must become more efficient than the one that was used for the majority of the observations in this thesis. Indeed, in the latter half of 1995 a new CCD was installed which gave a huge improvement in throughput in the blue region of the spectrum and now allows observations to go $\sim$ 1 magnitude deeper in comparable observing times to those used in this thesis. It would still be possible to improve on this new CCD in terms of readout noise etc. Thirdly, and perhaps most importantly, a proper automated fiber positioning system must be built and commissioned. Not only is the fibreing up procedure a tedious and laborious job for the observer it is also a bottleneck. While the exposure times are coming down, the time taken to fibre up is not and preparing each plateholder can take most of the night. This is obviously unacceptable given that the observations taken in each field in this thesis could take less than 5000s in total with the new system.

7.1.2 The Next Generation of Surveys

As was seen throughout this thesis, surveys the size of the Durham/UKST survey can give constraints on the observed large scale structure in the galaxy distribution, as well as implying information about the dynamics of the Universe. One can then use these measurements to constrain models of structure formation, such as CDM. Physically larger surveys, containing more galaxies to deeper magnitudes, will obviously decrease the statistical errors seen in these structural and dynamical measurements. However, it is very important to ask what new science they will achieve and to make sure that one is not merely "stamp collecting" galaxy redshifts. Two such surveys which will come fully into play in a couple of years time are the 2dF project (Efstathiou & Ellis *et al.* 1995) and the Sloan Digital Sky Survey (Gunn & Weinberg *et al.* 1995). These will contain at least an order of magnitude or more redshifts than any survey currently in existence.

Some of the questions which remain unanswered by current studies of large scale structure are :-

(i) What happens to $P(k)$ between those scales probed by the recent cosmic microwave background radiation anisotropy measurements ($\lambda > 300h^{-1}$Mpc) and those accessable from current redshift surveys ($\lambda < 100h^{-1}$Mpc) ? The COBE experiment (Smoot *et al.* 1992) indicates that $P(k) \sim k$ for $k \sim 0.001h\text{Mpc}^{-1}$, while galaxy catalogues (eg. Baugh & Efstathiou, 1993) measure $P(k) \sim k^{-1.3}$ for $k \sim 1h\text{Mpc}^{-1}$. Therefore, for these two measurements to join up, $P(k)$ must turn over in the intervening region between them. The scale at which the turn-over in $P(k)$ occurs could imply new knowledge about the dominant component of the matter distribution, particularly the microphysical processes which took place at the epoch of matter-radiation equality.

(ii) What is the value of $\beta \simeq \Omega^{0.6}/b$? Does b vary with scale ? What is the value of Ω ? The indications from current redshift surveys (eg. the Durham/UKST survey) are that $\beta \sim 0.5 \pm 0.1$. However, not only would one like to determine this parameter more accurately but also to larger scales and even as a function of scale. The current redshift surveys are very limited in these respects. Assuming that Ω does not vary with scale one can deduce how b behaves with scale by measuring $\Omega^{0.6}/b$ as a function of scale. Also, since the cosmic microwave background radiation anisotropy experiments measure the fluctuations in the dominant component of the matter distribution, one could deduce b directly from $P(k)_{gal} = b^2 P(k)_{mass}$ which then implies Ω from the measurements of $\Omega^{0.6}/b$.

(iii) How do galaxies cluster as a function of intrinsic luminosity and morphological type ? There exists only limited information on the answers to these questions (see Efstathiou, 1996), mainly due to a basic lack of statistics. Successful models of galaxy formation will have to address these questions and, conversely, the observations of clustering with luminosity and morphology should be able to constrain the galaxy formation models.

(iv) What is the morphological pattern of the galaxy distribution and can it be quantifiably described ? The current maps of galaxy redshifts have revealed a rich pattern of filaments, walls, voids and cells. One can attempt to analyse this morphological distribution and also test the gaussian random phase hypothesis of the Fourier components of the density field. However, the size of the current surveys implies a dependency on a few dominant structures. Therefore, whether one uses statistical methods of higher order moments, such as counts-in-cells (Efstathiou, 1990), or topological ones, such as the genus (Gott *et al.* 1986), they are limited by the lack of independent features in the observed distributions. This can only be improved with larger surveys.

(v) Other questions which a larger redshift surveys could answer are ; Does the galaxy luminosity function evolve with redshift and how does this affect the interpretation of the galaxy number counts ? How do voids and overdensities affect the local mean galaxy density and can they alter the interpretation of the galaxy number counts ? Given that the current redshift surveys are just approaching the volume within which the non-linear galaxy velocity dispersion is supposed to converge, what is the universal value of this quantity ?

7.2 Summary of Results

The 3-D Durham/UKST Galaxy Redshift Survey has been constructed to sample galaxies at a rate of 1 in 3 from the 2-D Edinburgh/Durham Southern Galaxy Catalogue. The observations of this survey were carried out using the FLAIR system on the UKST during the period 1991-1994. The completed survey contains over 2000 galaxy redshifts, accurate to ±150 kms^{-1}, down to $b_J \simeq 17.0$ in a $\sim$ 1500 sq. degree area over the South Galactic Pole. The survey probes to a depth $>$ $300h^{-1}$Mpc sampling a $\sim 4 \times 10^6 h^{-3}$Mpc^3 volume of space. The overwhelming visual impression of the survey is that the galaxy distribution appears "cellular" on 50-100h^{-1}Mpc scales. The galaxy number-distance histogram shows several large peaks, some of which agree with the Broadhurst *et al.* (1990) pencil-beam survey "spikes". However, the observed distribution is clearly more complex than a simple 1-D periodic pattern.

The optical galaxy luminosity function has been estimated from the Durham/UKST survey using parametric and non-parametric maximum likelihood techniques. The best fit parameters to the form of a pure Schecter function are $M^*_{b_J} = -19.72\pm0.09 + 5\lg h$ and $\alpha = -1.14\pm0.08$, with a normalisation of $\phi^* = 1.17\pm0.21\times10^{-2}h^3$Mpc^{-3}.

However, while this Schechter form does have the general features seen in the non-parametric estimates it does not provide a particularly good formal fit to the shape of the non-parametric estimates. This new determination of the luminosity function is consistent with those from similar redshift surveys. Overall, a Schechter function can be used to describe the luminosity function in this redshift range, $z < 0.1$. These fits favour a characteristic absolute magnitude of $M^{*}_{b_J} \sim -19.5$ and a flat faint end slope of $\alpha \sim 1.0$.

The significance of the observed large scale features in the galaxy distribution are investigated using the 2-point correlation function. This clustering statistic measures the excess probability of finding a galaxy at a given distance from another. The methods of determining this correlation function from a magnitude limited survey are empirically tested using mock catalogues of the Durham/UKST survey drawn from cosmological N-body simulations. The optimal method is then applied to the Durham/UKST survey and the results show good agreement with those from previous redshift surveys. A single power law fit to the *redshift* space correlation function, $\xi(s)$, gives an amplitude $s_0 = 6.8 \pm 0.3h^{-1}$Mpc and slope $\gamma = 1.18 \pm 0.04$ in the region $\sim$ 1-30h^{-1}Mpc. The projected correlation function, which should be independent of redshift space effects, is estimated for this survey. Using a single power law model for the *real* space correlation function, $\xi(r)$, gives a best fit amplitude $r_0 = 5.1 \pm 0.3h^{-1}$Mpc and slope $\gamma = 1.59 \pm 0.09$ in the region $\sim$ 1-10h^{-1}Mpc. There is some doubt over the significance levels of these parameters given that a simple χ^2 fit was used on non-independent points. Methods of inverting the projected correlation function to obtain the real space correlation function directly are investigated and a new application of the Richardson-Lucy technique is proposed and tested. The real and redshift space correlation functions from 3 different redshift surveys are combined. $\xi(r)$ appears to be well modelled by a featureless single power law out to $\sim 20h^{-1}$Mpc with $r_0 \simeq 5.0h^{-1}$Mpc and $\gamma \simeq 1.8$. However, $\xi(s)$ appears better modelled by a two power law with the change of shape occuring near $\xi \sim 1$, in the 4-7h^{-1}Mpc region. On scales larger than these $\xi(s)$ has a similar slope to $\xi(r)$ but with a higher amplitude. Therefore, redshift space effects alone are believed to be responsible for the differences seen in these correlation functions and there is no convincing evidence for any features, such as a "shoulder", in $\xi(r)$.

The effects of redshift space distortions are then investigated, again using the 2-point correlation function, and the non-linear and linear regimes are modelled separately. On small scales, the 1-D pairwise velocity dispersion of galaxies in the Durham/UKST survey is measured to be 416 ± 36 kms^{-1}. Again the significance levels are most likely an underestimate due to the non-independent nature of the correlation function. This value is consistent with the canonical value of ~ 350 kms^{-1} and also with other recent measurements, albeit on the slightly lower side of the new measurements. On larger scales, the dynamical infall of galaxies into overdense regions is measured to be $\Omega^{0.6}/b = 0.45 \pm 0.38$. This favours either an open Universe with galaxies tracing the mass distribution or, if galaxies do not trace the mass distribution, that the density of the Universe is nearer its critical value. An unbiased critical density Universe is less consistent with this estimate of $\Omega^{0.6}/b$.

Finally, one can compare all of the observational constraints from the Durham/UKST survey with the predictions from cosmological models of structure formation. The two models chosen are the standard cold dark matter model (SCDM), which is perhaps the most well-known and investigated cosmological model around, and a low density CDM model, with a cosmological constant to ensure spatial flatness, which is currently popular in the astronomical community (eg. Ostriker & Steinhardt, 1995). The 2-point correlation function from the Durham/UKST survey gives a significant detection, $> 3\sigma$, of large scale power above and beyond that of the SCDM model in the $\sim$ 10-40h^{-1}Mpc region. The LCDM model is more consistent in this region, although still 1-2σ low. The 1-D pairwise velocity dispersion from the Durham/UKST survey (see above) is inconsistent with the SCDM value of $\sim$ 1000 kms^{-1} at high levels of significance. The LCDM value of $\sim$ 800 kms^{-1} does not fair much better. However, the estimate of $\Omega^{0.6}/b = 0.45 \pm 0.38$ from the Durham/UKST survey cannot distinguish between the SCDM and LCDM values because they predict $\Omega^{0.6}/b \simeq$ 0.4-0.6. In conclusion, the SCDM model appears to have too much power on small scales but not enough on large scales. Therefore, the observational results argue for a model with a density perturbation spectrum more skewed towards large scales, such as LCDM.

Bibliography

Bardeen, J.M., Bond, J.R., Kaiser, N. & Szalay, A.S., 1986, *Astrophys. J.*, **304**, 15.
Baugh, C.M., 1996, *Mon. Not. R. astr. Soc.*, **280**, 267.
Baugh, C.M. & Efstathiou, G.P., 1993, *Mon. Not. R. astr. Soc.*, **265**, 145.
Baugh, C.M. & Gaztañaga, E., 1995, *private communication.*
Bean, A.J., 1983, *Ph.D. Thesis*, University of Durham.
Bean, A.J., Efstathiou, G.P., Ellis, R.S., Peterson, B.A. & Shanks, T., 1983, *Mon. Not. R. astr. Soc.*, **205**, 605.
Bertschinger, E., Dekel, A., Faber, S.M., Dressler, A. & Burstein, D., 1990, *Astrophys. J.*, **364**, 370.
Blumenthal, G., Faber, S.M., Primack, J.R. & Rees, M.J., 1984, *Nature*, **311**, 517.
Bond, J.R. & Efstathiou, G.P., 1984, *Astrophys. J. Lett.*, **285**, L45.
Broadbent, A., 1994, *private communication.*
Broadhurst, T.J., Ellis, R.S., Koo, D.C. & Szalay, A.S., 1990, *Nature*, **343**, 726.
Choloniewski, J., 1986, *Mon. Not. R. astr. Soc.*, **223**, 1.
Cole, S.M., Fisher, K.B. & Weinberg, D.H., 1994a, *Mon. Not. R. astr. Soc.*, **267**, 785.
Cole S.M., Frenk, C.S. & Eke, V.R., 1994b, *private communication.*
Collins, C.A., Heydon-Dumbleton, N.H. & MacGillivray, H.T., 1988, *Mon. Not. R. astr. Soc.*, **236**, 7p.
Collins, C.A., Nichol, R.C. & Lumsden, S.L., 1992, *Mon. Not. R. astr. Soc.*, **254**, 295.
Couchman, H.M.P, 1991, *Astrophys. J. Lett.*, **368**, L23.
Couchman, H.M.P, 1994, in *"Numerical Methods in Astrophysics"*, **v.II**, Springer-Verlag, New York.
Couchman, H.M.P. & Carlberg, R.G., 1992, *Astrophys. J.*, **389**, 453.
da Costa, L.N., Pellegrini, P.S., Davis, M., Meiksin, A., Sargent, W.L. & Tonry, J.L., 1991, *Astrophys. J. Suppl. Ser.*, **75**, 935.
Dalton, G.B., 1995, *private communication.*
Dalton, G.B., Efstathiou, G.P. & Lumsden, S.L., 1995, *in preparation.*
Davis, M., Efstathiou, G.P., Frenk, C.S. & White, S.D.M., 1985, *Astrophys. J.*, **292**, 371.
Davis, M. & Huchra, J., 1982, *Astrophys. J.*, **254**, 437.
Davis, M. & Peebles, P.J.E., 1983, *Astrophys. J.*, **267**, 465.
Dekel, A., Bertschinger, E., Yahill, A., Strauss, M.A., Davis, M. & Huchra, J.P., 1993, *Astrophys. J.*, **412**, 1.
Eadie, W.T., Drijard, D., James, F.E., Roos, M. & Sadoulet, B., 1971,

"Statistical Methods in Experimental Physics", North Holland, Amsterdam.
Efstathiou, G.P., 1988, in *"Comets to Cosmology"*, Proceedings 3rd IRAS Conference, ed. Lawrence, A., Springer-Verlag, 312.
Efstathiou, G.P., 1996, *"Observations of Large Scale Structure in the Universe"*, Les Houches Lectures, in press.
Efstathiou, G.P., Davis, M., Frenk, C.S. & White, S.D.M., 1985, *Astrophys. J. Supp.*, **57**, 241.
Efstathiou, G.P. & Ellis, R.S. *et al.*, 1995.
Efstathiou, G.P., Ellis, R.S. & Peterson, B.A., 1988a, *Mon. Not. R. astr. Soc.*, **232**, 431.
Efstathiou, G.P., Frenk, C.S., White, S.D.M. & Davis, M., 1988b, *Mon. Not. R. astr. Soc.*, **235**, 715.
Efstathiou, G.P., Kaiser, N., Saunders, W., Lawrence, A., Rowan-Robinson, M., Ellis, R.S. & Frenk, C.S., 1990, *Mon. Not. R. astr. Soc.*, **247**, 10p.
Eke, V.R., Cole, S.M., Frenk, C.S. & Navarro, J.F., 1995, submitted to *Mon. Not. R. astr. Soc.*
Ellis, R.S., Colless, M., Broadhurst, T.J., Heyl, J.S. & Glazebrook, K., 1995, *preprint.*
Fairall, A.P. & Jones, A., 1988, *Publs. Dept. Astr. Cape Town*, **10**.
Fong, R., Hale-Sutton, D. & Shanks, T., 1991, in *"Physical Cosmology"*, Proceedings 25th Anniversary of the Cosmic Background Radiation Discovery, eds. Blanchard, A. *et al.*, Editions Frontières, 289.
Fisher, K.B., 1995, *Astrophys. J.*, **448**, 494.
Fisher, K.B., Davis. M., Strauss, M.A., Yahil, A. & Huchra, J.P., 1994, *Mon. Not. R. astr. Soc.*, **266**, 50.
Gaztañaga & Baugh, C.M., 1995, *Mon. Not. R. astr. Soc.*, **273**, 1p.
Geller, M.J., Huchra, J.P. & de Lapparent, V., 1987, in *IAU Symposium 124, "Observational Cosmology"*, eds. Hewitt, A. *et al.*, Dordrecht, Reidel, 301.
Glazebrook, K., Peacock, J.A., Miller, L. & Collins, C.A., 1995, *Mon. Not. R. astr. Soc.*, **275**, 169.
Gott, J.R. III, Melott, A.L. & Dickinson, M., 1986, *Astrophys. J.*, **306**, 341.
Gunn, J.E. & Weinberg, D.H., 1995, in *"Wide Field Spectroscopy and the Distant Universe"*, 35th Herstmonceux Conference, Cambridge, UK, eds. Maddox, S.J. & Aragón-Salamanca, A., World Scientific Publishing, 3.
Guth, A.H., 1981, *Phys. Rev. D*, **23**, 327.
Hale-Sutton, D., 1990, *Ph.D. Thesis*, University of Durham.
Hamilton, A.J.S., 1992, *Astrophys. J. Lett.*, **385**, L5.
Hamilton, A.J.S., 1993, *Astrophys. J.*, **417**, 19.
Hawking, S.W., 1982, *Phys. Lett.*, **115B**, 295.
Holman, B. & Drinkwater, M.J., 1994, *"FLAIR Data Reduction with IRAF"*, Anglo-Australian Observatory Manual.
Hubble, E., 1929, *Proc. N.A.S.*, **15**, 168.
Huchra, J.P., Vogeley, M.S. & Geller, M.J., 1995, *in preparation.*
Hudson, M.J., Dekel, A., Courteau, S., Faber, S.M. & Willick, J.A., 1995, *Mon. Not. R. astr. Soc.*, **274**, 305.
Kaiser, N., 1986, *Mon. Not. R. astr. Soc.*, **219**, 785.
Kaiser, N., 1987, *Mon. Not. R. astr. Soc.*, **227**, 1.

Kendall, M., 1975, *"Multivariate Analysis"*, Charles Griffin & Company, London.
Kolb, E.W. & Turner, M.S., 1990, *"The Early Universe"*, Addison-Wesley Publishing Company, USA.
Landy, S.D., Shectman, S.A., Lin, H., Kirshner, R.P., Oemler, A.A. & Tucker, D.L., 1996, *Astrophys. J. Lett.*, **456**, L1.
Landy, S.D. & Szalay, A.S., 1993, *Astrophys. J.*, **412**, 64.
Lilly, S.J., Tresse, L., Hammer, F., Crampton, D. & Le Fevre, O., 1995, *Astrophys. J.*, **455**, 108.
Lin, H., Kirshner, R.P., Tucker, D.L., Shectman, S.A., Landy, S.D., Oemler, A.A. & Schechter, P.L., 1995a, *in preparation.*
Lin, H., Kirshner, R.P., Schectman, S.A., Landy, S.D., Oemler, A.A., Tucker, D.L. & Schechter, P.L., 1995b, *in preparation.*
Loveday, J., Efstathiou, G.P., Maddox, S.J. & Peterson, B.A., 1995a, submitted to *Astrophys. J.*
Loveday, J., Efstathiou, G.P., Peterson, B.A. & Maddox, S.J., 1992a, *Astrophys. J. Lett.*, **400**, L43.
Loveday, J., Peterson, B.A., Efstathiou, G.P. & Maddox, S.J., 1992b, *Astrophys. J.*, **390**, 338.
Loveday, J., Maddox, S.J., Efstathiou, G.P. & Peterson, B.A., 1995b, *Astrophys. J.*, **442**, 457.
Lucy, L.B., 1974, *Astron. J.*, **79**, 745.
Lucy, L.B., 1994, *Astron. Astrophys.*, **289**, 983.
Maddox, S.J., Sutherland, W.J., Efstathiou, G.P. & Loveday, J., 1990a, *Mon. Not. R. astr. Soc.*, **243**, 692.
Maddox, S.J., Sutherland, W.J., Efstathiou, G.P., Loveday, J. & Peterson, B.A., 1990b, *Mon. Not. R. astr. Soc.*, **247**, 1p.
Marzke, R.O., Geller, M.J., da Costa, L.N. & Huchra, J.P., 1995, *Astron. J.*, **110** 477.
Marzke, R.O., Huchra, J.P. & Geller, M.J., 1994, *Astrophys. J.*, **428**, 43.
Mecke, K.R., Buchert, T. & Wagner, H., 1994, *Astron. Astrophys.*, **288**, 697.
Metcalfe, N., Fong, R. & Shanks, T., 1995a, *Mon. Not. R. astr. Soc.*, **274**, 769.
Metcalfe, N., Fong, R., Shanks, T. & Kilkenny, D., 1989, *Mon. Not. R. astr. Soc.*, **236**, 207.
Metcalfe, N., Shanks, T., Fong, R., & Roche, N., 1995b, *Mon. Not. R. astr. Soc.*, **273**, 257.
Mo, H.J., Jing, Y.P. & Börner, G., 1993, *Mon. Not. R. astr. Soc.*, **264**, 825.
Ostriker, J.P. & Steinhardt, P.J., 1995, *Nature*, **377**, 600.
Parker, Q.A. & Watson, F.G., 1995, in *"Wide Field Spectroscopy and the Distant Universe"*, 35th Herstmonceux Conference, Cambridge, UK, eds. Maddox, S.J. & Aragón-Salamanca, A., World Scientific Publishing, 33.
Peacock, J.A. & Dodds, S.J., 1994, *Mon. Not. R. astr. Soc.*, **267**, 1020.
Peebles, P.J.E., 1973, *Astrophys. J.*, **185**, 413.
Peebles, P.J.E., 1980, *"The Large Scale Structure of the Universe"*, Princeton University Press, Princeton.
Peebles, P.J.E., 1993, *"Principles of Physical Cosmology"*, Princeton University Press, Princeton.
Penzias, A.A. & Wilson, R.W., 1965, *Astrophys. J.*, **142**, 419.

Peterson, B.A., Ellis, R.S., Efstathiou, G.P., Shanks, T., Bean, A.J., Fong, R., & Zen-Long, Z., 1986, *Mon. Not. R. astr. Soc.*, **221**, 233.

Richardson, W.J., 1972, *J. Opt. Soc. Am.*, **62**, 55.

Sandage, A., Tammann, G.A. & Yahil, A., 1979, *Astrophys. J.*, **232**, 352.

Saunders, W., Frenk, C.S., Rowan-Robinson, M., Efstathiou, G.P., Lawrence, A., Kaiser, N., Ellis, R.S., Crawford, J., Xia, X.-Y. & Parry, I., 1991, *Nature*, **349**, 32.

Saunders, W., Rowan-Robinson, M. & Lawrence, A., 1992, *Mon. Not. R. astr. Soc.*, **258**, 134.

Saunders, W., Rowan-Robinson, M., Lawrence, A., Efstathiou, G.P., Kaiser, N., Ellis, R.S. & Frenk, C.S., 1990, *Mon. Not. R. astr. Soc.*, **242**, 318.

Schechter, P.L., 1976, *Astrophys. J.*, **203**, 297.

Schmidt, M., 1968, *Astrophys. J.*, **151**, 393.

Shanks, T., 1990, in *"The Galactic and Extragalactic Background Radiation"*, IAU Symposium No. 139, eds. Bowyer, S. & Leinert, C., Kluwer Academic Publishers, 269.

Shanks, T., Bean, A.J., Efstathiou, G., Ellis, R.S., Fong, R. & Peterson, B.A., 1983, *Astrophys. J.*, **274**, 529.

Shanks, T. & Boyle, B.J., 1994, *Mon. Not. R. astr. Soc.*, **271**, 753.

Shanks, T., Hale-Sutton, D., Fong, R. & Metcalfe, N., 1989, *Mon. Not. R. astr. Soc.*, **237**, 589.

Shectman. S.A., Landy, S.D., Oemler, A.A., Tucker, D.L, Kirshner, R.P., Lin, H. & Schechter, P.L., 1995, in *"Wide Field Spectroscopy and the Distant Universe"*, 35th Herstmonceux Conference, Cambridge, UK, eds. Maddox, S.J. & Aragón-Salamanca, A., World Scientific Publishing, 98.

Smoot, G.F., Bennett, C.L., Kogut, A., Wright, E.L., Aymon, J., Boggess, N.W., Cheng, E.S., Deamici, G., Gulkis, S., Hauser, M.G., Hinshaw, G., Jackson, P.D., Janssen, M., Kaita, E., Kelsall, T., Keegstra, P., Lineweaver, C., Loewenstein, K., Lubin, P., Mather, J., Meyer, S.S., Moseley, S.H., Murdock, T., Rokke, L., Silverberg, R.F., Tenorio, L., Weiss, R. & Wilkinson, D.T., 1992, *Astrophys. J. Lett.*, **396**, L1.

Strauss, M.A. & Willick, J.A., 1995, *Phys. Lett.*, **261**, 271.

Tegmark, M., 1995, *private communication.*

Tonry, J.L. & Davis, M., 1979, *Astron. J.*, **84**, 1511.

Tucker, D.L., Oemler, A.A., Shectman, S.A., Kirshner, R.P., Lin, H., Landy, S.D., & Schechter, P.L., 1995, *in preparation.*

Watson, F.G., Oates, A.P., Shanks, T. & Hale-Sutton, D., 1991, *Mon. Not. R. astr. Soc.*, **253**, 222.

White, S.D.M., 1979, *Mon. Not. R. astr. Soc.*, **186**, 145.

Appendix A

The Durham/UKST Galaxy Redshift Catalogue

In this appendix the Durham/UKST Galaxy Redshift Catalogue is presented. Table A.1 gives information on all of the galaxies in the catalogue with a measured redshift. This includes the UKST field number, the (α,δ) coordinates (1950), the EDSGC b_J apparent magnitude (after the zero-point correction from an earlier chapter) and the measured radial velocity (from the FLAIR observations) of each galaxy.

Table A.1: The field numbers, the (α,δ) coordinates (1950), the COSMOS corrected apparent magnitudes and the FLAIR measured radial velocities for all the galaxies in the Durham/UKST survey.

α (h m s)	δ (° ′ ″)	b_J	v (kms^{-1})	α (h m s)	δ (° ′ ″)	b_J	v (kms^{-1})
531				531			
21 40 47.6	−25 34 50.0	13.83	3450	21 42 09.5	−25 15 38.3	14.47	3561
21 29 35.7	−24 10 12.1	14.81	19664	21 38 43.3	−26 49 13.0	15.22	9350
21 32 31.0	−26 52 58.6	15.27	15821	21 30 33.4	−27 06 42.2	15.40	16148
21 46 59.7	−26 14 32.5	15.53	9097	21 46 03.9	−25 56 17.2	15.74	9540
21 31 45.4	−24 26 20.9	15.78	16504	21 28 04.9	−24 02 31.7	15.84	19439
21 35 08.3	−27 22 51.6	15.96	9092	21 31 26.9	−27 06 04.0	16.03	19921
21 36 58.6	−22 48 39.7	16.07	9674	21 30 12.4	−22 55 15.1	16.11	9942
21 34 46.6	−25 09 51.5	16.21	7481	21 36 56.1	−22 37 59.3	16.23	10325
21 35 13.4	−26 55 31.0	16.25	11033	21 32 59.0	−26 40 33.0	16.27	9114
21 40 24.2	−24 31 04.4	16.36	9738	21 29 22.7	−25 46 42.1	16.38	5016
21 34 28.0	−26 31 07.5	16.45	19805	21 37 06.0	−22 52 30.2	16.49	9371
21 27 09.6	−23 22 08.3	16.51	10317	21 46 40.2	−26 36 03.6	16.65	9601
21 27 55.5	−25 27 25.0	16.72	9147	21 32 15.5	−24 27 17.6	16.77	16570
21 30 06.9	−23 22 38.1	16.80	19202	21 47 06.4	−26 21 11.1	16.83	21905
21 46 47.5	−24 30 51.0	16.85	9815	21 36 28.3	−22 37 36.7	16.89	9470
21 31 41.1	−27 22 17.8	16.92	20143	21 40 39.1	−24 01 34.1	16.95	16461
21 35 19.5	−22 40 35.3	16.96	9407	21 39 36.0	−27 29 24.4	17.08	15797
21 32 16.0	−24 49 36.2	17.08	15074	21 36 13.8	−22 53 51.9	17.12	16648
21 29 50.5	−26 32 49.9	17.14	16113	21 32 45.8	−26 27 18.5	17.18	19745
21 29 12.4	−25 15 51.2	17.20	16530	21 28 13.0	−25 36 42.8	17.25	10793
532				532			
22 10 19.4	−26 23 46.3	13.50	4850	22 08 05.7	−25 19 12.4	14.54	4917
22 05 25.2	−25 18 21.4	14.79	5553	21 59 03.7	−22 43 35.9	14.91	5330
22 00 22.5	−26 38 56.3	14.97	9759	22 08 44.1	−23 12 00.8	15.10	5407
22 01 53.2	−26 38 41.6	15.20	5549	22 06 34.3	−25 39 47.2	15.30	2476
22 09 09.6	−24 45 10.8	15.46	7437	22 03 14.0	−22 56 53.0	15.49	17262
22 08 20.8	−27 05 14.7	15.64	4743	21 58 22.6	−24 35 57.8	15.89	5343
22 03 14.6	−26 25 46.2	15.96	6672	22 10 59.0	−24 35 01.3	16.09	11341
22 09 32.9	−27 24 18.6	16.16	9609	21 54 58.7	−25 00 47.4	16.34	4966
22 05 56.0	−24 21 10.9	16.36	16730	22 07 53.5	−23 42 30.7	16.47	18659
22 10 36.2	−27 07 46.2	16.58	8872	21 53 01.3	−25 19 30.8	16.70	7139
22 09 16.2	−26 00 27.3	16.72	10918	21 57 20.1	−23 40 38.9	16.75	19931
21 56 04.0	−25 47 36.4	16.86	8869	22 07 38.1	−25 06 14.5	16.96	2603
22 08 28.6	−23 17 01.8	16.99	17612	22 01 11.8	−26 32 29.4	17.06	10756
22 05 22.3	−27 20 39.3	17.15	5800	22 06 28.8	−26 27 39.3	17.19	12400
22 05 12.9	−24 29 37.9	17.20	16150	21 54 09.6	−25 06 05.5	17.22	1711
21 50 35.9	−24 15 29.0	17.26	28966	22 04 02.4	−24 24 30.1	17.34	16256
22 10 06.8	−25 55 54.8	17.38	18817	—	—	—	—
533				533			
22 25 51.1	−25 05 57.3	13.00	4633	22 22 43.8	−25 53 59.9	13.92	4499
22 11 13.8	−27 11 12.4	14.29	2569	22 17 02.5	−26 35 35.0	14.61	2510
22 31 47.6	−22 57 00.7	14.87	5492	22 22 47.8	−24 29 44.5	15.17	7616
22 17 22.6	−25 18 01.7	15.21	10765	22 23 09.8	−24 59 06.0	15.29	10854

Table A.1: Information on the Durham/UKST galaxies.

α (h m s)	δ ($^\circ$ $'$ $''$)	b_J	v (kms^{-1})	α (h m s)	δ ($^\circ$ $'$ $''$)	b_J	v (kms^{-1})
22 19 24.1	−23 51 15.4	15.37	11579	22 19 45.7	−26 22 06.3	15.42	9752
22 22 09.7	−26 56 15.5	15.70	8949	22 32 46.6	−26 21 40.2	15.82	5783
22 30 18.5	−25 00 27.2	15.88	5638	22 20 00.2	−27 09 37.4	15.94	5473
22 12 02.1	−25 56 04.4	15.96	9310	22 13 32.5	−25 55 11.2	16.08	26170
22 12 45.5	−26 28 22.0	16.09	9923	22 12 36.6	−25 48 46.5	16.13	11612
22 19 32.8	−23 20 21.6	16.17	8001	22 28 46.1	−25 40 38.8	16.24	10070
22 16 50.9	−25 35 02.2	16.25	4707	22 29 56.9	−22 48 09.7	16.30	15298
22 32 32.8	−25 22 29.8	16.32	9823	22 13 04.1	−27 20 22.8	16.36	24395
22 14 10.2	−25 17 18.9	16.39	17836	22 19 40.2	−25 26 48.5	16.40	4369
22 16 43.5	−26 34 15.5	16.42	26625	22 30 12.1	−25 09 26.3	16.44	6132
22 32 37.4	−24 29 56.7	16.46	9932	22 12 34.1	−23 29 40.2	16.51	9387
22 23 36.5	−27 13 29.8	16.52	9755	22 15 44.0	−25 33 36.4	16.55	10419
22 28 40.5	−27 04 20.9	16.57	15182	22 15 56.0	−24 26 06.9	16.61	9216
22 14 10.2	−25 22 24.6	16.65	9212	22 13 41.5	−25 20 37.9	16.72	10331
22 25 44.8	−25 23 14.5	16.74	2587	22 26 45.5	−26 26 40.6	16.84	10187
22 13 31.3	−24 14 36.4	16.88	18042	22 28 32.3	−24 59 21.4	16.90	10168
22 12 00.1	−22 40 33.4	16.93	11030	22 29 28.0	−25 42 40.0	16.94	19158
22 15 08.6	−24 30 02.7	16.94	26856	22 19 18.1	−25 44 16.1	16.96	19317
22 23 41.2	−24 46 02.2	16.98	15748	22 31 20.8	−24 18 22.5	17.01	11268
22 30 38.6	−25 07 14.7	17.02	6234	—	—	—	—
		534				534	
22 33 00.4	−26 18 37.4	11.71	1503	22 35 56.3	−26 06 40.6	13.65	3408
22 54 02.6	−25 13 15.1	14.75	9345	22 34 23.0	−24 56 57.2	15.32	12942
22 40 28.5	−26 05 18.9	15.44	12544	22 33 51.0	−26 31 08.7	15.52	8096
22 34 58.0	−26 54 24.6	15.63	14484	22 43 10.2	−24 29 03.5	15.68	13607
22 42 33.8	−26 08 38.6	15.81	15679	22 36 28.5	−22 40 22.0	15.93	6422
22 34 55.6	−22 30 44.3	16.02	11131	22 42 33.8	−27 24 45.2	16.11	11004
22 34 04.7	−25 05 56.5	16.17	10688	22 33 33.2	−24 19 37.8	16.20	9845
22 41 26.1	−25 15 22.1	16.26	8205	22 33 09.0	−25 17 39.0	16.31	18047
22 35 58.6	−22 38 42.7	16.33	3444	22 47 11.4	−23 39 33.0	16.35	13989
22 33 35.5	−24 32 14.6	16.37	10340	22 39 14.3	−24 50 56.0	16.39	13820
22 48 05.5	−24 08 43.4	16.41	5951	22 39 48.8	−25 20 16.9	16.45	24095
22 33 31.9	−24 53 15.9	16.54	9957	22 44 15.0	−27 13 19.2	16.58	17376
22 38 56.4	−25 11 49.7	16.60	13375	22 36 41.2	−23 09 04.1	16.64	9005
22 35 50.0	−27 14 27.1	16.65	8476	22 52 23.2	−23 54 52.3	16.68	15429
22 40 35.4	−23 42 13.5	16.70	13490	22 35 06.4	−25 16 25.5	16.76	12383
22 52 25.3	−26 14 46.6	16.77	24359	22 53 11.1	−26 54 32.8	16.85	3067
22 38 28.4	−25 52 12.8	16.88	3030	22 46 31.2	−24 49 20.6	16.93	9963
22 37 15.9	−26 33 52.1	16.95	8064	22 38 11.2	−26 50 12.3	17.03	10844
22 38 44.0	−24 27 13.6	17.06	14919	22 52 26.9	−26 34 31.4	17.08	26856
22 52 51.8	−25 52 02.9	17.09	26218	22 48 18.5	−25 30 01.4	17.13	15423
22 48 02.9	−26 02 31.6	17.19	27134	22 40 06.4	−26 40 06.5	17.21	14417
22 37 57.3	−27 07 19.9	17.24	8351	22 36 59.1	−25 22 01.7	17.25	15840
22 43 30.1	−26 12 34.1	17.26	20744	22 49 49.0	−27 06 41.2	17.27	13265
22 51 05.6	−26 41 30.3	17.30	21198	—	—	—	—
		535				535	
22 56 18.7	−25 47 48.9	13.91	9222	23 16 36.5	−22 55 27.2	14.82	5983

Table A.1: Information on the Durham/UKST galaxies.

α (h m s)	δ ($^\circ$ $'$ $''$)	b_J	v (kms^{-1})	α (h m s)	δ ($^\circ$ $'$ $''$)	b_J	v (kms^{-1})
22 59 51.4	−24 35 32.8	15.43	9686	23 16 31.8	−23 43 06.8	15.54	7931
23 05 46.0	−26 32 43.3	15.99	8987	23 03 13.8	−25 30 59.7	16.20	15838
22 56 48.8	−26 06 41.0	16.26	8172	23 00 15.8	−26 11 32.2	16.34	14998
23 09 11.3	−25 28 58.8	16.41	9572	23 03 51.0	−25 41 52.3	16.51	15789
23 08 38.2	−27 11 27.7	16.70	15895	23 01 02.5	−26 36 47.9	16.86	15008
23 07 02.4	−23 13 47.1	16.93	9118	23 15 01.0	−25 53 06.7	17.16	20367
22 55 05.3	−25 12 32.2	17.18	26652	23 03 23.1	−27 08 28.7	17.22	8685
23 12 31.6	−25 26 40.4	17.32	9564	23 01 51.8	−22 41 20.2	17.39	26859
23 13 22.2	−24 18 07.0	17.41	18806	23 11 39.0	−25 58 14.5	17.43	8266
23 01 59.8	−23 57 49.1	17.45	7710	—	—	—	—
536				536			
23 19 22.5	−23 46 53.4	14.18	7746	23 34 12.2	−27 16 07.3	14.90	8691
23 22 44.9	−25 36 46.0	15.63	8596	23 37 13.9	−23 02 02.6	15.75	7686
23 33 57.9	−26 27 10.9	15.98	9425	23 28 09.4	−23 27 21.6	16.09	17751
23 35 26.1	−25 40 15.1	16.12	9659	23 32 36.8	−23 01 09.7	16.25	16592
23 18 15.7	−22 55 14.5	16.28	9114	23 38 44.8	−23 02 27.9	16.39	13858
23 29 49.8	−26 35 49.6	16.46	15021	23 35 37.2	−25 09 50.5	16.51	14301
23 36 02.9	−22 55 09.1	16.56	14723	23 37 35.2	−23 00 33.4	16.60	7714
23 23 49.5	−22 59 54.2	16.62	26061	23 29 52.7	−24 20 47.5	16.66	8040
23 29 29.6	−23 37 38.2	16.68	17504	23 23 49.8	−25 14 38.1	16.78	15035
23 35 56.5	−25 43 23.1	16.81	9464	23 31 54.0	−23 56 20.7	16.84	16170
23 27 54.8	−24 19 01.6	16.89	17945	23 31 25.6	−26 20 42.7	16.92	16237
23 37 12.0	−23 23 11.0	16.97	8942	23 24 19.3	−23 14 36.1	16.98	18355
23 38 42.6	−25 30 00.9	17.03	16417	23 26 28.0	−23 10 53.7	17.04	17841
23 22 32.5	−26 02 41.7	17.07	25932	23 22 23.0	−24 34 40.3	17.08	2576
23 17 52.8	−25 21 09.5	17.16	7977	23 22 24.7	−23 40 04.0	17.19	25974
23 36 09.7	−23 58 47.8	17.20	5170	23 38 34.0	−26 23 01.5	17.26	22132
23 25 50.8	−27 05 41.2	17.29	9567	23 20 01.6	−22 55 40.3	17.35	5159
23 24 11.2	−24 07 48.7	17.36	26605	23 31 37.2	−23 39 58.8	17.37	16069
23 28 09.6	−26 19 57.5	17.44	26636	—	—	—	—
537				537			
23 49 38.5	−25 40 59.2	14.12	3698	23 41 47.3	−24 15 55.0	15.17	14047
23 51 29.7	−25 43 58.9	15.36	2915	23 42 49.5	−27 10 36.7	15.68	14505
23 57 40.4	−27 00 32.4	15.90	17617	23 42 49.7	−24 03 04.1	15.99	14720
23 47 20.1	−24 18 13.5	16.06	16768	23 49 30.2	−22 38 03.5	16.09	13468
23 54 58.5	−25 12 16.9	16.18	19255	23 43 28.7	−23 10 34.8	16.24	13805
23 58 37.0	−27 17 54.6	16.27	8114	23 58 21.9	−26 11 02.1	16.28	14782
23 44 37.4	−24 05 01.0	16.31	22123	23 52 37.6	−22 54 04.1	16.35	14973
23 41 02.3	−26 12 03.8	16.39	16324	23 58 48.1	−25 28 25.8	16.43	8226
23 43 57.7	−23 10 32.4	16.46	8475	23 41 52.0	−26 19 02.8	16.47	14244
23 46 15.0	−27 01 28.8	16.48	9545	23 42 25.6	−26 54 07.4	16.50	14793
23 51 07.1	−23 40 09.8	16.51	14989	23 43 00.1	−27 17 58.7	16.51	14754
23 39 56.3	−27 11 50.4	16.53	18793	23 55 22.6	−22 59 45.0	16.54	15561
23 46 27.4	−25 27 49.5	16.56	15695	23 42 40.2	−26 19 54.1	16.57	15569
23 43 53.4	−25 24 05.0	16.59	16830	23 58 42.2	−26 04 50.5	16.62	15364
23 57 40.4	−25 31 25.2	16.63	8230	23 50 11.2	−26 54 49.6	16.65	17561
23 49 52.1	−27 10 01.3	16.70	19005	23 42 58.6	−23 36 21.2	16.72	14411

Table A.1: Information on the Durham/UKST galaxies.

α (h m s)	δ ($^\circ$ $'$ $''$)	b_J	v (kms^{-1})
23 42 53.1	−23 31 03.4	16.73	26833
23 46 24.8	−23 31 18.3	16.79	17107
23 40 27.7	−26 22 00.6	16.92	15199
23 41 52.5	−24 07 55.0	16.96	14163
23 55 02.2	−25 53 22.6	17.01	21934
23 43 45.2	−26 19 26.6	17.09	3777
23 58 17.1	−23 49 48.4	17.17	19972
472			
00 10 30.5	−24 29 33.7	14.12	10269
00 02 33.2	−27 22 42.2	16.32	8717
00 03 29.5	−26 36 17.9	16.77	8276
00 09 05.3	−23 57 16.8	17.26	16080
473			
00 16 33.4	−23 12 50.5	14.16	7718
00 12 23.4	−24 22 04.8	15.05	7606
00 27 40.6	−23 16 07.9	15.93	17248
00 28 49.5	−23 18 40.7	16.04	7958
00 12 48.6	−25 10 13.9	16.36	16668
00 14 06.5	−24 10 57.3	16.52	7595
00 24 37.3	−23 52 38.2	16.75	18993
00 18 12.1	−25 59 05.0	16.92	19133
00 13 06.7	−26 29 06.0	16.98	7830
00 20 51.6	−24 33 46.8	16.99	7851
00 22 59.9	−25 11 24.5	17.13	17037
00 22 48.7	−24 06 33.4	17.20	19238
00 29 15.6	−22 36 12.7	17.23	26023
474			
00 35 04.9	−22 49 26.4	14.18	3778
00 34 44.1	−22 51 41.7	14.69	3086
00 49 38.8	−22 57 07.2	15.35	13825
00 44 39.8	−24 38 36.9	15.45	16174
00 39 58.5	−23 54 10.4	15.73	6684
00 50 20.0	−25 56 34.8	15.98	9572
00 42 01.0	−23 34 13.8	16.09	18053
00 52 23.1	−26 38 31.0	16.17	17431
00 36 13.4	−25 49 51.0	16.31	18903
00 45 54.4	−25 23 57.7	16.35	19079
00 51 50.0	−23 49 25.2	16.40	17502
00 52 46.2	−24 18 53.2	16.44	17366
00 34 30.1	−22 47 21.1	16.52	19304
00 50 45.4	−26 21 54.1	16.60	20784
00 37 32.2	−25 08 22.2	16.67	18555
00 35 46.8	−23 10 43.0	16.70	27436
00 39 56.1	−25 21 11.6	16.79	19142
00 53 10.4	−24 05 49.4	16.90	13534
00 34 41.9	−26 42 25.8	16.92	18563
00 36 30.9	−24 37 32.5	16.98	21638

α (h m s)	δ ($^\circ$ $'$ $''$)	b_J	v (kms^{-1})
23 57 28.6	−23 38 47.7	16.75	19728
23 50 09.0	−24 19 58.2	16.89	15129
23 42 47.3	−25 11 04.6	16.92	17373
23 43 54.6	−23 35 59.7	16.96	13323
23 59 08.8	−25 51 18.0	17.05	4550
23 56 03.2	−23 00 32.9	17.11	902
—	—	—	—
472			
00 02 17.6	−25 38 08.2	16.13	18656
00 00 56.8	−23 13 19.5	16.69	25964
00 09 46.7	−24 01 42.7	16.84	10082
00 07 56.6	−24 38 30.0	17.36	15601
473			
00 32 53.4	−23 38 58.6	14.38	3804
00 28 45.5	−22 50 10.6	15.57	8031
00 12 50.5	−24 20 16.4	16.01	7467
00 14 09.9	−27 07 54.2	16.22	16660
00 19 04.6	−24 23 15.4	16.49	5720
00 19 52.2	−23 04 08.5	16.65	5997
00 12 34.5	−24 54 10.8	16.90	16623
00 16 48.8	−24 26 35.2	16.96	18708
00 13 11.6	−23 58 41.5	16.99	19267
00 19 05.8	−26 18 15.0	17.03	16900
00 14 59.3	−24 56 56.5	17.19	28406
00 16 19.6	−25 23 02.2	17.22	10583
—	—	—	—
474			
00 40 17.2	−23 50 07.6	14.54	6713
00 35 20.5	−26 55 27.2	14.82	5649
00 38 33.8	−25 29 29.7	15.43	16270
00 46 15.5	−23 50 02.5	15.58	16842
00 37 29.2	−22 45 54.1	15.91	15764
00 45 55.7	−27 16 49.1	16.00	5445
00 34 45.8	−25 47 50.2	16.12	18503
00 43 18.8	−26 11 35.6	16.28	11120
00 45 01.5	−25 42 47.2	16.34	20883
00 52 16.8	−23 47 28.7	16.38	9668
00 37 38.2	−25 25 22.4	16.43	7495
00 54 33.7	−23 36 55.8	16.47	2657
00 48 25.4	−23 21 20.8	16.56	35375
00 46 11.8	−27 00 12.6	16.64	6667
00 51 38.2	−23 27 58.1	16.68	16534
00 47 42.0	−23 33 07.8	16.77	16297
00 41 46.4	−24 36 05.7	16.84	20398
00 40 06.8	−22 57 42.2	16.91	15204
00 38 43.9	−23 37 41.2	16.95	15780
00 54 54.2	−27 05 48.1	17.03	21785

Table A.1: Information on the Durham/UKST galaxies.

α (h m s)	δ (° ′ ″)	b_J	v (kms^{-1})	α (h m s)	δ (° ′ ″)	b_J	v (kms^{-1})
00 40 56.1	−25 34 00.5	17.03	19250	00 54 36.7	−22 41 22.4	17.07	18589
00 37 33.8	−24 44 37.2	17.08	15769	00 35 40.0	−22 46 44.2	17.09	26988
00 40 12.7	−27 05 34.2	17.11	2003	00 43 32.1	−26 46 41.3	17.14	25759
00 40 14.1	−26 56 43.2	17.15	10656	00 52 34.9	−24 08 26.6	17.16	8116
00 42 52.8	−27 13 50.8	17.18	36264	00 40 22.9	−26 21 10.9	17.20	33076
00 43 07.0	−24 31 18.8	17.23	15758	—	—	—	—
	475				475		
01 13 23.1	−27 06 24.1	13.85	3592	01 13 10.1	−26 42 43.7	14.41	3688
01 16 49.7	−25 47 36.1	14.86	16028	00 56 29.3	−26 02 22.7	15.07	5583
01 01 02.3	−25 59 07.5	15.38	5525	01 15 30.2	−27 17 29.1	15.78	16992
01 12 29.6	−26 50 29.5	15.85	13303	01 06 16.7	−26 22 22.7	16.16	11750
01 03 42.8	−24 25 06.3	16.17	11745	00 59 48.1	−25 46 22.4	16.20	11858
01 00 44.4	−23 39 45.8	16.27	12127	01 15 23.9	−25 46 05.7	16.31	13409
00 55 57.2	−23 29 39.5	16.41	16575	01 06 49.4	−24 23 34.8	16.79	16879
01 01 58.4	−25 57 09.0	16.91	13258	00 56 28.1	−27 16 02.5	16.91	32001
01 11 35.8	−26 38 21.3	16.98	17256	01 03 27.9	−27 04 27.9	17.00	16239
01 01 41.1	−27 19 06.4	17.05	17543	01 11 59.5	−25 59 52.5	17.09	16885
01 05 36.6	−24 24 11.2	17.12	19276	00 59 53.7	−22 30 35.1	17.27	16413
	476				476		
01 28 06.0	−22 55 29.8	11.32	1588	01 18 45.2	−26 59 15.8	13.85	5775
01 28 24.5	−23 50 42.5	14.58	5890	01 38 45.3	−26 16 28.7	14.89	16629
01 33 46.2	−22 46 32.7	15.11	14663	01 35 55.7	−23 10 57.0	15.28	14078
01 28 56.7	−26 44 28.9	15.38	5689	01 25 15.2	−25 22 50.2	15.44	12942
01 22 17.7	−23 05 19.3	15.47	9430	01 29 18.4	−25 48 10.6	15.60	5992
01 24 28.2	−23 12 43.5	15.66	9876	01 27 31.0	−25 18 48.2	15.94	21030
01 24 37.8	−23 03 55.0	16.00	9434	01 31 07.0	−26 05 41.8	16.03	21340
01 17 11.1	−26 44 35.6	16.14	5662	01 33 20.1	−22 58 40.9	16.20	15885
01 30 36.9	−27 18 20.9	16.33	11601	01 31 31.3	−25 48 42.9	16.35	5780
01 24 27.6	−26 37 01.4	16.41	15028	01 38 31.0	−23 39 01.7	16.43	15210
01 33 49.3	−22 55 14.2	16.46	17861	01 31 26.7	−23 01 20.0	16.51	18091
01 28 51.0	−24 55 44.8	16.56	13151	01 33 25.1	−25 53 30.1	16.61	25563
01 36 13.5	−25 47 48.2	16.63	1495	01 37 40.9	−26 12 16.7	16.74	9380
01 29 06.6	−27 07 19.3	16.74	5970	01 23 07.4	−23 57 49.1	16.76	5584
01 21 51.8	−26 20 36.4	16.77	12764	01 33 04.4	−23 00 20.0	16.83	14897
01 24 48.2	−24 37 56.1	16.85	21357	01 22 05.2	−22 58 49.8	16.98	9458
01 30 21.5	−25 21 32.7	17.02	33718	01 19 56.0	−25 55 44.6	17.04	5620
01 25 10.4	−24 31 23.4	17.07	21329	01 28 26.9	−27 18 08.9	17.08	27416
01 22 26.3	−24 06 15.7	17.11	9440	01 23 44.1	−23 13 20.9	17.17	5548
01 20 11.0	−26 16 25.9	17.19	4626	01 31 56.1	−23 13 20.2	17.20	12484
01 23 11.9	−27 16 35.4	17.21	23871	01 24 26.6	−22 44 51.0	17.22	9950
01 23 48.4	−27 03 24.8	17.23	9600	01 27 50.2	−27 06 30.0	17.29	32704
	477				477		
01 56 15.2	−26 32 09.3	13.27	4525	01 51 25.8	−24 00 12.7	13.74	1486
01 59 13.0	−25 09 56.7	14.34	22815	01 47 32.5	−26 31 54.6	14.76	9455
01 46 31.3	−27 23 23.6	15.03	1359	01 48 35.0	−27 17 10.5	15.64	16440
01 46 42.5	−27 19 43.4	15.74	8774	01 40 46.2	−25 35 10.5	15.78	3920
01 50 27.9	−26 33 41.1	15.92	5745	01 46 08.1	−24 24 35.3	16.08	4724

Table A.1: Information on the Durham/UKST galaxies.

α (h m s)	δ ($^\circ$ $'$ $''$)	b_J	v (kms^{-1})	α (h m s)	δ ($^\circ$ $'$ $''$)	b_J	v (kms^{-1})
01 50 49.3	−26 34 00.8	16.09	5352	01 43 00.7	−22 34 38.4	16.19	12283
01 40 45.5	−26 32 23.2	16.33	8653	01 54 59.6	−25 33 05.2	16.38	9018
01 43 56.5	−26 51 20.3	16.47	17960	01 49 23.2	−25 46 14.0	16.56	12891
01 57 48.0	−23 37 58.2	16.58	6045	01 55 44.9	−23 36 01.9	16.66	12713
01 47 58.9	−25 50 02.8	16.68	16644	01 51 10.4	−26 54 39.6	16.69	17014
01 54 48.8	−25 21 20.6	16.71	16400	01 48 17.2	−25 02 57.6	16.73	13030
01 51 38.8	−24 01 49.4	16.76	21050	01 50 05.3	−24 16 15.3	16.78	17818
01 40 02.5	−26 04 52.5	16.82	5874	01 56 45.1	−24 44 26.8	16.85	25007
01 44 41.8	−27 08 27.2	16.93	9839	01 50 23.1	−24 33 53.3	17.16	17608
01 54 41.1	−23 17 35.1	17.20	5918	02 00 17.7	−27 20 10.0	17.26	12193
01 52 43.6	−24 44 03.7	17.32	12317	01 53 14.4	−26 54 58.4	17.34	24979
01 48 33.7	−25 47 26.1	17.35	16644	—	—	—	—
478				478			
02 22 48.5	−25 00 54.2	12.71	2976	02 10 11.5	−22 42 18.0	14.15	12356
02 16 19.5	−25 59 11.3	14.66	10792	02 07 57.4	−22 39 58.3	15.12	5585
02 15 36.8	−23 36 51.3	15.26	11026	02 10 33.2	−26 41 36.0	15.40	17451
02 09 04.8	−25 15 15.1	15.67	9709	02 10 46.5	−22 43 29.0	15.79	12164
02 09 48.4	−25 58 43.9	15.98	16922	02 22 19.4	−23 11 13.9	16.13	10548
02 03 01.4	−23 56 13.6	16.21	9065	02 12 38.9	−25 05 14.0	16.27	11067
02 11 51.1	−23 02 33.0	16.29	12217	02 20 58.9	−23 08 54.5	16.36	15696
02 07 05.2	−24 06 54.1	16.40	16679	02 10 05.1	−27 08 15.5	16.48	9590
02 06 42.6	−23 54 32.4	16.52	16653	02 13 46.4	−22 56 51.7	16.54	9721
02 16 46.1	−26 47 28.4	16.75	15024	02 17 08.9	−27 26 08.5	16.84	17206
02 21 37.2	−25 21 48.1	16.88	17832	02 18 18.4	−26 36 00.6	16.94	17768
02 21 02.7	−26 22 50.8	17.00	17544	02 13 25.8	−27 28 01.1	17.11	17430
02 14 59.8	−24 29 21.6	17.15	13265	02 14 16.9	−23 50 15.9	17.19	9792
02 18 50.7	−23 25 03.7	17.34	11633	02 12 49.6	−26 40 59.5	17.36	11461
02 12 57.7	−25 34 20.7	17.38	16868	02 05 02.3	−22 37 23.1	17.40	16315
02 11 29.5	−27 14 09.2	17.42	16799	—	—	—	—
479				479			
02 24 05.8	−24 30 48.0	12.69	1390	02 39 52.6	−24 20 40.6	14.42	1566
02 27 14.2	−26 45 23.4	14.55	4823	02 44 01.0	−26 30 59.8	14.87	6892
02 29 10.4	−23 13 35.3	15.24	17309	02 41 26.2	−24 24 35.9	15.28	7389
02 36 13.2	−27 26 43.3	15.40	13433	02 29 20.0	−23 14 10.1	15.48	16565
02 25 05.8	−24 09 07.4	15.59	5291	02 42 52.4	−26 39 36.0	15.72	7111
02 43 34.4	−23 26 35.5	15.74	6850	02 25 01.3	−26 52 01.7	15.83	4952
02 29 58.2	−24 55 46.2	15.91	11766	02 40 38.4	−25 47 37.5	16.06	7049
02 42 16.7	−24 45 01.5	16.14	6857	02 35 12.6	−23 44 56.5	16.19	15419
02 37 48.9	−23 08 12.6	16.21	9865	02 29 43.0	−26 16 22.1	16.26	13816
02 31 15.5	−26 59 38.2	16.30	12828	02 37 39.0	−25 20 57.4	16.33	7322
02 23 25.5	−23 31 12.1	16.37	15750	02 28 31.0	−25 51 47.4	16.43	10107
02 26 10.5	−24 02 16.7	16.45	24839	02 43 29.8	−25 58 17.9	16.52	10373
02 27 50.9	−22 32 24.8	16.67	16489	02 36 02.4	−23 03 47.0	16.75	16198
02 40 10.0	−25 46 28.0	16.77	7195	02 43 59.7	−25 07 55.3	16.80	6919
02 27 45.5	−25 44 44.3	16.83	16706	02 25 16.0	−24 37 01.1	16.86	10587
02 23 43.4	−26 47 29.9	16.87	17617	02 26 31.0	−25 34 09.3	16.89	16658
02 32 41.1	−23 19 41.5	16.95	15703	02 41 15.4	−22 38 55.3	16.97	9850

Table A.1: Information on the Durham/UKST galaxies.

α (h m s)	δ ($^\circ$ $'$ $''$)	b_J	v (kms^{-1})
02 31 54.7	−27 23 11.5	16.99	30728
02 29 49.4	−25 38 28.8	17.06	4754
480			
03 00 23.8	−23 03 41.7	11.41	1356
03 01 53.0	−26 47 25.1	15.01	3790
02 59 33.3	−25 30 33.7	15.26	10814
02 57 27.6	−24 29 29.6	15.47	10586
03 03 31.1	−23 26 34.3	15.65	11687
02 59 47.3	−24 01 12.3	15.79	10401
03 04 31.5	−26 20 15.9	15.96	11108
02 52 11.2	−22 42 20.5	16.13	8418
03 02 49.9	−22 33 07.2	16.32	4274
03 06 03.9	−23 45 15.3	16.44	19938
02 49 12.1	−25 08 57.3	16.48	33754
03 03 55.7	−23 33 16.2	16.52	10230
03 06 44.0	−23 26 05.1	16.58	23310
03 03 29.0	−23 20 37.7	16.65	11307
02 57 25.7	−27 02 06.7	16.73	15131
02 53 29.9	−26 37 38.3	16.80	18542
02 57 13.0	−27 25 57.1	16.90	5335
02 56 08.3	−24 00 53.6	16.94	19173
02 52 10.8	−25 15 48.1	17.00	18672
02 45 37.2	−22 48 56.8	17.11	25529
02 56 41.2	−24 05 20.9	17.17	10697
02 55 09.4	−23 36 08.1	17.21	4563
02 49 17.8	−24 09 17.2	17.21	4742
03 06 12.6	−23 05 57.1	17.33	10347
02 46 50.8	−26 13 35.2	17.38	31466
481			
03 17 42.5	−26 14 26.1	11.56	1710
03 18 53.8	−25 41 29.6	14.33	1471
03 09 08.1	−25 17 48.0	15.38	6324
03 09 16.4	−27 07 10.3	15.74	20642
03 09 08.8	−26 07 21.8	16.06	19932
03 24 23.3	−23 06 48.5	16.17	15775
03 16 42.3	−24 09 24.7	16.23	15284
03 25 41.6	−26 21 52.5	16.27	12599
03 13 13.5	−27 22 02.2	16.42	20602
03 17 28.3	−26 20 07.9	16.52	21032
03 28 08.0	−24 31 20.5	16.55	16146
03 20 52.1	−23 22 00.2	16.57	15603
03 24 28.0	−25 26 41.1	16.61	12183
03 20 34.5	−26 00 59.3	16.78	19216
03 09 19.5	−23 04 55.6	16.83	16194
03 19 46.3	−23 14 04.8	16.92	15365
03 08 15.4	−26 12 02.3	17.11	22659
466			

α (h m s)	δ ($^\circ$ $'$ $''$)	b_J	v (kms^{-1})
02 28 15.6	−26 10 13.5	17.00	14062
02 34 42.5	−22 55 23.5	17.15	15855
480			
03 05 58.6	−23 06 48.6	14.46	10237
02 49 23.9	−25 54 26.4	15.06	6700
02 49 08.1	−27 10 26.7	15.41	3467
02 57 01.5	−23 51 33.5	15.56	2762
03 05 37.2	−27 15 41.0	15.72	6432
02 56 07.7	−23 14 59.7	15.90	7987
02 51 38.7	−27 01 59.6	16.02	18197
02 47 47.4	−25 58 28.2	16.25	13588
02 51 21.1	−26 48 27.0	16.40	18935
02 59 02.8	−25 31 15.0	16.46	11083
02 51 12.6	−27 20 52.5	16.50	20313
03 04 54.3	−26 35 37.5	16.57	6368
02 47 58.6	−26 56 01.9	16.63	18132
03 06 33.6	−24 11 41.3	16.66	20717
03 04 40.4	−23 16 03.2	16.80	12178
03 06 36.0	−23 37 29.9	16.87	19523
03 03 06.2	−25 16 24.9	16.92	19460
03 05 41.2	−27 20 42.8	16.98	20156
03 06 01.2	−24 52 56.2	17.03	9570
02 48 26.6	−25 11 29.9	17.15	10491
02 49 46.9	−24 25 28.0	17.19	22621
02 59 28.8	−23 14 06.1	17.21	19494
02 51 33.8	−26 23 47.2	17.23	15107
02 48 39.7	−26 54 25.9	17.36	7017
02 53 16.6	−25 22 47.7	17.40	34246
481			
03 16 23.7	−26 01 07.0	13.42	1764
03 23 36.8	−26 33 45.7	14.88	12904
03 10 07.1	−25 20 05.5	15.67	6242
03 12 34.2	−25 03 33.3	15.80	15405
03 07 05.5	−23 59 58.2	16.14	21901
03 13 39.0	−26 55 08.6	16.19	4329
03 26 43.0	−26 47 10.0	16.25	13133
03 26 42.6	−23 10 47.7	16.40	15954
03 08 13.1	−25 54 58.5	16.50	23043
03 26 06.3	−27 15 11.3	16.53	11199
03 23 02.9	−24 10 05.9	16.56	21017
03 22 39.2	−26 42 17.6	16.59	19430
03 13 20.2	−23 00 12.5	16.65	10651
03 10 51.1	−25 58 21.4	16.79	12876
03 21 36.5	−24 25 37.3	16.87	10793
03 16 44.6	−22 54 12.9	16.94	26572
—	—	—	—
466			

Table A.1: Information on the Durham/UKST galaxies.

α (h m s)	δ (° ′ ″)	b_J	v (kms^{-1})
21 59 11.4	−32 13 36.8	12.07	2508
21 45 36.4	−32 24 35.0	14.33	5309
21 54 09.2	−28 51 25.0	14.69	6095
21 44 42.0	−29 55 32.7	15.02	6795
21 59 20.9	−31 27 42.7	15.25	2820
21 54 36.3	−29 37 57.5	15.39	10887
21 43 35.3	−30 15 30.2	15.56	7112
21 57 08.9	−30 25 27.4	15.65	5153
21 58 38.7	−27 44 28.5	15.96	19762
21 53 11.5	−29 28 57.9	16.18	9664
21 44 24.5	−28 30 34.2	16.26	14260
21 56 35.0	−29 26 05.6	16.39	11127
21 42 44.1	−29 23 16.4	16.58	13955
21 58 45.3	−31 08 03.1	16.64	11470
21 55 57.7	−27 49 30.5	16.70	20281
21 47 28.7	−30 23 34.8	16.80	28186
21 47 29.8	−30 19 08.7	16.85	27720
21 54 40.3	−27 56 41.2	16.88	24373
21 40 15.2	−29 15 50.2	16.95	21380
22 01 36.5	−28 20 29.5	17.04	28082
21 44 23.5	−28 55 09.3	17.12	21778
21 47 50.5	−28 29 55.6	17.14	28301
	467		
22 08 23.0	−30 48 35.1	13.05	4341
22 22 50.8	−31 27 17.8	14.02	8507
22 23 21.0	−31 23 59.9	14.43	4433
22 16 25.1	−28 39 16.7	14.78	8398
22 23 16.0	−31 07 20.5	15.07	8532
22 04 20.1	−30 04 56.0	15.22	8823
22 04 00.0	−29 11 33.8	15.44	18173
22 25 29.0	−30 31 27.6	15.67	15871
22 19 59.5	−32 19 03.0	15.89	8286
22 06 22.8	−27 48 46.9	16.05	6985
22 05 33.2	−30 27 43.8	16.10	12334
22 22 37.8	−27 57 17.8	16.17	15234
22 05 40.9	−30 50 05.2	16.27	18131
22 05 37.6	−29 07 09.5	16.42	16791
22 07 54.7	−29 13 36.1	16.59	7324
22 21 15.5	−29 25 34.0	16.64	18336
22 09 09.6	−28 20 33.5	16.73	24876
22 25 15.1	−30 56 31.7	16.76	18551
22 07 37.6	−30 36 14.5	16.81	10949
22 25 26.3	−30 16 16.4	16.90	17053
22 08 11.9	−29 08 26.8	16.91	18170
22 17 34.1	−29 18 45.6	16.95	24783
	468		
22 39 31.1	−30 19 08.2	12.93	1358

α (h m s)	δ (° ′ ″)	b_J	v (kms^{-1})
21 56 25.5	−32 07 23.3	13.56	3033
22 00 53.5	−28 02 27.0	14.51	6829
21 58 26.1	−31 46 14.7	14.86	2468
21 39 37.2	−29 35 46.0	15.08	7005
21 59 21.3	−31 59 52.0	15.30	2814
21 51 36.0	−28 35 56.9	15.51	9844
21 55 16.7	−28 54 00.5	15.61	6420
21 43 27.5	−29 33 14.9	15.80	14030
21 54 28.2	−31 55 52.9	16.03	16730
21 55 56.3	−28 57 42.8	16.20	6353
21 55 29.9	−30 33 52.7	16.30	16224
21 47 09.2	−31 09 27.5	16.43	5044
21 58 49.5	−31 12 23.6	16.62	11509
22 01 39.6	−31 13 30.1	16.67	27679
21 56 43.8	−29 00 31.6	16.73	17739
21 46 53.8	−32 04 04.1	16.82	28171
21 42 56.5	−30 27 22.1	16.85	7044
21 49 26.7	−29 07 28.6	16.91	27390
21 46 00.8	−27 54 32.8	16.97	22090
21 56 24.1	−31 52 02.6	17.10	20818
21 52 07.3	−31 12 31.9	17.13	22198
—	—	—	—
	467		
22 03 50.5	−31 24 25.8	13.76	4205
22 13 25.7	−27 39 10.8	14.23	5316
22 13 14.9	−30 37 06.5	14.59	7833
22 11 33.0	−30 13 47.7	14.93	4515
22 24 04.0	−31 08 34.9	15.15	3947
22 13 28.6	−32 01 37.8	15.36	8320
22 06 25.9	−27 58 33.5	15.56	7417
22 24 37.6	−31 38 31.0	15.85	8371
22 23 34.8	−28 21 03.5	16.01	3518
22 07 58.3	−30 27 24.3	16.08	18010
22 11 20.4	−28 48 20.0	16.13	17671
22 24 34.2	−30 45 03.2	16.24	16802
22 13 30.6	−28 59 18.3	16.35	18116
22 05 45.4	−31 07 52.0	16.58	2613
22 21 56.0	−31 12 21.0	16.63	17611
22 13 13.6	−28 11 54.2	16.67	18455
22 18 44.3	−31 12 51.2	16.74	17297
22 13 26.0	−29 02 02.2	16.77	18339
22 05 24.5	−29 34 56.9	16.88	25496
22 16 48.9	−28 35 03.4	16.91	17889
22 21 03.8	−30 44 26.2	16.92	24598
22 18 44.9	−27 52 35.4	16.98	18069
	468		
22 28 31.1	−28 39 27.8	14.88	10874

Table A.1: Information on the Durham/UKST galaxies.

α (h m s)	δ (° ′ ″)	b_J	v (kms^{-1})
22 35 30.3	−28 29 38.9	15.20	9459
22 27 17.0	−28 43 28.3	15.71	8410
22 41 50.6	−32 19 57.3	15.97	8572
22 28 58.0	−27 33 33.9	16.14	2040
22 27 53.8	−30 47 18.1	16.25	4161
22 29 34.6	−31 26 27.2	16.36	16997
22 29 41.0	−30 43 10.9	16.56	16663
22 31 03.8	−29 12 21.9	16.69	8351
22 31 54.9	−27 56 23.7	16.75	11873
22 31 02.5	−29 09 34.7	16.82	8871
22 39 09.2	−30 38 17.6	16.88	17468
22 40 20.5	−32 02 11.3	17.01	23610
22 47 15.5	−28 19 05.9	17.03	8860
22 36 25.5	−31 21 01.4	17.07	8426
22 25 52.3	−30 21 22.2	17.14	8591
22 43 29.0	−30 58 43.2	17.34	17574
22 44 50.1	−31 49 15.4	17.40	24179
22 30 42.1	−31 19 15.6	17.47	17086
22 48 02.1	−29 11 16.6	17.52	9644
469			
23 09 26.1	−28 48 39.9	11.94	1444
23 06 12.8	−31 07 47.2	15.02	1740
22 54 34.3	−31 43 23.7	15.50	9556
22 49 23.0	−28 52 25.3	15.63	12424
23 01 07.7	−29 00 41.4	15.76	1763
22 49 49.3	−30 07 17.9	15.85	4611
23 02 56.2	−32 25 25.3	15.93	17873
22 48 58.6	−29 42 41.8	16.25	11230
23 09 19.8	−31 10 57.0	16.34	32633
22 50 12.6	−31 23 43.2	16.47	22953
22 50 35.9	−29 49 18.0	16.50	23750
23 10 51.8	−29 17 25.8	16.55	8740
22 50 10.0	−28 59 55.3	16.65	20909
23 02 06.1	−30 32 37.5	16.69	21591
22 54 05.3	−28 58 15.5	16.87	12053
22 58 33.6	−28 22 57.3	16.95	24962
23 03 11.1	−31 00 29.8	16.98	8617
23 03 17.0	−31 34 58.1	17.04	11415
22 58 44.5	−31 48 02.3	17.13	16395
23 08 17.8	−29 38 51.9	17.16	31058
22 59 41.3	−31 22 00.0	17.21	24999
23 01 17.4	−32 06 21.2	17.25	25154
23 01 07.5	−29 23 46.5	17.28	21620
470			
23 21 07.2	−29 39 43.9	13.73	6989
23 19 52.8	−29 33 18.1	14.90	6852
23 16 44.3	−28 17 47.9	15.38	8504

α (h m s)	δ (° ′ ″)	b_J	v (kms^{-1})
22 29 45.2	−31 10 32.0	15.63	8573
22 39 42.5	−28 50 45.8	15.92	8544
22 34 34.6	−31 00 21.8	16.06	8491
22 28 53.0	−31 44 38.7	16.17	17441
22 39 23.9	−31 21 08.7	16.31	8689
22 27 34.2	−31 51 55.1	16.42	14586
22 28 33.5	−28 21 23.9	16.62	8394
22 34 03.9	−32 09 35.6	16.70	11407
22 40 21.7	−30 22 10.1	16.78	8261
22 45 09.2	−28 48 34.4	16.86	10086
22 36 38.6	−28 14 37.1	16.96	14663
22 45 48.2	−29 49 23.2	17.01	9718
22 32 33.7	−27 46 15.1	17.06	11742
22 31 32.6	−28 58 47.7	17.08	19329
22 47 52.2	−31 30 58.7	17.25	31544
22 39 31.0	−31 20 48.3	17.37	8484
22 48 21.2	−28 51 31.3	17.41	14832
22 45 24.6	−29 47 09.8	17.49	24058
—	—	—	—
469			
22 56 14.1	−30 45 43.0	14.46	8799
22 49 53.5	−29 19 17.5	15.23	11367
22 59 23.3	−32 22 13.9	15.54	8304
23 02 04.1	−30 41 19.6	15.72	8537
23 11 09.0	−29 51 27.4	15.84	8587
23 04 47.0	−27 36 46.8	15.88	8667
22 56 42.7	−32 02 42.7	16.12	17560
22 49 12.7	−31 36 10.6	16.29	20407
23 04 49.0	−29 05 18.6	16.44	14843
23 03 59.2	−31 25 37.5	16.48	20950
23 03 10.2	−31 10 21.4	16.53	8517
22 48 38.0	−30 13 23.9	16.59	13276
23 00 14.6	−29 44 55.2	16.68	15097
23 07 32.5	−31 30 33.8	16.75	20187
22 50 49.0	−29 39 29.3	16.93	23178
22 50 26.4	−30 19 41.3	16.97	13206
23 06 52.5	−28 51 11.4	17.01	14907
22 48 35.0	−32 11 38.9	17.06	23350
23 08 41.0	−30 52 55.5	17.14	22565
23 09 31.7	−27 45 38.6	17.16	31623
22 53 58.6	−30 50 27.4	17.22	24184
23 07 13.0	−31 20 30.5	17.26	16339
—	—	—	—
470			
23 29 46.8	−28 02 49.2	14.67	8755
23 28 17.4	−27 56 46.8	15.19	8530
23 29 36.4	−31 25 16.0	15.42	18218

Table A.1: Information on the Durham/UKST galaxies.

α (h m s)	δ ($^\circ$ $'$ $''$)	b_J	v (kms^{-1})
23 28 21.7	−27 48 04.1	15.49	8420
23 20 28.3	−29 02 11.4	15.89	13475
23 12 30.6	−28 11 06.4	16.03	8830
23 19 35.4	−29 39 29.2	16.09	15277
23 21 01.6	−30 15 21.3	16.29	15489
23 26 08.4	−27 32 49.3	16.41	9555
23 28 37.9	−32 08 32.6	16.48	16373
23 32 32.8	−31 14 21.8	16.51	15671
23 27 25.2	−29 12 18.4	16.59	13248
23 29 50.5	−30 16 15.2	16.65	15394
23 28 30.9	−30 14 18.4	16.71	15376
23 30 57.7	−29 02 44.7	16.89	14829
23 26 55.8	−31 38 59.3	16.93	10696
23 30 45.6	−28 56 01.9	16.98	19638
23 18 00.7	−28 19 54.5	17.00	16427
23 33 57.2	−31 40 13.1	17.06	19796
23 25 45.2	−29 25 11.4	17.08	20844
23 24 58.2	−30 41 23.0	17.14	10467
23 31 15.7	−31 45 11.1	17.16	18753
23 29 36.4	−30 30 23.9	17.17	31340
23 16 54.5	−29 49 31.0	17.20	15345
23 16 47.1	−32 15 33.7	17.22	35721
	471		
23 45 08.2	−28 25 01.2	13.67	8587
23 49 56.4	−30 27 33.4	14.89	8745
23 44 52.8	−28 24 48.0	14.97	8210
23 46 40.1	−29 18 28.8	15.20	10507
23 39 14.1	−28 18 07.0	15.25	8282
23 56 05.2	−30 07 24.3	15.49	8946
23 49 49.0	−29 18 04.3	15.62	8606
23 51 51.6	−29 09 57.5	15.72	8810
23 44 02.3	−28 59 17.2	15.80	19082
23 36 32.2	−31 50 52.4	15.99	15733
23 46 08.4	−29 16 20.6	16.03	10977
23 34 58.7	−31 17 41.9	16.28	14943
23 49 51.0	−27 55 01.6	16.33	8710
23 45 51.8	−28 54 45.9	16.35	10734
23 38 29.0	−32 11 14.9	16.39	18268
23 44 19.0	−29 22 13.4	16.45	10391
23 54 05.8	−29 34 14.6	16.51	8795
23 42 32.4	−28 32 52.2	16.54	8265
23 50 15.9	−29 54 35.0	16.62	12824
23 35 38.5	−31 35 08.1	16.65	25845
23 35 43.6	−31 46 35.1	16.70	15280
23 41 54.7	−28 07 00.6	16.75	22610
23 42 19.0	−29 49 08.3	16.80	9625
23 43 15.9	−28 29 17.5	16.82	15547

α (h m s)	δ ($^\circ$ $'$ $''$)	b_J	v (kms^{-1})
23 23 26.8	−32 07 33.8	15.79	18136
23 23 28.9	−30 48 51.8	15.99	18857
23 11 34.3	−29 28 19.6	16.06	14962
23 17 29.0	−29 47 56.5	16.12	15134
23 33 33.7	−31 50 21.7	16.38	19805
23 25 14.2	−31 57 09.8	16.46	18911
23 24 22.9	−29 22 09.1	16.49	20710
23 33 05.6	−29 19 14.3	16.56	10203
23 31 00.8	−29 59 18.5	16.62	15147
23 24 12.0	−27 37 06.8	16.68	16018
23 32 40.6	−29 15 03.8	16.80	15192
23 34 15.8	−30 26 29.2	16.91	18636
23 14 43.8	−28 08 02.3	16.97	26554
23 31 47.4	−27 45 11.2	16.99	16193
23 12 35.6	−29 47 27.9	17.03	8666
23 29 30.7	−27 55 29.6	17.06	7922
23 32 02.2	−28 06 22.9	17.13	8295
23 33 44.7	−30 13 07.2	17.15	15295
23 13 43.3	−30 47 18.3	17.17	33775
23 22 43.0	−29 48 48.0	17.18	22449
23 26 58.4	−31 24 04.0	17.21	18541
23 18 44.9	−31 47 28.1	17.29	28358
	471		
23 49 01.5	−28 38 35.4	14.07	8321
23 38 52.8	−29 35 52.9	14.96	15628
23 44 38.8	−28 14 08.2	15.10	8455
23 49 19.2	−28 12 29.8	15.24	8646
23 45 47.5	−28 21 10.1	15.36	10153
23 45 20.2	−28 35 55.9	15.52	9966
23 48 56.0	−28 17 58.4	15.63	10242
23 49 54.9	−28 37 15.5	15.74	8640
23 47 49.3	−28 13 06.6	15.84	8750
23 55 51.9	−32 01 50.3	15.99	17747
23 48 34.2	−31 36 59.1	16.27	13140
23 51 52.8	−27 47 57.5	16.31	15179
23 47 07.9	−29 38 58.8	16.34	9059
23 49 45.8	−29 46 26.5	16.38	8902
23 45 50.4	−29 01 29.7	16.44	15599
23 43 41.1	−30 28 15.2	16.48	16393
23 46 52.7	−30 41 56.7	16.53	13619
23 47 10.5	−27 58 45.5	16.61	19360
23 40 51.0	−29 22 05.5	16.64	15294
23 44 04.9	−28 22 39.4	16.69	17013
23 52 29.7	−27 56 39.2	16.71	21006
23 40 48.0	−32 06 56.2	16.78	16449
23 38 04.7	−29 33 10.5	16.81	15565
23 49 00.2	−31 45 27.4	16.82	13131

Table A.1: Information on the Durham/UKST galaxies.

α (h m s)	δ ($^\circ$ $'$ $''$)	b_J	v (kms^{-1})
23 43 40.0	−27 47 13.9	16.84	8646
23 48 00.2	−28 24 23.1	16.87	8767
409			
00 05 48.4	−30 11 35.5	13.88	1476
00 03 57.0	−32 14 05.7	14.93	8583
00 09 14.9	−30 24 43.7	15.33	7720
00 10 31.7	−30 59 54.8	15.53	9238
00 09 36.5	−31 02 40.3	15.75	9546
00 08 13.2	−30 14 30.7	15.96	7725
00 05 17.9	−28 22 07.8	16.21	8427
00 09 51.2	−29 34 06.8	16.29	16864
23 58 59.9	−28 41 48.1	16.32	19273
00 07 44.9	−30 35 53.1	16.38	14528
00 06 32.3	−27 52 36.8	16.41	17892
23 58 00.2	−30 24 14.2	16.48	17749
23 58 05.6	−31 15 55.2	16.63	18388
23 59 29.0	−27 31 56.8	16.68	11702
00 07 42.2	−29 37 57.1	16.79	7427
00 04 17.3	−31 53 07.7	16.91	12177
00 10 32.8	−31 21 03.3	16.97	18572
23 58 34.7	−28 05 23.1	16.98	18628
23 57 39.3	−27 54 41.1	17.07	18911
00 10 54.8	−28 43 52.6	17.19	4292
23 58 07.5	−27 42 47.3	17.21	8620
410			
00 31 47.1	−28 04 46.8	12.10	1671
00 26 34.8	−31 06 52.9	14.52	7340
00 24 09.3	−30 49 36.7	15.54	5981
00 20 37.4	−28 25 35.3	15.85	18437
00 33 18.1	−28 45 33.5	16.03	6997
00 34 04.2	−30 51 13.4	16.16	18081
00 32 32.3	−27 38 29.6	16.23	21909
00 33 22.4	−28 31 51.1	16.27	7179
00 33 33.2	−31 28 26.1	16.41	16117
00 19 18.7	−30 43 37.6	16.57	27013
00 31 37.3	−28 29 27.4	16.62	4958
00 20 20.1	−29 21 45.8	16.75	20791
00 28 52.1	−29 25 29.1	16.80	28783
00 27 44.5	−29 53 28.1	16.87	29459
00 31 43.3	−28 52 38.3	16.95	33789
00 14 40.9	−28 31 27.8	16.98	16810
00 32 36.0	−30 34 23.9	17.01	1905
00 31 36.8	−29 39 32.2	17.06	18471
00 23 35.7	−28 51 51.4	17.16	16451
00 13 58.0	−29 26 57.8	17.19	14292
411			
00 55 21.8	−27 46 16.2	13.25	5573

α (h m s)	δ ($^\circ$ $'$ $''$)	b_J	v (kms^{-1})
23 43 19.8	−28 52 40.2	16.86	15614
23 44 21.5	−31 00 39.2	16.88	26369
409			
23 59 58.8	−30 54 01.7	14.59	9080
00 02 26.6	−30 47 03.5	15.05	8281
00 02 29.5	−27 59 34.2	15.42	9872
00 02 58.2	−30 51 54.7	15.60	8565
23 59 02.2	−29 53 37.4	15.80	8285
00 09 23.2	−29 00 31.2	16.05	19975
00 00 32.1	−30 08 41.9	16.26	18379
00 00 00.3	−31 00 47.9	16.30	18470
00 06 11.0	−31 43 57.3	16.37	16847
00 04 53.0	−28 37 52.0	16.40	18366
23 59 42.9	−30 46 37.4	16.42	8721
00 09 52.6	−29 28 51.7	16.57	16667
00 08 08.4	−31 56 18.7	16.65	17934
00 05 05.0	−31 25 12.6	16.75	16916
00 01 17.9	−28 11 23.3	16.85	19068
00 04 23.7	−28 07 31.6	16.96	18549
00 00 49.0	−31 06 31.6	16.97	29341
00 01 20.6	−29 03 30.8	16.98	20445
00 02 54.8	−29 09 20.0	17.12	18856
23 57 49.9	−30 56 50.2	17.20	9505
23 59 07.7	−29 46 26.9	17.25	18855
410			
00 31 42.9	−31 02 50.3	13.95	1536
00 31 51.8	−31 52 13.9	15.36	9513
00 32 38.1	−28 32 50.1	15.77	7060
00 11 43.9	−31 56 12.2	15.93	6838
00 16 25.5	−28 31 00.0	16.11	18731
00 33 47.2	−30 34 37.7	16.19	18140
00 13 37.4	−29 11 24.1	16.26	18145
00 16 08.1	−30 50 10.8	16.37	4681
00 14 08.5	−28 03 12.7	16.45	32758
00 21 40.6	−28 42 59.0	16.58	11821
00 22 59.8	−29 32 48.8	16.68	10318
00 14 49.0	−31 54 08.1	16.76	30998
00 15 57.1	−31 00 52.3	16.86	18631
00 19 44.5	−31 11 44.8	16.88	32105
00 25 53.9	−31 13 56.8	16.97	15350
00 33 54.2	−29 43 08.3	16.99	16055
00 29 58.5	−29 16 30.0	17.05	28903
00 27 17.4	−30 31 59.2	17.10	7487
00 26 23.0	−29 38 27.3	17.19	22873
—	—	—	—
411			
00 54 28.7	−32 14 00.4	14.59	5798

Table A.1: Information on the Durham/UKST galaxies.

α (h m s)	δ ($^\circ$ $'$ $''$)	b_J	v (kms^{-1})
00 48 17.7	−31 39 21.9	14.87	6262
00 47 53.5	−30 45 29.2	15.42	12938
00 52 20.3	−31 17 41.3	15.69	9991
00 36 10.6	−28 17 32.7	15.90	17275
00 41 07.2	−30 50 41.6	16.08	14424
00 45 34.1	−32 14 31.2	16.12	1730
00 44 25.3	−31 48 51.4	16.35	1703
00 40 26.4	−28 44 36.2	16.41	24742
00 40 45.8	−32 00 01.4	16.46	9936
00 35 11.0	−27 44 28.7	16.55	18527
00 52 53.2	−31 35 32.9	16.58	9929
00 54 57.5	−29 43 07.2	16.60	23165
00 53 54.8	−29 21 25.6	16.68	22699
00 49 13.5	−28 46 04.7	16.77	32607
00 36 50.8	−31 13 53.9	16.85	17873
00 37 29.1	−29 11 02.5	16.89	34331
00 56 30.4	−30 29 20.3	16.93	10146
00 38 33.5	−29 54 46.3	17.00	33572
00 47 01.2	−31 05 11.8	17.05	17594
00 53 16.6	−29 04 25.6	17.13	22566
00 40 29.7	−30 32 03.9	17.21	18934
	412		
01 11 26.5	−32 00 45.1	12.69	5722
01 03 49.3	−30 26 44.7	13.84	9607
01 18 28.2	−31 22 35.7	14.83	9454
01 14 20.5	−31 41 51.3	15.20	10524
01 03 47.5	−30 44 32.0	15.36	6907
01 10 28.5	−31 27 54.5	15.46	5543
01 20 12.2	−30 14 37.6	15.63	11112
01 08 42.9	−32 26 12.3	15.86	10559
01 03 43.2	−30 39 55.6	15.99	10080
01 09 28.7	−31 43 23.1	16.10	9864
01 00 15.6	−29 17 29.3	16.24	17316
01 07 18.1	−30 48 04.4	16.33	24579
01 14 28.7	−28 54 37.2	16.43	18687
01 16 52.9	−29 17 37.5	16.54	8634
01 17 21.4	−31 10 35.5	16.60	17350
01 18 54.2	−30 02 51.6	16.66	20377
01 12 55.1	−28 10 52.7	16.72	11247
01 09 38.5	−30 19 02.0	16.80	26801
01 04 17.7	−30 27 28.7	16.85	27423
01 14 39.0	−27 55 07.1	16.89	17732
01 03 59.1	−27 39 01.2	16.91	15911
01 18 56.3	−31 01 22.6	17.01	9133
01 14 30.7	−31 22 06.0	17.04	10633
01 11 13.1	−30 59 46.9	17.07	17028
01 07 05.6	−29 58 16.0	17.11	18248

α (h m s)	δ ($^\circ$ $'$ $''$)	b_J	v (kms^{-1})
00 36 51.3	−30 13 12.4	15.04	7298
00 41 49.0	−28 54 21.1	15.53	13047
00 54 55.3	−31 12 28.5	15.80	9443
00 47 16.5	−30 34 03.8	16.04	14418
00 42 16.3	−31 00 27.6	16.10	21424
00 45 48.5	−30 57 32.0	16.19	13056
00 37 37.7	−32 23 24.8	16.37	9337
00 35 44.2	−27 49 04.0	16.43	18276
00 37 34.2	−29 56 10.2	16.48	13233
00 47 17.7	−31 43 02.0	16.57	24615
00 51 19.1	−27 52 33.0	16.59	22615
00 55 22.0	−28 33 10.9	16.65	15569
00 49 53.1	−27 37 02.8	16.72	11791
00 37 10.2	−29 10 50.0	16.82	33599
00 50 32.2	−29 38 55.4	16.85	34821
00 52 33.4	−32 11 22.4	16.92	20211
00 44 31.7	−29 07 56.7	16.97	22225
00 40 43.0	−31 28 56.9	17.03	26605
00 46 01.6	−29 28 46.1	17.08	14443
00 43 25.1	−29 39 05.4	17.14	16290
00 54 11.0	−31 09 13.6	17.29	23419
	412		
01 08 39.1	−30 42 16.2	13.34	5940
01 10 36.0	−31 42 55.0	14.79	5571
01 09 58.3	−32 19 38.5	15.07	10179
01 11 32.9	−32 28 53.0	15.24	5985
01 11 22.4	−32 06 30.2	15.44	6242
01 15 55.0	−31 02 11.5	15.49	10780
00 57 56.0	−30 10 55.0	15.71	9883
01 11 07.1	−30 29 26.3	15.89	5660
01 05 13.1	−31 18 44.2	16.01	9557
01 15 52.1	−30 10 55.6	16.16	11319
01 19 09.8	−30 12 15.2	16.31	10915
01 11 17.1	−31 55 05.0	16.40	5683
01 09 00.8	−31 43 26.9	16.48	5685
01 11 06.6	−32 03 28.6	16.57	5868
01 20 26.6	−30 48 11.3	16.61	17942
01 11 24.1	−31 54 32.9	16.70	5840
01 09 47.2	−32 08 30.1	16.77	5737
00 57 34.7	−30 45 19.0	16.84	9807
01 20 00.8	−28 20 11.2	16.86	24515
01 08 23.8	−31 14 23.9	16.90	5535
01 12 12.9	−31 26 56.8	16.94	5773
00 57 48.2	−29 48 34.6	17.02	10025
00 58 25.6	−28 26 26.5	17.06	29041
01 11 49.7	−28 35 44.6	17.09	11240
01 09 16.0	−29 22 57.5	17.13	18151

Table A.1: Information on the Durham/UKST galaxies.

α (h m s)	δ ($^\circ$ $'$ $''$)	b_J	v (kms^{-1})
413			
01 31 59.7	−29 40 23.0	10.86	1757
01 36 30.7	−32 04 33.1	14.87	8958
01 37 38.1	−28 12 34.0	15.35	17026
01 30 03.4	−31 20 57.1	15.51	21276
01 28 35.7	−27 57 46.9	15.72	6032
01 20 34.0	−28 15 10.8	16.00	16047
01 25 04.3	−28 37 11.6	16.11	10184
01 30 30.4	−29 34 12.7	16.27	19372
01 34 29.4	−28 34 48.3	16.37	16000
01 30 52.0	−29 12 46.8	16.45	10086
01 24 20.0	−28 40 48.0	16.52	9344
01 21 24.8	−27 51 09.6	16.56	28481
01 42 33.0	−28 26 46.9	16.64	9283
01 24 13.9	−31 47 41.1	16.66	31894
01 27 56.9	−28 51 51.5	16.71	9927
01 27 29.1	−29 47 20.2	16.77	21023
01 24 27.6	−28 25 52.6	16.80	21229
01 32 10.8	−31 48 21.1	16.84	20418
01 33 33.9	−29 38 30.1	16.87	21879
01 26 40.0	−29 17 52.1	16.92	26162
01 21 35.4	−31 23 42.8	16.96	32778
01 39 44.2	−29 34 34.4	17.09	12287
01 31 31.7	−29 05 33.8	17.14	13674
414			
01 53 25.9	−30 10 00.9	13.25	4412
01 43 37.4	−29 17 17.3	14.69	5867
02 03 52.7	−30 28 40.6	15.34	10646
01 47 39.5	−28 01 32.7	15.49	13384
02 00 29.3	−29 36 14.0	15.65	18407
01 53 14.5	−31 20 58.9	15.98	8276
01 44 47.8	−31 47 38.5	16.08	8684
02 00 41.8	−27 41 38.1	16.34	22906
02 05 25.2	−27 51 24.1	16.37	20837
01 51 11.4	−32 10 55.5	16.53	10383
01 49 37.7	−27 36 27.4	16.65	27328
01 45 18.0	−31 51 45.9	16.73	18390
01 44 59.2	−28 51 55.9	16.80	18613
01 57 05.9	−28 08 46.8	16.83	17758
02 03 37.1	−30 43 24.4	16.86	8557
01 44 48.0	−29 51 30.9	16.90	10957
01 56 37.6	−31 06 52.2	16.93	4939
02 05 15.7	−29 47 47.7	16.98	11638
01 51 55.8	−28 06 38.8	16.99	17885
02 06 23.0	−28 15 36.1	17.01	18146
01 50 57.5	−29 08 05.6	17.12	18185
01 55 58.1	−28 22 11.9	17.16	26492

α (h m s)	δ ($^\circ$ $'$ $''$)	b_J	v (kms^{-1})
413			
01 38 03.3	−29 09 57.5	13.93	5371
01 26 37.1	−32 16 17.9	15.12	6291
01 43 29.4	−28 09 57.6	15.42	8998
01 20 34.9	−31 02 48.1	15.62	9483
01 25 00.7	−28 59 36.2	15.95	11432
01 39 37.2	−28 47 59.3	16.05	11576
01 35 56.0	−28 53 20.6	16.20	9111
01 40 19.7	−31 03 44.4	16.29	15043
01 29 08.8	−31 30 39.7	16.40	9135
01 21 31.0	−30 18 32.2	16.49	7400
01 35 16.1	−28 08 54.8	16.52	11681
01 25 20.7	−32 22 16.6	16.62	18018
01 33 14.7	−29 20 07.3	16.65	12689
01 21 30.3	−30 39 28.2	16.69	29821
01 30 28.6	−29 34 00.0	16.72	19125
01 41 40.6	−30 24 23.6	16.80	17762
01 41 41.6	−30 24 47.6	16.83	17867
01 28 06.3	−28 43 27.4	16.85	20680
01 29 00.1	−29 26 14.5	16.89	11094
01 31 13.8	−30 38 43.2	16.95	21420
01 21 34.3	−28 38 59.6	17.03	16036
01 29 44.9	−28 26 47.9	17.12	17106
01 26 26.0	−29 54 19.9	17.14	28488
414			
01 56 55.5	−28 03 10.6	14.33	4769
01 59 01.6	−31 58 13.1	14.87	5520
02 01 16.2	−29 59 17.7	15.42	12667
01 58 42.0	−32 09 43.3	15.57	5450
01 47 38.9	−28 03 58.2	15.84	12945
01 52 20.0	−30 55 16.6	16.03	20414
01 57 23.8	−29 43 31.5	16.31	3074
01 56 00.4	−30 49 21.1	16.35	17166
01 48 52.6	−27 58 03.5	16.41	18310
01 45 17.1	−30 30 39.1	16.57	12892
01 57 47.1	−31 28 45.8	16.67	37381
01 53 59.2	−27 54 34.8	16.79	19320
01 51 33.4	−31 35 14.5	16.80	19526
02 01 42.2	−31 17 32.3	16.85	20203
01 57 59.9	−29 29 18.0	16.87	4767
01 56 06.7	−27 49 21.0	16.92	25263
01 55 21.5	−28 19 53.6	16.96	22074
01 47 33.0	−29 00 28.1	16.99	27970
01 44 38.0	−30 18 35.6	16.99	18367
02 00 12.8	−29 01 43.5	17.05	25510
01 47 07.3	−29 56 33.8	17.14	18425
02 02 59.8	−28 02 49.1	17.16	22647

Table A.1: Information on the Durham/UKST galaxies.

α (h m s)	δ ($^{\circ}$ $'$ $''$)	b_J	v (kms^{-1})
01 53 41.2	−27 39 08.2	17.17	19146
	415		
02 13 38.7	−31 26 00.6	13.02	3455
02 12 01.5	−31 22 56.2	14.86	3734
02 08 44.5	−31 50 04.4	15.45	12747
02 23 33.2	−29 50 26.8	15.78	18674
02 15 33.5	−28 01 10.6	15.92	17665
02 09 09.9	−30 36 44.0	16.05	11631
02 21 20.9	−29 07 31.4	16.35	18382
02 10 24.6	−30 00 56.8	16.42	10552
02 14 06.2	−30 17 58.7	16.54	19657
02 26 20.5	−29 44 39.3	16.59	17992
02 09 44.4	−30 41 48.3	16.65	12539
02 16 09.5	−30 09 02.3	16.75	23770
02 26 59.3	−29 46 58.0	16.83	17996
02 20 04.5	−31 36 14.0	16.95	8152
02 14 37.6	−31 18 33.5	17.10	21562
02 10 21.4	−31 41 01.0	17.12	17823
02 07 34.3	−31 35 51.9	17.26	17776
02 24 59.9	−29 41 05.2	17.31	19010
02 29 07.2	−27 55 18.9	17.40	18342
	416		
02 41 35.1	−29 12 49.6	12.75	1493
02 47 28.8	−30 47 05.0	14.67	1179
02 50 20.6	−30 58 50.8	14.92	6730
02 34 46.8	−29 24 26.2	15.56	4874
02 30 23.6	−29 54 55.1	15.99	5075
02 41 27.3	−29 50 31.5	16.24	6659
02 32 31.7	−28 30 40.3	16.72	15121
02 47 50.8	−31 22 60.0	16.90	6130
02 45 20.9	−32 01 29.1	17.14	6838
02 52 11.3	−29 06 38.0	17.30	16609
	417		
02 53 30.8	−27 37 30.8	13.39	5272
02 59 07.1	−28 39 50.1	14.49	6571
03 02 59.3	−27 31 50.6	15.13	6048
03 13 22.9	−31 42 16.2	15.83	20068
03 02 41.1	−28 14 20.9	16.18	12500
03 06 27.8	−31 55 16.6	16.44	19978
03 10 03.6	−29 39 27.1	16.56	20251
03 03 27.5	−27 37 34.4	16.60	15141
03 07 56.5	−30 31 00.5	16.64	20665
03 11 44.4	−30 20 14.7	16.70	16381
03 02 59.4	−30 11 33.0	16.78	16219
03 13 59.2	−31 08 42.3	16.85	18579
03 14 34.4	−29 02 51.3	16.97	6900
03 04 07.2	−31 23 05.9	17.01	19440

α (h m s)	δ ($^{\circ}$ $'$ $''$)	b_J	v (kms^{-1})
02 04 19.7	−28 38 46.5	17.19	24624
	415		
02 28 27.6	−31 49 03.7	14.60	4635
02 14 27.3	−30 10 54.3	15.13	3765
02 12 04.9	−32 17 12.1	15.58	3492
02 07 53.3	−31 56 53.5	15.89	4489
02 08 28.9	−31 39 22.4	16.05	12643
02 17 47.8	−28 50 30.0	16.31	17924
02 22 43.3	−28 28 51.0	16.40	10006
02 18 31.4	−28 42 28.8	16.48	17888
02 15 55.4	−28 06 44.7	16.58	8032
02 25 21.9	−29 43 35.8	16.63	17917
02 09 48.4	−29 15 50.1	16.69	10732
02 09 06.2	−29 31 35.0	16.81	14529
02 28 44.5	−31 39 50.4	16.85	24304
02 16 50.1	−27 55 53.6	17.02	17380
02 11 55.3	−31 28 40.5	17.10	18247
02 13 48.6	−27 55 48.8	17.24	19718
02 08 10.6	−30 45 40.5	17.28	21827
02 24 42.6	−31 38 45.5	17.33	24492
02 22 52.2	−31 32 39.5	17.42	19179
	416		
02 46 57.4	−31 22 49.6	14.59	5866
02 46 34.6	−31 44 35.1	14.87	4992
02 46 31.6	−27 40 05.2	15.38	6952
02 49 27.6	−30 25 00.8	15.93	5740
02 36 32.7	−31 33 45.8	16.18	4929
02 29 51.8	−29 49 23.6	16.35	4932
02 40 54.7	−32 15 56.1	16.85	4491
02 29 36.9	−30 05 17.6	17.08	16308
02 47 46.3	−31 09 41.7	17.18	16093
—	—	—	—
	417		
02 54 17.0	−32 23 13.9	14.37	5010
03 07 53.9	−31 19 45.5	14.58	4781
02 53 08.7	−30 02 07.2	15.45	6694
03 14 33.0	−31 10 17.7	16.07	18730
03 10 45.3	−31 40 24.2	16.27	4132
03 10 22.1	−28 28 37.1	16.47	19615
03 06 45.4	−28 07 05.9	16.58	20598
02 57 26.8	−30 55 14.0	16.61	19208
03 05 33.0	−29 34 34.5	16.69	21249
03 06 06.3	−31 45 50.6	16.72	19961
03 00 16.3	−32 22 50.1	16.83	16930
03 14 08.5	−29 24 50.5	16.92	20977
03 13 28.6	−32 02 29.5	17.00	20036
03 04 51.2	−30 51 30.7	17.02	18305

Table A.1: Information on the Durham/UKST galaxies.

α (h m s)	δ ($^\circ$ $'$ $''$)	b_J	v (kms^{-1})	α (h m s)	δ ($^\circ$ $'$ $''$)	b_J	v (kms^{-1})
03 07 50.4	−29 42 12.1	17.03	20508	03 09 44.8	−28 26 18.6	17.07	19766
03 12 18.5	−29 01 13.4	17.13	19579	02 59 29.7	−29 27 45.9	17.16	17996
03 05 36.5	−27 40 04.8	17.19	21939	03 09 30.9	−30 23 28.2	17.22	20241
03 10 08.6	−29 04 27.1	17.31	18857	03 11 43.8	−32 28 51.3	17.38	19902
03 11 27.9	−30 43 35.8	17.41	19873	—	—	—	—
404				404			
21 54 09.5	−34 49 14.1	12.98	2717	22 00 53.1	−32 31 38.5	13.60	2478
21 59 11.1	−33 07 40.3	14.40	4251	22 09 37.8	−36 11 01.3	14.62	9707
21 51 16.9	−34 03 37.2	14.75	4900	22 08 47.2	−34 07 57.8	14.93	2661
22 04 30.4	−33 37 35.9	15.01	2769	21 59 02.9	−36 15 39.3	15.24	9586
22 10 56.0	−33 38 48.7	15.41	4247	21 55 21.7	−34 32 51.7	15.55	10574
21 52 47.6	−34 53 50.3	15.56	4683	21 57 14.6	−37 11 37.9	15.66	16540
22 07 05.7	−33 04 32.8	15.71	14015	22 05 46.6	−35 16 12.1	15.77	9235
22 08 43.8	−35 32 43.7	15.98	17625	22 11 57.3	−34 20 32.1	16.09	8347
22 11 49.0	−36 02 41.3	16.28	3734	22 06 29.0	−36 08 28.1	16.34	17554
22 10 47.5	−35 34 34.1	16.40	3933	22 07 44.0	−34 49 42.9	16.44	8305
22 03 41.3	−36 52 12.6	16.49	27468	22 07 45.2	−32 54 31.8	16.51	12853
22 06 29.7	−34 53 04.6	16.56	8450	21 59 55.1	−32 49 07.3	16.58	2221
22 08 21.8	−35 20 38.5	16.59	9440	22 11 38.2	−34 03 21.9	16.61	8384
22 06 24.8	−35 26 38.4	16.62	8208	22 05 26.8	−33 55 15.2	16.70	18321
22 08 02.8	−32 38 11.5	16.72	10622	22 11 01.6	−34 35 58.3	16.75	17624
21 59 06.5	−36 37 29.7	16.77	17185	22 11 56.4	−37 10 14.2	16.83	10742
22 04 50.8	−32 49 42.5	16.83	17700	21 53 14.6	−34 54 01.8	16.86	4895
22 11 03.3	−36 46 18.3	16.96	9632	22 06 38.0	−36 55 27.2	16.99	17305
21 57 37.2	−35 26 59.8	17.00	10755	22 08 56.2	−37 22 31.4	17.03	17216
22 01 29.3	−35 38 40.2	17.04	27226	22 11 23.8	−37 08 49.5	17.05	17189
22 01 17.2	−33 32 27.1	17.07	9541	22 04 07.2	−34 22 08.8	17.09	16276
22 05 09.2	−34 09 43.6	17.10	4345	21 54 08.9	−35 51 07.5	17.12	20564
22 07 54.0	−35 19 11.4	17.14	4894	—	—	—	—
405				405			
22 13 13.2	−37 05 35.8	12.74	3343	22 26 27.7	−35 43 41.0	14.33	8458
22 13 53.3	−36 38 59.5	14.68	3500	22 19 00.2	−35 27 28.8	14.88	3422
22 18 36.6	−37 17 03.0	15.12	9276	22 23 06.3	−32 44 13.6	15.42	3278
22 33 00.9	−35 06 23.1	15.62	26770	22 26 06.4	−36 41 27.8	15.64	12965
22 23 39.2	−34 28 00.4	15.74	8974	22 32 39.5	−37 24 09.2	15.85	8667
22 18 39.3	−32 50 08.4	15.96	4136	22 23 17.7	−34 58 24.1	16.00	17724
22 26 34.8	−33 16 40.7	16.04	8581	22 32 46.3	−34 53 47.1	16.12	17766
22 14 14.7	−33 18 49.9	16.14	4009	22 24 47.2	−36 44 21.5	16.27	8472
22 34 59.1	−32 37 22.0	16.32	14523	22 32 22.7	−33 25 27.4	16.33	9275
22 27 45.9	−35 40 14.8	16.37	17655	22 35 46.8	−36 38 20.7	16.38	27709
22 35 42.6	−37 14 46.0	16.42	17315	22 26 08.9	−35 35 50.8	16.45	8440
22 18 31.9	−32 45 17.4	16.47	9038	22 29 46.7	−35 51 59.0	16.52	29266
22 16 00.4	−36 29 10.8	16.55	8996	22 14 39.5	−32 32 30.7	16.57	15196
22 26 36.9	−35 48 33.8	16.60	8219	22 32 32.2	−36 34 38.2	16.61	12493
22 15 32.2	−33 43 02.8	16.63	17200	22 13 45.2	−36 24 40.1	16.67	9102
22 26 20.1	−35 45 26.8	16.68	8762	22 17 23.2	−34 55 11.6	16.70	12270
22 16 37.7	−37 04 32.0	16.73	17133	22 16 10.4	−34 48 02.3	16.74	20777

Table A.1: Information on the Durham/UKST galaxies.

α (h m s)	δ ($^\circ$ $'$ $''$)	b_J	v (kms^{-1})
22 33 29.0	−36 25 58.4	16.78	12351
22 20 26.2	−34 45 48.9	16.83	20567
22 16 29.2	−35 07 51.0	16.86	11218
22 31 19.5	−37 27 51.8	16.88	21942
22 18 32.2	−33 11 58.3	16.90	24108
22 35 21.6	−35 11 25.7	16.95	18365
22 19 56.9	−32 36 02.0	16.99	17724
22 30 50.8	−36 56 45.6	17.01	23392
22 33 54.9	−34 06 51.2	17.03	8626
22 26 24.7	−35 45 03.1	17.06	9056
22 27 47.7	−37 05 07.4	17.16	5493
	406		
22 54 23.1	−36 43 45.9	11.40	1659
22 54 56.5	−36 17 37.0	13.58	2307
22 53 53.5	−37 02 25.7	14.31	2076
22 40 39.9	−37 07 41.6	15.08	11857
22 40 56.6	−32 59 29.7	15.26	8508
22 45 50.2	−37 11 03.3	15.40	8217
22 42 49.1	−35 24 48.6	15.57	8946
22 54 55.5	−33 30 30.1	15.64	8763
22 50 55.6	−34 24 48.6	15.75	8503
22 52 31.9	−34 11 14.1	15.93	8788
22 45 24.8	−32 50 40.6	16.04	16505
22 42 54.2	−33 12 36.4	16.09	9281
22 47 47.8	−34 26 29.8	16.13	9056
22 46 38.7	−33 19 28.7	16.23	11769
22 53 57.9	−34 03 01.4	16.31	8775
22 52 32.5	−34 38 53.5	16.39	8807
22 37 21.8	−37 14 18.9	16.44	17608
22 46 14.7	−33 05 03.4	16.50	16683
22 37 18.8	−36 39 00.2	16.52	18071
22 43 37.7	−34 17 52.0	16.58	23523
22 51 54.0	−34 45 07.1	16.63	17091
22 53 12.0	−37 21 01.3	16.67	11025
22 59 32.3	−36 53 34.5	16.67	16448
22 48 05.0	−37 23 55.6	16.71	11006
22 44 18.8	−36 50 10.4	16.75	20362
22 36 45.5	−36 58 34.4	16.79	17676
22 38 36.0	−33 21 54.9	16.83	8542
22 47 56.5	−35 15 53.1	16.84	26908
22 54 50.5	−33 26 47.7	16.86	16633
22 43 21.2	−35 42 42.5	16.87	24196
22 38 29.4	−36 56 17.0	16.91	21414
22 42 56.5	−37 22 27.2	16.93	8856
22 44 30.9	−34 34 09.8	16.95	27416
22 42 29.7	−35 41 31.4	16.95	28318
22 44 19.3	−36 30 02.2	16.97	20838

α (h m s)	δ ($^\circ$ $'$ $''$)	b_J	v (kms^{-1})
22 32 55.6	−35 04 33.9	16.81	8283
22 24 51.5	−35 59 50.0	16.84	17851
22 17 13.2	−35 49 47.8	16.87	7740
22 35 31.7	−35 49 25.2	16.90	18703
22 24 15.5	−35 17 22.8	16.94	17673
22 12 33.8	−36 56 30.3	16.97	11011
22 20 17.6	−33 55 05.0	16.99	2432
22 14 23.5	−37 11 46.6	17.02	17456
22 26 06.0	−32 35 51.4	17.04	29488
22 26 58.5	−35 17 29.6	17.13	23731
—	—	—	—
	406		
22 55 08.0	−36 07 33.2	13.03	2323
22 58 02.1	−35 38 18.5	14.14	1753
22 40 03.5	−35 20 11.1	14.83	12308
22 43 09.8	−36 30 03.0	15.20	8690
22 54 48.7	−34 21 18.6	15.36	8886
22 44 53.4	−36 03 32.8	15.43	8686
22 41 33.8	−36 48 33.4	15.61	12040
22 46 45.5	−33 28 10.3	15.67	8782
22 37 41.9	−35 19 17.3	15.86	8621
22 46 20.4	−33 59 41.4	16.00	20406
22 44 09.5	−33 12 50.7	16.05	16832
22 37 22.3	−36 28 41.3	16.12	17648
22 51 32.2	−32 40 47.8	16.19	16208
22 39 32.1	−32 38 11.8	16.27	17487
22 51 12.2	−33 16 12.4	16.37	17233
22 48 15.1	−32 42 14.2	16.41	12228
22 38 31.9	−33 52 12.5	16.48	18201
22 36 20.3	−36 25 40.9	16.52	17731
22 41 23.1	−36 37 11.3	16.56	17648
22 48 59.6	−35 57 04.1	16.60	24839
22 56 15.4	−33 50 26.4	16.64	8691
22 52 55.0	−34 24 52.0	16.67	8486
22 36 33.0	−32 58 17.5	16.69	17203
22 50 06.7	−34 52 45.1	16.74	16991
22 58 24.8	−37 09 30.1	16.77	8983
22 59 23.6	−32 57 34.6	16.81	4009
22 54 35.6	−33 19 27.4	16.84	16781
22 41 16.3	−36 25 18.1	16.85	20167
22 41 39.5	−37 19 56.8	16.87	19790
22 48 16.2	−36 53 35.4	16.87	19595
22 43 00.7	−33 30 37.3	16.92	21984
22 43 31.1	−37 15 21.2	16.94	11366
22 40 47.3	−36 42 05.2	16.95	20674
22 46 03.3	−37 17 15.1	16.97	31692
22 46 24.1	−36 36 31.4	16.98	12106

Table A.1: Information on the Durham/UKST galaxies.

α (h m s)	δ ($^{\circ}$ $'$ $''$)	b_J	v (kms^{-1})
22 55 25.1	−33 25 57.5	16.99	16584
22 41 17.5	−35 31 23.3	17.01	22200
22 46 27.9	−37 14 04.3	17.03	32223
22 49 12.3	−36 36 45.2	17.05	20116
22 37 04.6	−34 33 28.6	17.06	8817
22 46 10.0	−34 30 09.3	17.09	35710
22 59 14.0	−36 45 10.9	17.10	1624
407			
23 04 19.5	−36 32 54.5	12.96	2728
23 14 04.7	−35 47 50.8	15.03	10753
23 03 50.0	−36 31 14.4	15.85	18040
23 01 38.2	−33 26 34.5	15.98	16526
23 05 54.2	−32 52 33.4	16.24	16209
23 03 16.6	−36 41 38.3	16.33	11666
23 03 22.7	−34 32 25.8	16.40	16856
23 06 13.5	−33 51 24.3	16.46	18470
23 01 50.5	−32 47 30.4	16.53	25201
23 20 19.0	−34 19 00.1	16.60	24237
23 04 47.9	−33 08 46.1	16.62	16451
23 19 50.0	−37 15 40.7	16.68	16364
23 07 31.8	−37 24 29.5	16.73	25767
23 18 12.7	−36 51 20.1	16.78	25782
23 04 38.2	−33 38 01.9	16.83	8561
23 11 51.4	−36 09 00.3	16.85	26707
23 20 17.7	−34 19 06.6	16.91	24276
23 02 14.9	−32 58 45.0	16.93	18033
23 10 08.3	−32 53 17.9	16.97	11519
408			
23 41 09.9	−36 59 28.8	14.76	12482
23 27 42.2	−35 13 22.3	15.23	16172
23 27 36.1	−33 20 56.2	15.35	16057
23 39 43.9	−36 41 34.8	15.71	16199
23 41 12.8	−36 33 30.9	15.85	9792
23 41 21.4	−33 00 14.6	15.96	11442
23 44 05.9	−36 02 25.2	16.01	13518
23 45 43.2	−35 30 31.5	16.09	17135
23 47 26.5	−35 11 37.0	16.12	13466
23 39 17.8	−37 21 55.0	16.17	15599
23 43 44.4	−35 44 10.5	16.31	10804
23 41 51.2	−36 11 42.6	16.39	11120
23 40 30.8	−36 13 27.4	16.45	16733
23 47 41.8	−35 26 34.4	16.47	14831
23 42 07.9	−35 33 48.5	16.53	12069
23 41 04.9	−34 26 27.5	16.59	13481
23 29 31.4	−34 13 08.0	16.61	25919
23 47 01.6	−36 51 20.3	16.65	17229
23 40 23.9	−35 15 28.1	16.68	11820

α (h m s)	δ ($^{\circ}$ $'$ $''$)	b_J	v (kms^{-1})
22 49 55.2	−33 56 37.0	17.00	22752
22 54 28.0	−33 31 44.3	17.03	20131
22 39 49.5	−33 26 02.0	17.03	17279
22 42 21.8	−35 52 17.3	17.06	8797
22 53 58.4	−34 13 37.5	17.08	9765
22 44 42.3	−34 36 51.5	17.10	8558
22 55 57.7	−36 17 47.3	17.10	17611
407			
23 06 54.5	−36 41 28.4	14.33	1657
23 10 39.2	−34 25 23.8	15.57	10404
23 02 25.5	−33 19 24.8	15.94	16779
23 04 19.9	−33 48 37.2	16.06	8665
23 16 27.5	−33 09 56.7	16.28	18657
23 15 48.6	−33 36 06.3	16.39	16197
23 22 10.3	−35 50 23.1	16.42	16444
23 02 09.6	−37 05 34.8	16.48	18085
23 02 06.4	−32 49 16.3	16.57	24460
23 12 13.6	−35 41 45.5	16.60	10741
23 01 45.9	−34 10 07.6	16.66	25391
23 21 11.3	−35 56 47.2	16.71	16442
23 00 57.5	−33 27 59.2	16.76	16453
23 09 19.2	−33 41 47.2	16.80	19546
23 16 56.8	−35 03 40.2	16.84	15873
23 22 22.5	−35 53 59.4	16.88	16318
23 19 16.1	−32 54 05.1	16.92	12016
23 06 59.5	−32 46 24.5	16.94	16422
23 14 19.3	−34 16 23.0	17.02	16306
408			
23 44 21.4	−36 04 21.6	14.95	12609
23 33 28.6	−32 47 05.4	15.32	15612
23 47 28.8	−36 01 32.6	15.52	12975
23 44 58.1	−36 28 33.5	15.78	16846
23 26 37.2	−35 16 03.5	15.90	16430
23 39 55.6	−33 05 26.3	15.99	15562
23 35 39.1	−36 00 27.5	16.02	16151
23 31 52.8	−35 12 23.0	16.10	11906
23 43 35.5	−37 02 32.9	16.15	16864
23 44 49.7	−34 34 13.6	16.26	11617
23 46 35.5	−35 20 03.8	16.38	13109
23 43 38.8	−33 29 42.1	16.43	11590
23 41 55.6	−36 21 46.1	16.46	11358
23 28 55.7	−33 03 15.9	16.51	16340
23 46 25.9	−35 16 51.1	16.56	19593
23 45 36.0	−35 24 05.2	16.61	16618
23 41 50.9	−36 51 15.9	16.63	16938
23 39 23.9	−37 14 51.1	16.66	15821
23 41 35.5	−34 40 24.1	16.71	12679

Table A.1: Information on the Durham/UKST galaxies.

α (h m s)	δ (° ′ ″)	b_J	v (kms^{-1})
23 46 41.4	−36 46 51.3	16.74	14698
23 25 59.3	−35 06 01.4	16.78	25794
23 35 18.4	−35 33 43.9	16.82	16070
23 37 41.2	−36 32 58.5	16.87	13714
23 28 45.3	−34 21 50.4	16.91	15903
23 44 54.0	−35 17 43.3	16.95	17727
23 45 36.4	−33 09 11.3	17.04	26862
23 44 13.6	−35 39 52.5	17.07	12856
	349		
23 54 26.0	−35 02 20.2	13.76	14800
00 03 08.6	−36 13 43.8	14.77	9320
23 55 27.0	−34 34 09.1	14.94	14656
23 59 30.2	−33 44 43.2	15.22	8755
00 07 21.5	−36 55 05.8	15.54	7140
23 48 32.5	−36 39 47.9	15.66	13913
23 52 13.7	−36 26 13.3	15.71	13853
23 56 24.4	−35 21 07.6	15.80	14784
23 53 08.8	−34 26 13.7	15.87	15025
00 08 18.5	−37 26 16.4	15.93	6814
00 10 48.1	−35 47 11.9	15.98	27743
00 09 43.1	−33 44 32.7	16.02	7661
00 00 21.1	−36 00 02.5	16.06	14750
23 54 55.9	−36 52 48.3	16.14	8363
00 03 04.3	−35 05 32.9	16.20	8643
23 57 18.4	−35 16 23.7	16.26	14342
00 03 27.2	−36 23 28.8	16.29	8643
23 48 09.2	−36 25 57.5	16.33	14156
23 51 12.8	−34 57 43.8	16.37	16555
00 06 54.2	−35 25 06.5	16.43	14703
23 57 49.5	−34 02 27.5	16.49	14415
23 54 09.5	−34 51 20.7	16.52	16211
23 57 16.6	−32 46 05.9	16.56	12369
23 56 28.0	−33 30 25.3	16.59	17715
23 57 35.9	−36 30 28.9	16.62	17919
23 50 36.5	−34 16 28.7	16.66	17868
23 54 21.2	−35 06 55.6	16.69	14086
23 50 24.1	−34 57 59.8	16.71	16651
00 08 28.8	−35 41 49.3	16.73	15084
23 57 31.9	−35 56 12.3	16.76	8360
00 10 45.7	−35 48 55.8	16.77	29636
00 10 29.5	−34 14 36.3	16.78	6680
00 10 56.5	−35 47 12.8	16.80	7949
23 59 05.3	−36 23 56.0	16.84	21813
00 00 33.6	−36 13 12.0	16.87	14685
23 50 53.5	−34 35 15.9	16.88	17007
23 51 13.1	−35 46 53.3	16.90	17333
23 53 13.1	−34 44 33.4	16.93	15735

α (h m s)	δ (° ′ ″)	b_J	v (kms^{-1})
23 27 28.2	−36 05 54.9	16.76	5800
23 33 29.6	−32 48 48.2	16.80	15819
23 39 14.2	−36 25 32.5	16.85	11600
23 45 01.2	−32 38 20.7	16.90	11246
23 46 43.0	−35 12 34.3	16.92	10567
23 43 35.3	−35 50 02.0	16.98	12557
23 26 50.0	−35 14 50.6	17.06	23799
—	—	—	—
	349		
00 00 20.9	−34 30 50.4	14.25	6842
23 52 22.6	−34 52 46.6	14.79	16002
23 49 35.7	−34 52 06.8	14.99	8568
23 54 29.6	−36 19 23.6	15.51	13707
23 59 59.4	−36 33 15.6	15.60	13680
00 03 24.4	−36 23 32.3	15.70	8657
23 56 53.0	−35 27 40.5	15.74	14909
00 02 54.8	−36 13 15.9	15.85	8826
00 08 21.5	−35 24 30.7	15.91	14402
23 48 31.0	−35 54 03.4	15.96	16816
00 01 58.9	−32 31 39.7	16.00	8338
23 50 37.4	−33 12 34.0	16.05	17880
00 03 57.1	−32 34 57.0	16.11	13531
23 54 36.8	−35 37 59.3	16.19	15148
23 53 02.3	−36 45 11.1	16.23	15289
23 50 27.4	−35 05 18.6	16.27	13137
00 07 59.5	−33 24 46.4	16.31	7807
23 53 10.5	−33 47 09.9	16.36	17291
00 07 32.0	−35 39 28.2	16.39	14573
00 02 51.5	−35 21 11.4	16.47	9079
00 07 44.5	−37 08 29.4	16.50	8530
00 06 04.7	−33 43 10.6	16.53	14648
00 03 30.1	−32 58 55.5	16.58	13762
23 54 48.1	−32 54 02.8	16.60	17916
23 49 31.9	−36 13 56.6	16.65	14079
23 52 25.1	−33 13 44.3	16.69	17009
23 54 29.3	−35 04 54.7	16.70	15153
00 10 40.7	−35 39 33.5	16.72	22228
00 07 11.6	−35 54 41.3	16.75	18428
00 07 19.6	−35 35 31.2	16.76	15824
23 54 36.6	−34 47 14.3	16.77	10097
00 05 49.9	−35 36 56.6	16.79	14856
00 10 09.6	−36 17 55.7	16.81	21612
00 06 24.4	−35 57 15.1	16.86	14874
00 07 13.9	−36 45 21.6	16.87	15111
00 02 38.9	−34 59 17.1	16.90	34412
23 48 23.0	−34 43 52.3	16.91	17102
23 50 04.6	−35 25 42.2	16.94	19962

Table A.1: Information on the Durham/UKST galaxies.

α (h m s)	δ ($^\circ$ $'$ $''$)	b_J	v (kms^{-1})
00 09 48.5	−37 21 46.4	16.95	15771
23 48 14.4	−33 15 19.1	16.97	21060
	350		
00 27 53.5	−33 31 16.0	11.23	1545
00 23 02.3	−33 19 11.4	14.32	14940
00 28 34.8	−37 09 59.1	14.90	7298
00 14 48.1	−32 47 37.1	15.26	7834
00 29 54.3	−36 59 28.8	15.41	9092
00 23 51.6	−33 41 24.5	15.64	9543
00 17 24.7	−36 19 32.7	15.84	7333
00 34 16.1	−36 31 52.0	15.90	12411
00 15 24.2	−32 48 15.4	15.99	7480
00 35 16.6	−33 58 37.5	16.13	8639
00 28 56.1	−37 21 35.9	16.18	7042
00 20 45.1	−35 02 39.8	16.22	18469
00 25 44.1	−35 44 25.4	16.31	32214
00 20 00.9	−34 23 52.9	16.35	15112
00 15 26.6	−34 10 31.7	16.42	8819
00 24 18.6	−33 03 25.0	16.47	14803
00 12 32.8	−34 20 51.8	16.55	6630
00 28 10.3	−37 21 15.6	16.58	6967
00 17 35.0	−34 33 56.5	16.65	7364
00 32 31.8	−36 42 14.6	16.69	18698
00 16 18.7	−35 02 11.8	16.70	28597
00 22 20.2	−35 53 21.2	16.73	32867
00 26 09.4	−33 20 12.9	16.75	14199
00 23 14.0	−33 18 14.6	16.78	14453
00 22 57.3	−33 19 18.6	16.81	14723
00 34 21.0	−32 30 31.6	16.83	27009
00 12 30.2	−34 09 21.4	16.87	14903
	351		
00 57 02.0	−34 35 57.3	13.77	3427
00 52 37.1	−35 35 33.1	14.89	17368
00 58 38.4	−35 30 40.9	15.35	11598
00 46 54.4	−33 42 13.5	15.67	9062
00 58 24.5	−36 38 19.6	15.93	11742
00 54 50.0	−36 51 45.2	16.12	16988
00 49 59.6	−32 54 58.8	16.20	6020
00 47 43.4	−33 23 08.2	16.26	23633
00 37 21.8	−33 08 41.5	16.45	15199
00 37 07.6	−36 04 44.3	16.49	6347
00 43 55.9	−34 42 24.9	16.58	14559
00 53 32.3	−35 45 54.5	16.64	17164
00 39 12.7	−34 40 48.0	16.70	11442
00 47 07.8	−33 22 26.0	16.74	13381
00 42 05.2	−36 58 05.2	16.78	20694
00 45 16.9	−35 11 35.1	16.83	6898

α (h m s)	δ ($^\circ$ $'$ $''$)	b_J	v (kms^{-1})
23 52 29.4	−36 28 37.5	16.96	14778
23 53 02.5	−34 49 41.2	16.98	10383
	350		
00 27 10.1	−33 32 10.2	14.03	1415
00 13 12.8	−33 18 30.0	14.61	7363
00 33 39.3	−32 52 43.8	15.09	4421
00 12 28.2	−33 11 19.0	15.29	18349
00 20 27.4	−34 51 44.2	15.58	14842
00 30 17.5	−33 26 47.4	15.78	14797
00 34 36.4	−32 48 14.5	15.86	14935
00 15 32.3	−33 12 24.3	15.93	7677
00 19 25.1	−33 33 27.9	16.03	14325
00 19 39.0	−34 32 50.0	16.16	18303
00 28 44.1	−32 36 00.8	16.22	13663
00 16 42.5	−36 52 28.2	16.26	19794
00 33 37.6	−36 50 51.2	16.35	18797
00 18 07.2	−34 44 59.6	16.38	7577
00 14 34.8	−34 49 35.2	16.46	15183
00 22 02.5	−33 21 53.1	16.54	14431
00 21 28.6	−33 42 32.6	16.56	15309
00 19 02.9	−34 11 57.2	16.63	32629
00 22 10.9	−33 32 40.1	16.67	14749
00 23 34.6	−36 05 54.5	16.69	20477
00 19 45.1	−33 30 57.0	16.71	14270
00 24 04.7	−36 47 37.5	16.74	13225
00 34 33.2	−36 06 29.6	16.76	16484
00 21 02.8	−34 31 34.8	16.78	14783
00 19 33.8	−33 33 12.5	16.82	21919
00 26 57.2	−33 15 02.0	16.85	15618
00 34 15.7	−34 18 23.8	16.89	9772
	351		
00 39 30.8	−33 14 40.4	14.79	9642
00 40 25.4	−37 09 09.8	15.19	7100
00 52 14.1	−36 07 22.4	15.56	13681
00 53 30.3	−34 41 18.0	15.69	10236
00 46 43.0	−34 25 13.3	16.08	14395
00 53 53.4	−35 31 28.3	16.18	14526
00 43 47.3	−34 39 21.7	16.22	19249
00 38 38.6	−33 52 28.9	16.35	14471
00 37 41.7	−36 28 47.1	16.47	13278
00 51 59.3	−35 42 56.3	16.55	17072
00 55 37.2	−36 10 48.5	16.60	14617
00 50 32.4	−35 18 12.4	16.68	13538
00 38 21.7	−37 22 54.3	16.72	10383
00 47 29.7	−34 23 03.8	16.76	6668
00 47 16.4	−34 28 34.7	16.82	13967
00 53 05.2	−35 52 03.0	16.83	17388

Table A.1: Information on the Durham/UKST galaxies.

α (h m s)	δ ($^\circ$ $'$ $''$)	b_J	v (kms^{-1})
00 49 31.4	−34 07 52.0	16.87	17835
00 51 35.2	−35 56 13.9	16.89	10138
00 49 20.6	−33 16 51.1	16.95	11621
00 36 35.7	−33 41 21.7	16.97	14355
00 38 38.0	−36 28 25.5	16.99	8730
00 44 30.6	−34 04 02.3	17.01	11514
	352		
01 11 46.6	−32 54 57.2	13.62	3564
01 17 46.2	−34 09 43.6	14.12	3539
01 18 48.0	−36 22 48.9	14.39	9652
01 16 01.7	−37 22 01.9	14.96	9519
01 17 28.4	−33 20 44.3	15.14	9369
01 05 01.0	−37 01 19.9	15.32	3964
01 16 43.8	−36 11 15.2	15.52	15130
01 11 23.7	−34 10 45.2	15.62	6642
01 04 58.4	−36 56 09.1	15.78	14508
01 02 49.2	−34 48 00.7	15.87	14833
01 11 58.7	−35 23 04.4	15.93	9488
01 16 56.2	−33 16 35.6	16.02	9263
01 05 00.9	−34 17 57.8	16.09	19777
01 00 18.1	−33 31 37.7	16.18	10625
01 15 08.4	−34 59 57.8	16.20	15491
01 20 16.4	−33 46 20.3	16.25	10256
01 15 48.1	−36 46 08.1	16.29	7158
01 06 00.5	−36 33 18.5	16.33	6483
01 23 17.1	−33 30 36.2	16.37	9337
01 12 02.7	−33 59 42.4	16.42	20313
01 14 05.0	−33 12 33.0	16.51	5538
01 07 45.6	−36 19 23.5	16.57	5471
01 14 39.4	−37 02 03.0	16.65	20321
01 18 15.3	−36 56 38.5	16.73	11475
01 22 05.1	−34 01 27.1	16.79	9024
01 01 36.2	−33 19 39.1	16.81	15005
01 20 32.2	−32 59 43.8	16.87	20931
01 15 32.5	−35 52 26.8	16.89	22559
	353		
01 47 02.9	−32 59 24.1	13.30	4986
01 35 20.5	−34 10 42.3	13.94	5778
01 28 07.5	−33 17 37.4	14.39	4850
01 47 31.0	−35 04 42.3	14.62	8342
01 33 05.0	−33 01 54.3	14.86	10655
01 31 20.9	−36 51 14.9	15.07	9211
01 32 06.0	−33 05 28.2	15.20	19109
01 29 48.0	−34 03 35.8	15.41	20791
01 37 04.3	−36 32 47.0	15.50	8874
01 41 13.2	−33 43 37.3	15.64	8772
01 33 40.7	−36 10 05.3	15.84	9347

α (h m s)	δ ($^\circ$ $'$ $''$)	b_J	v (kms^{-1})
00 50 22.2	−36 17 44.6	16.89	9802
00 55 42.9	−36 19 56.5	16.91	9177
00 56 31.0	−36 07 60.0	16.97	11727
00 47 44.4	−36 00 38.8	16.99	17843
00 55 48.2	−33 02 57.4	17.01	17949
00 57 20.8	−34 32 54.2	17.03	19703
	352		
01 12 10.8	−32 31 45.2	14.08	5262
01 07 59.8	−36 00 08.4	14.23	3938
01 22 16.3	−33 26 02.2	14.47	9250
01 06 27.3	−36 36 41.4	14.97	6684
01 15 07.5	−36 02 48.2	15.23	9607
01 21 17.7	−35 11 46.8	15.39	6041
01 17 22.3	−33 22 06.1	15.55	5881
01 16 17.1	−33 46 40.1	15.74	5799
01 03 11.2	−34 01 54.5	15.81	5859
01 18 56.1	−33 28 54.2	15.91	5662
01 23 26.2	−37 18 52.7	15.98	9365
01 14 18.6	−33 11 28.1	16.06	5477
01 12 42.0	−33 17 05.8	16.13	6614
01 20 48.7	−32 56 38.2	16.19	9183
01 08 36.3	−33 48 57.2	16.24	9941
01 21 39.5	−34 03 45.4	16.27	1502
01 00 44.2	−36 09 49.7	16.32	14441
01 16 27.0	−33 23 46.7	16.36	9059
01 21 51.7	−35 32 38.5	16.39	3560
01 17 21.2	−35 55 35.8	16.46	10042
01 17 48.5	−33 11 36.6	16.55	20280
01 19 35.4	−32 54 25.0	16.62	9216
01 11 19.2	−33 19 19.4	16.70	6665
01 16 51.0	−33 12 58.1	16.77	20289
01 14 09.4	−33 57 48.4	16.79	11412
01 06 34.9	−36 35 28.8	16.84	17434
01 05 18.8	−36 26 26.5	16.88	6016
—	—	—	—
	353		
01 25 41.0	−35 58 35.7	13.64	5679
01 26 07.0	−36 14 58.8	14.24	5456
01 40 55.6	−34 29 36.3	14.53	3846
01 33 55.3	−36 33 29.1	14.72	9797
01 31 48.8	−34 42 01.8	14.90	3759
01 36 27.2	−33 16 40.1	15.12	10785
01 39 59.9	−33 30 40.5	15.32	5828
01 45 03.5	−32 49 16.5	15.49	10526
01 41 31.1	−34 33 11.6	15.55	3754
01 33 19.2	−34 52 51.3	15.72	5968
01 29 52.0	−34 55 35.6	15.90	9262

Table A.1: Information on the Durham/UKST galaxies.

α (h m s)	δ ($^\circ$ $'$ $''$)	b_J	v (kms^{-1})
01 27 04.8	−33 06 26.7	15.93	19500
01 35 04.2	−33 35 07.7	16.02	13580
01 43 19.4	−34 36 48.6	16.07	8542
01 37 11.2	−34 15 54.5	16.13	8778
01 47 38.7	−36 35 28.4	16.19	9880
01 26 29.9	−35 23 26.7	16.24	5647
01 39 10.2	−35 15 40.5	16.32	8795
01 25 39.2	−32 53 43.6	16.40	17902
01 37 37.4	−34 20 47.4	16.52	20270
01 44 10.5	−36 14 52.2	16.56	18349
01 30 08.9	−33 20 10.7	16.59	10709
01 42 31.1	−36 36 29.8	16.65	20309
01 40 59.5	−35 29 35.2	16.72	8470
01 33 21.6	−36 20 12.9	16.80	16001
01 45 54.4	−35 29 49.1	16.82	8113
01 33 12.4	−36 16 50.8	16.86	12120
01 37 16.4	−33 50 36.1	16.88	10580
01 41 38.6	−34 06 27.7	16.90	8630
01 41 24.4	−35 41 37.0	16.91	20656
	354		
02 07 55.6	−33 10 32.7	13.48	3299
01 58 18.3	−34 29 50.9	14.08	4814
01 59 03.8	−34 36 18.2	14.80	4752
01 52 40.2	−35 24 23.4	15.19	5135
01 52 36.8	−34 58 12.8	15.51	15443
01 50 21.6	−36 05 10.9	15.71	7592
01 52 31.8	−35 54 47.3	15.91	9988
01 48 27.5	−32 51 06.1	16.00	16203
01 48 35.6	−33 02 00.8	16.14	3359
01 55 01.2	−37 06 01.3	16.18	13449
02 08 01.9	−36 43 19.7	16.35	9835
01 51 58.9	−33 35 45.9	16.46	20529
01 53 49.4	−34 53 26.6	16.52	24259
02 02 21.6	−35 39 28.2	16.60	8990
02 09 17.5	−35 04 19.4	16.68	13768
02 07 57.4	−36 38 47.5	16.71	16829
02 04 57.8	−34 18 51.2	16.75	14230
02 04 18.2	−32 35 15.5	16.79	7092
02 06 52.3	−36 16 29.2	16.81	24700
	355		
02 35 30.0	−33 08 25.9	12.93	4406
02 31 07.7	−37 04 45.5	14.77	9434
02 30 35.4	−33 13 20.2	15.41	10806
02 15 13.5	−37 08 28.0	15.83	9467
02 20 54.8	−37 06 22.3	15.99	12913
02 35 19.8	−33 26 58.9	16.15	6375
02 14 14.9	−36 05 16.1	16.22	9394

α (h m s)	δ ($^\circ$ $'$ $''$)	b_J	v (kms^{-1})
01 30 56.8	−33 16 00.4	15.97	4981
01 33 14.3	−33 13 33.0	16.04	18956
01 33 41.2	−36 42 37.9	16.09	9412
01 43 44.3	−35 04 10.5	16.16	20450
01 46 07.7	−35 05 02.4	16.20	18307
01 41 55.1	−36 26 30.5	16.25	8312
01 24 27.7	−33 09 21.4	16.36	20625
01 34 43.7	−35 44 09.4	16.48	8927
01 32 04.5	−35 37 53.5	16.55	24560
01 27 14.3	−33 12 38.5	16.58	11369
01 41 52.0	−35 30 58.4	16.62	20994
01 33 26.5	−33 23 29.4	16.67	21042
01 47 19.5	−33 16 27.7	16.75	11336
01 45 24.5	−36 37 54.3	16.80	8984
01 45 06.3	−37 15 47.5	16.82	20790
01 38 33.3	−37 21 46.8	16.86	21144
01 34 36.4	−36 43 53.7	16.89	5312
01 31 58.1	−33 44 48.7	16.90	14982
—	—	—	—
	354		
02 04 45.4	−36 41 27.5	13.80	5836
02 05 41.1	−35 26 20.1	14.64	6070
01 58 43.6	−34 58 32.5	14.99	10923
02 05 53.8	−37 09 57.8	15.41	6964
02 05 02.1	−37 18 13.9	15.58	18234
01 49 53.7	−33 46 33.1	15.77	8703
02 02 56.9	−35 41 53.1	15.93	18332
02 02 01.8	−35 21 00.7	16.04	10382
01 48 51.2	−36 22 27.8	16.16	5735
01 57 20.9	−35 51 23.2	16.19	8830
01 51 51.9	−33 15 28.7	16.43	8624
01 48 52.2	−33 01 35.1	16.48	8092
02 10 44.7	−35 26 27.0	16.54	5996
01 53 04.3	−33 30 54.1	16.62	20435
01 58 32.9	−33 19 56.1	16.69	22603
02 05 02.5	−37 13 22.7	16.73	18212
01 50 08.6	−36 07 08.4	16.77	9785
01 52 40.3	−33 26 17.7	16.81	26852
—	—	—	—
	355		
02 28 43.5	−34 26 31.3	14.50	4483
02 35 56.7	−33 55 13.1	14.96	4991
02 32 55.2	−34 05 10.3	15.62	6282
02 23 42.1	−37 01 36.8	15.93	5769
02 34 51.7	−33 07 45.8	16.08	21429
02 33 06.2	−37 11 39.0	16.19	13670
02 24 41.7	−36 47 49.5	16.30	9553

Table A.1: Information on the Durham/UKST galaxies.

α (h m s)	δ ($^\circ$ $'$ $''$)	b_J	v (kms^{-1})	α (h m s)	δ ($^\circ$ $'$ $''$)	b_J	v (kms^{-1})
02 16 20.7	−33 04 26.6	16.31	10224	02 34 26.4	−37 28 39.3	16.35	18456
02 28 47.3	−36 13 25.3	16.39	4696	02 18 24.8	−36 57 40.8	16.53	9256
02 17 38.6	−34 10 21.6	16.56	19741	02 15 35.7	−37 22 06.8	16.62	12486
02 26 29.9	−36 27 34.2	16.65	13059	02 14 04.0	−35 12 14.3	16.68	15972
02 19 36.9	−33 02 40.4	16.71	10509	02 26 11.4	−34 51 39.8	16.72	4892
02 16 35.2	−33 59 54.5	16.77	20385	02 28 48.8	−32 57 52.3	16.82	10071
02 32 31.0	−33 26 24.8	16.84	19294	02 24 46.5	−36 33 16.0	16.86	9499
02 34 17.1	−35 28 04.6	16.91	3009	02 13 45.6	−35 03 19.9	17.03	19550
02 26 05.7	−34 27 39.2	17.04	9575	02 19 44.0	−34 37 32.9	17.16	6103
02 20 41.4	−34 16 52.4	17.22	19188	02 12 57.2	−36 07 45.2	17.24	9393
356				356			
02 55 50.4	−36 55 04.6	12.89	6154	02 46 47.0	−36 55 19.8	14.12	5129
02 58 23.6	−37 07 06.8	15.03	1612	02 44 56.0	−36 02 40.4	15.36	6192
02 46 18.6	−35 23 46.1	15.42	5042	02 45 08.3	−34 38 10.2	15.58	6332
02 51 01.0	−34 56 35.2	15.65	4374	02 46 14.4	−36 14 02.3	15.66	4452
02 52 09.5	−33 55 18.7	15.69	18897	02 50 25.3	−36 10 01.1	15.82	16782
02 52 48.3	−35 11 04.9	16.06	6331	02 52 03.3	−36 34 22.9	16.12	18828
02 42 07.1	−36 14 04.9	16.22	6337	02 48 13.9	−35 01 18.9	16.37	10888
02 56 31.5	−34 02 05.8	16.39	4832	02 58 25.5	−37 17 40.5	16.45	19816
02 48 19.2	−35 12 59.2	16.49	10463	02 50 06.4	−36 24 19.7	16.51	28593
02 46 13.6	−37 06 52.8	16.57	11693	02 55 49.6	−36 11 07.9	16.58	15743
02 45 25.4	−35 17 29.3	16.63	25976	02 56 32.7	−34 14 16.4	16.65	19122
02 53 51.8	−34 26 43.5	16.66	19162	02 56 46.4	−37 24 58.6	16.77	19757
02 50 04.3	−35 56 01.9	16.82	16371	02 48 49.9	−35 17 14.4	16.83	11369
02 38 17.2	−33 38 56.1	16.85	10648	02 49 01.6	−35 00 56.1	16.86	11465
02 57 56.6	−36 17 54.1	16.88	23000	02 52 41.3	−36 23 12.5	16.89	19053
02 44 09.3	−36 35 34.0	16.91	10497	02 55 12.0	−32 30 19.4	16.92	4746
02 51 28.0	−33 42 13.6	16.96	4617	02 57 03.7	−36 53 38.4	17.00	7638
02 47 09.3	−33 21 38.4	17.02	10823	02 49 34.3	−35 16 47.3	17.04	10389
02 57 13.9	−37 29 43.1	17.06	19380	02 50 47.4	−33 04 12.3	17.07	4946
02 54 55.2	−35 45 04.6	17.08	26392	02 45 26.9	−34 55 43.7	17.11	24846
02 59 05.0	−32 55 14.9	17.15	28087	02 47 35.2	−36 18 37.5	17.19	4060
02 46 30.6	−35 02 09.8	17.29	18876	—	—	—	—
357				357			
03 20 47.6	−37 23 07.8	10.60	1521	03 15 11.9	−32 45 29.7	12.59	4333
03 23 04.0	−37 11 05.7	14.44	1913	03 08 22.8	−33 20 41.5	14.60	1110
03 21 40.9	−35 57 18.1	15.32	1823	03 23 09.7	−37 06 09.9	15.43	1802
03 19 08.1	−36 54 15.6	15.68	12478	03 19 04.4	−35 52 29.1	16.00	12944
03 17 24.0	−32 49 47.5	16.04	1673	03 15 52.4	−33 14 25.4	16.06	4569
03 08 13.8	−36 49 22.3	16.16	10480	03 18 58.8	−35 46 30.5	16.22	4139
03 00 56.0	−35 42 21.8	16.28	4451	03 06 09.7	−34 22 08.3	16.30	16796
03 17 20.0	−32 56 29.6	16.35	13161	03 06 55.5	−36 55 02.4	16.43	18767
03 16 33.5	−33 17 55.3	16.56	15536	03 12 51.5	−33 43 09.1	16.60	20010
03 04 02.2	−35 26 40.3	16.69	19876	03 06 16.4	−36 53 45.8	16.73	19712
03 12 26.6	−35 59 16.8	16.77	19500	03 05 42.4	−35 41 05.1	16.82	4456
03 05 59.0	−36 54 33.2	16.85	20010	03 02 15.9	−33 11 39.9	16.93	16799
03 05 56.8	−35 32 53.1	16.96	18284	03 00 29.3	−37 05 30.3	17.04	29305

Table A.1: Information on the Durham/UKST galaxies.

α $(h\ m\ s)$	δ $(^\circ\ '\ '')$	b_J	v (kms^{-1})	α $(h\ m\ s)$	δ $(^\circ\ '\ '')$	b_J	v (kms^{-1})
03 01 09.0	−36 48 42.8	17.09	16017	03 21 53.9	−37 25 39.0	17.09	17652
03 07 33.3	−32 54 09.3	17.11	19176	03 03 42.5	−35 02 05.9	17.14	19326
	344				344		
21 59 12.7	−41 19 53.2	14.35	10683	22 03 07.9	−41 00 27.5	14.64	10957
22 11 44.0	−39 03 19.2	14.81	11658	22 15 28.6	−38 17 20.8	14.91	10629
21 54 02.8	−38 29 04.1	15.33	9601	21 54 07.3	−38 29 05.9	15.33	9774
22 13 02.4	−41 18 25.5	15.56	14753	22 01 30.5	−37 44 15.3	15.74	9965
22 14 25.9	−38 15 38.3	15.89	21529	22 07 38.7	−41 25 45.9	15.99	8242
21 58 42.1	−39 59 52.0	16.04	20826	22 17 41.8	−39 07 20.7	16.22	14350
22 07 49.5	−37 53 12.6	16.28	10431	22 09 52.4	−38 43 32.0	16.32	10822
22 05 15.0	−38 27 04.6	16.35	11039	22 15 38.9	−39 54 30.7	16.43	18788
21 57 55.0	−40 30 30.0	16.43	20196	22 00 16.4	−38 18 34.4	16.45	16991
22 08 24.0	−41 58 10.6	16.49	16360	22 17 11.1	−41 55 37.7	16.51	20557
21 56 24.5	−40 25 46.0	16.55	18946	22 06 00.5	−40 58 36.6	16.57	18655
22 03 21.9	−39 10 04.3	16.68	11044	22 14 14.6	−40 40 05.3	16.84	14304
22 12 34.1	−38 24 05.1	16.85	16942	22 07 54.8	−41 07 50.0	16.87	17240
21 58 40.3	−37 47 22.4	16.87	2687	22 12 17.4	−40 28 06.9	16.95	19125
22 18 19.3	−38 52 44.6	17.02	17302	22 04 44.7	−39 18 08.9	17.09	10825
22 15 23.0	−39 46 13.8	17.12	18348	22 09 01.1	−38 47 21.1	17.24	11206
22 09 51.4	−40 49 05.7	17.26	22303	22 03 05.6	−39 34 45.0	17.34	21318
21 57 28.8	−40 10 43.2	17.37	20372	21 59 07.8	−41 33 52.5	17.45	19050
	345				345		
22 30 57.0	−41 11 31.5	12.83	2014	22 19 19.9	−40 20 33.0	14.01	2282
22 20 34.6	−38 17 27.9	14.85	8250	22 29 44.1	−38 18 22.1	14.92	3058
22 31 00.1	−39 39 23.5	15.16	17100	22 23 47.2	−41 49 44.4	15.35	19834
22 40 21.6	−40 18 40.4	15.43	9157	22 30 38.8	−37 48 07.7	15.52	10800
22 20 13.5	−38 14 48.3	15.67	8428	22 21 48.4	−38 49 31.6	15.81	2570
22 40 20.1	−39 44 26.2	15.88	9586	22 19 35.6	−38 53 06.9	15.90	8366
22 33 52.7	−39 14 42.2	15.97	2023	22 32 11.3	−38 30 50.3	16.09	9016
22 28 37.0	−38 27 38.2	16.17	21790	22 22 23.5	−38 14 34.7	16.19	11291
22 39 32.3	−40 14 11.8	16.27	9040	22 42 18.0	−40 10 59.8	16.31	9793
22 31 51.2	−39 05 25.1	16.33	17343	22 29 24.2	−41 53 23.2	16.43	2624
22 19 17.1	−39 54 47.8	16.44	15152	22 26 09.2	−40 00 55.7	16.49	10721
22 38 02.6	−39 36 49.6	16.52	16497	22 44 31.3	−41 08 47.0	16.55	19906
22 20 11.1	−39 41 42.0	16.60	16168	22 31 44.5	−37 50 17.0	16.62	11034
22 35 25.0	−38 52 36.0	16.63	18207	22 36 39.7	−37 47 18.7	16.67	13483
22 35 27.2	−40 32 18.0	16.68	17417	22 31 01.7	−40 35 34.6	16.77	15630
22 30 30.3	−38 27 36.1	16.79	21614	22 24 03.6	−40 10 33.7	16.93	21517
22 43 06.9	−37 40 21.0	16.94	10804	22 42 39.8	−40 50 20.6	16.98	17293
22 28 22.5	−42 07 12.1	17.00	17302	22 24 37.8	−40 55 18.6	17.01	17752
22 32 49.7	−41 45 41.9	17.06	22447	22 41 38.6	−41 28 20.0	17.09	20156
22 37 05.3	−41 32 02.3	17.13	9088	—	—	—	—
	346				346		
22 52 10.6	−39 55 49.2	11.82	1448	22 46 33.0	−37 44 10.8	13.78	8538
22 59 17.9	−41 26 00.5	14.91	1688	23 01 22.8	−39 31 55.9	15.56	16916
23 02 29.0	−40 42 07.0	15.77	16585	22 49 33.0	−40 34 40.7	15.85	10001
22 57 56.5	−37 36 30.5	16.03	8358	22 51 24.3	−40 24 55.7	16.09	9421

Table A.1: Information on the Durham/UKST galaxies.

α ($h\ m\ s$)	δ ($^\circ\ '\ ''$)	b_J	v (kms^{-1})
22 56 12.8	−40 53 25.1	16.29	17043
23 04 45.1	−40 05 02.1	16.46	17915
22 49 37.6	−38 14 12.0	16.56	8411
23 08 43.3	−40 50 15.6	16.66	13455
22 53 38.0	−39 38 39.2	16.84	8371
22 49 03.8	−40 33 51.5	16.88	9677
23 03 22.6	−37 39 18.4	16.97	11676
23 00 12.8	−39 50 29.9	17.09	16856
23 00 33.2	−38 33 38.8	17.13	16082
22 48 59.6	−40 03 23.8	17.30	17012
22 56 48.5	−40 41 18.2	17.52	9711
347			
23 33 36.0	−38 12 52.0	11.44	688
23 12 07.9	−38 07 41.0	14.62	2834
23 28 50.2	−42 25 24.1	15.19	1685
23 33 14.9	−41 00 10.4	15.47	15697
23 22 42.0	−38 43 19.7	15.66	10717
23 19 02.1	−38 41 11.8	15.83	10542
23 23 42.4	−39 29 28.1	15.90	10877
23 23 14.0	−39 34 47.8	16.07	10344
23 34 51.1	−40 59 36.0	16.17	15843
23 30 46.8	−38 55 11.9	16.20	16128
23 17 07.2	−41 04 01.3	16.33	15496
23 32 18.2	−40 43 19.6	16.44	13516
23 23 46.4	−39 48 50.4	16.52	15041
23 34 10.1	−39 34 52.1	16.54	17033
23 29 46.3	−41 03 03.7	16.58	14754
23 16 00.4	−39 43 00.8	16.66	17307
23 29 34.8	−38 04 01.3	16.69	10799
23 23 18.9	−38 23 42.9	16.73	10897
23 34 08.8	−37 34 43.6	16.76	11492
23 27 19.1	−37 59 30.9	16.82	27734
23 17 58.3	−41 37 21.1	16.87	17222
23 27 15.5	−39 43 39.1	16.93	17009
23 30 59.5	−39 52 14.3	16.98	16097
348			
23 48 17.5	−41 00 34.1	12.96	1634
23 42 45.7	−38 36 52.0	15.12	12736
23 40 03.3	−39 20 34.0	15.18	12502
23 45 13.0	−37 52 29.6	15.42	13005
23 50 38.1	−42 01 38.9	15.53	8731
23 41 55.8	−37 39 49.5	15.77	12534
23 51 09.2	−37 57 08.4	15.90	13306
23 58 34.5	−38 24 17.2	16.03	13400
23 42 08.0	−40 22 39.5	16.08	15309
23 56 33.4	−38 55 23.1	16.23	15028
23 52 15.5	−39 13 49.8	16.34	18222

α ($h\ m\ s$)	δ ($^\circ\ '\ ''$)	b_J	v (kms^{-1})
23 10 51.8	−42 16 03.7	16.41	1766
22 57 00.5	−38 53 48.9	16.50	10333
23 06 10.9	−39 48 20.1	16.64	5307
22 50 51.4	−39 56 54.0	16.70	8610
23 05 42.6	−40 34 42.9	16.86	16653
23 00 05.8	−38 07 41.7	16.89	8432
22 45 40.6	−39 26 46.1	17.00	2639
23 09 01.9	−38 59 22.2	17.11	9762
23 01 37.6	−39 37 07.4	17.21	935
23 04 49.7	−38 03 50.9	17.33	18029
23 03 28.8	−42 15 17.7	17.53	22268
347			
23 12 47.6	−38 48 27.3	13.78	2884
23 20 30.6	−38 06 50.8	14.90	16015
23 17 46.6	−42 02 37.2	15.36	16749
23 31 41.2	−38 02 24.6	15.64	11377
23 27 58.7	−41 30 57.1	15.67	17064
23 33 34.3	−37 45 37.9	15.87	16033
23 20 39.9	−40 33 02.1	16.03	15445
23 34 55.6	−37 33 40.4	16.11	15947
23 26 35.7	−38 11 15.1	16.20	16131
23 26 28.0	−38 40 43.0	16.27	10825
23 31 41.7	−39 53 56.8	16.40	18341
23 29 51.9	−41 30 04.5	16.47	17111
23 19 53.3	−40 55 17.8	16.53	17017
23 27 12.3	−37 48 39.6	16.55	15999
23 27 28.5	−38 11 03.3	16.63	16042
23 31 56.8	−40 20 52.7	16.67	15980
23 35 33.8	−40 53 36.6	16.71	15370
23 35 39.7	−40 40 01.8	16.73	24874
23 33 31.3	−40 56 51.5	16.78	15114
23 15 46.4	−37 34 14.2	16.84	18263
23 11 16.9	−41 38 55.2	16.90	10287
23 19 33.0	−42 16 35.7	16.96	27095
23 22 14.9	−41 28 08.9	16.98	16204
348			
23 44 06.9	−38 44 47.7	14.87	12370
23 41 03.0	−38 57 27.1	15.14	12529
23 53 27.8	−41 10 09.2	15.29	18449
23 59 22.9	−40 56 26.7	15.49	14984
23 44 58.2	−38 20 38.1	15.62	13279
23 39 26.8	−39 29 37.5	15.78	12835
23 42 54.7	−37 53 04.1	15.93	15649
23 54 41.9	−41 10 20.1	16.07	14980
23 50 44.7	−40 01 28.0	16.10	15533
23 47 23.1	−38 52 48.5	16.24	12220
23 49 23.7	−39 43 13.2	16.36	11956

Table A.1: Information on the Durham/UKST galaxies.

α $(h\ m\ s)$	δ $(^\circ\ '\ '')$	b_J	v (kms^{-1})
23 54 38.7	−38 58 23.8	16.40	15158
23 54 51.2	−41 20 21.4	16.43	14864
23 47 02.4	−38 51 31.2	16.51	12838
23 42 17.2	−41 29 01.1	16.53	12287
23 58 28.7	−41 04 53.5	16.57	20566
23 39 24.2	−38 06 54.3	16.64	32858
23 38 01.0	−42 14 26.3	16.68	18697
23 55 38.8	−39 49 15.0	16.74	12845
23 47 36.0	−38 13 42.1	16.79	12994
23 49 19.6	−41 26 25.8	16.87	19898
23 52 10.5	−38 18 46.8	16.88	17428
23 40 35.6	−41 27 04.6	16.91	15362
23 54 21.9	−39 28 01.6	16.93	15701
23 59 45.6	−38 01 43.3	16.94	14786
23 51 11.3	−40 16 48.4	16.98	12277
23 52 42.7	−38 57 19.5	17.01	20060
23 58 01.9	−40 51 14.9	17.04	14948
293			
00 04 34.1	−41 38 06.5	14.41	13919
00 02 53.1	−39 11 00.8	15.52	6619
00 04 56.6	−42 01 56.2	16.00	16035
00 10 24.3	−41 37 20.4	16.21	12246
00 05 55.1	−41 08 09.7	16.34	18500
00 00 45.8	−42 18 31.5	16.50	12655
00 00 42.1	−39 23 46.5	16.70	15146
00 11 00.0	−42 20 53.5	16.77	25527
00 02 39.6	−42 16 31.5	16.99	9147
00 02 03.5	−40 58 12.7	17.23	13304
294			
00 32 47.2	−37 49 59.7	14.57	6954
00 15 36.0	−37 59 14.6	15.34	7044
00 21 26.7	−42 24 01.1	15.78	15974
00 27 24.7	−41 13 14.7	16.08	11999
00 22 57.5	−41 52 47.9	16.16	8018
00 18 51.1	−41 23 33.8	16.25	20724
00 36 43.9	−41 30 23.2	16.38	14515
00 33 32.7	−38 07 12.9	16.49	18760
00 13 03.3	−42 07 01.9	16.53	26232
00 30 23.7	−42 02 28.1	16.57	9138
00 16 08.3	−41 56 08.1	16.62	28559
00 18 50.5	−41 40 50.8	16.66	12123
00 31 40.8	−38 10 19.7	16.71	9088
00 17 32.8	−39 36 23.3	16.94	14236
00 30 37.1	−39 49 26.5	17.00	19086
00 24 17.0	−40 00 36.2	17.03	8868
00 13 19.0	−41 25 35.2	17.09	24785
00 27 20.5	−40 07 01.2	17.16	19396

α $(h\ m\ s)$	δ $(^\circ\ '\ '')$	b_J	v (kms^{-1})
23 47 45.8	−38 27 22.6	16.42	12617
23 59 26.6	−39 38 04.2	16.46	8637
23 42 34.2	−37 47 28.1	16.52	9736
23 42 52.8	−40 51 01.4	16.56	19909
23 38 36.2	−39 14 08.9	16.62	13636
23 54 10.6	−37 50 23.5	16.67	15204
23 48 02.6	−42 23 34.3	16.73	26220
23 50 05.2	−37 42 02.6	16.78	10398
23 54 27.2	−40 09 12.1	16.84	20850
23 44 38.4	−38 51 02.3	16.88	12747
23 54 35.7	−41 28 16.3	16.89	17926
23 45 50.8	−38 33 30.2	16.92	12437
23 40 57.6	−39 53 10.3	16.94	12191
23 56 44.8	−41 53 03.7	16.96	15746
23 38 44.0	−38 42 55.3	17.00	12417
23 47 08.6	−38 06 57.7	17.03	12866
—	—	—	—
293			
00 10 48.7	−37 47 32.4	15.10	15117
00 08 37.5	−39 15 54.8	15.59	3280
00 07 22.1	−40 08 03.8	16.15	17604
00 01 20.4	−39 29 16.5	16.27	19869
00 08 03.0	−41 09 53.2	16.49	20776
00 04 35.5	−41 45 21.3	16.61	13115
00 05 43.6	−39 16 01.7	16.71	15286
00 12 51.7	−41 13 04.0	16.95	8512
00 06 17.7	−41 30 58.6	17.13	15403
—	—	—	—
294			
00 24 42.1	−41 15 42.0	14.96	7829
00 36 40.3	−39 07 54.2	15.70	19052
00 20 48.3	−41 29 45.2	15.81	8064
00 20 35.7	−42 21 51.1	16.09	15982
00 38 59.6	−38 07 42.1	16.19	7382
00 30 18.0	−39 44 58.0	16.33	19903
00 27 19.0	−38 05 07.3	16.46	6955
00 22 32.3	−42 29 14.5	16.50	12469
00 23 22.5	−42 15 48.7	16.55	27461
00 28 06.9	−41 05 47.2	16.60	20509
00 29 40.7	−40 22 23.2	16.64	20920
00 24 50.6	−38 27 24.7	16.68	20396
00 18 22.6	−42 06 31.1	16.73	16019
00 22 14.3	−39 59 21.6	16.96	19029
00 33 54.9	−39 32 19.7	17.02	18607
00 20 16.8	−38 23 30.0	17.08	35673
00 29 43.2	−38 55 46.2	17.13	13973
00 24 59.3	−40 02 54.4	17.16	20794

Table A.1: Information on the Durham/UKST galaxies.

α (h m s)	δ ($^\circ$ $'$ $''$)	b_J	v (kms^{-1})
00 32 06.9	−38 22 25.8	17.17	22573
00 32 16.1	−39 39 23.4	17.19	19856
00 29 52.9	−40 12 29.4	17.23	20732
00 35 00.2	−39 23 33.9	17.24	19234
00 17 43.8	−39 10 14.7	17.28	27622
00 29 55.7	−42 22 19.3	17.35	20906
	295		
00 57 27.3	−40 36 11.6	13.59	6890
01 02 22.6	−37 54 16.7	14.72	3906
00 52 44.8	−40 59 40.8	15.26	17919
01 00 15.8	−42 17 10.5	15.39	6992
00 50 58.6	−39 07 54.3	15.54	19439
00 51 20.4	−37 36 10.4	15.93	14946
00 49 32.6	−40 18 58.6	16.19	16520
00 47 58.4	−37 39 56.0	16.51	11962
00 45 50.6	−42 17 37.5	16.57	5189
01 04 23.7	−38 50 56.2	16.73	6599
00 52 06.0	−38 17 36.1	16.80	16767
00 59 41.2	−38 47 34.2	16.82	16496
00 46 42.2	−39 01 59.8	16.85	11510
00 51 45.8	−37 42 21.3	16.93	16310
00 55 10.3	−38 45 18.9	17.00	19347
00 44 54.4	−39 19 18.8	17.09	7243
00 40 06.7	−41 17 32.4	17.14	18173
00 41 44.8	−41 12 04.5	17.17	24340
00 46 40.8	−39 14 39.5	17.23	11212
00 54 50.6	−41 40 48.8	17.26	19103
00 49 50.0	−41 05 35.3	17.28	31787
	296		
01 30 14.5	−38 56 09.9	13.66	3716
01 28 28.0	−37 58 42.7	14.58	9540
01 28 16.8	−41 33 13.9	14.78	6518
01 24 28.7	−40 14 28.2	15.16	5988
01 10 21.8	−41 04 47.4	15.36	15659
01 29 23.9	−41 47 19.0	15.62	6427
01 28 57.2	−37 55 56.0	15.81	5896
01 28 10.4	−41 30 26.1	15.99	6580
01 29 39.6	−41 55 56.3	16.04	8287
01 21 47.5	−38 53 35.7	16.26	6229
01 28 55.1	−38 06 39.6	16.39	5863
01 06 02.1	−41 49 08.8	16.46	19362
01 18 14.6	−39 37 34.1	16.51	28120
01 08 14.4	−39 20 22.2	16.58	9057
01 17 36.8	−38 39 31.2	16.65	9465
01 09 08.3	−39 49 20.4	16.70	20217
01 25 28.6	−39 12 09.9	16.80	27497
01 07 24.6	−41 13 00.2	16.85	16232

α (h m s)	δ ($^\circ$ $'$ $''$)	b_J	v (kms^{-1})
00 34 47.3	−41 31 55.8	17.18	29159
00 18 11.2	−41 07 55.0	17.22	21267
00 30 36.6	−41 53 47.8	17.23	9394
00 13 26.0	−39 17 29.6	17.24	15501
00 33 40.0	−40 00 21.8	17.29	20547
00 27 56.2	−38 36 41.7	17.35	12018
	295		
01 04 54.3	−42 11 03.3	14.39	6811
00 49 08.6	−37 55 37.5	15.00	7048
00 53 24.1	−37 40 44.1	15.32	16851
00 48 12.6	−42 19 28.0	15.51	16135
00 49 59.1	−41 20 02.5	15.76	7219
01 00 35.7	−38 02 42.0	16.06	13357
00 58 58.3	−38 53 10.0	16.23	16411
00 42 18.0	−38 27 22.5	16.56	6922
00 48 08.3	−42 24 30.7	16.65	22993
00 54 38.7	−39 12 18.9	16.78	20421
00 56 26.2	−39 25 34.5	16.81	16802
00 54 02.9	−38 25 36.8	16.84	9824
00 50 46.4	−39 59 23.8	16.86	9851
00 56 11.8	−39 48 03.4	16.97	16998
00 46 32.0	−42 11 47.1	17.02	16279
00 47 07.4	−42 19 35.1	17.10	9977
00 48 17.4	−40 46 37.5	17.15	22632
00 50 35.8	−39 44 39.3	17.18	25629
00 50 30.7	−37 39 44.2	17.24	14363
00 48 45.5	−39 10 04.6	17.26	11368
00 51 55.3	−41 36 13.4	17.29	19096
	296		
01 22 29.8	−38 23 19.3	14.30	5762
01 23 35.6	−37 35 37.3	14.62	9224
01 10 19.9	−38 09 44.6	15.00	6444
01 15 53.0	−42 07 07.7	15.21	6395
01 23 55.3	−38 54 55.7	15.58	10081
01 23 17.7	−38 32 36.3	15.75	5955
01 07 59.6	−41 15 33.9	15.94	13959
01 26 51.7	−41 08 50.5	16.01	6404
01 12 22.6	−41 08 25.0	16.15	9920
01 14 10.8	−42 04 44.9	16.36	23993
01 27 34.0	−42 23 33.6	16.44	6495
01 28 55.1	−41 28 03.7	16.50	26144
01 21 41.8	−41 08 26.4	16.55	9033
01 13 56.7	−39 50 12.3	16.60	15832
01 25 27.1	−41 14 18.5	16.69	15709
01 28 20.5	−41 09 59.8	16.71	28650
01 21 31.6	−40 54 51.7	16.83	9355
01 09 34.9	−41 01 39.5	16.87	16232

Table A.1: Information on the Durham/UKST galaxies.

α (h m s)	δ ($^\circ$ $'$ $''$)	b_J	v (kms^{-1})	α (h m s)	δ ($^\circ$ $'$ $''$)	b_J	v (kms^{-1})
01 11 36.3	−38 53 06.2	16.88	9635	01 16 42.5	−42 16 40.2	16.89	16835
01 14 37.1	−41 05 04.9	16.89	15945	01 10 52.6	−37 45 32.3	16.92	15892
01 23 24.0	−38 07 39.0	16.98	9429	01 08 28.2	−39 53 40.3	17.02	14996
01 23 53.5	−39 05 45.5	17.07	27971	01 24 27.9	−38 24 34.7	17.07	9274
01 20 23.2	−39 15 07.1	17.08	15473	01 09 41.0	−41 37 07.8	17.10	9894
01 25 48.6	−39 38 45.1	17.14	9136	01 14 12.5	−39 25 07.9	17.21	28538
01 24 49.2	−41 46 15.5	17.22	31614	01 08 32.1	−41 08 23.4	17.23	16575
01 06 20.6	−39 39 42.5	17.24	22051	01 18 38.8	−39 41 32.1	17.26	27991
297				297			
01 42 20.1	−40 54 55.2	14.44	10253	01 32 00.8	−38 52 20.1	14.70	5873
01 43 18.7	−38 48 08.0	14.84	9876	01 55 50.6	−38 15 45.0	14.95	11202
01 33 28.7	−41 32 36.0	15.12	7336	01 38 26.2	−38 56 10.0	15.31	5878
01 42 17.7	−42 04 58.1	15.39	6171	01 43 53.4	−38 19 24.6	15.48	6192
01 56 00.3	−39 17 05.0	15.71	17101	01 42 45.3	−38 59 00.9	15.83	5991
01 32 20.8	−42 26 38.4	15.90	9897	01 31 47.9	−39 23 00.3	15.94	5876
01 31 49.1	−39 42 37.1	16.00	13700	01 31 19.7	−39 43 16.8	16.02	8866
01 42 28.9	−40 49 13.5	16.13	10171	01 40 56.6	−40 25 59.4	16.15	16078
01 32 40.8	−39 54 00.6	16.19	5911	01 54 57.1	−40 29 33.4	16.21	6253
01 34 10.4	−41 20 23.3	16.23	7392	01 43 29.7	−40 55 01.7	16.32	16338
01 50 03.0	−37 47 26.3	16.34	1376	01 43 37.0	−42 12 24.0	16.38	8665
01 33 32.2	−37 54 46.7	16.42	22227	01 55 08.4	−38 55 11.0	16.57	17212
01 31 36.7	−39 20 39.4	16.59	8908	01 55 48.4	−38 49 28.9	16.61	17288
01 54 42.0	−40 54 57.0	16.61	17081	01 34 24.0	−41 47 33.9	16.65	20152
01 32 34.8	−40 42 44.9	16.67	8816	01 43 51.3	−41 47 01.0	16.69	17543
01 49 09.7	−41 46 52.2	16.75	16569	01 45 54.7	−40 32 30.3	16.77	17802
01 41 47.7	−38 39 53.4	16.79	6291	01 44 08.4	−40 59 24.7	16.84	16265
01 34 18.2	−41 36 35.0	16.92	11198	01 31 56.0	−37 47 20.7	16.96	17222
01 42 03.0	−40 26 09.4	16.98	16171	01 54 47.5	−39 15 27.1	17.00	5792
01 37 49.5	−40 08 28.5	17.00	11129	01 55 59.0	−37 57 44.2	17.03	6148
01 42 34.3	−41 54 46.6	17.05	22936	01 31 36.1	−38 49 04.2	17.05	28196
01 55 36.9	−41 56 24.1	17.09	16893	01 48 34.7	−38 02 34.8	17.09	18955
01 35 49.3	−40 12 30.5	17.15	17064	01 38 47.1	−40 22 10.2	17.19	16223
01 38 58.8	−41 27 55.2	17.23	20684	01 33 53.5	−41 21 57.8	17.27	23008
01 31 23.5	−39 35 53.5	17.34	8949	01 32 50.5	−39 47 24.8	17.34	20669
01 32 49.4	−41 18 41.5	17.38	23028	—	—	—	—
298				298			
02 17 33.5	−38 02 52.7	13.33	4948	02 08 36.3	−41 09 11.7	13.91	1480
02 09 52.2	−39 26 21.5	14.12	5261	02 04 35.9	−41 23 41.8	14.29	5307
02 19 12.7	−42 13 47.5	14.76	4873	02 11 35.0	−39 58 31.2	14.93	5100
02 03 46.9	−38 20 17.7	15.27	11553	02 13 25.4	−41 55 37.7	15.30	17041
01 58 49.8	−41 40 59.7	15.53	5592	02 08 23.2	−42 19 27.4	15.60	4178
02 04 40.2	−37 31 35.8	15.68	18332	02 11 11.7	−40 02 54.1	16.03	5175
02 05 51.0	−39 47 04.3	16.08	27950	01 57 57.8	−38 50 48.5	16.12	26821
02 10 44.8	−41 04 16.3	16.17	11350	02 07 57.8	−39 51 11.5	16.22	5173
02 22 17.3	−40 28 00.5	16.26	8789	02 14 21.7	−41 44 43.5	16.28	11249
02 01 40.4	−42 26 27.9	16.30	16065	02 18 18.5	−40 07 29.1	16.36	21116
02 17 53.8	−41 53 33.2	16.43	3785	02 05 48.5	−40 50 29.3	16.44	8704

Table A.1: Information on the Durham/UKST galaxies.

α (h m s)	δ (° ′ ″)	b_J	v (kms^{-1})	α (h m s)	δ (° ′ ″)	b_J	v (kms^{-1})
02 09 47.5	−40 26 28.1	16.46	11594	02 15 03.3	−39 18 16.0	16.47	11487
02 05 30.4	−41 01 02.2	16.60	21334	02 19 52.8	−38 40 24.0	16.65	18321
02 13 35.2	−41 37 21.9	16.69	11136	02 11 09.4	−42 15 50.3	16.70	5337
02 21 45.2	−40 13 23.5	16.75	18039	01 57 36.8	−41 12 34.7	16.77	19460
02 17 29.7	−38 40 31.2	16.77	17838	02 09 31.1	−38 54 53.7	16.88	28264
02 00 42.8	−41 58 04.5	16.90	5200	01 58 00.5	−40 22 42.5	16.93	16717
02 16 27.5	−41 54 21.2	16.95	11241	02 06 26.9	−38 17 00.9	16.97	5127
01 58 10.0	−41 29 40.8	17.00	15340	02 13 51.8	−40 01 36.6	17.01	11577
02 06 05.0	−41 52 55.0	17.12	16914	02 05 35.4	−39 46 09.5	17.13	27770
02 19 05.6	−37 51 06.7	17.17	21055	02 16 10.7	−41 50 12.2	17.18	11193
		299				299	
02 31 34.0	−39 15 49.4	11.50	1959	02 30 41.9	−39 30 55.0	14.26	1406
02 23 41.7	−38 31 26.8	15.33	5025	02 41 45.8	−37 46 02.4	15.43	5099
02 46 15.8	−39 19 20.6	15.49	18654	02 32 37.2	−37 50 23.1	15.84	21418
02 40 23.1	−37 40 53.2	16.03	18305	02 34 30.5	−42 14 53.0	16.15	16321
02 40 31.8	−40 19 04.7	16.33	7870	02 32 40.9	−38 04 33.0	16.42	21090
02 42 42.5	−39 01 25.1	16.46	18514	02 36 20.9	−37 34 15.1	16.50	18386
02 32 24.1	−40 17 08.7	16.56	11652	02 46 21.8	−41 51 40.5	16.58	20082
02 41 03.2	−38 34 30.6	16.62	9581	02 47 03.4	−41 55 55.7	16.68	13611
02 26 44.7	−40 50 01.0	16.72	20933	02 44 08.0	−41 03 21.5	16.74	28350
02 36 51.8	−40 51 33.2	16.76	18393	02 44 59.9	−40 52 47.8	16.84	21035
02 29 07.3	−41 55 55.9	16.94	21768	02 41 38.3	−38 09 38.3	16.98	18544
02 40 39.2	−38 32 20.5	17.06	21184	02 39 31.8	−41 26 25.3	17.15	18647
02 37 53.6	−37 46 27.1	17.17	13711	02 45 16.6	−39 29 56.1	17.19	18776
02 42 51.7	−37 52 15.0	17.19	5756	02 36 41.3	−40 02 10.2	17.23	1877
02 32 27.2	−41 52 51.6	17.26	26740	02 42 30.1	−41 08 01.8	17.27	30343
02 40 43.0	−38 20 58.9	17.33	9995	02 37 15.3	−42 14 39.5	17.36	5131
02 32 47.7	−38 43 20.3	17.39	31847	—	—	—	—
		300				300	
03 04 11.6	−39 13 33.0	13.34	6224	03 05 46.9	−39 47 47.4	14.77	4413
03 02 17.2	−39 33 00.5	15.67	5945	03 00 39.2	−39 01 07.5	15.71	12523
03 04 43.8	−42 11 05.8	15.81	9298	02 50 07.6	−40 57 04.8	15.85	14286
03 05 42.5	−41 49 18.5	15.88	9261	02 54 52.9	−42 19 21.4	15.94	13754
02 57 25.2	−38 42 10.4	16.08	11346	03 13 27.5	−38 06 01.7	16.12	19358
02 56 25.4	−40 41 34.0	16.18	9796	03 09 45.5	−39 19 16.3	16.21	8077
03 03 18.4	−41 52 20.1	16.23	9312	03 12 19.8	−39 22 24.5	16.31	16929
03 02 15.6	−39 44 09.4	16.33	6056	02 52 29.2	−37 42 05.5	16.42	19665
02 57 53.4	−41 20 18.0	16.45	21987	03 00 02.0	−40 52 43.5	16.47	6212
03 01 04.1	−37 54 07.5	16.56	19452	03 08 02.0	−40 09 41.3	16.62	2053
03 11 53.5	−39 54 56.3	16.66	12157	03 01 27.6	−39 50 52.7	16.77	19423
03 07 26.4	−41 37 45.8	16.78	9216	03 14 36.8	−37 31 21.4	16.85	19551
03 13 57.3	−42 29 09.8	16.86	18404	03 03 10.4	−39 32 39.6	17.02	15140
03 08 34.5	−39 49 04.7	17.07	4579	03 01 36.6	−41 23 32.0	17.10	9438
02 56 38.4	−41 16 44.3	17.18	16522	—	—	—	—
		301				301	
03 15 28.8	−41 17 24.4	10.92	791	03 21 08.2	−42 22 01.9	14.35	1208
03 16 52.1	−41 52 59.4	15.52	19308	03 23 43.0	−39 37 55.0	15.57	18869

Table A.1: Information on the Durham/UKST galaxies.

α (h m s)	δ ($^\circ$ $'$ $''$)	b_J	v (kms^{-1})
03 39 39.3	−41 07 37.8	15.63	18410
03 22 01.9	−40 23 21.5	15.83	16286
03 21 40.0	−39 49 16.9	16.17	18848
03 16 43.8	−41 37 38.0	16.21	9534
03 26 25.1	−41 44 20.4	16.45	21745
03 30 06.2	−40 37 13.3	16.50	21905
03 35 53.6	−38 58 57.3	16.68	33845
03 27 04.4	−38 14 24.2	16.74	19847
03 32 23.8	−40 50 30.0	16.85	18741
03 23 09.1	−40 34 48.7	16.89	9161
03 35 31.3	−37 44 56.7	16.99	24596
03 23 18.5	−42 04 48.4	17.04	18470
03 27 37.8	−37 38 46.2	17.06	18971

α (h m s)	δ ($^\circ$ $'$ $''$)	b_J	v (kms^{-1})
03 22 49.0	−40 24 55.2	15.67	9073
03 36 24.7	−37 43 19.1	15.90	13814
03 25 52.2	−37 46 37.0	16.18	9270
03 33 03.4	−38 51 01.8	16.41	20301
03 16 40.8	−41 49 23.2	16.46	19356
03 31 49.6	−38 31 46.3	16.54	20246
03 32 48.0	−39 14 14.3	16.70	18205
03 20 18.2	−41 30 30.2	16.83	20822
03 20 48.5	−40 07 35.9	16.88	15848
03 37 14.4	−38 26 17.2	16.95	18122
03 35 08.1	−38 45 41.6	16.99	20182
03 39 15.3	−39 05 31.8	17.05	7238
—	—	—	—

Appendix B

Completeness of the Durham/UKST Galaxy Redshift Catalogue

In this appendix the completeness rates of the Durham/UKST Galaxy Redshift Catalogue are presented for three different magnitude limits. For each field information is given about the magnitude limit of the field, m_{lim}, the total number of galaxies to this magnitude limit, n_{tot}, the number of measured redshifts, n_z, the number of unobserved galaxies, n_{unobs}, the number of missed galaxies, n_{miss} and the completeness rate calculated from these numbers. Table B.1 presents this information using a uniform limit of $b_J = 16.75$, table B.2 uses the "best" limit chosen as a compromise between having a faint magnitude limit in each field and keeping the completeness levels quite high ($> 60\%$) and table B.3 uses an "all" limit which includes every measured redshift from the 1 in 3 catalogue.

Table B.1: Field information and completeness for a uniform magnitude limit of $m_{lim} = 16.75$.

Field #	m_{lim}	n_{tot}	n_z	n_{unobs}	n_{miss}	Completeness (%)
531	16.75	33	25	0	8	75.8
532	16.75	34	22	0	12	64.7
533	16.75	50	37	2	11	74.0
534	16.75	32	29	0	3	90.6
535	16.75	13	11	0	2	84.6
536	16.75	28	17	2	9	60.7
537	16.75	38	34	1	3	89.5
472	16.75	8	4	0	4	50.0
473	16.75	32	13	1	18	40.6
474	16.75	40	31	1	7	77.5
475	16.75	26	13	1	12	50.0
476	16.75	34	27	1	6	79.4
477	16.75	29	22	0	7	75.9
478	16.75	33	19	1	13	57.6
479	16.75	45	26	3	16	57.8
480	16.75	34	29	2	3	85.3
481	16.75	40	26	1	13	65.0
466	16.75	41	30	4	7	73.2
467	16.75	47	34	6	7	72.3
468	16.75	28	19	3	6	67.9
469	16.75	31	28	1	2	90.3
470	16.75	29	27	0	2	93.1
471	16.75	68	43	14	11	63.2
409	16.75	40	28	3	9	70.0
410	16.75	31	23	3	5	74.2
411	16.75	33	28	1	4	84.8
412	16.75	39	33	2	4	84.6
413	16.75	33	30	0	3	90.9
414	16.75	30	23	0	7	76.7
415	16.75	35	23	0	12	65.7
416	16.75	31	13	0	18	41.9
417	16.75	23	20	0	3	87.0

Table B.1: Field information and completeness for a uniform magnitude limit of $m_{lim} = 16.75$.

Field #	m_{lim}	n_{tot}	n_z	n_{unobs}	n_{miss}	Completeness (%)
404	16.75	40	30	3	7	75.0
405	16.75	34	34	0	0	100.0
406	16.75	49	49	0	0	100.0
407	16.75	29	25	0	4	86.2
408	16.75	44	39	0	5	88.6
349	16.75	63	58	0	4	92.1
350	16.75	46	45	0	1	97.8
351	16.75	27	27	0	0	100.0
352	16.75	51	47	0	4	92.2
353	16.75	50	48	0	2	96.0
354	16.75	45	33	0	12	73.3
355	16.75	32	24	1	7	75.0
356	16.75	31	23	3	5	74.2
357	16.75	33	20	1	12	60.6
344	16.75	33	23	0	10	69.7
345	16.75	49	29	2	18	59.2
346	16.75	28	16	0	12	57.1
347	16.75	56	36	2	18	64.3
348	16.75	54	37	5	12	68.5
293	16.75	25	14	0	10	56.0
294	16.75	30	26	0	4	86.7
295	16.75	36	19	3	14	52.8
296	16.75	40	32	3	5	80.0
297	16.75	39	31	0	8	79.5
298	16.75	33	29	1	3	87.9
299	16.75	23	18	0	5	78.3
300	16.75	35	21	1	13	60.0
301	16.75	41	19	1	21	46.3

Table B.2: Field information and completeness for the "best" magnitude limit.

Field #	m_{lim}	n_{tot}	n_z	n_{unobs}	n_{miss}	Completeness (%)
531	16.96	44	33	0	11	75.0
532	16.58	24	19	0	5	79.2
533	17.02	69	47	2	20	68.1
534	17.27	61	46	0	15	75.4
535	16.93	19	13	1	5	68.4
536	17.08	44	28	3	13	63.6
537	16.79	40	35	2	3	87.5
472	16.32	4	3	0	1	75.0
473	16.04	12	7	1	4	58.3
474	16.70	38	31	1	5	81.6
475	16.31	17	12	0	5	70.6
476	16.85	39	31	1	7	79.5
477	16.82	33	25	0	8	75.8
478	16.54	25	18	1	6	72.0
479	17.00	58	36	4	18	62.1
480	17.23	59	46	3	10	78.0
481	16.65	36	26	1	9	72.2
466	16.97	58	38	9	11	65.5
467	16.98	63	44	8	11	69.8
468	17.14	46	31	5	10	67.4
469	17.16	56	40	6	10	71.4
470	17.22	63	49	7	7	77.8
471	16.88	80	52	16	12	65.0
409	16.68	36	27	1	8	75.0
410	17.06	52	35	5	12	67.3
411	17.14	54	42	4	8	77.8
412	16.94	50	42	3	5	84.0
413	16.96	46	41	1	4	89.1
414	17.01	49	39	0	10	79.6
415	16.85	40	26	0	14	65.0
416	16.24	17	11	0	6	64.7
417	17.07	38	30	0	8	78.9

Table B.2: Field information and completeness for the "best" magnitude limit.

Field #	m_{lim}	n_{tot}	n_z	n_{unobs}	n_{miss}	Completeness (%)
404	17.14	65	45	4	16	69.2
405	16.87	40	40	0	0	100.0
406	16.81	52	52	0	0	100.0
407	17.02	44	38	0	6	86.4
408	16.98	58	50	0	8	86.2
349	16.98	91	80	0	10	87.9
350	16.89	55	54	0	1	98.2
351	17.05	46	44	0	2	95.7
352	16.89	59	55	0	4	93.2
353	16.91	64	59	0	5	92.2
354	16.81	50	37	0	13	74.0
355	16.86	38	28	2	8	73.7
356	17.11	58	40	4	14	69.0
357	16.43	20	16	0	4	80.0
344	16.87	42	27	0	15	64.3
345	16.68	45	29	2	14	64.4
346	16.89	35	20	0	15	57.1
347	16.90	65	42	3	20	64.6
348	17.04	83	55	6	22	66.3
293	16.71	23	14	0	8	60.9
294	16.73	30	26	0	4	86.7
295	16.86	46	26	3	17	56.5
296	16.92	53	40	3	10	75.5
297	17.09	59	44	1	14	74.6
298	17.01	45	38	1	6	84.4
299	16.76	24	19	0	5	79.2
300	16.66	30	21	0	9	70.0
301	16.45	25	13	1	11	52.0

Table B.3: Field information and completeness for the "all" magnitude limit.

Field #	m_{lim}	n_{tot}	n_z	n_{unobs}	n_{miss}	Completeness (%)
531	17.36	74	40	9	25	54.1
532	17.38	78	33	1	44	42.3
533	17.02	69	47	2	20	68.1
534	17.31	66	47	0	19	71.2
535	17.47	42	21	1	20	50.0
536	17.44	77	37	5	35	48.1
537	17.18	76	45	10	21	59.2
472	17.40	35	8	0	27	22.9
473	17.29	83	25	4	54	30.1
474	17.23	88	51	9	27	58.0
475	17.34	63	22	7	34	34.9
476	17.32	76	44	3	28	57.9
477	17.39	61	33	1	27	54.1
478	17.42	81	31	7	43	38.3
479	17.18	73	38	9	26	52.1
480	17.40	71	50	5	16	70.4
481	17.17	76	33	10	33	43.4
466	17.14	72	43	12	17	59.7
467	17.09	73	44	12	17	60.3
468	17.54	72	39	11	22	54.2
469	17.29	72	45	11	16	62.5
470	17.30	70	50	9	11	71.4
471	16.88	80	52	16	12	65.0
409	17.28	77	42	18	17	54.5
410	17.19	69	39	13	17	56.5
411	17.29	65	44	10	11	67.7
412	17.13	64	50	5	9	78.1
413	17.14	59	46	3	10	78.0
414	17.19	63	46	3	14	73.0
415	17.42	86	38	3	45	44.2
416	17.37	65	19	0	46	29.2
417	17.41	62	37	0	25	59.7

Table B.3: Field information and completeness for the "all" magnitude limit.

Field #	m_{lim}	n_{tot}	n_z	n_{unobs}	n_{miss}	Completeness (%)
404	17.19	69	45	4	20	65.2
405	17.27	76	55	6	15	72.4
406	17.10	84	84	0	0	100.0
407	17.08	47	38	0	9	80.9
408	17.07	66	53	0	13	80.3
349	16.98	91	80	0	10	87.9
350	16.89	55	54	0	1	98.2
351	17.05	46	44	0	2	95.7
352	16.89	59	55	0	4	93.2
353	16.91	64	59	0	5	92.2
354	16.91	58	37	0	21	63.8
355	17.33	76	34	12	30	44.7
356	17.29	76	43	15	18	56.6
357	17.17	65	30	4	31	46.2
344	17.47	82	36	1	45	43.9
345	17.13	83	39	6	38	47.0
346	17.54	82	30	2	50	36.6
347	17.05	82	46	3	33	56.1
348	17.07	87	55	8	24	63.2
293	17.30	53	19	1	32	35.8
294	17.38	85	48	3	34	56.5
295	17.35	89	42	8	39	47.2
296	17.27	87	52	6	29	59.8
297	17.42	85	51	6	28	60.0
298	17.24	60	42	1	17	70.0
299	17.39	67	33	1	33	49.3
300	17.20	69	29	4	36	42.0
301	17.15	82	29	2	51	35.4

Acknowledgements

This is the one chance that I get to stand up and thank everyone who I have ever known for being so wonderful and fantastic, and I'm going to do it ! If you like the Oscars then you'll love this section, darling's...

Firstly, I would like to thank my family for their support throughout my studies, from school to doctorate level. I would also like to thank the Physics Department at the University of Durham for giving me the one chance I needed to show what I could do. I acknowledge the receipt of a PPARC research studentship for the period in which this research was carried out. I thank STARLINK for the use of their computing facilities and in particular Alan Lotts for keeping the systems running at all times of the day and night when I was using the CPU's. The staff of the UKST and AAO are thanked for their help with the observations and fibreing, especially Malcolm Hartley and Quentin Parker who made the long nights pass quicker with their undeniable sense of humour. Alison Broadbent deserves thanks for her efforts in the early years of the Durham/UKST project. Of course, my gratitude goes to all my collegues in the Physics Department at Durham who have helped me along the way. However, Carlton Baugh deserves a special mention for actually reading the early version of my thesis and making constructive comments. Having written this thesis I know how much effort it takes to read it and hopefully my payment of Mars Bars was enough for him ! I would also like to thank my viva examiners, George Efstathiou and Carlos Frenk, for a very entertaining day. To say I was not on top form is an understatement and their patience was appreciated. And last but certainly not least, I am hugely indebted to the guidance, knowledge and passion that my supervisor, Tom Shanks, has shown me in the past 3 years. Without him it would not have all been possible and I wish him big hugs and kisses in the future...

I believe that I have been very lucky to know and associate with a special group of people in the second term of my sentence at Durham, these people I call my friends. I start by thanking my past and present office-mates (wherever my office has been !). In particular, the members of room 157 (Omar Almaini, Scott Croom, Douglas Burke and Claire Halliday) did constantly put up with my inane sense of humour and sponge basketball games on a daily basis. I'm sure they all regret the day Doug brought that hoop and ball into the office. However, I believe we produced an excellent research atmosphere, with just the right blend of fun, frolics and hard work. I cannot remember the number of evenings I came into the department at midnight to find 2 or 3 other lost souls also working late. I think we made a good team. Also, I must say a big thanks to the early group of students who made me feel welcome when I was just starting out, Rafael Guzman, Lilian Graham, Susan Watkin, Neasa Foley and Kathy Romer get the nod here. The past and present set of postdocs in Durham also deserve mention, especially Mike and Chloe Hudson, Glenn Baggley, Michiel van Haarlem, Ana Campos, Peter Doel and Carlton Baugh. Similar sentiments go to the students Gillian Wilson, James Steel, Luis Teodoro, Vincent Eke, Paul Young and Paul Alton. The more recent additions to the department, both postdocs and students, will ensure that Durham remains a lively place for a few more years to come as people such as Enzo Branchini, Katherine Gunn, Harald

Kuntschner, Ale Terlevich etc. take over. Also, Roelof de Jong deserves thanks for producing some excellent theme parties in the past year, his party Web page will no doubt become legendary in Durham.

I would like to thank those past and present members of the "Cosmic" 5-a-side football team... and other men I have given blood with ! Rather than live up to the typical image of a physicist, I believe we showed just how "committed" we could be (or is that should be ?) in reaching the dizzy heights near the top of the table for a year (or two). This commitment culminated in a 2 month period which started with my sending off and ended triumphantly with us lifting the knockout Cup ! The players that I remember most vividly are Steve Fullerton, Luis Teodoro, Roger Haynes, Nigel Metcalfe, Douglas Burke, Ray Sharples and James Gourlay. The majority of our games were battles and I could not pick any better players to go to war with than these. I can also remember in every detail each of the 5 goals I scored in actual match competition over a period of almost 4 years. Strange that, isn't it ?

I feel I must mention the people from other academic institutions who have helped me along the way, mainly in terms of providing floors to sleep on when I was visiting. Creidhe O'Sullivan, Helen Tadros, Chris & Russell Pearson, Wendy Groom and Mark Jex all supplied hospitality at one time or another. However, Wendy Groom and Helen Tadros deserve a special mention as good friends and former "veterans" of the Les Houches Summer School. We suffered together for a month on a mountain and I still get the flashbacks...

Individually, I have some special mentions ; Scott Croom, a quality person who is also a superior cosmologist, is thanked for his many helpful moments when I all but forgot how to spell my name, never mind cosmological matters ! Jane Chapman, who was undoubtly the backbone of the Astronomy Department in Durham (before she left for Cambridge !), constantly amazed me with her resilience and sense of humour against the brickwall of red tape she faced every day. Her leaving party was one of the highlights of my time here. Gillian Wilson deserves mention as a good friend over the past 3 years. A class act if ever I met one (I have to say this otherwise I'll never get a holiday in Hawaii !). And finally, I owe a great deal (an infinite amount in fact) to Omar Almaini who was my best friend and main confidant during his 3 years in Durham. I have fond memories of our late night conversations in the physics department and I wish him all the best for the future.